Ground Response Analyses and Design Spectra for UDOT Bridges on Soft Soil Sites

A Research Report Submitted to the
Utah Department of Transportation

by

Steven F. Bartlett

January 8, 2004

Department of Civil and Environmental Engineering
University of Utah
Salt Lake City, Utah 84112

ACKNOWLEDGMENTS

This guidance was funded by the Utah Department of Transportation Research Division. We are grateful to this agency for its support. Technical review and comments were also provided by the UDOT Geotechnical and Structures Divisions. We would also like to acknowledge the help of Clifton Farnsworth, who was the project manager for this research.

We would also like to thank Drs. Abbas Abghari (CALTRANS), Farhang Ostadan (Bechtel) and James Pechmann (University of Utah) for their review of this document. Their suggestions and detailed discussions have greatly improved its technical content. Ivan Wong (URS) also provided data and suggestions that are contained in this report. Some of the preliminary analyses were completed by Michelle Flint and Ryan Broadbent (University of Utah) and we acknowledge their assistance.

Table of Contents

List of Figures

List of Tables

List of Attachments

Introduction

Background

Current seismic design requirements for highway bridges and retaining wall are found in AASHTO (1996). The design peak ground acceleration (pga) for rock is based on probabilistic hazard mapping having a 10 percent probability of exceedance in 50 years (i.e., approximate 500-year return period event). However, state DOTs have the option to use more stringent seismic design requirements and incorporate a design event with a longer return period. This was the approach used by the Utah Department of Transportation (UDOT) in establishing the seismic design requirements for the I-15 Reconstruction Project in Salt Lake City, Utah. For this project, a site specific probabilistic seismic hazard assessment (PSHA) was performed by Dames and Moore (1996). Strong motion hazard curves were calculated at various locations along the I-15 alignment for a 500 year and a 2500 year return period event. Based on the results of the PSHA and recommendations of a UDOT seismic advisory panel, the 2500 year return period earthquake was selected as the design basis earthquake for bridge structures. Retaining wall were designed to a 500 year return period event. The design spectra were uniform hazard spectra with spectral acceleration values that varied according to location and soil type along the alignment.

UDOT's current usage of a more stringent design earthquake for interstate bridge design has a strong technical basis that is reflected in current trends in building and bridge code design (NEHRP 1997a, b; 2000a, b; IBC 2000; MCEER 2001a, b). After I-15 Reconstruction Project, UDOT has continued the policy of using a 2500 year return period design for the design of critical structures. Bridge structures which fall under this more stringent design earthquake are interstate and lifeline bridges. Further, UDOT recommends that spectral values for the design response spectra be obtained from the national seismic hazard maps (Frankel et al. 1996).

However, the spectral acceleration values obtained from the seismic hazard maps (Frankel et al., 1996) are only appropriate for outcropping soft rock conditions (NEHRP site classification B to C). These rock spectral values cannot be used directly for design at soil sites because they do not account for important amplification and/or deamplification effects.

The effects that soil has on strong motion are particularly important at soft and/or deep soil sites. Many valleys adjacent to the Wasatch Front are filled with interbedded alluvium and lacustrine deposits that extend to considerable depths. Thus, soil effects will play a significant role in modifying the nature of the strong motion caused by a major earthquake. For example, Figures 1 and 2 show a typical soil and shear wave velocity profile, respectively, for the central part of the valley near the I-15 alignment. The clayey silt and silty clay of the upper Bonneville Lake deposits are especially soft between depths of about 5 to 10 meters. These lacustrine sediments have moisture content values ranging from 35 to 70 percent and plasticity index (PI) values ranging from 30 to 40 percent. Also, geotechnical investigations for the I-15 Reconstruction Project show that the undrained shear strength of this soft layer is about 20 to 30 kPa (Saye and Ladd, 2000). Thus, this soil profile classifies as site class "E" using NEHRP (1997a, 2000a) and MCEER (2001a) soil classification systems. Because of the soft nature of these deposits, we expect that the character of the strong motion will be significantly modified by the near surface soil profile.

Objectives and Scope of Guidance

The purpose of this research is to provide design guidance to the Utah Department of Transportation (UDOT) for developing design spectra and performing site specific ground response analyses for bridges located on soft and/or deep soil profiles (i.e., NEHRP classes D and E soils). The University of Utah Civil and Environmental Engineering Department has contracted with the Utah Department of Transportation Research Division to develop this guidance which has been peer reviewed by a panel of seismic experts established by the UDOT Research Division. The methods discussed herein have been integrated with the

guidance outlined in: Recommended LRFD Guidelines for the Seismic Design of Highway Bridges, Part I: Specifications (MCEER, 2001a, b) which has not been adopted by UDOT for design, but its adoption is anticipated. We have also reviewed design guidance given in NEHRP Recommended Provisions for Seismic Regulations for New Buildings and Other Structures," Part 1: Provisions (FEMA 368), Building Seismic Safety Council (NEHRP, 2001a, b) and other technical documents (CALTRANS 1996a, b, c) provided by the UDOT Technical Advisory Committee (TAC).

The methods discussed herein are applicable for interstate bridges and other critical lifeline bridges founded on soft and/or deep soil sites. These are bridges that UDOT requires to remain operational following a seismic event. In the language of MCEER (2001a) performance levels, this guidance is applicable to UDOT interstate and lifeline bridges which shall immediate operation following the earthquake and have a minimal damage for a design basis earthquake which corresponds to a "rare earthquake." The design ground motion for the rare earthquake is defined in terms of an acceleration response spectrum with spectral values that have a 3 percent probability of exceedance in 75 years. (This event is equivalent to a response spectrum having spectral values corresponding to a 2 percent probability of exceedance in 50 years (MCEER 2001b), or an event with an average return period of 2500 years). UDOT and MCEER (2001a) require that the 0.2 and 1.0 second soft rock (NEHRP Type B) spectral acceleration values be obtained from the national seismic hazard maps (Frankel et al., 1996).

This guidance describes the process of developing site specific amplification factors and design spectra using ground response analyses and empirical attenuation relatons. We recommend that this guidance be applied to NEHRP Type D and E soil profiles. This guidance should be not applied to sites where liquefaction is a concern. Guidance for developing design ground motions for potentially liquefiable sites has been developed for UDOT by Brigham Young University.

This design guidance contains examples, figures and supporting files and programs, so that UDOT and/or its geotechnical consultants can complete the ground response and design spectra development. For illustration purposes, the UDOT TAC has recommended that we use two soft soil sites located in the Salt Lake Valley. The sites that were selected by the TAC are: 1) I-15 / I-80 / Highway 201 Interchange near 2100 South and 2) the 600 South Interchange near downtown Salt Lake City (Figure 3). These will be referred to as the "I-80 interchange" and the "600 South interchange," respectively.

Amplification Factors Used in Current Building and Bridge Design Codes

Current AASHTO (1996) seismic provisions use site coefficients (S_1, S_2, S_3, S_4) to adjust the rock spectral shape for soil effects. These site coefficients are the same coefficients included in NEHRP and Uniform Building Code (UBC) provisions before 1994 and 1997, respectively. However, the widespread adoption of more recent seismic codes clearly demonstrate that the seismic provisions found in AASHTO (1996) have been superseded by recent developments that make the current AASHTO provisions somewhat dated (Dobry et al., 1997).

Current building code and draft bridge design guidelines use soil amplification factors to adjust rock spectra for soil effects (NEHRP 1997a, b; NEHRP, 2000a, b; MCEER 2001a, b). Recommendations developed during the NCEER/SEAOC/BSSC Site Response Workshop (Rinne and Dobry, 1992) use a two factor approach. This method has been adopted by building and draft bridge codes and also uses site coefficients to adjust bedrock spectral values for soil effects (NEHRP 1997a, b; NEHRP, 2000a, b; MCEER 2001a, b). In this approach, the short period acceleration (0.2 s), S_S, is multiplied by a short-period site coefficient F_a. The long period spectral values are represented by a curve that is equal to the one second period acceleration, S_1, divided by the period (i.e., S_1 / T) and multiplied by the long-period site coefficient, F_v. Values of F_a and F_v are dependent on the soil conditions and the level of ground shaking. Ultimately in the building code approach ((NEHRP 1997a, b;

2000a, b), the spectral values described above are multiplied by 0.67 (i.e., 2/3) to determine the final design spectrum for non-critical facilities. However, in both the building code (NEHRP 1997a, b; 2000a, b) and in the draft bridge code (MCEER, 2001a, b) for the rare earthquake (maximum considered earthquake), the design spectral values are not reduced by the 0.67 factor for critical facilities.

Furthermore, NEHRP (1997a) and IBC 2000 require site specific geotechnical investigations and dynamic site response analysis for site class E profiles having mapped 0.2-second period accelerations (i.e., S_S) greater than 1.25 or mapped 1.0-second period accelerations (i.e., S_1) greater than 0.5. Also, the same requirements are placed on all site class F profiles, regardless of the mapped spectral acceleration values. In contrast, NEHRP (2000a) and MCEER (2001a) do not require site specific response analysis for site class E soils with S_S greater than 1.25 g or S_1 greater than 0.5 g. Instead, the NEHRP (2000a) has provided amplification factors for site class E soils at higher acceleration values. The same amplification factors given in NEHRP (2000a) are repeated in MCEER (2001a). The reason and technical basis for the change between the two versions of NEHRP (i.e., 1997a and 2000a) are not explained in the commentary (NEHRP 2000b). Nonetheless, the development of site amplification factors for soft soil sites experiencing high levels of strong ground is an area of active research and warrants further investigation (Dobry et al., 1997; Borcherdt, 1997; Seed et al., 2001).

Even though the amplification factors calculated from recent modeling studies and published in current building codes represent significant improvements over amplification factors given in AASHTO (1996), the NEHRP (1997a; 2000a), site amplification factors for site class E soils represent simplifications and/or extrapolations of strong ground motion records that were available in 1992 (NCEER, 1997). Extrapolations have been made based on amplification estimates at the 0.1 g level from the Loma Prieta earthquake and have been extrapolated to higher ground motion levels based on laboratory and theoretical modeling

(NEHRP, 2000b). This was done because few or no strong motion recording have been obtained at higher levels of motion on soft soils (NEHRP, 2000b).

Because of the uncertainty associated with soft soil amplification factors as published in current building and bridge codes, especially at high levels of strong motion, we recommend that site specific response analyses be performed for all site class E profiles. We also recommend that consideration be given to performing site specific response analysis for site class D profiles. This is because of the considerable thickness of unconsolidated sediments found in the intermountain valleys near the Wasatch Fault. For example, Arnow et al., (1970) have estimated the depth of Quaternary fill ranges from 300 to 640 m around the downtown Salt Lake area. This deep sediment profile may produce a surface soil response that is significantly different that estimated by using the generic soil amplification factors found in NEHRP (2000a) and MCEER (2001a).

Previous Research Regarding Soft Soil Response

Summary of Previous Research

Many researches have used site specific response analyses for soft soil sites. Typically, 1-D response analyses are performed from bedrock to the ground surface. This is generally sufficient to capture the dominant response of most soil deposits for periods less than about 2 seconds. Often, the state-of-practice is to use the results of ground response modeling to extrapolate of soil amplification factors for soft soil sites at levels greater than about 0.1g (Borcherdt, 1994; Dobry et al., 1997). This extrapolation is typically done based on laboratory and theoretical modeling results and is necessary because very few strong-motion recordings have been obtained at higher levels of motion for soft soil sites (NEHRP, 2000b).

In addition, research from past earthquakes suggests that at high levels of strong motion, soft soils will yield and behave plastically. Such yielding produces a strong nonlinear soil behavior. Research studies by Seed et al. (1976a, 1992) suggest that nonlinear behavior may significantly reduce the high frequency spectral accelerations at the ground surface (Seed et al., 1976a, 1992). For example, Seed et al. (1976a) conducted a statistical study of peak ground accelerations developed at locations with different site conditions using 147 records from each western U.S. earthquake of about magnitude 6.5. Based on this analysis, they proposed the general relations shown in Figure 4. This figure suggests a deamplification of the maximum surface acceleration for deep cohesionless soils and for soft to medium stiff clay and sand when compared with the maximum acceleration on rock. However, the database for this study did not include soft clay sites; thus the curve for these soils was drawn based on judgment and has more uncertainty (Seed et al., 1976a).

Subsequently, Idriss (1990) compared earthquake records from the 1985 Mexico City and 1989 Loma Prieta earthquakes for soft soil sites and used ground response modeling at higher levels of ground motion to modify the Seed et al. (1976a) soft soil curve (Figure 5). The

Idriss (1990) curve shows a significant amplification of the peak acceleration due to soil effects at low to moderate levels of strong ground motion. For these earthquakes, relatively low values of peak rock accelerations of 0.05 g to 0.10 g were amplified about 1.5 to 4 times for sites with soft clay layers. The clay layers at these sites ranged in thickness from a few feet to more than a hundred feet and the depth to bedrock was up to several hundred feet below the surface. However, not all of the Idriss (1990) curve is drawn using empirical data. Ground response modeling was used to extrapolate the curves for accelerations greater than about 0.2 g. The ground response analyses suggest that the median amplification factor for soft soil sites tends to decrease as the rock acceleration increases and approaches a cross-over point of 1.0 for a rock acceleration of about 0.4 g.

More recently, Chang et al. (1997) and Seed et al. (1997) have compared maximum accelerations for soil sites with those recorded at adjacent rock sites. The study by Chang et al. (1997) compared accelerations on deep, stiff, cohesive sites (i.e., generally site classification C_3 from Table 1) with maximum rock accelerations (Figure 6). This study suggests an amplification of the maximum soil acceleration when compared with the maximum rock acceleration for accelerations below about 0.6 g. It also suggests a slight deamplification for acceleration values above 0.6 g. Seed et al. (1997) used these results and previous studies to suggest the relations between maximum soil and maximum rock accelerations shown in Figure 7 for the soil types listed in Table 1. Figure 7 suggests that deamplification of maximum soil acceleration compared to rock begins at about 0.35 g for soil types C4, D and E and at about 0.5 g for soil types B, C1 and C2.

The above results, if true, have particular importance for soil sites along the Wasatch Front. A significant portion of the central part the valleys that comprise Utah, Salt Lake, Davis and Weber Counties are underlain by thick, unconsolidated soils consisting generally of type C, D and E soil profiles. Also, the expected maximum rock acceleration expected for most of this area significantly exceeds 0.4 g for the 2500 year return period event (Figure 8). Thus,

Figure 7 suggests a possible deamplification of maximum rock acceleration resulting from soil effects in the central parts of the Wasatch Front valleys.

In addition to peak ground acceleration, the spectral shape of rock motion can be significantly modified by soil sites. The effects of soil nonlinearity (i.e., greater amount of shear strain and damping) at high levels of ground motion are generally recognized as: (1) a deamplification of high frequency spectral accelerations and (2) a shift in the predominant period of the spectral response to longer period (Seed et al., 1976b; Seed et al., 1992). Figure 9 shows representative spectral shapes for different soil conditions from a study by Seed et al. (1976b). These spectral shapes have been normalized according to peak ground acceleration and were calculated for 104 earthquake records from 21 earthquakes from the western U.S., Japan and Turkey. The earthquake magnitudes included in this study are between 5.0 to 7.8 and have peak ground accelerations between 0.04 to 0.43 g. Of most importance to this study is that the soft to medium clay and sand spectral shape suggests a deamplification of high frequency spectral accelerations and a shift of the predominate period to longer periods. However, we should note that this spectrum was obtained from peak accelerations in the soil that were less than 0.10 g. Thus, this spectrum may not accurately represent the spectral shape for soft soil sites at higher acceleration levels, like those expected along the Wasatch Front.

One of the first published ground response modeling studies for soft soils sites in the Salt Lake Valley was performed by Wong and Silva (1993). They performed site specific analyses to characterize the strong ground motion in Salt Lake Valley at three locations, one of them was the Salt Lake City Airport, which is a soft soil site. Wong and Silva (1993) used a methodology that combines the Band-Limited-White-Noise Point Source Model and Random Vibration Theory (BLWN-RVT). This method allows for modeling the effects of a finite source, including rupture propagation, directivity, and source-site geometry, which can be significant for near source earthquakes. The computational scheme employed by Wong and Silva (1993) uses BLWN-RVT to calculate power spectral density and spectral

acceleration of the rock or input motion. This motion is propagated to the surface using an equivalent linear model similar to SHAKE and appropriate strain-dependent soil moduli and damping values. In the equivalent linear method employed by Wong and Silva (1993), the estimates of peak shear strain and 1-D oscillator response are, because of RVT, fundamentally probabilistic in nature. The procedure of generating BLWN power spectrum, computing equivalent-linear layered soil response, and estimating peak time domain values has been validated by comparison with SHAKE (Toro et al., 1988).

Wong and Silva (1993) show a significant deamplification of surface motions at high frequencies (f > 2 Hz) for the very deep soil site analyzed at the East Salt Lake City Airport. Peak ground acceleration was reduced by approximately 30 percent and spectral accelerations at 10 Hz were reduced by about 50 percent. This equates to amplification factors of about 0.7 and 0.5, respectively for 100 Hz and 10 Hz input motions. The East Salt Lake City Airport has shear wave velocities as low as 130 m/s in the upper 8 m and V_s values ranging from 175 m/s to 223 m/s in the interval between 8 m and 30 m below ground surface. Wong and Silva (1993) concluded that near surface site geology has an extremely important influence on strong motion in the Salt Lake Valley, both in terms of the amplitude of the response and the soil damping.

In addition to the study of Wong and Silva (1993) equivalent linear (i.e., SHAKE) analyses was performed by Gerber (1996) for the 600 South and I-80 Interchanges in Salt Lake City, Utah for the I-15 Reconstruction Project. In short, these analyses predict spectral acceleration values that are less than those estimated from western U.S. empirical attenuation relations for soil sites (Figure 10). This modeling estimated short period spectral acceleration values that are approximately 50 percent of those obtained by applying the Abrahamson and Silva (1997) attenuation relation for deep soil sites at periods ranging from 0.1 to 0.01 s (Figure 10). For longer periods greater than about 1 s, there is reasonable agreement between the Gerber (1996) equivalent linear analysis and the Abrahamson and Silva (1997) attenuation relation.

We believe that the Abrahamson and Silva (1997) is the best attenuation relation to compare with the Gerber (1996) SHAKE results because this relation has regression coefficients that have been developed for deep soil sites and the 600 South profile is a deep soil profile. However, we note that the 600 South soil profile classifies a NERHP site class E soil and is probably softer (i.e., lower shear wave velocity) than most of the soil sites used by Abrahamson and Silva (1997) attenuation relation. We should also note that the Gerber (1996) 600 South soil spectrum is a mean spectrum with 5 percent damping which was averaged for SHAKE runs using 13 different input time histories. All time histories used by Gerber (1996) were scaled to a pga value of 0.76 g, but no spectral matching of the time histories was performed. The other response spectra shown in Figure 10 are calculated from empirical attenuation relations for soil sites (i.e., Spudich et al. (1997) and Boore, Joyner and Fumal (1997)). As input to these relations, we used M = 7.2 and a R = 3.9 km, which is the earthquake magnitude and source distance for the Wasatch Fault obtained from the 0.2 second period deaggregation given in Table 3a. Also, we used the regression coefficients corresponding to a deep soil and soil for the Abrahamson and Silva (1997) and Spudich et al. (1997) relations, respectively. For the Boore, Joyner and Fumal (1997) relation, a Vs_{30} value of 190 m/s was used, where Vs_{30} represents the average shear wave velocity in the upper 30 meters of the profile at the 600 South interchange.

A detailed comparison cannot be made between the Gerber (1996) SHAKE average soil spectrum and those obtained from the various attenuation relations because of differences in the various methods and issues regarding the applicability of empirical attenuation relations to soft soil sites at high levels of ground motion. However, the trends in Figure 10 do suggest that equivalent linear (EQL) analyses may underestimate the lower short-period spectral acceleration values for the 600 S. interchange. At present, it is unclear whether the deamplification is real or if it is a bias in the EQL method at high strain levels.

More recently, EQL modeling was performed by Silva et al. (1999) for California sites. Silva et al. have made extensive use of the EQL analysis to estimate soil amplification

factors for soil and rock profiles in the San Francisco and Los Angeles areas. Their amplification factors were computed using random vibration theory (RVT) and equivalent-linear methods for various geologic units found in those areas. Silva et al. (1999) have compared their results with the NEHRP (1994) amplification factors and concluded that their results are in reasonable agreement with NEHRP values, except for the San Francisco Bay mud profile. For this profile and for bedrock input motion ranging between 0.2 and 0.4 g pga, the effects of strong soil nonlinearity appear to be important. Their analyses show that nonlinearity reduces the high frequency motion ($f > 10$ Hz) and increases the low frequency motion ($f < 1$ Hz). For the highest input motions analyzed (0.75 g to 1.25 g outcropping rock pga), the Quaternary Alluvium and San Francisco Bay mud profiles suggest very strong nonlinearity. For the 0.75 pga input motion case, the calculated median amplification factors are about 0.3 and 0.6 at 10 Hz and 100 Hz, respectively (Figure 11). This means that the predicted peak ground acceleration (i.e., 100 Hz) is approximately 60 percent of the input rock motion and that the 10 Hz spectral acceleration value is only 30 percent of the input rock motion.

Like the Gerber (1996) results, Silva et al. (1999) found that the EQL method suggests a significant deamplification of spectral values at frequencies between about 2 Hz and 100 Hz at high levels of ground motion (e.g., 0.75 to 1.25 g). These analyses, although done for a Bay Mud profile, have relevancy to the Salt Lake Valley soft soils because of the similarities of the Vs profiles. Shear wave velocity profiles at the 600 South and I-80 interchanges in Salt Lake City compare reasonably well with the Bay mud profile (Figure 12). Also, the estimated pga for soft to stiff soil sites in the Salt Lake Valley is about 0.64 to 0.77 g, respectively, as estimated for the I-15 Reconstruction Project by Dames and Moore (1996) for a probabilistic event having spectral acceleration values with a 2 percent probability of exceedance in 50 years. Thus, estimates of pga for the Salt Lake Valley surficial soils are relatively similar to the levels of input rock ground motion analyzed by Silva et al., 1999 for San Francisco Bay muds. However, we should noted that the Dames and Moore (1996)

estimates for the Salt Lake Valley are for soil conditions, whereas the 0.75 g value used by Silva et al. (1999) is an outcropping rock value.

The analyses performed by Silva et al. (1999) do suggest a significant deamplification of spectral accelerations between 2 to 100 Hz for soft soil sites experiencing high levels of strong motion (Figure 11). However, Silva et al. (1990) state that the degree of deamplification may be overestimated by the EQL model. They believe that their results may be overdamped for high levels of ground motion (i.e., 0.75 to 1.25 g pga rock) when compared with modeling results obtained from a fully nonlinear ground response model. Silva et al. (1999) also note their outcropping rock peak ground accelerations of 0.75 g to 1.25 g are greater than any values found in the strong motion database. Thus, they conclude that there is insufficient empirical data to constrain the actual amount of deamplification predicted by EQL model. They suggest a reasonable lower limit for amplification factors at high frequencies of about 0.5 to 0.6 for the Bay mud profile. This lower limit comes from their experience with empirical strong motion data and attenuations relations developed for deep soil sites at moderate levels of ground motion (Abrahamson and Silva, 1997).

Most recently, Wong et al. (2002) have used the methods of Silva et al. (1999) to produce strong motion scenario maps for the Salt Lake Valley. They divided the valley into similar geologic units, one of which is a lacustrine-alluvial silt and clay unit, which comprises the softest soils in the Salt Lake Valley (Figure 13). This figure shows the median and 16^{th} and 84^{th} percentile profiles for this unit. It also compares the Vs measurements with those obtained from the Bay mud profile (Silva et al., 1999). Wong et al. (2002) chose to use the Bay mud profile to represent the lacustrine-alluvial silt and clay unit in their development of hazard maps for the Salt Lake Valley. This was done because of the similarity of the two profiles (Figure 13) and the much larger database that was available for the Bay mud. They felt that the Bay mud database provided a more statistically robust data set from which the effects of variability in the V_s measurements could be better assessed in their hazard calculations. Based on the average V_s profile, 30 randomized profiles were computed for the

Bay mud profile to account for horizontal and vertical variability in velocities and these were used in the simulations to calculate amplification factors for the Salt Lake Valley. The randomizations were done using a correlation model for soil velocity profiles developed by Walt Silva of Risk Engineering Inc.

To represent the strong ground motion, Wong et al. (2002) used a stochastic numerical ground motion modeling approach that is coupled with the equivalent linear methodology to calculate amplification factors for 5 percent damped acceleration response spectra. The amplification factors were computed for various site response units as a function of thickness of the underlying unconsolidated sediments and the level of input rock motion (Figure 14). An M = 6.5 event was placed a several distances to produce input peak accelerations of 0.05, 0.10, 0.20, 0.40, 0.50 and 0.75 g to produce these amplification factors. Figure 14 shows that deamplification begins at about 2 Hz and the median amplification factors are about 0.30 and 0.65 for 10 Hz and 100 Hz, respectively for the 0.75 g input motion. These median amplification factors compare well with those computed by Silva et al. (1999) which are 0.30 and 0.65 for 10 and 100 Hz, respectively. This is not surprising given that both studies (Silva et al., 1990 and Wong et al., 2002) used the same methods and the same Bay mud profile for their analyses.

Research Needs and Guidance Approach

Topics regarding soft soil response in deep alluvial valleys that warrant additional research include: 1) effects of high levels of ground motion and the nonlinear response of soft soils, 2) better understanding of rate of loading effects and effects of soil softening on site response, 3) site effects and amplification of long period strong motion by deep soil sites, 4) improved understanding of the interaction between near source fault mechanisms and site effects and 5) better incorporation of other seismological factors into ground response analysis (e.g., 2-D and 3-D basin and deep structure effects) (Dobry et al., 1997; Seed et al., 2001). Based on these considerations, we believe there is a need to develop practical

guidance for performing ground response analysis and developing design spectra for soft soil sites. We believe that this guidance should incorporate, as much as possible, the state of knowledge regarding the above effects, yet be simple enough so that it can be applied by the practicing geotechnical engineer.

However, we fully recognize the difficulty in developing an engineering description of strong motion that captures all relevant features. Generation of seismic waves from an earthquake source and their propagation and interaction with near surface soil conditions are complex phenomena. This complexity, which includes source, path and site effects, introduces large, systematic and random spatial variations into the ground motion. Regarding this variation, Somerville (1998a) concludes that for earthquakes of a given tectonic regime and for M > 6 earthquakes, the resulting event-to-event variability is small compared to the intra-event variability. This means that while the average ground motions from one earthquake are very similar to those of another earthquake, crustal and near surface conditions cause the resulting ground motion for a particular event to vary significantly from one location to another, even at the same source-to-site distance (Somerville, 1998a). Much of this intra-event variation is attributed to earthquake source processes, the propagation of seismic waves from the source to a given site and the interaction of the seismic waves with a very heterogeneous surficial geology and soil conditions.

Although the importance of the above factors have been recognized for some time, it is not a simple matter to incorporate their influence into a comprehensive model. Current seismological research is focused on developing wave propagation models that include source, path and local site conditions (Somerville, 1998a). Certainly, wave propagation models offer the promise of significant improvements over empirical attenuation relations; however such models have not gained widespread usage in engineering practice. Further, no generally accepted 2-D or 3-D basin model has developed for the Salt Lake Valley.

The widespread adoption and use of probabilistic-based seismic hazard maps as outlined in current design codes and engineering practice is an important trend and one that we cannot ignore (NEHRP 1997a, b; NEHRP, 2000a, b; MCEER (2001a, b). The application of probabilistic-based strong motion estimates is a key component of performance-based design. In this approach, the desired seismic performance of a structure, system or component (SSC) is linked to the strong motion exceedance probability of the design earthquake. In applying performance based design, the SSC must be categorized according to its relative importance, critical function or role in post-earthquake recovery and the expected seismic performance for each performance category must be defined. For important or essential structures, such as a lifeline bridge, the design event is generally a "maximum considered earthquake (MCE)" having spectral acceleration values for 0.2 and 1.0 second periods obtained from the national hazard maps (Frankel et al., 1996; NEHRP 1997a, b; 2000a, b; IBC 2000; MCEER 2001a, b). These spectral values have a 2 percent probability of exceedance in 50 years (i.e., an approximate 2500-year return period event). For the design to be deemed adequate, it must be demonstrated that the SSC will have the expected seismic performance for the appropriate MCE.

In developing the guidance found herein, the UDOT TAC has given us direction that whatever methods are developed, they must be consistent with guidelines proposed in MCEER (2001a, b) "Recommended LRFD Guidelines for the Seismic Design of Highway Bridges, Part I (Specifications) and Part II: (Commentary and Appendices)." Further our guidance must be implementable by UDOT and its geotechnical consultants. Thus, it must be relatively user friendly.

The MCEER (2001a, b) guidance for developing design spectra is very similar to the guidance found in building codes (NEHRP 1997a, b; NEHRP, 2000a, b). The basic steps are: 1) selection of a short period (0.2 second) and 1-second period spectral acceleration values from national hazard maps for the appropriate design event and damping, 2) modification of the mapped rock spectral acceleration values to a soil values by applying the

appropriate amplification factor, 3) using the modified spectral acceleration values to develop the design spectrum using typical spectral shapes as outlined in the guidance.

Our guidance follows a similar approach with some important additions and modifications. In short, the steps we discuss in the method part of this document consist of: 1) performing site specific geotechnical characterization to define the dynamic properties at a candidate bridge site, 2) obtaining the 0.2 and 1-second spectral acceleration values from the national hazard maps (Frankel et al, 1996), 3) determining the controlling fault and its distance using the deaggregation published by the U.S.G.S, website 4) developing a deterministic design rock spectrum for the controlling earthquake using appropriate attenuation relations, 5) comparing the results of the deterministic spectrum with the 0.2 and 1 second spectral acceleration values and making adjustments to the deterministic target spectrum, as necessary, 6) adjusting the target rock spectrum for fault directivity effects for sites with 15 km of the controlling fault, 7) performing spectral matching of the candidate time histories to the target rock spectrum, 8) deconvolving the rock motion to a depth of 5 km using a generic western U.S. rock V_s profile, 9) convolving the motion obtained in step 8 to the surface using the site specific V_s profile to predict the free-field response of the soft soil profile, 10) calculating site specific amplification factors from the results of the EQL analysis, 11) comparing these amplification factors with those predicted from attenuation relations for deep soil sites and the general requirements of MCEER (2001a, b), 12) developing enveloping design spectra that bound the EQL analysis results and the results from the Abraham and Silva (1997) deep soil attenuation relation for the controlling earthquake magnitude and source distance, 13) ensuring that none of the spectral values are less than two-thirds of the spectral values for a MCEER (2001a) type E soil spectrum.

Ground Response Analysis Methodology

Introduction

The most popular method for performing site specific response analysis is the equivalent linear (EQL) method as employed in the computer program SHAKE (Schnabel et al., 1972). We have performed the site specific response analysis in this guidance using 1-D EQL (i.e., SHAKE) analysis using the computer program ProShake (ProShake, Ver. 1.1). ProShake is a commercial version of the lastest version of SHAKE 91 (Idriss and Sun, 1992). The user's manual for ProSHAKE gives examples that show that ProSHAKE produces results that are essentially the same as SHAKE 91 (Idriss and Sun, 1992).

For large strain problems, however, nonlinear analyses are often used. For these analyses, the cyclic behavior of the soil is modeled in a more realistic manner than is used in EQL methods. The nonlinear methods apply constitutive relations to define the soil's hysteresis loops, thus these methods can more accurately model non-linear moduli and shear strains. However, the soil's parameters for these constitutive relations are usually poorly defined or unknown and must be determined by specialized soil testing or by some other means. Thus, nonlinear analyses have not been widely used in engineering practice.

CALTRANS (1996b) states that using appropriate modulus and damping relations, EQL methods will usually result in reasonable estimates of soil response for depths of soil to about 500 feet, however the results should be examined for reasonableness. Also, the soil's peak shear strain should be limited to about 2 percent to produce reliable results using the EQL method (CALTRANS, 1996b). However, this is still debate about the appropriateness of EQL methods at this high strain level (Abbas Abghari, personal communication). Nonetheless, our preliminary SHAKE analyses for the Salt Lake Valley soil profiles indicate that peak shear strains are about 2 percent or less, thus we have chosen to use the EQL methods over nonlinear methods because of their simplicity and widespread engineering use.

However for some analyses, non-linear methods may be more appropriated and warranted; but such analyses are beyond the scope of the research agreed to by UDOT and its technical advisory committee.

Strong ground motion modeling studies and comparison with actual earthquake records have shown that the EQL method adequately predicts recorded ground response for moderate-sized earthquakes (Idriss, 1990; Seed et al., 1992; and Geomatrix, 1996). The EQL method treats the non-linear soil behavior in an approximate manner by using an EQL stress-strain model (Seed and Idriss, 1970). This method is an approximate method for modeling the non-linear stress-strain behavior of a soil deposit using the 1-D wave equation for a viscoelastic solid (i.e., Kelvin-Voigt solid) (Kramer, 1996). The EQL method approximates the 1-D wave equation, which is a second-order nonlinear differential equation, over a limited range by a linear equation. Formally, this is done in such a way that an average difference between the second-order differential equation and its linear approximation is minimized. This approximation has been used in practice in somewhat of an ad-hoc manner by defining an effective shear strain, which is used in the analysis to iterate toward strain compatible shear modulus and damping properties.

The use of effective shear strain instead of peak shear strain by EQL analyses is often justified because the peak shear strain occurs only once during a given time history, thus making its use somewhat anomalus. The effective shear strain is somewhat less than the peak shear strain and has been found to vary between about 40 to 75 percent of the peak shear strain (Idriss and Sun, 1992). Thus, it is common practice to use effective shear strain instead of peak shear strain to define the strain level used in the EQL computations.

An iterative process is implemented by the EQL method to calculate strain compatible properties and complete the ground response analysis. For the first iteration, initial estimates of shear modulus, G, and damping, ξ, are made for each soil layer. The initial estimates are usually based on the elastic (i.e., low-strain values) for each layer. These initial estimates

are then used to compute the ground response, including shear strain time histories, peak strain and effective strain for each layer. Using the calculated effective strain, values of G and ξ are updated to values that more closely approximate the level of strain calculated from the previous step. The next iteration is performed with updated estimates of G and ξ until differences between the updated and computed values of G and ξ converge within about 5 percent. This convergence can usually be obtained in about five iterations (Schnabel et al., 1972).

The advantage of the EQL method is that the use of a complex, multi-parameter nonlinear soil model is avoided and the simplicity of linear analysis is maintained. Non-linear modeling requires the determination of the shapes of the soil hysteresis curves and their variation with the number of cyclic reversals. Depending on the complexity of the non-linear model, more soil testing and more parameters are required. In contrast, the laboratory soil test data for the EQL method are simpler to obtain because each iteration is a linear problem and the material properties are treated as frequency independent and the damping is rate independent (Silva et al., 1999).

Although the 1-D EQL method is widely accepted and used by geotechnical engineers, it can lead to some difference in the calculated response when compared with nonlinear models. The major differences have been EQL and nonlinear models have been researched by Joyner and Chen (1975); Martin and Seed (1978); Dikmen and Ghaboussi (1984); Kramer (1996). In summary these are: (1) spurious resonance (high levels of amplification) can occur from the coincidence of a strong component of the input motion with one of the natural frequencies of the equivalent linear soil deposit, (2) use of effective shear strain in an equivalent linear analysis can lead to an over-softened and overdamped system when the peak shear strain is much larger than the remainder of the shear strains in the record, or to an underdamped system when the shear strain amplitude is nearly uniform, (3) nonlinear methods can be formulated in terms of effective stress allowing the modeling of the

generation, redistribution and dissipation of excess pore pressure during earthquakes. Effective stress analyses cannot be performed using the results of EQL methods.

Screening of Bridge Sites for Site Specific Ground Response Analyses

Introduction

We recommended that the site be classified according to the guidance given in NEHRP (2000a). If the site classification is a NEHRP A, B, or C, we recommend the design spectrum be developed using the generalized method outlined in MCEER (2001a). For NEHRP site class D or E sites having:

$$S_S < 1.25 \text{ g and } S_1 < 0.5$$

we also recommend that the design spectrum be developed according to the generalized method give in MCEER (2001a).

For NEHRP site class D or E sites, we recommend that this guidance be used for cases where the outcropping rock spectral accelerations exceed the following values:

$$S_S > 1.25 \text{ g and/or } S_1 > 0.5$$

The recommendation to use site specific analysis for site class E soils meeting the above criteria is consistent with NEHRP (1997a) and IBC (2000). However, we note that the recommendation to use site specific response analyses for site class D soils meeting the above criteria is not required by NEHRP (1997a, 2000a) and MCEER (2001a). Thus, it is left to the discretion of UDOT and the design team whether or not to use site specific analyses. However, we emphasize that many of the site class D sites along the Wasatch Front are deep soil sites, which may not be adequately represented by the generalized procedures given in NEHRP (2000a) and MCEER (2001a) as discussed in more detail below.

We further note that NEHRP (2000a) has published amplification factors for site class E soils for spectral acceleration values meeting the criteria above, but these are not found in IBC (2000), which is based on NEHRP (1997a). The differences between the amplification factors published in NEHRP (1997a) and those of NEHRP (2000a) are not explained in the commentary (NEHRP, 2000b). Thus, we have no basis to judge the technical merit of the change in soil amplification factors between these versions. However, based on experience offered to us by our peer reviewers and our ground response analyses, we believe that the long period (i.e., T = 1 s) amplification factor F_V given in NEHRP (2000a) and MCEER (2001a) may not completely describe the long period response for site class D and E profiles found in the Wasatch Front deep sedimentary basins. Also, we note that the F_V factor of NEHRP (2000a) and MCEER (2001a) does not account for ground motion amplification caused by near source effects and basin-generated surface waves. These effects may be important for structures with fundamental frequencies exceeding about 1 to 2 seconds. Therefore, for long-period structures founded on deep (i.e., z > 30 m) NEHRP D and E soil profiles, we recommend that this guidance be followed.

We do not recommend the use of this guidance for NERHP site class F soils. These soils can exhibit extremely nonlinear behavior for the design earthquakes anticipated along the Wasatch Front. EQL methods are not appropriate for these types of soils. Guidance for developing design spectrum for class F liquefiable soils is being developed by Brigham Young University.

Site Characterization

Introduction

The purpose of site characterization is to obtain an adequate description of the subsurface soils and their variability so that engineering analyses can be completed to ensure adequate structural and foundation performance. Site characterization should be performed for each substructure element, as appropriate, to provide the necessary information for design and construction. The site characterization should be extensive enough to reveal the nature and types of soil deposits and/or rock formations, their engineering properties, and the potential for liquefaction and ground water conditions (MCEER, 2001b).

As a minimum, the subsurface investigations and testing program should obtain the necessary information required to analyze foundation stability and settlement. Information should be obtained with respect to: geologic formation; location and thickness of soil and rock units; engineering properties of these units (including density, shear strength, and compressibility); groundwater conditions; surface topography; local considerations (such as expansive or dispersive soil deposits, collapse potential, underground voids from solution weathering or mining, slope instability); behavior of soils under seismic loading (including liquefaction, seismic-induced settlement, lateral spread, flow failure and ground motion amplification or attenuation) (MCEER, 2001b).

Required Information for Ground Response Analysis

The soil layers in a 1-D EQL model are characterized by their thickness, density and shear wave velocity, V_S. From V_S and density measurements, the low-strain shear modulus, G_{max}, is calculated. Also, shear modulus degradation and damping curves, which define how the shear modulus and damping change as a function of shear strain, are required. Typically, modulus reduction and damping curves are used from published relationships for appropriate

soil types (e.g., Seed and Idriss, 1970; Seed et al., 1986; Sun et al., 1988; Vucetic and Dobry, 1991; Electric Power Research Institute, 1993; Kramer, 1996). However, in some cases, site specific dynamic laboratory tests can be done to develop the required curves. The most commonly performed dynamic tests are: resonant column, ultrasonic pulse, piezoelectric bender element, cyclic triaxial, cyclic direct simple shear and cyclic torsional shear tests (Kramer, 1996). These dynamic laboratory tests are done on undisturbed soil samples to establish their nonlinear soil behavior for cases where published relations are judged inadequate for the type of soil present at a given site.

Development of Subsurface Profile for Ground Response Analysis

The first step in a ground response analysis is the development of a site specific geotechnical profile of the soil column. Typically, a 1-D soil column extending from the ground surface to bedrock, or to a very dense material, is adequate to capture first-order site response characteristics. However, 2-D or 3-D models may be considered for critical projects where 2-D and 3-D wave propagation effects are deemed to be significant (e.g., sedimentary basins) (MCEER, 2001a).

The required data are soil description, soil classification, Atterberg limits, thickness of soil layers, water table depth, depth to bedrock, soil unit weights and Vs measurements. This information can be obtained from geotechnical testing and/or correlated from CPT soundings. Normally, borings are sampled every 1.5 m (5 feet) in order to provide a reasonably continuous soil profile. The number of borings for a candidate bridge is dependent upon the variation of the soil and rock properties at the site. As a minimum, we recommend that one bore hole be completed at each abutment area, intermediate bent, or support. In addition to the geotechnical data, geophysical measurements of Vs should be obtained at the borehole locations. The recommended frequency of sampling with depth for geotechnical and V_s measurements for UDOT bridge projects is:

a. Shallow soil profile (depth to bedrock less than 30 meters)
   1.5 m (5-foot) sampling intervals for soil classification and V_s measurements

b. Deep soil profile (depths to bedrock greater than 30 meters)
   1.5 m (5-foot) sampling intervals for the first 30 meters
   3.0 m (10-foot) sampling intervals for the remaining depth

There are several methods of obtaining the required V_s measurements. These include (in order of preference): cross-hole surveys, down-hole Seismic Cone Penetrometer (SCPT), other downhole geophysical methods, spectral Analysis of Surface Waves (SASW) and other correlations based on soil density, plasticity, void ratio, etc. However, we note that cross-hole geophysical surveys require multiple cased boreholes and are often cost prohibitive. Also, SCPT surveys can only be performed to depths of about 30 to 40 m in the central part of the Salt Lake Valley. Below these depths, the CPT truck does not have enough reaction capacity for deeper soundings.

For deep (i.e., greater than 30 meters) V_s profiles at important bridge sites, or major interchanges with multiple bridges, the recommended technique is the downhole V_s suspension logging using the Oyo™ (1992) suspension logger (CALTRANS, 1996b). We note, however, that Utah State University has proposed the use of SASW testing to characterize deep V_s profiles. SASW has been used for deep soil profiling using high energy harmonic sources. However, because this technique needs to generate long wave lengths for deeper depths, the basic assumption used in SASW must hold, that is the site must be horizontally layered. This is not a great concern for shallow depths where very short wave length is used. However, it is more of a concern for deep profiles, especially in basin deposits, where the soil layers may not always be horizontal.

CALTRANS (1996b) recommends that the depth of V_s profiles at bridge sites extend at least 15 m into competent rock or rock-like material at shallow soil sites. However, for the central parts of the Wasatch Front Valleys, the depth to this layer may be much greater than 150 m.

For ground response modeling purposes, bedrock can be considered at a layer where the V_s measurements are 600 m/s (2000 ft/s) layer or greater. However, for very deep, soft profiles at important interchanges, we believe it is prudent to measure or estimate the V_s profile to depths greater than 150 m in at least one cased bore hole. If this not possible, then V_s estimates for deeper layers may be obtained from regional seismological reports, geophysical surveys (i.e., SASW) and other ground motion modeling studies (e.g., Wong et al., 2002; Wong and Silva, 1993; Murphy, 1989; Hill, 1988). This is the approach that we have taken in defining the deep V_s profile used in this guidance because no deep V_s measurements (i.e., $z > 70$ m) are available for the I-80 and 600 South interchange sites.

Generation of Spectrum Compatible Time Histories

Introduction

Most acceleration time histories when taken at face value without modification do not provide a very good match to the target spectrum, thus they must be scaled, adjusted or matched to the target design spectrum. CALTRANS (1996a) list four methods of modifying time histories commonly used in engineering practice: (1) method 1 - Response-Spectrum Compatibility Time History Adjustment Method, (2) method 2 - Source-to-Site Numerical Model Time History Simulation Method, (3) method 3 - Multiple Actual Recorded Time-History Scaling method, (4) Connecting Accelerogram Segments Method.

Spectrum compatible time histories are acceleration time histories that have been matched to a target acceleration response spectrum using numerical techniques. The general objective of spectral matching is to generate a design acceleration time history that approximately achieves a mean-based fit to the target spectrum (NUREG CR-6728). That is, the average ratio of the spectral acceleration calculated from the accelerogram to the target spectrum as a function of frequency is only slightly greater than 1. An additional aim is to achieve an acceleration time history that does not have significant gaps in the Fourier amplitude spectrum, but is not biased too high with respect to the target spectrum. An accelerogram that exceeds the target spectrum at most frequencies may overdrive a site soil column or structure where nonlinear response is of interest (NUREG CR-6728).

For our analyses, we will apply method 1 (above) to perform the spectral matching. Spectral matching may be done in either the time domain or the frequency domain in such a way that the spectral acceleration values of the spectrally matched time history matches a target response spectrum within a prescribed tolerance. The spectral matching can be done throughout the full spectral range or only over a portion of a specified range that is of interest to the design.

In performing method 1 above, it is important that to use a technique the retains the phase characteristics of the ground motion time history that is to be modified (Somerville, 1998a). Many techniques that use method 1 involve the addition of sinusoidal waveforms to the time history by modifying its Fourier spectrum. However, this approach has the disadvantage of not retaining the phase characteristics of the time history that is being modified. Preservation of phase characteristics is important for non-linear time domain analyses, because the non-linear solution can be sensitive to the phasing of the individual time history.

To minimize modification of the phase characteristics of the input time history, we have performed the spectral matching using the RSPMATCH software developed by Arahamson (1992). The user's manual for RSPMATCH is included in Attachment A. RSPMATCH adjusts the initial accelerogram iteratively in the time domain to achieve compatibility with the target spectrum. RSPMATCH does this by adding "wave packets" having specified period ranges and limited durations to the input time history. These wave packets are added at times where there is already significant amplitude in that period range in the time history (Somerville, 1998a). This method preserves the overall phasing characteristics and the time-varying (i.e., non-stationary) frequency content of the ground motion (Somerville, 1998a).

Development of Target Acceleration Response Spectrum

The design acceleration spectrum used by MCEER (2001a) is an outcropping rock spectrum with 5 percent damping. Spectral values are required to have a 3 percent exceedance probability in 75 years for critical or essential facilties. This is essentially equivalent to the "maximum considered earthquake" or MCE of Frankel et al. (1996) which has spectral values with a 2 percent exceedance probability in 50 years. The spectral acceleration values for developing the target spectrum can be obtained from the national hazard maps (Frankel et al., 1996) for the 0.2 s and 1.0 s periods. An updated version of these maps is also found on the U.S.G.S. web site, which requires the user to input the latitude and longitude of the proposed site.

As a parenthetical note, we mention that the U.S.G.S. uses the term "maximum considered earthquake," instead of "maximum credible earthquake" to represent the design event for critical structures. This distinction is important because the U.S.G.S. found that for sites located close to the active fault(s), the probabilistically estimated MCE can reach acceleration levels that exceed acceleration levels calculated from deterministic methods. Thus, to solve this problem, a deterministic cap has been placed on the MCE estimates for such cases (Frankel et al., 1996). The deterministic cap is defined as 1.5 times the median ground motion calculated using the appropriate attenuation relations assuming the occurrence of the maximum magnitude earthquake on the fault. However, this limit must not be less than 1.5 g for the short-period (0.2 s) acceleration value and 0.6 g for the 1.0 s spectral acceleration value (MCEER, 2001b).

The MCEER (2001a) design spectrum for the I-80 interchange is shown in Figure 15. Guidance for constructing this spectrum is also found in NEHRP (1997a, 2000a) and IBC 2000. The MCEER (2001a) spectrum is equivalent to an IBC (2000) design spectrum for critical facilities and either guidance is an acceptable reference. Note that we have developed the MCEER (2001) spectrum according to the 0.2 s and 0.1 s spectral acceleration values found in Table 2 for the I-80 interchange for the latitude and longitude coordinates given in Figure 3.

Initially, we spectrally matched time histories to the MCEER (2001a) response spectrum and used these time histories in our initial analyses of the I-80 site. However, these initial attempts yielded questionable results, especially when the deconvolved motion was once again convolved to the surface through the site specific I-80 interchange profile. It appeared that these deconvolved / convolved motion had long period spectral accelerations that were excessive. Ivan Wong (personal communication) cautioned us against using spectrally matched time histories that matched a "flat topped" building code spectrum, such as the building code spectrum, and subsequently using these time histories in the ground response analyses. Such a process may produce unreasonable results. He recommended that we use

more "realistic" spectral shapes based on attenuation relations for the appropriate magnitude and source distance obtained from the seismic deaggregation. This is the approach we have used as explained in the remainder of this section. This approach is also recognized by MCEER (2001a), which allows that:

"Alternatively, deterministic spectra may be defined for each fault, and each spectrum, or the spectrum that governs bridge response, may be used for the analysis of the bridge."

However, it is important to note that MCEER (2001a) also requires that when response spectra are determined from a site specific studies, the final design spectra (including the soil response) shall not be less than two thirds of the response spectra developed using the generalized procedures outlined in Article 3.4.1 of MCEER (2001a).

To develop the target rock spectrum for our ground response analyses, we recommend deaggregation of the national seismic hazard maps for the specific bridge location to determine the controlling earthquake magnitude and distance to the seismic source(s). For example, Table 3 gives the deaggregated hazard for the 600 South and I-80 sites, respectively obtained from the U.S.G.S web site (http://geohazards.cr.usgs.gov/eq/). This table has columns of source distance (km), earthquake magnitude (Mw) and percent contribution (i.e., ALL-EPS) to the total seismic hazard for the 0.2 second spectral acceleration values at a return period of 2500 years. For example, in Table 3b (I-80 site), we can see that the two major contributors to the seismic hazard are a M = 6.51 earthquake at a distance of 0.7 km which contributes 56.599 percent of the hazard and a M = 7.2 km earthquake, which contributes 37.037 percent of the hazard for the 0.2 s spectral acceleration.

The deaggregations like that found in Table 3 are useful for many purposes. We will use them to: (1) determine the controlling earthquake magnitude and source distance to develop the target deterministic rock spectrum, (2) evaluate whether or not the candidate site is close enough to a major active fault(s) to require adjustment of the target rock spectrum for

directivity effects, and (3) determine the approximate magnitude and source distance range for selection of candidate time histories for spectral matching and subsequent ground response analyses. Further, if liquefaction and lateral spread analyses are also required for a bridge evaluation, we recommend that the controlling earthquake magnitude and source distance be used as input to these evaluations.

Determining the controlling earthquake and source distance from a hazard deaggregation requires some knowledge about the nearby faults and their relationships. Sometimes it is possible that more than one nearby fault may be a significant contributor to the seismic hazard. Also, it must be remembered that the percent hazard contribution of each fault may varies as a function of period or frequency. Often, the short period (0.2 s) spectral acceleration values are controlled by a moderate-sized nearby earthquakes, whereas the long period (1.0 s and greater) spectral acceleration values are dominated by a more distance, large earthquake.

For our example, we used Table 3b to show that the West Valley Fault and the Salt Lake City segment of the Wasatch Fault are the major contributors to the seismic hazard. The average (mean source) distance and magnitude from this table are: mean src-site R= 2.9 km; M= 6.78. These means are the average for all earthquake source and distance combinations that produce the 0.2-second spectral acceleration hazard at this site. Sometimes, it is appropriate to use these mean values to define the controlling source distance and earthquake magnitude for deterministic evaluations. However, we do not recommend the use of mean values to define the controlling source distance and earthquake magnitude, if the seismic hazard is bimodial. For our example, Table 3b shows that the West Valley Fault and the Salt Lake City Segment of the Wasatch Fault contribute 54.71 and 37.03 percent of the 0.2 second spectral hazard, respectively, for the I-80 interchange. These percentages suggests that the seismic hazard at this site is bimodial and that perhaps, each fault is not well represented by mean values of R = 2.9 km and M = 6.78. Also, the West Valley Fault system is believe to be an antethetic fault system to the Wasatch Fault system and as such it is not considered to

be the primary source of seismic energy. With this consideration in mind, we do not believe that a bimodal hazard exists at this site, thus we selected the Salt Lake City segment of the Wasatch Fault as the controlling fault and source distance.

Care must also be exercised when determining the earthquake source distance. For example, Table 3b reports that the Salt Lake City segment of the Wastach Fault is capable of a M = 7.2 earthquake at a mean distance of 3.8 km. However, we must caution against using the source distance of 3.8 km reported in Table 3b as the input source distance for empirical attenuation relations. It is not apparent which definition of source distance is given in this table. It appears to be an average of the different source definitions used in the attenuation relations. Therefore, care is warranted in selecting a source distance that is consistent with that used in the selected attenuation relation when developing the target spectrum..

If the deaggregated hazard does truly suggest a bimodal hazard distribution, then we recommend consideration be given to using two design basis earthquakes (DBEs) to more fully represent the earthquake hazard at a given site at all frequencies of interest. For such a case, it is possible that the high frequency spectral acceleration values are dominated by a near-field, moderate-sized earthquake, while the low frequency spectral acceleration values may be controlled by a more distance, larger earthquake. Thus, two earthquakes may be required to better represent the entire spectral content. If two DBEs are deemed necessary, each DBE should have a magnitude and source distance that represents its respective modal average. Also, we recommend that spectral matching of the candidate time histories be done for each DBE spectrum and the respective time histories for each DBE be carried throughout the remaining engineering evaluations.

Once the controlling earthquake fault and magnitude have been identified, it is a simple matter to construct a deterministic rock spectrum for the controlling earthquake magnitude and source distance. As an example, we have developed a mean deterministic rock acceleration response spectrum for the I-80 interchange (Figure 15). This spectrum was

developed using M = 7.2 and a source distance of R = 2.5 km, which is the closest distance from the I-80 site to the rupture plane of the Wasatch Fault. This definition of R is consistent with that given by Abrahamson and Silva (1997) for their attenuation relation. We selected this attenuation relation because it gives the best match to the MCEER (2001a) design spectrum for the appropriate M and R values and is a common attenuation relation used in adjusting for fault directivity and basin generated surface waves, as discussed later.

Figure 15 shows the rock spectrum developed for the I-80 interchange using Abrahamson and Silva (1997). We believe this spectrum adequately represents the seismic hazard for this site, due to the relatively good match between this spectrum and the MCEER (2001a) design spectrum (Figure 15). We note that the Abrahamson and Silva (1997) spectrum has a reasonably good match at pga, is slightly high at 0.2 s period, and is somewhat low at 1.0 s period. However, an adequate match may not be always obtained for other sites at all frequencies. In some cases, small adjustments of the inputted M and R may be tried until a reasonable match is obtained at the frequencies of interest. However, one must be careful not to make large changes in the inputted earthquake magnitude and source distance. This may produce a target spectrum that is too rich (i.e., has excessively high) in the long-period spectral acceleration values. What is important is that the target spectrum has sufficient spectral acceleration values for the frequencies most important to structural response.

Adjustment of the Target Spectrum for Fault Directivity Effects

Near source effects that are important to the characteristics of horizontal ground response are: (1) higher levels of ground motions due to the close proximity of the active fault; (2) directivity effects that increase the ground motions for periods greater than about 0.5 s, if the fault rupture propogates toward the site (i.e., forward directivity) and 3) directionality effects that increase ground motions for periods greater than 0.5 s in the direction normal (perpendicular) to the strike of the fault (MCEER, 2001b). If the active fault is included and appropriately modeled in the development of the national hazard maps, then effect 1 is

already included in those maps. However, effects 2 and 3 are not present in the current hazard maps and are collectively referred to as fault directivity effects.

Near source effects, such as fault directivity effects, are generally significant for sites located within 10 to 15 km from the causative fault (Somerville, 1998b). MCEER (2001a) requires that for sites located within 10 km of an active fault, studies shall be considered to quantify near fault effects on ground motion, if these effects could significantly influence bridge response. However, our peer reviewers recommend that near source effects be considered for sites within 15 km of the causative fault.

Fault directivity (or fault rupture directivity) is a well documented near source effect that influences the long-period bridge response. Fault directivity is a pulse or pulses of seismic energy that is preferentially generated in the direction of fault rupture. An earthquake is generated by a shear dislocation that begins on a small area of a fault and spreads with a velocity that is almost equal to the velocity of shear wave propagation. Often this causes much of the seismic energy produced by fault rupture to arrive in a single, large, long-period pulse of motion that occurs near the beginning of the record (Somerville, 1997). This pulse of motion is referred to as fault directivity and is similar to a Doppler effect for sound waves. Often the directivity pulse represents the cumulative effect of much of the seismic radiation from the fault.

The radiation pattern of fault dislocation causes the largest pulses to be oriented in a direction that is perpendicular to the strike of the fault for normal and reverse faults and parallel to the strike of the fault for strike-slip faults. For normal faults, this radiation pattern produces a strike-normal peak velocity that is larger than the strike-parallel peak velocity. The magnitude of the directivity pulse(s) is a function of earthquake magnitude and the relationship between the site location, length of fault rupture and the point of rupture initiation (Somerville et al., 1997). Forward rupture directivity occurs when the rupture front propagates toward the site and the direction of fault slip is aligned with the site (Somerville,

1997). This alignment produces the maximum peak velocity in the velocity time history. Backward rupture directivity occurs when the rupture front propagates away from the site or the direction of fault slip is not aligned with the site. Forward directivity can cause peak velocity pulses that are approximately twice the value of those produced by backward directivity.

In addition to fault directivity, a "fling" effect may also be present in near source time histories. The "fling" effect results from an elastic rebound of the ground resulting from the seismic deformation and can also produce long-period pulses in the time history. However, fault fling should not be confused with fault directivity, because the former does not result from rupture propagation. However, in practice both effects produce long-period pulses and may be difficult to distinguish from each other without more detailed seismological studies.

The Abrahamson and Silva (1997) spectrum (Figure 15) does not account for near source effects (such as fault directivity) and should be adjusted for sites that are within 15 km of the controlling fault. (Also, we should note that the 1.0 s spectral values obtained from the national hazard maps do not fully account for fault directivity.) However, one of the future research goals of the U.S.G.S. is to incorporate near source effects, such as fault directivity, in its future maps (Frankel and Safak, 1998).

Because the seismic hazard in Utah is largely dominated by normal faulting, the effects of fault directivity for normal or dip-slip faults is most germane for our study area. The conditions required for forward rupture directivity are also met for normal faulting. The alignment of both the rupture direction and the slip direction in a direction that propagates up the fault plane produces rupture directivity effects at sites located near the surface exposure of the fault (or its updip projection, if the fault does not break the surface) (Somerville, 1997). Because most large normal faults initiate their rupture near the base of the seismogenic crust, sites on or near the fault trace will experience the maximum effect of both directivity and systematic fault-normal-to-fault-parallel differences in ground motion

(Geomatrix, 2001a). Forward directivity effects begin to be apparent at a spectral period of about 0.5 seconds and increase with increasing period. For normal faulting, the amplification effect is the range of about a 20 percent increase for sites that are within 15 km of the causative fault

Sommerville et al. (1997) provide a more detailed method to adjust deterministic spectra for directivity effects. Their model assumes that amplitude variations in the spectrum resulting from rupture directivity are dependent upon geometrical parameters defined in Figures 16a. Figure 16b shows a surface projection of the fault and the area affected by fault directivity. Sommerville et al. (1997) found a statistical dependence of the residuals (i.e., differences between the recorded and modeled spectral accelerations) on the phi angle, d and W parameters shown in Figure 16a. The phi angle is the angle between the dip of the fault and the line that connects the site with the hypocenter. The values of W and d are the width of the fault and depth to the hypocenter as measured down the dip of the fault.

In their regression analysis, Sommerville et al. (1997) chose to retain the magnitude and distance dependence of the Abrahamson and Silva (1997) attenuation relation, so the functional form of their regression equation for the residuals has no magnitude or distance dependence. They fit the residuals with an equation having the form:

$$\mathbf{y = C_1 + C_2\, Y \cos(\theta)}$$

where y is the residual of the natural logarithm of the spectral acceleration at a given period and Y is the updip distance ratio and θ is the zenith angle (Figure 16a). This equation is valid for dip-slip faults and for values of M greater than 6.5. Sommerville et al. (1997) explain that the regression coefficients C_1 and C_2 are dependent upon the spectral period. Also, the C_1 term has been reduced by a constant value that was obtained by setting C_2 equal to zero. This adjustment was done to remove any bias between the Sommerville et al. (1997)

data set and that used by Abrahamson and Silva (1997) for their attenuation relation. Sommerville et al. (1997) state that this adjustment improves the applicability of their model to other attenuation relations besides that of Abrahanson and Silva (1997).

We applied the Sommerville et al. (1997) directivity model to adjust the Abrahmason and Silva (1997) target spectrum to include directivity effects. We recommend that this adjustment be made for all sites that are found within 15 km of the controlling fault. However, in a later paper which focused on normal faulting in the Basin and Range Province, Sommerville et al. (1998b) state that the results of their model can be reduced by 25 percent to account for differences between normal faults and reverse faulting. Thus, we have used 75 percent of the values predicted by the Sommerville (1997) model to amplify the long-period spectral accelerations of the I-80 interchange target spectrum (Figure 17).

To apply the Sommerville et al. (1997; 1998b) model, we used the results of the deaggregated seismic hazard to determine the controlling fault and source distance. Once the controlling fault is identified, it is possible to determine phi, d, and W based on the location of the candidate bridge site and the location and dip of the controlling fault. For the example found in Figure 17, we used vertical depth to the base of the fault of 15 km ($\pm$ 5 km) and a fault dip angle of 50 degrees ($\pm$ 20 degrees) and a distance from the site to the fault plane of 2.5 km. The maximum fault directivity effect was calculated for these ranges and the calculations are included in Attachment B. The directivity effect produced the following increases in spectral acceleration as shown below as a function of period.

Period (s)	Increase due to directivity effect (%)
0.6	0.0
1.0	6.79
1.5	12.44
2.0	16.60
3.0	28.88
4.0	27.43

If more than one fault is found within 15 km of the bridge site, we recommend using the fault which gives the largest directivity effect to define the target spectrum. For example, in the case of the 600 South and I-80 Interchanges, we expect that the Salt Lake City segment of the Wasatch Fault is the controlling earthquake because the West Valley fault may not act independently from the Salt Lake City segment and thus is not the primary seismogenic source. Thus, we used the Salt Lake City segment of the Wasatch Fault to define the parameters for the Sommerville et al. (1997) model.

The forward directivity effects shown above were calculated using fault and site parameters that produced the maximum acceleration increase from the Sommerville et al. (1997) model. This increase in most applicable to bridges whose alignment is perpendicular to the fault trace. However, for bridges that are oblique to the fault or parallel the fault, the directivity effect may be somewhat less. Thus, we recommend the development of two target spectra for each site, one that has the maximum directivity effect and one that has no increase for fault directivity. These two spectra (i.e., fault normal and fault parallel spectra) and their associated time histories can then be used to analyze for any rocking or torsional modes of vibration that might be introduced into the structure due to directional variations in the design ground motion. For the remaining discussion presented in the following sections, we will use the fault normal (i.e., maximum) directivity effect spectrum as a working example. However, we will also analyze cases without fault directivity and use these to develop amplification factors and design spectra presented later in this report.

Selection of Candidate Time Histories

For ground response and other dynamic analyses, spectrally matched free field time histories are required. Because the I-80 target response spectrum was adjusted for the forward rupture directivity effect, it is important to select some acceleration time histories having this effect. We should emphasize that the adjustment of the target spectrum for fault directivity and spectrally matching a time history to that target spectrum does not mean that the directivity

effect (i.e., pulse) will be present in the spectrally matched time history. Somerville (1998a) states that if time histories are to be used in conjunction with near-fault response spectra, it is important to select time histories that appropriately include forward rupture directively effects. This is true even if the time histories are being matched to a design spectrum, and even if the design spectrum explicitly incorporates near-fault conditions, because the spectrally matching process cannot build a forward rupture directivity pulse into a record where none is present in the first place (Somerville, 1998a). Based on this consideration, we have selected time histories that have forward directivity effects (Table 4). Many of these records have moderate to large v_{max} / v ratios, which the ratio of the peak velocity, v_{max}, compared to the peak velocity measured in the orthogonal direction, v. High v_{max} / v ratios suggest a velocity pulse is present in the record.

In addition to capturing pulses from fault directivity, one of the primary goals of spectral matching is to generate a set of realistic time histories that satisfy other seismological and geological conditions which are appropriate for the seismic source and site conditions. The main considerations for selecting time histories are: appropriate earthquake magnitude, faulting mechanism, source-to-site distance and geological structure. The candidate time histories should be selected from earthquake events that have similar conditions, when possible. The following describes the steps we used for selecting and preparing time histories for spectral matching:

1. The candidate time histories for SHAKE analyses should come from earthquakes that have earthquake magnitude and source-to-site distance that are approximately the same as the controlling earthquake magnitude and source distance determined from the seismic hazard deaggregation.

2. We recommend that the candidate time histories be selected from the National Geophysical Data Center (NGDC), U.S.G.S., PEER and California Strong Ground Motion Instrumentation Program, or other appropriate strong motion databases. We

found that the PEER web site was particulary useful because its records had been already pre-processed for engineering evaluations.

3. We recommend that the earthquake magnitude, M, of candidate time histories be within $\pm$ 0.5 M of the controlling fault magnitude obtained from the hazard deaggregation. For example, a site with a controlling earthquake magnitude of 7.0 should have candidate time histories selected from earthquakes with M between 6.5 and 7.5.

4. In addition to earthquake magnitude, it is important that the candidate time histories have the appropriate source-to-site distance. This criterion is often difficult to meet for moderate to large earthquake that are close to the seismic source because there is only a handful of appropriate records. To aid in determining the appropriate distance for the candidate time history, we propose dividing the source-to-site distance into the following four categories:

    a. $R < 15$ km
    b. $15 < R < 30$ km
    c. $30 < R < 50$ km
    d. $R > 50$ km

    We recommend that the candidate time histories be selected for the appropriate M and from events that fall within the same source-distance category. For example, if the controlling source distance for the design event is 20 km, then candidate time histories should be selected from source distances that fall between 15 and 30 km.

5. Whenever possible, we recommend the selection of candidate time histories from extensional tectonic regimes. Two of the five records in Table 4 are from extensional regimes. We note that there is a lack of abundant records from this tectonic regime

for moderate to large earthquakes with source distances less than 10 to 15 km. Thus, we have included additional records in our study that have high levels of ground motion and are located close to the seismic source, but are from other tectonic regimes (Table 4).

6. Whenever possible, we recommend that the candidate time histories have peak ground acceleration (PGA), peak ground velocity (PGV) and peak ground displacement (PGD) with minus 25 percent and plus 50 percent of the target spectral values (CALTRANS 1996a). This will allow the spectral matching process to be completed with less difficulty. In addition, the spectral matching process will not introduce as large of change in the spectral content of the matched time history. However, for some of the extensional tectonic regime records listed in Table 4, it was not possible to strictly adhere to this guideline. Some of these records we used from extensional tectonic regimes have pga values that are less than this criterion. However, we have nonetheless used these records, because they are from extensional tectonic regimes with the appropriate magnitude and distance to the earthquake source and hence are important to our study.

7. We recommend the selection of at least 3 and as many as 5 time histories for the ground response analyses. MCEER (2001b) does not specify the number of time histories required for site specific analysis. However the number of time histories to be used in nonlinear dynamic analyses should take in account the dependence of the response on the time domain characteristics of the time history (e.g., duration, pulse shape, pulse sequencing) and its spectral response content (MCEER 2001b). ASCE 4-98 recommends that at least 3 independent time histories be used for non-linear analyses.

   For the working example contained herein, we have used five acceleration time histories listed in Table 4. These time histories have been spectrally matched to the

target spectrum and used in the response analyses of the I-80 and 600 South interchanges. The unmatched, rotated and spectrally matched records are included in the electronic files in this report.

8. We recommend the use of acceleration time histories obtained from rock or stiff soil sites, whenever possible. Records from deep or soft soil sites should not be used. All of the records in Table 4, except for the 1992 Erzincan, Turkey record, are from rock sites. This record is from a stiff soil site (Table 4).

9. The candidate time histories should be independent motions (i.e., should have no statistical or spatial correlation).

10. We recommend that synthetically generated time histories not be used for ground response analyses. Such time histories do not have near field and other effects, which may be important for non-linear time domain analyses.

11. We have not modified the duration of our candidate time histories. We do not believe that this is necessary because we have selected time histories that have approximately the same earthquake magnitude and distance from the seismic source as the controlling earthquake hazard for our selected bridge sites. Thus in doing so, we believe that the selected time histories will have approximately the appropriate duration.

Rotation of Time Histories

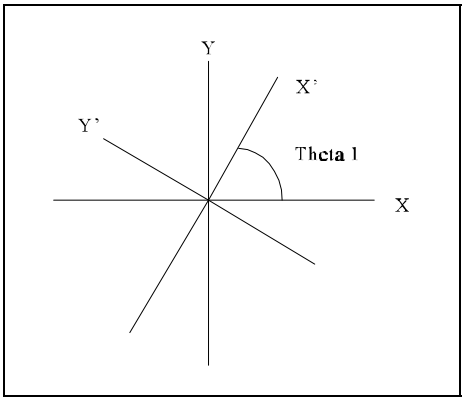

For a given target spectrum, a set of spectrum-compatible time histories should be generated for ground response analysis as described below.

1. Because the candidate time histories selected in Table 4 have been selected to represent near-field motions having strong velocity pulses in the fault-normal component, it is important the horizontal components of these motions be transformed into their principal components. The major and minor principal components are the directions which should reasonably correlate with the fault-normal and fault-parallel directions discussed in the fault directivity section. To accomplish this, the horizontal motion of the two recorded components, ax(t) and ay(t) are transformed into a new set of orthogonal axes x' and y' as shown in the above figure.

   The transformed accelerations in the x' and y' directions are calculated from:

   $ax'(t) = ax(t) \cos \theta_1 + ay(t) \sin \theta_1$
   $ay'(t) = -ax(t) \sin \theta_1 + ay(t) \cos \theta_1$

   The principal components are found by minimizing the covariance between ax'(t) and ay'(t). The covariance is calculated from:

$$\mu_{xy} = \frac{1}{t_d}\int_0^{t_d}\left[a_x(t) - \overline{a_x(t)}\right]\left[a_y(t) - \overline{a_y(t)}\right]dt$$

   Substituting x' and y' for x and y, respectively, in the above equation yields the corresponding relations that define the covariance of components ax'(t) and ay'(t).

   For example, Figure 18 shows the unrotated 1987 Superstition Hills acceleration and velocity time histories. The covariance between the ax(t) and ay(t) is minimized at a θ_1 angle of 25 degrees (counterclockwise). At this angle, the rotated 135 degree component becomes the major principal component (i.e., the principal component is

found at an azimuth of 95 degrees). The rotated time histories are shown in Figure 19. Note that the peak acceleration and peak velocity have increased in each of the rotated time histories in the major principal component direction. The Excel spreadsheet (rotation.xls) used to perform the rotations have been included with the electronic files in this report.

Filtering of Input Time Histories in RSPMATCH

1. Filtering of the input time history is also required prior to performing spectral matching. This is necessary because the ground response analysis assumes that surface rock motion is a result of vertically propagating shear waves. However, Silva (1988), Kramer (1996) and Geomatrix (1999) have noted that some recorded surface motions may consists of higher mode surface waves. Thus to remove these waves, they recommend that the candidate time histories be filtered to remove frequencies above 15 Hz. This was done by Geomatrix (1999) during the spectral matching process to reduce the potential for the overestimation of the deconvolved motion at depth.

   Also, any additional unwanted noise in the candidate time history is reduced through the use of filters at both high and low pass frequencies. The BAP manual (1992) suggests that high frequency noise (i.e., between 30 and 50 Hz) may originate in several ways: (1) from earthquake-induced vibrations in equipment close to the recorder, (2) from an unexpected higher-mode oscillation in the mechanical transducer, (3) or from the inability of the automatic trace-following digitizer to cope with an unclear photographic trace. The BAP manual suggests that unless it can be verified that high-frequency content is in fact useful earthquake input, the high frequencies should be filtered out. The use of a high and low pass filtering removes unwanted noise and produces a frequency range over which the recorded signal of the earthquake ground motion significantly exceeds the noise level. Generally it is

recommended that an anti-aliasing filter such as a Butterworth filter should be used rather than an abrupt cut-off frequency that is used by the program SHAKE.

We have used a low pass Butterworth filter to remove frequencies greater than 15 Hz from the rotated acceleration time histories during spectral matching within the RSPMATCH program. We have also used a high pass Butterworth filter for frequencies less than 0.14 Hz (T = 7.0s) as used by Geomatrix (1999). The high and low pass filters are include within the RSPMATCH program (Attachment A) and are done during the spectral matching process. The RSPMATCH input file requires that the number of poles be specified for the high and low pass Butterworth filters. We will use a 4-pole Butterworth filter based on the default values recommended by the BAP (1992) user's manual.

However, high and low pass filtering may not always be necessary, depending upon the source of the original time history. Some time history databases, like the PEER database, have time histories that have already been processed and filtered. However, if one is uncertain regarding whether or not filtering has been performed on the candidate record, repeating the filtering process by using the RSPMATCH filters does not appear to produce any deleterious effects.

Spectral Matching Using RSPMATCH

1. Spectral accelerations for the target rock spectrum (5 percent damping) should be computed at a minimum of 100 points per frequency decade, uniformly spaced over the logarithmic frequency scale (NUREG/CR-6728). RSPMATCH requires that linear interpolation on a logarithmic scale be used to interpolate the intermediate spectral values between those defined by the target spectrum. For each time history, we have carried out the response spectral matching at 250 spectral frequencies ranging from 100 Hz (0.01 s) to 0.25 Hz (4.0 s). We have used an Excel spreadsheet

to develop the target spectrum and create the 250 spectral frequencies. This spreadsheet is called "targetspectrum.xls" and is contained with the electronic data files that are part of this report. Also, the RSPMATCH input files we used to generate the spectrally matched time histories are included in Attachment C.

2. The sampling rate or time step increment (Δ t) of the spectrally matched time history is also an important consideration. RSPMATCH recommends that the Nyquist frequency of the spectrally matched time history should be about twice the maximum frequency. The Nyquist frequency is the highest frequency in the Fourier series and is calculated by $w_N = \pi / \Delta t$ (Kramer, 1996). For our case we have selected a maximum frequency of 25 Hz for our response analysis, thus the Nyquist frequency should be 50 Hz or w_N = 314 radians per second. This means that the maximum time step or Δ t for the spectrally matched time history should be:

$$\Delta t = \pi / w_N$$

which results in a Δ t of about 0.01 s. If frequencies above 25 Hz are of interest, then the time step interval should be decreased to provide a Nyquist frequency that is about twice that of the maximum frequency of interest.

We have used a Δ t value of 0.005 to 0.01 s for our spectrally matched time histories, which meets the above recommendation. In no case do we recommend using a Δ t value that is larger than 0.01 s. If interpolation to a smaller time step is required, RSPMATCH handles this interpolation with a parameter called "dtFlag." This parameter is the integer number of the interpolation requested for the original time history. RSPMATCH will then interpolate based on 1 / dtFlag of the input time step. For example, if the original time history has a Δ t of 0.02 seconds and Δ t of 0.01

seconds is wanted in the spectrally matched time history, then dtFlag should be set to 2.

On the other hand, some of the records that we obtained from the PEER website are already digitized to time steps of 0.005 s. For these records, we used the time step in the original PEER record. We did not attempt to average or integrate these records to a larger time step.

3. RSPMATCH has the option of scaling the pga value of the input time history to the value of the target spectrum pga. The user's manual recommends to scale the initial time history before the spectral matching procedure is performed, but not to scale the record after subsequent iterations. RSPMATCH suggests that scaling to the initial pga is useful and can reduce the number of iterations necessary when the spectral shape of the original time history is similar to the target spectrum's spectral shape. Also, scaling to the initial pga will help preserve the high frequency content of the time history, especially if the target spectrum is substantially higher than the spectrum from the initial input time history.

4. We recommend that the 5 percent damped spectrum of a spectrally matched time history should not fall more than 10 percent below the target spectrum at any frequency (NUREG CR-6728). This is a slightly more restrictive requirement than that found in MCEER (2001a). The latter design guidance requires that the mean spectrum of the target time histories not be more than 15 percent lower than the design target spectrum at any period, and the average of the ratios of the mean spectrum shall be equal to or greater than unity (MCEER 2001a). We do not believe that it is necessary to calculate the ratio of the mean to the design target spectrum to verify that it is greater than 1, on average. Our experience with RSPMATCH suggests that this ratio will be very close to 1, because RSPMATCH does not have any bias (high or low) in the spectral matching process.

Also NUREG CR-6728) requires that not more than 9 adjacent spectral points to fall below the target spectrum at any frequency. Also, the 5 percent damped spectrum of the spectrally matched time history should not exceed the target spectrum at any frequency by more than 30 percent (i.e., factor of 1.3) in the frequency range between 0.25 Hz and 25 Hz (NUREG CR-6728).

5. We recommend that the input acceleration time history be matched in a two pass process. The guidance for RSPMATCH suggests that a tapered cosine wave model (Model 6) should be used to make initial adjustments to the time history. This is followed by an oscillator impulse response function in reverse time order model (Model 1) to refine the match to the target spectrum. The user guide and manual for RSPMATCH gives the function for the taper as:

$$a(f) = a1 * f \qquad \text{for } f < f1$$

$$a(f) = (a1 + (f-f1) * (a2-a1)/(f2-f1)) * f \qquad \text{for } f1 \leq f \leq f2$$

$$a(f) = a2 * f \qquad \text{for } f > f2$$

where a1, a2, f1, f2 are the model parameters for frequency dependence of the taper of the adjustment time history. The recommended values for a1, a2, f1 and f2, respectively are 1.25, 0.25, 1.0, 4.0. We have used these recommended values for our spectral matching process. The RSPMATCH input files used in the two pass process are included in Attachment C.

The response spectrum for the spectrally matched time history are shown in Figures 20a and 20b. Figure 20a compares the spectrum of the original time history (i.e., rotated 1987 Superstition Hills record) with the target response spectrum developed from the Abrahamson and Silva (1997) attenuation relation for the I-80 interchange. Figure 20b compares the response spectrum of the spectrally matched time history

with the I-80 target response spectrum. In addition, Figure 21 compares the input time history (Figure 21a) with the spectrally matched time history (Figure 21b). From this comparison, it can be seen that the frequency content and amplitude of the matched time history has been modified by the spectral matching, but the spectrally matched time history still contains many of the characteristics of the input time history.

Baseline Correction of Spectrally Matched Time Histories

1. Geomatrix (1999) recommends that a baseline correction be performed on the candidate time history before spectral matching is done. This is required to remove any spurious low frequency motions prior to the filtering and spectral matching. However, baseline correction had already been performed on the records we obtained from the PEER web site, so this step may not be required, depending on the source of the candidate time history.

   However, the spectral matching process does introduce drift into the processed record. We found that a baseline correction is required of the spectrally matched time history (Figure 22a). Drift in the time history is best seen by plotting the displacement time history, because any errors are accentuated by the double integration process used to obtain displacement. Note that drift has occured in Figure 22a because the displacement time history does not terminate at zero. Correction of this drift is important if the spectrally matched time history is to be used in analyses where displacement is to be predicted from the analysis. It is less important if only the accelerations or forces are to be obtained. We should note that some displacement time histories have a “real” drift” as opposed to a “processed drift.” Real drift can be a result of permanent tectonic or ground displacement after the earthquake and is not an artifact of the record processing. However, our analyses are

not interested in estimating this part of drift and we recommend that all records be baseline corrected, even if they have some real drift.

We have used the computer program BASELINE.EXE (Attachment D) to baseline correct the spectrally matched time history (Figure 22b). The excel spreadsheet (Plot.exe) was made as an interface with BASELINE. Also, a compiled version of BASELINE are contained in the computer file attachments to this guidance. BASELINE performs a least squares inversion of the input displacement time history using a user specified polynomial of degree n, where n is less than or equal to 10. We have found that a 4^{th} order polynomial fit generally produces reasonable results (i.e., n = 4). The reasonableness of the baseline correction can be judged by inspecting the corrected displacement time history. First, one should ensure that there is no drift remaining by inspecting the end of the displacement time history record to verify it goes back to zero displacement. One should also check to see that there is approximately the same number of excursions above and below the zero displacement line (i.e., the number of positive displacement peaks is approximately equal to the number of negative displacement peaks).

Quiet Zone and Comparison with Target Spectrum

1. One last detail that should be discussed involves the number of trailing zeros that should be present in the record. Because the Fourier series used in EQL analyses implies periodicity (it is assumed that the total time history repeats itself indefinitely), there should be enough trailing zeros at the end of the acceleration time history to form a "quiet zone." This zone should have sufficient duration to allow the periodic response to die out before the next motion begins. The ProShake manual states that the best results are usually obtained when the last third or more of the total time history is quiet. This can be accomplished by increasing the number of terms in the Fourier series that is found on the input motion screen of ProShake in the input

manager menu. For example, if the input time history has 8192 (i.e., 2^{13}) terms or greater in the input motion, then a quiet zone can be added by increasing the number of terms to 16,384 (i.e., 2^{14}). ProShake will then automatically add the required number of trailing zero acceleration values to bring the total length of the acceleration time history to 16,384 terms. We recommend that approximately the last third of the spectrally matched time history contain a quiet zone. We should note that the number of terms in the Fourier series should be 2^N terms and the maximum number of terms allowed by ProShake is 2^{14} terms or 16,384 terms. However, we have found that this is not a significant limitation for the time histories we have processed.

2. As a final step, we recommend that the spectrally matched time histories be compared with the target response spectrum to ensure that no errors have been introduced in the spectral matching and baseline correction processes. Figures 23 and 24 show the results of the spectral matching process for the time histories listed in Table 4. Figures 23a and 23b compare the 5 candidate time histories matched to the I-80 Interchange target spectrum for the case with and without fault directivity, respectively. Figures 24a and 24b compare the 5 candidate time histories matched to the 600 South Interchange for the case with and without fault directivity, respectively. The closeness of the spectral match appears to be reasonable throughout the entire frequency range that was specified for matching (i.e., 100 Hz to 0.25 Hz, or 0.01 s to 4.0 s) and within the ± 10 percent tolerance that was specified in the RSPMATCH program.

Deconvolution Analysis

Introduction

Before convolution analysis is used to calculate the soil response at a given site, we recommend that a deconvolution analysis be performed. Because the EQL method is a linear method, it is possible to determine the response spectrum at any point in the profile. Deconvolution analysis involves the computation of bedrock motion from a free surface motion. The deconvolution analysis is necessary to fully account for the characteristics of the shallow crust V_s profile at the candidate site.

Unfortunately, NEHRP (2000b) and MCEER (2001b) guidance do not recognize the importance of this step and give no guidance for its completion. However, our peer reviewers have emphasized the importance of performing deconvolution analysis at our candidate sites because the shallow crustal rock V_s profile in the Salt Lake Valley is significantly different from that of the average western U.S. rock V_s profile (Figure 25). These marked differences in the shallow crustal Vs profiles can produce significant differences in the outcropping rock motion for the Salt Lake Valley when it is compared with a site having a rock profile more similar to the "average western U.S. rock profile." To correct for these differences, a deconvolution analysis followed by a convolution analysis is used by this guidance.

To this end, we recommend that the spectrally matched time histories be deconvolved down to a depth of 5 km to a point where the generic western U.S. Vs profile and the Salt Lake Valley Vs profiles are reasonably matched (Figure 25). The deconvolved motion will be subsequently convolved to the surface using the site specific Vs profile for the Salt Lake Valley in order to estimate the surface soil response, as described later.

The following steps and discussion outlines the approach we recommend for completing the deconvolution analysis. Geomatrix (1999) and Kramer (1996) further explain the deconvolution / convolution process.

V_s Profile for Deconvolution Analyses

1. We recommend that the average western U.S. V_s profile values developed by Boore and Joyner (1997) be used in the deconvolution analysis (Figure 25). This shear wave velocity profile is considered to be reasonably representative of the crustal V_s values found in the attenuation relations used in developing the national seismic hazard maps.

Performing Deconvolution Analysis Using ProShake

1. We recommend that EQL analyses be used to deconvolve the surface motion to a depth of at least 5 km in the Salt Lake Valley.

2. When using the ProShake program, deconvolution analysis is done by assigning the spectrally matched input rock motion to the surface layer (i.e., layer 1) as an "outcropping" motion.

3. The output object motion at a depth of 5 km should be requested by the user as an "outcropping rock" motion. This is selected using the selection output option in the input menu of ProShake. For our ProShake V_s model, the "outcropping rock motion" for the 5-km deep layer corresponds to layer 336. This layer is also the beginning of the infinite half space. Output from this layer will be later used as input to the convolution analysis.

4. In our ProShake model, the infinite half space (layer 336) has been assigned the same material, Vs and damping properties that was used in the last rock layer (layer 335) in the deconvolution model. Below this depth the V_s values are relatively constant (Figure 25).

Shear Modulus and Damping Curves for Deconvolution Analysis

1. Shear modulus reduction (i.e., G/Gmax) curves appropriate for the generic western U.S. rock profile are also needed for the deconvolution analysis. We have used the rock G/Gmax and damping curves used by Geomatrix (1999) (Figure 26). These curves are appropriate for weathered and fractured rock for the depths given in this figure. The solid line is appropriate for depths from 0 to 6 m and the dotted line is appropriate for depths from 6 m to a depth where the V_s value is 1220 m /s (i.e., 4000 ft /s). For the generic western U.S. V_s profile, this corresponds to a depth of 70 m (Figure 25). Thus, we have used the dotted G/Gmax curve for depths between 6 and 70 m.

2. For depths below 70 m, where V_s values are equal to or greater than 4000 ft/s, we assumed that the rock behaves linearly (i.e., no shear modulus reduction is used). Note that a linear G/Gmax relation can be specified in ProShake by making all G/Gmax values equal to 1.0 for all levels of shear strain.

3. In addition to G/Gmax curves, estimates of material damping as a function of strain are also required to complete the deconvolution analysis. The damping curves shown in Figure 26 were used for the appropriate depth intervals. These curves were used from a depth of 0 m to 70 m.

Damping Calculations for Linear Rock Portion of Deep Profile

1. For the linear rock layers found between a depth of 70 m to 1.5 km, the damping value for each sub layer was calculated using seismic attenuation parameter kappa, κ. Values of κ are related to the near surface shear wave velocity quality factor, Q_s, by:

$$\kappa = H / (Q_s V_s)$$

where H is the portion of the crust over which the energy loss occurs and V_s is the average shear wave velocity over H (Geomatrix, 1999). For their calculations, Geomatrix used H equal to 1.5 km and we have used the same value. Silva and Darragh (1995) and Boore and Joyner (1997) found that the total κ for the upper 1.5 km of the crust is approximately equal to 0.04 s for western U.S. rock conditions.

It is important to note that a κ value of 0.04 s includes the total damping in the upper portion of the crust (i.e., upper 1.5 km) including that portion found in the upper 70 m. However, because we have used rock damping curves for the upper 70 m, it is important to account for the portion of κ associated with this part of the profile. Once this is calculated, then the κ associated with the upper 70 m can be subtracted from the total κ in order to calculate the remaining κ. The remaining κ is then distributed to the layers found between 70 m and 1500 m.

To distribute κ for each sublayer, we have used the procedures outlined by Geomatrix (1999). First, the low strain damping, λ, must be estimated from the curves shown in Figure 26 for each sublayer above 70 m. Geomatrix did not define what level of strain should be used to define the low strain damping, but a review of their calculations suggests that they have used a low strain damping value, λ, that

corresponds to a shear strain of of 1 x 10^{-3}. Once the low strain damping value for each layer has been estimated from Figure 26, then Q_s and damping can be calculated from the following:

$$Q_s = 1 / (2\lambda)$$

Then κ for that sublayer is calculated from:

$$\kappa = H / (Q_s V_s)$$

Ultimately, the κ values for each sublayer are then summed in the upper 70 m and this value is subtracted from the total κ of 0.04 s to determine the κ remaining between 70 and 1500 m. This calculation is shown in Table 5 and the Excel spreadsheet used to make these calculations is also found in the electronic files provided with these guidelines.

For the depth between 70 m and 1.5 km, the appropriate κ value is the total κ (i.e., 0.04 s) minus the κ value contributed by the upper 70 m of the profile (i.e., 0.0063618). Silva and Darragh (1996) found that the Q_s for western U.S. rock is proportional to the shear wave velocity. This assumption can be used to calculate the damping for each sublayer.

However, before calculating damping, the values of H/V_s^2 are summed for each sublayer in the 0 m to 1.5 km interval:

$$\Sigma H / V_s^2$$

From this sum, the weighting factor, γ ,can be calculated from:

$$\gamma = (\Sigma H / V_s^2) / \kappa$$

Then the κ value for each sublayer can be calculated from:

$$\kappa = (1 / \gamma) (H / V_s^2)$$

Once the κ value for a sublayer is known, then the quality factor is calculated from:

$$Q_s = H / (\kappa V_s)$$

Ultimately, the damping is calculated from:

$$\lambda = 1/ (2 Q_s)$$

The damping calculations for the 70 m to 1.5 km interval are shown in Table 6. Note that the damping values, λ, are in decimal fraction and must be multiplied by 100 to convert them into percent damping that is used in ProShake.

2. Below a depth of 1.5 km, damping is calculated from the crustal quality factor, Q. Geomatrix (1999) used the following formula to calculate the Q below 1.5 km:

$$Q = 150 f^{0.6}$$

where f is the frequency in Hz. This formula is for the California crustal Q and was applied by Geomatrix (1999) to the generic western U.S. profile. Using f equal to 3 Hz, the Q factor below 1.5 km is approximately 290 (unitless). Damping values below 1.5 km are not thickness or shear wave velocity dependent, thus the damping for each layer is the same and calculated from:

$$\lambda = 1/ (2\ Q)$$

This formula yields a damping of 0.0017 or 0.17 percent for each of the sublayers below 1.5 km to a depth of 5 km.

Other Rock Properties

1. Estimates of total unit weight or density of the rock are also required to complete the deconvolution analysis. We have used the total unit weight, Vs, and other soil properties given in Table 7 to complete the deconvolution analysis. This table shows the properties for the weathered rock portion of the profile (upper 75 m). The complete ProShake file is found in Attachment E.

Checking of Deconvolution Analysis Profile

1. We recommend that the convolution analysis be checked for reasonableness by convolving the deconvolved motion to the surface using the same generic western U.S. profile. This is done by taking the time history record calculated for the bottom of the generic profile (depth = 5 km) and assigning it as an non-outcropping rock motion in the ProShake model at this depth and having ProShake calculate the outcropping rock motion for layer 1 (surface layer). This convolution process in essence uses the object motion calculated at a depth of 5 km and convolves it back to the ground surface. This process is useful to check for errors or numerical inaccuracies in the deconvolution/convolution process. In theory, deconvolution analysis should in theory produce a unique solution, but in practice it usually does not, especially when strain levels are large (Kramer, 1996).

Results of Deconvolution Analysis

The spectrally matched response spectra representing the input target surface rock motions for the initial deconvolution analyses are shown in Figures 23 and 24 for the I-80 and 600 South Interchanges, respectively for these cases without and with fault directivity. The matching tolerance for these response spectra was set to ± 10 percent in the RSPMATCH program. These surface rock motions were deconvolved using the generic western U.S. rock profile properties given in Table 7.

In our first deconvolution attempts, the surface rock motions (Figures 23 and 24) were deconvolved to a depth of 5 km by setting the cutoff frequency in ProShake to 25 Hz. However, these preliminary analyses produced spurious high frequency spikes in some of the deconvolved motion response spectra (Figure 27). For example, note the prominent spikes in the response spectra at a period of about 0.04 s (25 Hz). These spikes were present in some but not all of the resulting spectra. Subsequent 5 km convolution analysis with the deconvolved time histories used as input revealed that the high frequency spikes also produced spurious results in the convolution analysis. Thus, we found that it is desirable to remove these spikes prior to performing convolution analysis.

Silva (1988) recommends a deconvolution procedure that uses pre-filtering of the input motion by applying a 15 Hz low-pass filter to eliminate the tendency of the deconvolution analysis to develop unrealistically large accelerations at depth. Regarding this point, we did a considerable number of preliminary ProShake runs to see if the magnitude of the spurious high frequency spikes could be reduced. We found that these spikes are reduced when ProShake's cutoff frequency is set at 20 Hz, but they do not completely disappear until ProShake's cutoff frequency is set to 15 Hz (Figure 28).

Thus, based on our peer reviewers advice and the recommendations of Silva (1988), we recommend the following additional steps and procedures.

Butterworth Filtering of Input Time Histories

1. We recommend that a Butterworth filter be used to pre-filter the input time histories to remove any high frequency spikes prior to the deconvolution analysis. We used a 4th order, low-pass Butterworth filter starting at 15 Hz to filter the spectrally matched input time histories. The filtering was done using the SeismoSignal program included in the electronic files included in this report. (This program is also available at: http://www.seismosoft.com/). Figures 29 and 30 show the response spectra for the input time histories after the Butterworth filter has been applied but prior to the deconvolution analysis.

   We should note that 15 Hz Butterworth filtering does have the slightly undesirable consequence of decreasing the high frequency spectral acceleration values of the input time histories (Figures 29 and 30). Note that in these figures, the spectral acceleration near zero period are less than the input target spectrum (Figures 23 and 24). In essence, this means that the subsequent deconvolution analysis output will be slightly to somewhat deficient in its high frequency (i.e., greater than 15 Hz) portion of the spectrum.

2. After filtering, we performed the subsequent deconvolution analysis by setting the cutoff frequency in ProShake to 25 Hz and by using a strain ratio of 0.60. The maximum number of iterations was set to 10 and an error tolerance of 5 percent was used for all deconvolution analyses.

3. ProShake's output manager can be used to inspect the deconvolution time histories and response spectra. The results of the deconvolution analyses are shown in Figures 31 and 32 for the I-80 and 600 S. Interchanges, respectively. The response spectra shown in these plots are outcropping rock spectra for layer 336 (i.e., the deepest layer of the generic western U.S. profile). The ground motions that correspond to these

plots will be used as input to the subsequent convolution analysis, as described in the next section.

Convolution Analysis

Introduction

The results of deconvolution analysis described in the previous section will be used to estimate the site specific rock and soil effects for the candidate sites in this section. In the following section, the results of the convolution analyses will be used to estimate the design spectral shape and amplification factors for the I-80 and 600 South interchanges. The following explains the steps, analyses and recommendations we recommend for completing the convolution analyses.

Summary of Previous Steps

1. As discussed in the previous sections, the design team should select candidate time histories from the appropriate magnitude and distant ranges and spectrally match them to a target spectrum, which includes near source effects, as appropriate.

2. The spectrally matched time histories should be deconvolved to a depth where the site specific V_s profile matches the generic western U.S. V_s profile and outcropping rock motion should be obtained for the deepest layer in the deconvolution model, as discussed in the previous sections.

Development of Soil Profiles

1. To perform the convolution analysis, site specific geotechnical soil and V_s profiles should be developed using the information obtained from geotechnical and geophysical investigations at the candidate sites. For example, Figure 33 shows a generalized geotechnical profile for the I-80 interchange developed by Woodward-Clyde for the I-15 Reconstruction Project (unpublished). We have used this

information and site specific V_s soil measurements for the I-80 and 600 S. interchanges to develop best-estimate (i.e., mean) V_s profiles for the upper 60 m of the subsurface profile. The V_s measurements were obtained from geotechnical reports published for the I-15 Reconstruction Project (Dames and Moore, 1996; Gerber, 1996) and are presented in Figures 34 and 35.

2. V_s measurements are also required for depths greater than 60 m for most convolution analyses. The depth of the unconsolidated Quaternary sediments in the Salt Lake Valley is considerable and extends to depths of about 300 m at the I-80 and 600 S. interchanges. Often deep V_s measurements are not available, except for very large and/or important projects. This is the case with the sites we have selected where V_s measurements were not made for depths below about 60 m. Thus, for the depth interval between 60 m to 152 m, we have used the median V_s profile for the lacustrine/alluvial silts and clays unit of Wong et al. (2002). For depths between 152 and about 300 m, we used the unpublished V_s profile used by Wong et al. (2002). Figures 34 and 35 show the ProShake V_s profiles to depths of about 300 m for the I-80 interchange and 600 South interchanges, respectively. These same data are also tabulated in Tables 8 and 9. These data in these figures and tables are considered to be “best-estimate” or mean values.

3. Below a depth of about 300 m, semi-consolidated sediments having much higher V_s values are found (Figure 36). However, the depth to the semi-consolidated interface varies significantly throughout the Salt Lake Valley (Figure 37). This figure shows the depth to the top of the semi-consolidated sediments (in meters) as contoured by Wong et al. (2002) from data published by Arnow et al. (1970). It is important to remember these depth variations when constructing V_s profiles for other locales within the Salt Lake Valley and the depth to the semi-consolidated interface should be adjusted accordingly.

4. At a depth of about 1000 m, the semi-consolidated sediments change to consolidated sediments with another marked increase in V_s values (Figure 36). Consolidated sediments are found to a depth of about 2600 m. Below this depth, bedrock is encountered with V_s values of about 3400 m / s.

Sublayer Thickness

1. Because the EQL method is based on a continuum solution, there is no theoretical limitation to the thickness of the sublayer used in the SHAKE Vs profile. However, if nonlinear soil effects are important and one is interested in accurately predicting the level of strain in a highly nonlinear zone, there should be some practical limitation placed on the maximum thickness of any sublayer used in the SHAKE analysis profile. For such cases, we recommended a maximum thickness of any sublayer be calculated from the following:

$$H \leq Vs /(4 * f_c)$$

where H = maximum thickness of the sublayer, Vs = shear wave velocity in the layer and f_c = the cutoff frequency in Hz.

However, for medium stiff to stiff soils and rock layers, reasonably thick layers can be used without greatly affecting the accuracy of the SHAKE results. It is only at or near the ground surface where the thickness of the sublayers should be reduced to about 3 to 5 m maximum. We have also noted that if thin layers (i.e., less than 3 to 5 m) are input into the profile, then high strain can be concentrated in these thin layers, especially if they are soft (i.e., have low V_s values). Such soft, thin layers can cause convergence and numerical errors in the ProShake Program and should be avoided, whenever possible.

The ProShake manual suggests that a cutoff frequency of 15 to 20 Hz is usually adequate for most soil profiles, because high frequency motion has little effect on most civil structures. We have completed all of our convolution analyses using a cutoff frequency of 25 Hz. However, we should note that the time histories for the deconvolution analysis were filtered using a 15 Hz Butterworth filter and therefore are somewhat deficient in the high frequency part of the spectrum, as previously discussed. Thus a frequency of 15 Hz for the above equation is generally sufficient.

Uncertainty Considerations

1. Because large uncertainty exists in the deep V_s profile in the Salt Lake Valley, we believe it was important to capture some of this variability in the ProShake analyses. Thus, we used two alternatives for the deep V_s profile for the I-80 and 600 South Interchanges (Figure 36). These are labeled "Deep V_s Profile I" and Deep V_s Profile II." The V_s velocities for "Deep V_s Profile I" were obtained from Hill et al. (1990) for the Salt Lake Valley and were adjusted for the appropriate depths to the major lithological interfaces (J. Pechmann, personal communication). The V_s velocities for "Deep V_s Profile II" were obtained from Wong et al. (2002, unpublished) and are average V_s velocities from the Pacific Engineering and Analysis database compiled by Walt Silva. The complete ProShake input files for these "best-estimate" V_s profiles are included in Attachments F and G for the I-80 and 600 S. Interchanges, respectively.

2. In addition to convolution analyses using best estimate V_s values, it is important to consider potential variability the shallow V_s profile. ASCE 4-98 recommends that a 50 percent variation in the maximum shear modulus (G_{max}) be considered for ground response analyses. (Note that a 50 percent variation in G_{max}, corresponds to a 22.5 percent variation in V_s). Thus, we have performed additional ProShake runs that increase the V_s values in the upper profile by a factor of 1.225. This increase

was applied to all layers having V_s values less than 4000 ft/s (1220 m/s) at both the I-80 and 600 S. Interchange sites. We have called these profiles our "upper bound" V_s profile. The "upper bound" V_s profiles for the I-80 and 600 S. Interchanges are found in Attachments H and I, respectively. Also, EQL analyses have performed and tabulated for the upper bound case and are used to calculate the final design response spectra discussed in the next section.

However on the other hand, we do not recommend that the shear modulus in the shallow profile be decreased by 50 percent and analyzed using EQL analysis. Our experience with ProShake has shown that such an excessively softened V_s profile will cause convergence and other numerical run-time problems. Furthermore, we believe that an excessively softened V_s profile will cause additional damping and deamplification of the high frequency spectral accelerations produced by the EQL method. This is an outcome that we wish to avoid for design purposes because of the potential for underestimating spectral accelerations at frequencies that may be important for bridge design. Many typical bridges and overpass structures have fundamental frequencies that are generally greater than about 1 to 2 Hz and are in the range of severe deamplification suggested by the EQL analysis.

We have performed 40 Shake runs for each site to capture some of the variability found in the deep and shallow Vs profiles. This combination of computer runs was obtained by the following combinations: 2 shallow V_s profiles (upper bound and mean) x 2 deep V_s profiles (deep V_s Profile I and II) x 5 time individual time histories x 2 input motions (cases with and without fault directivity). The results are plotted and discussed in the convolution analysis section of this report.

Shear Modulus and Damping Curves for Soils

1. We have used shear modulus reduction and damping curves appropriate for the soil descriptions for the upper 200 m of the site specific soil profiles. We have used the curves by Vucetic and Dobry (1991) for the soft and medium stiff clayey soils as provided in ProShake (Figure 38). We have used the curves of Seed and Sun (1989) and Sun et al. (1988) for overconsolidated or stiff clayey soils (Figure 39) as provided in ProShake. For the granular and/or deeper sediments (60 to 220 m), we have used Electric Power Research Institute (EPRI, 1993) curves for saturated sands (Figure 40). Although we did not encounter any significant amounts of gravel in our profiles, we recommend that the shear modulus and damping curves developed by Rollins et al. (1998) be used for these soils.

Damping Calculations for Linear Rock Part of Profile

1. Damping values for the linear rock part of the profile (i.e., depths 320 km to 1.5 km) were calculated in the same manner as the deconvolution analysis. The damping calculations are given in Attachments J and K for the I-80 and 600 S. Interchanges, respectively.

   The seismic attenuation parameter kappa, κ, for the upper 1.5 km of the profile was estimated to be 0.05 s (J. Pechmann, personal communication). The κ value is slightly higher than the 0.04 s used for the generic western U.S. rock profile. It was increased to account for the higher attenuation that is expected in the shallow crust beneath the Salt Lake Valley.

Below a depth of 1.5 km, damping values were calculated from the crustal quality factor, Q for Utah. Geomatrix (1999) used the following formula to calculate the Q below 1.5 km:

$$Q = 500f^{0.2}$$

where f is the frequency in Hz. This formula is for Q and was applied by Geomatrix (1999) in their seismic evaluations of the proposed Private Fuel Storage Facility at Skull Valley. Using f = 3 Hz, the Q factor below 1.5 km is approximately 623 (unitless). Damping below 1.5 km is not thickness or shear wave velocity dependent, thus the damping for each layer is the same and calculated from:

$$\lambda = 1/ (2\ Q)$$

This formula yields a damping of 0.0008 or 0.08 percent for each of the sublayers below 1.5 km.

Other Considerations

1. If the input ground motion is high, the calculated shear strain in softer layers may be large. This introduces the possibility that the calculated shear strain will exceed the maximum shear strain values defined in the G/Gmax and damping curves during an a given iteration step. If this happens, ProShake generates the following error message:

M6201: MATH
-)-cexp: DOMAIN error

Often this error message can be eliminated by extending the G/Gmax and damping curves to higher levels of strain. CALTRANS (1996c) has a procedure for extending these curves for to higher strain for clayey soils (Figure 41). However, we do not recommend extending these curves beyond about 2 to 3 percent shear strain. If such large strains are truly possible, then a non-linear model should be considered.

The maximum shear strain levels developed in our ProShake analyses were about 2 percent, thus we did not find it necessary to greatly extend the shear modulus and damping curves to higher shear strain. However, we did extend the EPRI (1993) saturated sand curves to higher strain levels by using the modulus and damping values at 1 percent strain (Figure 40).

2. EQL analyses use the "effective shear strain" and not the peak shear strain to determine if strain compatible properties have been obtained during a given iteration step (see discussion in introduction to ground response analysis). Thus, ProShake requires that the ratio of the effective shear strain to peak shear strain be known as an input parameter. We have used the relation of Idriss and Sun (1992) to calculate the effective strain ratio, n, where n is the effective shear strain, $\gamma_{(eff)}$, divided by the peak shear strain, $\gamma_{(peak)}$. The effective shear strain ratio is a function of earthquake magnitude and is equal to:

$$n = (M - 1)/10$$

where M is the controlling earthquake magnitude. For the Salt Lake City Segment of the Wasatch Fault, the design earthquake is generally about a M = 7 event, thus the effective shear strain ratio is about 0.6. This is the value we have used in both our deconvolution and convolution analyses. However, perhaps even a smaller ratio

may be justifiable. Seed et al. (1992) suggest that n is between 0.30 and 0.55 for M_s = 6 to 7 events and n is between 0.5 to 0.65 for M_s = 7 to 8 events.

3. During the convolution analyses, it is possible that softer clay layers may be brought to a failure condition (i.e., the peak shear stress predicted by SHAKE may exceed the peak strength of this layer). EQL analyses cannot predict when a failure condition has been reached, thus it is necessary to manually check to see if the failure state has been reached. In a similar manner, Seed et al. (1992) point out that EQL analyses performed in a conventional manner may not accurately model the softening or failure condition. This may result in the overprediction of peak ground acceleration and other high frequency spectral acceleration values for the post yield (i.e., failure) condition. They suggest that EQL analyses be modified iteratively to model the overstressed (i.e., post-yield) behavior of layers by using lowered G/G_{max} values for these layers.

   We recommend the following criterion to determine if a layer has reached the yield (i.e., failure) condition:

$$\tau_{yield} = 2\ S_u$$

   where τ_{yield} = yield stress and S_u is the peak undrained shear strength of the clay. The coefficient of 2 is recommend by CALTRANS (1996c) and takes into account strain rate effects and the effective versus peak strain ratio. We recommend that the evaluator inspect the SHAKE results to verify that the peak stress predicted by SHAKE does not exceed 2 times the undrained shear strength of that layer. If this condition is not met, then the evaluator should consider that this layer has reached the failure condition. (The peak shear stress may be obtained directly from the output manager in ProShake.) The peak shear strength can be calculated from undrained

shear strength testing or estimated from empirical relations that are based on the preconsolidation stress, or the effective vertical stress.

For layers reaching the failure condition, Seed et al. (1992) recommend that a slightly lower G/G_{max} value be used in the appropriate strain range to account for post-failure softening (i.e., the G/G_{max} curve is slightly decreased in the large strain portion of the curve). However, the damping curve for the overstressed layers are usually not adjusted. The SHAKE analysis is then repeated using the slightly softened G/G_{max} curve and the output is reexamined to verify that peak stress has decreased below the failure criterion. This process is done iteratively, until the softened G/G_{max} values are sufficient to produce a non-yielding condition. In essence, this softening of the G/G_{max} curve will produce a lower peak stress for the appropriate layer, but it will also increase that amount of strain that is predicted for that layer.

4. Convolution analysis in soft soil profiles can also cause convergence problems. For most of our ProShake runs, we used a convergence error tolerance of 5 percent and a maximum number of iterations of 10. This parameter is set in the input motion menu of the input manager of ProShake. The error tolerance is the difference between the assumed shear modulus and damping value used at the beginning of the iteration step and that calculated at the end of the iteration step. This parameter is required to set the convergence tolerance as SHAKE iterates to obtain strain-compatible properties.

   ProShake continues to iterate until the convergence error tolerance is met, or until the maximum number of iterations is reached. Convergence problems are indicated by excessively long run times in the solution manager or run-time errors. We recommend that if convergence difficulties are encountered, then the convergence error should be slightly increased to allow ProShake to come to a solution. We found

this to be necessary for the 600 S. Interchange “best-estimate” profile using some of the input motion that included fault directivity.

Calculation of Site Specific Amplification Factors

Introduction

Design response spectra for site specific soil conditions can be calculated from the results of the convolution analyses. Also site specific amplification factors for each location can be calculated. Using the guidelines given in this section, we calculate soil response spectra and amplification factors from the SHAKE results. For each site, there are 20 SHAKE runs that have been performed (i.e., five spectrally matched time histories times two V_s profiles for each site (i.e., mean and upper bound cases) times 2 target rock spectra (with and without directivity). However, before we develop the final design spectra for the I-80 and 600 South interchanges, it is important that we compare our modeling results with previous modeling efforts and empirical attenuation relations. From this comparison it is possible to judge the "reasonableness" of our results and make any adjustments, as necessary.

Previous Amplification Factors

Amplification factors developed by Silva et al. (1999) and Wong et al. (2002) have been previously discussed in the section entitled "Summary of Previous Research." In this section we only discuss the potential bias of these amplification factors for high levels of ground motion at soft soil sites.

Silva et al. (1999) found that amplification factors calculated from random vibration theory and the EQL method for the Los Angeles and San Francisco, California have good agreement with the NEHRP (1997a) amplification factors at low levels of ground motion (i.e., pga $\leq$ 0.10 g). However, at higher levels of ground motion, they found that their long period amplification factors significantly exceeded those of NEHRP. Conversely, their short period (i.e., high frequency) amplification factors were significantly less than those of NEHRP.

This lead to the conclusion that NEHRP factors appear to have considerable conservatism for shorter periods (Silva et al., 1999).

From a design perspective, if the EQL method provides higher amplification of the long period ground motion when compared with NEHRP amplification factors, then it is conservative to use the modeling results, because a larger design margin will be obtained. However, regarding the short period ground motion, the conclusion of Silva et al. (1999) begs the question: "Are the NEHRP factors really conservative for spectral values at short period (high frequencies) or is the EQL method simply underestimating the spectral acceleration at those frequencies?" Regarding this issue, we have no definitive answer. Unfortunately, it is not possible to use the empirical dataset to entirely resolve this question, due to paucity of recorded ground motions for soft soil sites that have experienced high levels of ground motion. However, Silva et al., (1999) recognized this potential unconservatism and suggested a potential for overdamping by EQL methods at high levels of strain, especially for spectral acceleration values greater than about 2 Hz. They reached this conclusion by comparing EQL modeling results with the Abrahamson and Silva (1997) attenuation relation for deep soil sites. Based on this comparison, Silva et al. (1999) suggest that a reasonable lower limit for soil amplification factors at high frequencies is about 0.5 to 0.6 for the Bay mud profile.

Also, Wong et al. (2002) used the methods to Silva et al. (1999) to produce strong motion scenario maps for the Salt Lake Valley. Amplification factors were computed for various site response units as a function of thickness of the underlying unconsolidated sediments and the level of input rock motion (Figure 14). An M = 6.5 event was placed a several distances to produce input peak accelerations of 0.05, 0.10, 0.20, 0.40, 0.50 and 0.75 g to produce the amplification factors as a function of frequency. The median amplification factors of Wong et al. (2002) compare well with those computed by Silva et al. (1999). Wong et al. (2002) calculated median amplification factors of 0.30 and 0.65 for 10 and 100 Hz, respectively.

Thus, based on these considerations, we believe that it is potentially unconservative to rely solely on EQL methods to develop the final design spectra, especially if spectral accelerations have been underestimated at higher frequencies. Thus, we strongly recommend that the SHAKE results be compared with spectral values from the appropriate attenuation relations and amplification factors calculated from previous studies of soft soil sites before the ground response analyses are used as design input.

Calculation and Comparison of Amplification Factors

From the results of the convolution analysis, it is possible to calculate site specific amplification factors as a function of frequency or period (Silva et al., 1999). These amplification factors are the ratio of the surface soil spectral acceleration values divided by the input outcropping rock spectral acceleration values as a function of frequency. The surface soil spectral values come from the results of the convolution analyses at each site. The input outcropping rock spectra values are the average spectral acceleration values from the spectrally-matched time histories that were used as input to the deconvolution analyses.

We recommend that amplification factors be calculated for each candidate site. Then these factors can then be used to compare with results of other modeling studies and empirical attenuation relationships. The following describes the steps we recommend in calculating site specific amplification factors.

1. We recommend that 5 percent damped median spectral acceleration values as a function of frequency be calculated from the surface soil response spectra using the SHAKE results. We recommend that these median spectral values be calculated for the best-estimate soil profile for the following two cases: Case (1) where the input target spectrum includes fault directivity effects and Case (2) where the input target spectrum has no directivity effects.

In determining the median value for a specific case, we recommend that the results from the best-estimate V_s profiles for be treated as equally likely possibilities and used to calculate the median amplification factors for each site. For our example, there are 5 time histories and two deep Vs profiles (Deep V_s profiles I and II). For our case, this produces approximately 10 equally likely possibilities from which to calculate the median value Figures 42 and 43 show ProShake response spectra obtained from the 5 km convolution analysis for the I-80 and 600 South interchanges, respectively, for cases without and with fault directivity. Note that in developing these figures, we have not included the results for the upper bound V_s profile cases in calculating the median values. The upper bound V_s cases were not included in order to more directly compare our results with the median amplification factors calculated by Wong et al. (2002).

2. For each case discussed above, median amplification/deamplifcation factors as a function of period or frequency are calculated by dividing the median SHAKE spectral acceleration values by the spectral acceleration values from the spectrally matched input time histories after these time histories have been filtered with a 15 Hz Butterworth filter, but before they have been deconvolved. For example, Figures 44 and 45 show median amplification/deamplification factors for the I-80 and 600 South interchanges, respectively, for the cases with and without fault directivity. These have been calculated using the median values from Figures 42 and 43 and the filtered input spectral acceleration values shown in Figure 29 and 30.

3. To check the reasonableness of the calculated amplification/deamplification factors, we recommend that the amplification factors estimated from the SHAKE results be compared with previous results and studies, if available. For example Figures 44 and 45 show our results compared with the Wong et al. 2002 amplification factors calculated for the lacustrine-alluvial silt and clay unit for a M = 6.5 earthquake with an input pga of 0.75 g.

Figure 44a shows that the median SHAKE soil amplification factors calculated for the I-80 interchange are relatively similar to those calculated by Wong et al. (2002) for frequencies between 5 and 100 Hz. At frequencies less than 5 Hz, our analyses show less deamplification.

In addition, Figures 44b and 45a and 45b show the site specific amplification factors calculated for the I-80 and 600 South interchanges for the cases without and with fault directivity, respectively. A comparison of these figures suggests that our soil amplification factors are relatively similar to those calculated by Wong et al. (2002) in the frequency range between 1 to 5 Hz. For frequencies above about 5 Hz and below about 1 Hz, the our results show slightly less deamplification than that of Wong et al. (2002). At pga, the median soil amplification factor predicted by our analyses is about 0.8, whereas that estimated by Wong et al. (2002) is about 0.65. For frequencies less than about 1 Hz, the amplification factors estimated from our analyses are somewhat higher than those calculated by Wong et al. (2002). For example at 0.5 Hz (2.0 s), amplification factors estimated by SHAKE are about 3 to 3.5, whereas those estimated by Wong et al. (2002) are about 2.

However, we believe that it is important to keep these differences in context. The analysis of Wong et al. (2002) produced median estimates from a large statistical sampling of lacustrine-alluvial silt and clay units from northern California sites, whereas our estimates are from site specific analyses of two sites, which have less statistical support. Thus, our results probably fall within the uncertainty ranges of the Wong et al. (2002) results.

4. In addition to comparing with previous studies, we also recommend that amplification factors be calculated using empirical attenuation relations that are appropriate for soil sites and compared with those factors obtained from the SHAKE

analyses. To this end, we recommend that attenuation relation of Abrahamson and Silva (1997) be used for this comparison.

We prefer this attenuation relation for two reasons: (1) it has regression coefficients that have been specifically developed for deep soil sites, and (2) it is the same attenuation relation that we used to develop the target spectrum; thus it is relatively straightforward to calculate amplification factors using this attenuation relation. The amplification factors calculated from the Abrahamson and Silva (1997) attenuation relation are the deep soil spectral values divided by the rock spectral values as a function of frequency for the appropriate earthquake magnitude and source distance at the I-80 and 600 South interchanges, respectively. However, we should note that strictly speaking, the Abrahamson and Silva (1997) attenuation relation has not been completely validated for soft deep soil sites. Notwithstanding, we consider it to the best available attenuation relation for the comparison with our results.

From Figures 44 and 45 we note that the amplification factors from our analyses are generally less than those estimated from the Abrahamson and Silva (1997) attenuation relation for the mid-range frequencies. This is to be expected because this attenuation relation was developed for deep soil sites, but not necessarily for deep soft soil sites. We believe that deep soft soil sites will have more attenuation (i.e., deamplification) in the short to mid-range frequencies based on observations from previous earthquakes. However, it is also possible that SHAKE analyses are artificially overestimating the amount of deamplification in the mid-range frequencies. If true, this underestimation would be unconservative (i.e., unsafe) from an engineering standpoint. Thus, we believe that it is potentially unconservative to accept the SHAKE results at face value and rely solely on them for developing design spectra.

Amplification Factors and Their Use in Current Seismic Codes

1. MCEER (2001a) places limits on the amount of deamplification allowed by site specific ground response analyses. For site specific studies (such as our examples), the final design spectra shall not be less than two-thirds of the response spectra determined using the general procedures given in MCEER (2001a). The short period (i.e., 0.2 s) amplification factor, S_s, is 0.9 and the 1 second period amplification factor, S_1, is 2.4 for type E soils at high levels of ground motion (MCEER, 2001a). This means that the minimum allowable amplification factor is 0.6 for S_s and 1.6 for S_1. Thus, this requirement must be considered when developing the final design spectra from the SHAKE results.

2. We do not recommend that the SHAKE amplification factors calculated above be applied to the MCEER (2001a) procedure for developing a generic MCEER (2001a) design spectral shape for type D and E soils. There are important reasons why this should not be done: (1) The target spectrum from which our SHAKE amplification factors were calculated is different from that of MCEER (2001a); thus our results cannot be used directly to modify a MCEER (2001a) surface rock spectrum. (2) The MCEER (2001a) rock spectrum may have a different spectral shape, particulary at longer period than our spectrum. This difference is not accounted for by simply scaling a MCEER (2001a) rock spectrum by the procedures given in MCEER (2001a). (3) Our target rock spectrum has been adjusted for fault directivity effects, which are not contained in the MCEER (2001a) rock spectrum.

3. After a review of the convolution results and amplification curves, the final design spectra are ready to be developed, as described in the next section.

Calculation of Design Spectra

Introduction

Before we develop the design spectra, we will present the results of the convolution analyses for all cases analyzed. Figures 46 and 47 present the results of the 5 km convolution analysis for the I-80 and 600 interchanges, respectively, for the case without fault directivity. Figures 48 and 49 present the results for these interchanges for the case with fault directivity. We should note that in developing the average response spectra for the cases shown in Figure 46, we chose not to include the results for the Cape Mendocino record. This record produced a response spectrum that was considerably lower than the other results for the period ranging between 1 to 2 seconds. Also, the Erzican Turkey record is not included in the average response spectra for the 600 S. interchange for the case with fault directivity (see Figures 49a, c, d). For some reason, this record caused convergence problems for this case, thus it could not be processed. Thus, it has not been included in the average in these plots.

As expected the results from the convolution analysis show a significant deamplification of the shorter period motion and a shift of the predominate period to longer periods (Figures 46 to 49) when compared with the input rock motions. These figures also suggest that the 600 S. interchange site is a softer soil site than the I-80 interchange, because of the more pronounced short to mid frequency range deamplification and a period shift as seen in the response spectra.

The convolution analysis also suggest that reasonably large differences in the deep V_s profile produce relatively minor differences in the average surface response (Figures 46 to 49). This can be seen by inspecting the average spectral values for these two cases (Deep V_s Profile I and II). This suggests that difference in the input deep V_s profiles does not strongly influence the response analysis, or at least it is not as important as the shallow V_s profile in determining the ground response.

Once the convolution analyses and amplification factors have been reviewed and deemed reasonable, the final design spectra can be generated. MCEER 2001(a,b) and NEHRP 2000(a, b) do not give extensive guidance regarding the calculation of design spectra from the results of site specific analyses. In computing design spectrum, MCEER guidance only states that typically a "smoothed" average of the individual responses is used. This smoothing is done by: "slightly decreasing spectral peaks and increasing spectral valleys (MCEER, 2001b)."

Development of Enveloping Design Spectra

For the reasons discussed in the previous sections, and to guard against potential unconservatism in the SHAKE analsyes, we recommend that a "smoothed" enveloping design spectrum be developed. We recommend that the enveloping design spectrum bound the following cases: (1) average spectral values calculated from the SHAKE convolution analysis, (2) an MCEER (2001a) design spectrum for soil type E scaled to two-thirds of the spectral acceleration values using the maximum considered earthquake (i.e., 2500 return period event) and (3) the spectral acceleration values obtained from the Abrahamson and Silva (1997) attenuation relation for deep soil sites using the appropriate magnitude and source distance for the controlling earthquake.

The steps for constructing the enveloping design spectrum are:

1. Make a composite plot the following soil spectra for 5 percent damping:

    a. Mean response spectrum from the SHAKE results using the average of the best-estimate and upper bound soil profiles. The best-estimate and upper bound cases should be treated as equally-likely cases and averaged together.
    b. Abrahamson and Silva (1997) deep soil spectrum for the appropriate magnitude (M) and distance (R).

c. MCEER 2001(a) soil spectrum scaled to two-thirds (i.e., 0.67 times) a soil class E spectrum developed using the MCEER guidance.

2. The above steps should be done for cases with and without fault directivity and these cases plotted and bounded separately. Separate design spectra should be constructed for cases without and with fault directivity. For example, Figures 50 through 53 show the various spectra developed in steps 1a, b, and c. above.

3. From the composite plots, construct a smoothed enveloping spectrum which bound all of the spectra plotted in steps 1a, b, and c. We have found that this smoothing and enveloping is not easily done numerically, thus we recommend that it be done by using a french curve or simply smoothed by eye, as we have done. The enveloping smoothed design spectra for the I-80 and 600 South interchanges are shown in Figures 50 through 53, respectively. We recommend that similar smoothed enveloping spectra be developed as the final design spectra for bridge projects on soft soil sites.

4. It is interesting to note that the SHAKE results suggest more deamplification is occurring in the short to mid period range for cases with fault directivity than is occurring for cases without fault directivity. This can be seen in mean spectra for both the I-80 and 600 S. sites (compare Figures 50 with 51 and 52 with 53). Thus, the SHAKE results suggest that the long period spectra content of the input record (i.e., periods greater than 0.6 s) is affected the short period response. However, it is unclear if this is phenomenon is real or if it is simply an artifact of the EQL analyses. To guard against underestimating the short to mid period spectral response for design spectra with fault directivity, we recommend that enveloping spectral values for the case without directivity be used as a guide in constructing the spectrum for the case with directivity for periods less than about 1 second. For example, the spectral shape in Figure 51 is identical to the spectral shape in Figure 50 for periods less than 1

second. This same approach was also used in creating the spectral shape for 600 S. interchange for the case with fault directivity (compare Figure 53 with Figure 52).

Other Considerations

1. For cases where linear or nonlinear time domain analyses is to be conducted for bridge structures, the frequency differences between spectra representing fault normal and fault parallel motions should be recognized for sites within 15 km of the causative fault. The time histories and design spectra that include fault directivity are most appropriate for analyses where the longitudinal axis of the bridge is oriented in a direction that is perpendicular to the fault trace (i.e., fault normal). The time histories and design spectra that do not include fault directivity are most appropriate for cases where the longitudinal axis of the bridge is oriented in a direction that is parallel to the fault trace (i.e., fault parallel). For bridges with oblique orientations to the fault trace, we recommend that the components of strong motion parallel and perpendicular to the longitudinal axis of the bridge be calculated by rotating the time histories. The required equations are the same as those used to rotate the time histories when we calculated the maximum and minimum principal components of the time histories as described in the spectral matching section of this report.

2. When two or more sets of time histories are used for input into a linear or nonlinear time domain analysis, the resulting responses shall be averaged (ASCE 4-98). The average structural response can then be used for design purposes. Thus for our case, which used 5 time histories, the response from these time histories can be averaged. If fault directivity effects are important, we recommend that separate averages should be developed for cases without and with fault directivity effects.

3. For cases where linear or nonlinear-time domain analyses are not required, a single surface soil response spectrum is often used for design purposes. For such cases, we

recommend that a smoothed enveloping design spectrum be developed that envelopes both cases with and without fault directivity.

4. The process and results that we have presented in this guidance appears to produce reasonable spectral acceleration values for periods less than about 4.0 s. We performed spectral matching up to a period of 4 seconds when developing the input time histories for the deconvolution analysis. However, for very long period structures (i.e., greater than about 4.0 s), the applicability of the process described herein is questionable. Long period ground response is dominated by other wave forms other than vertically propagating SH waves and is also influenced by basin generated surface waves. These issues should be considered by the designer.

5. In addition to the above procedure, there are other factors which ultimately influence the selection and development of the design ground motion and design spectra. These are discussed in the following sections.

Other Design Considerations

Convolution Analysis Using Methods of NEHRP (2000b) and MCEER (2001b)

Current bridge MCEER (2001a, b) and building code guidance (NEHRP 2000a, b) do not recognize the need for deconvolution analysis for deep sedimentary basins, such as the Salt Lake Valley. These documents allow for a shallow convolution analysis, which does not consider the deep V_s profile and its effects on the surface response.

The spectrally matched acceleration time histories developed in "Generation of Spectrum Compatible Time Histories" section of this report defines the expected surface motion for a generic NEHRP site class B/C V_s profile. NEHRP (2000b) and MCEER (2001b) allow the spectrally matched acceleration time histories to be input into the site specific soil column at a depth with the V_s measurements are equal to a Site Class C soil. In performing soil response analysis, these documents recommend that the spectrally-matched design motion be assigned to a layer within the subsurface profile as follows:

> "*For profiles having great depths of soil above Site Class A or B rock, consideration can be given to defining the base of the soil profile and the input rock motions at a depth at which soft rock or very stiff soil of Site Class C is encountered.*"

Once this assignment is made, the spectrally matched acceleration time history is convolved to the surface as an outcropping rock motion using the site specific soil profile to determine the surface soil response. Site Class C soils have V_s values ranging from 360 m/s to 760 m/s (1200 to 2500 ft/s). However, as a more refined estimate, Boore and Joyner (1997) have calculated a generic rock Vs profile for the western U.S.. Their average V_s profile has V_{s30} values of 618 m/s (2027 ft/s), where V_{s30} is the average shear wave velocity in the upper 30 m (100 ft) of the profile.) The Vs value of 618 m/s (2027 ft/s) is considered to be the mean

value for rock sites in western North America and is our best estimate of the average rock V_s value used in current empirical attenuation relations. Thus, if one is to perform convolution analysis using NEHRP (2000b) and MCEER (2001b) guidance, a layer with a V_s value of about 2000 feet per second should be selected as the input rock motion layer. The target ground motion should be assigned at the depth of this layer as an outcropping rock motion in the ground response model.

We do not recommend that this process be used for deep sedimentary basin, but we have done convolution analysis according to the guidance of NEHRP (2000b) and MCEER (2001b) to explore what affect it has on the ground response. Figures 54 and 55 show the results of these convolution analyses. The response spectra in these figures are mean, 5 percent damped surface acceleration response spectra which have been calculated by convolving the earthquake motion to the surface from a depth of 200 m using the site specific geotechnical data and V_s profiles for the I-80 and 600 S. interchanges, respectively. (Note that some of the time histories used in these analyses differ from those used in Figures 50 through 53. The results shown in Figures 54 and 55 were done at an earlier time, and some of the time histories were later replaced with different time histories, as our analyses evolved and were peer reviewed.)

Figures 56 and 57 compare the mean spectra obtained from the 5 km deconvolution / convolution analysis with those obtained from the 200 m convolution analysis. In short, the 200 m convolution analysis shows a higher acceleration response at short period and a lower acceleration response at longer periods. Thus, for the sites that we analyzed, it appears that the 200 m convolution analysis is somewhat conservative for short periods and grossly unconservative at longer periods. However, we caution about over-generalizing these results to other sites with varying subsurface conditions and seismic inputs. We believe that prudent design should carry out the full deconvolution / convolution analysis for sites underlain by deep sediments as given in this guidance document.

Basin Generated Surface Waves

We recommend that basin generated surface waves be considered at candidate bridges whose fundamental period is 3 seconds or greater, or at bridges where inelastic (i.e., ductile) behavior may cause a shift of the fundamental period to 3 seconds or greater during the seismic event. We do not recommend adjustment to the final design spectrum for bridges with fundamental periods that are less than 3 seconds.

Basing generated surface waves are an important component of long period ground motion in sedimentary basins. In these basins, like the Salt Lake Valley, long-period surface waves are created by the conversion of body waves to surface waves at the basin boundary. These boundary generated waves increase the amplitude of the strong ground motion at longer periods. Also, body waves can be "trapped" within the basin and generate surface waves that propagate across the basin (Sommerville, 1998). The phenomenon of wave trapping may explain why larger long-period amplification occurs when the earthquake is located at the edge of or outside the basin (Sommerville, 1998). Wave trapping causes a lengthening of duration and amplifies intermediate and long-period seismic wave amplitude (Sommerville, 1998). In addition to basin effects, long-period surface waves can be a significant in large, distant earthquakes due to lower attenuation rate of these waves when compared with body waves (Joyner, 2000).

Notwithstanding the importance of basin generated surface waves and their potential impact on the structural response of long-period bridges, this issue may not be crucial to the design of most of UDOT bridges. Many, if not most of UDOT bridges are relatively short-span overpass structures having fundamental period of vibrations generally less than 1 second (UDOT, personal communication). This is below the period at which the effects of basin generated surface waves become significant (Joyner, 2000).

If basin generated surfaces are considered to be important for design due to the expected long period response of the structure, the following items should be considered.

1. The intermediate to long period increase in spectral acceleration caused by basin effects cannot be incorporated in the input rock target spectrum like was done for the case of fault directivity. This cannot be done because: (1) basin amplification is a soil response effect and will not be present in the input rock spectrum, (2) 1-D EQL response analyses are based on the assumption that soil and bedrock boundaries are horizontal and that the response of a soil deposit is predominantly caused by vertically propagating SH-waves and not by surface waves. Thus, 1-D EQL methods are not entirely appropriate for modeling basin generated surface waves.

2. In addition, long-period amplification caused by basin generated surface waves is not fully included in most commonly used attenuation relations. For example, Joyner (2000) indicates that median estimates of pseudovelocity response from attenuation relations may be underestimated by as much as a factor of three for periods ranging from 3 to 6 seconds for deep sedimentary basins where the earthquake source is located outside of the basin. Thus, bridge code-based spectra, which are based on attenuation relations used in the national strong ground motion maps (Frankel et al., 1996), are likely to underpredict the amplitude of the long-period ground motion for such cases. Also, most empirical attenuation relations, such as those used in developing the national seismic hazard maps, do not distinguish between shallow soil sites and soil sites located in deep sedimentary basins. These attenuation relations have a limited set of input parameters such as earthquake magnitude, style of faulting, distance and site category and tend to ignore basin considerations.

3. Seismological-based models, like the 3-D elastic wave propagation model proposed by Olsen et al. (1994), have been used to model the complex behavior of body wave propagation and surface wave generation with a sedimentary basin. However, these

elastic models generally do not completely capture the highly non-linear soil behavior that occurs near the surface. Such anelastic and nonlinear behavior is very important at soft soil sites. Joyner (2000) recommends that anelastic attenuation be included in any model which is used to predict ground motion in deep sedimentary basins. Joyner (2000) believes that body waves dominate the ground motion in such basins for periods less than about 3 seconds. This is because surface waves at shorter periods are reduced in amplitude by anelastic attenuation and possibly scattering. If Joyner (2000) is correct, then wave propagation models that do not include anelastic attenuation will predict excessive surface wave amplitudes for waves with periods of 3 seconds or less. Joyner (2000) concludes that future progress in understanding basin surface waves and predicting their amplitude will require additional data and research.

4. In the meantime, Joyner (2000) recommends that the consequences of basin generated surface waves be considered for structures having fundamental periods of vibration equal to three seconds or greater, or for cases where shorter-period structures may lengthen to 3 seconds due to inelastic deformation. Joyner (2000) suggests the potential lengthening of a structure's fundamental period of vibration under inelastic deformation is approximately a factor of 2; thus the effects of surface waves may need to be considered for structures with elastic natural periods greater than about 1.5 seconds.

Joyner (2000) presents a regression equation to adjust the pseudovelocity response values predicted by an attenuation relation developed by Abrahamson and Silva (1997) and Joyner and Boore (1982). The adjustment was made to the 1982 version of the Joyner-Boore attenuation relation instead of the most recent vesion (Boore et al., 1997) because the former includes periods up to 4 seconds; whereas the latter only considers periods up to 2 seconds.

However, we must point out that the use of the Joyner (2000) equation is limited to peak horizontal particle velocities equal to or less than about 10 cm/s. Above this value, there is a potential for of peak particle velocity resulting from the lack of completely accounting for anelastic and nonlinear soil behavior (Joyner, 2000). This is a severe limitation for the case of Salt Lake Valley, where peak particle velocities for the design basis earthquake will greatly exceed 10 cm/s. Nonetheless, the use of the Joyner (2000) equation may provide a conservative estimate of basin effects for higher levels of ground motion and we recommend its use until a better method is available.

The pseudovelocity amplitudes of basin-edge-generated surfaces waves can be represented by an equation of the form (Joyner, 2000):

$$\log y = f(M, R_E) + c + bR_B$$

where y is the pseudovlocity response, $f(M, R_E)$ is the attenuation relation result from Joyner and Boore (1982), M is the moment magnitude, R_E is the distance from the source to the edge of the basin and R_B is the distance from the edge of the basin to the recording site and c and b are regression coefficients. For cases where the earthquake originates at the edge of the basin (such as the Wasatch Fault), we recommend that R_E be set to zero, or a very small value, and R_B be set to the distance from the edge of the fault-bounded basin margin to the candidate bridge site. The fitted parameter c is a measure of coupling between the incident body waves and the surface waves in the basin and the b parameter controls the attenuation with distance within the basin. The form of the above equation implies negligible geometric spreading for the surface waves within the basin.

We recommend that the above equation be applied to the Abrahamson and Silva (1997) attenuation relation to calculate the increase in spectral acceleration caused

by basin generated surface waves at longer period. We have used this attenuation relation and have adjusted it both for basin generated surface wave and fault directivity effects. However, for our sites, the combined basin generated surface wave and fault directivity effects added to the Abrahamson and Silva (1997) attenuation relation for deep soils sites were not greater than the enveloping design spectra constructed in Figures 50 through 53. Thus, basin generated surface wave effects do not constitute the controlling spectrum for the long period part of our final design spectra. However, this conclusion should be verified for other candidate sites.

Amplification of Surface Waves at Deep Soil Sites

Potential amplification of surface waves by deep soil profiles is another important issue, especially for large earthquakes that occur at relatively long distances. In the case of the 1985 Mexico City earthquake, the combination of soil amplification of longer period waves acting in conjunction with basin effects caused a significant amplification of the ground motion in the sedimentary basin that underlies parts of the city (Seed et al., 1987). The Mexico City earthquake was a relatively distance large event (M = 8.1) that occurred about 240 miles from the downtown area (Seed and Sun, 1989). Normally, such a distance event would not be expected to cause significant damage However, in the northwest part of Mexico City, very damaging ground motion occurred resulting from soil amplification of long period waves by the soft soil profile. This part of the city is underlain by 30 to 50 m of soft clay deposits which have shear wave velocities ranging from about 40 to 90 m/s (Seed et al., 1987). Nearby rock and hard soil records from the National University of Mexico showed pga values of about 0.04 g and had additional spectral acceleration peaks of about 0.1 g occurring both at periods of 0.9 and 2.0 seconds. Spectral acceleration values ranged from abut 0.04 to 0.02 g for periods between 3 and 5 seconds.

The bedrock/stiff soil ground motion was greatly amplified by the soft soil column and caused significant damage where the deposits had the greatest thickness. For example, at a

nearby soft soil site (SCT site), recorded peak ground acceleration was amplified to about 0.13 g and the spectral peaks at 0.9 and 2 seconds were amplified to about 0.25 g and 0.75 g, respectively. This corresponds to a 325 percent increase in pga and a 250 and 750 percent increase in the 0.9 second and 2 second spectral acceleration values. The 3 to 5 second spectral acceleration values were not greatly amplified at the SCT site, but other soil sites (CAO and CAF sites) showed amplifications of about 500 to 700 percent in these periods of their spectra.

The amplification of the 2 second spectral acceleration was particularly damaging to many buildings in Mexico City. Damage surveys showed that the severest damage occurred in structures ranging from 6 to 18 stories in height (Seed et al., 1987). Seed et al. (1987) inferred that buildings of this height had the greatest damage because their fundamental period of structural response matched the resonance created in the soil column by the soft soil deposits. Damage surveys also showed that the zone of severe damage was well defined by soil depth contours, which ranged from 26 to 44 meters in this area (Seed et al., 1987). On shallower soil deposits that flanked this zone, damage was relatively minor.

Seed et al. (1987) completed a series of ground response analyses of the Mexico City earthquake using a 1D EQL model (i.e., SHAKE). One of the purposes of their study was to see if 1D response analyses could replicate the soil amplification observed in parts of the city. Seed et al. (1987) used rock and hard soil records from the University of Mexico as input outcropping rock motions to the soil column analyses. They noted that the predicted response spectra at soil sites were generally in reasonable agreement with the recorded spectra. Some differences were noted however and attributed to uncertainties in the shear wave velocity profiles and other input parameters.

Seed et al. (1987) concluded that 1D EQL analyses provide a useful tool for assessing the affect of local soil conditions on ground motions at clayey sites where ground motions are likely to vary widely due to differences in the depth and stiffness of the clay deposits. Thus,

the conclusions reached by Seed et al. (1987) suggest that even though 1D EQL analyses are based on the assumption of 1D vertically propagating SH waves, perhaps this type of analysis can reasonably replicate possible soil amplification resulting from surface waves with periods about 2 seconds or less. The ability of 1D EQL analyses to reasonably estimate soil amplification for periods greater than 2 seconds is much less certain, because this long period ground motion is dominated by surface waves and not SH waves. Use of EQL methods to estimate strong motion for periods greater than about 2 seconds should be check and verified against other methods and/or attenuation relations as we have done in developing our final design spectra.

Vertical Ground Motion

The impact of vertical ground motion may be ignored if the bridge site is greater than 50 km from an active fault (MCEER, 2001a). If the bridge is located between 10 and 50 km of an active fault, a site specific study may be performed including the effects of appropriate vertical ground motion. However, in lieu of a dynamic analysis that includes vertical ground motion, MCEER (2001a) allows an approach that incorporates the effects of vertical ground motion by variations in the column axial loads and superstructure moments and shears.

If the bridge site is located within 10 km of an active fault, then a site specific study is required, if it is determined that the response of the bridge could be significantly and adversely affected by vertical ground motion characteristics. In such cases, response spectra and acceleration time histories as appropriate shall be developed for use and shall include appropriate vertical ground motions for inclusion in the design and analysis of the bridge (MCEER, 2001a).

Recent seismological studies have shown that the ratio of vertical response to horizontal response (i.e., V/H) can differ substantially from the nominal two-thirds ratio commonly used in engineering practice (MCEER, 2001b). This ratio is a function of tectonic

environment, subsurface soil or rock conditions, earthquake magnitude, earthquake source-to-site distance and period of vibration (MCEER, 2001b). In many cases, at shorter periods, the ratio of vertical to horizontal response may exceed two-thirds and even substantially exceed unity for very near field earthquakes at periods less than about 0.2 seconds (MCEER, 2001b).

At present, detailed procedures have not been developed for constructing vertical response spectra having an appropriate relation to the horizontal spectra developed using the guidelines of MCEER (2001a, b). However, Silva (1997) has developed empirical V/H ratios for soil sites for distances of 1 and 20 km for M = 5.5, 6.5 and 7.5 (Figure 58). Silva (1997) states that these empirical V/H ratios are reasonable well constrained and can provide the basis for developing smooth design ratios for western U.S. deep, moderately stiff, soil sites. For cases where estimates of a vertical spectrum are required, we recommend the use of this figure until generalized procedures are developed and/or adopted by FHWA or MCEER. Also, the reasonableness of the developed vertical response spectrum should be compared with a vertical response spectrum developed from the Abrahamson and Silva (1997) attenuation relation for deep soil parameters and for the appropriate magnitude and source-to-site distance obtained from the deaggregation of the seismic hazard.

Use of Response Spectrum Method versus Non-linear Time Domain Analyses

UDOT's current structural design approach is a force-based approach using an acceleration response spectrum to calculate the magnitude of the inertial force for the appropriate resonant frequency of the structure. However, our review of design trends shows that there is an increasing practice of using near-field time histories in nonlinear time-domain analyses to evaluate structural response. This evolution of practice is partly a result of a increasing computational capabilities in applying non-linear time domain analyses to ductile structural design and also in part by shortcomings of the response spectrum approach in capturing important near source effects.

Regarding the latter issue, near-fault ground motion is often very distinct from more moderate to distant ground motion in that near-fault motions often contain strong, coherent, long-period pulses and permanent ground displacements (Somerville, 2002). Review of recorded near source time histories shows that these records are often dominated by a large, long-period pulse or pulses that occurs in the velocity or displacement component of the time history, as discussed in the previous section. Somerville (1998a) states that near fault ground motion is often characterized by relatively simple, long-period pulses of strong ground motion having relatively short duration instead of a stochastic process having relatively long duration that is characteristic of moderate to distant ground motion. Thus, the resonance phenomenon, which a response spectrum is calculated to represent, has no time to build up in the near field. Somerville (1998a) cautions that any design practice that is based solely on the design response spectrum approach does not always provide a reliable basis for incorporating near source seismic effects.

Because ductile design and/or nonlinear analysis has a growing usage in engineering practice, we believe there will be an increasing need for development of representative time histories to use be used in nonlinear time-domain analyses. Thus, we have included guidance regarding the development of such time histories for soft soil sites using SHAKE analyses. Also, because nonlinear analyses are sensitive to the amplitude of velocity pulses and their phasing in the input time history, we recommended that five different time histories be used in performing ground response analyses in order to capture the potential variability in the response due to near source effects. Thus, we have taken great care in selecting the time histories used in our analyses. Three of the five selected time histories have a significant velocity pulse resulting from near fault rupture directivity.

Use of Regional versus Site Specific Strong Motion Hazard Studies

The adoption of the national hazard maps (Frankel et al. 1996) allows a performance-based approach to strong motion assessment without the need of performing site specific

probabilistic hazard assessment for each bridge or construction project. This constitutes a major advancement in seismic design over previous approaches. However, the national hazard maps provide probabilistic estimates of rock spectral acceleration values on a grid that covers the conterminous United States. Because of the relatively large grid spacing, these maps may not always capture important near fault details and spatial variations. For important projects or bridges, consideration should be given to performing site specific hazard studies to provide a more detailed representation of these factors. In addition, an economy in design might be obtained from site specific hazard studies.

MCEER (2001a) allows for site specific probabilistic ground motion analyses which should include the following: (1) characterization of seismic sources, (2) use of ground motion attenuation relations that incorporates current scientific interpretations, including uncertainties in the seismic source and ground motion models and parameter values, (3) detailed documentation, and (4) peer review.

For example, a site specific probabilistic seismic hazard assessments (PSHA) was performed for the I-15 Reconstruction Project (Dames and Moore, 1996. Site specific PSHAs include a higher level of detail and complexity in the geological and seismological assessment than the national hazard maps. Recently, the U.S.G.S. has recognized the need for more detailed hazard maps in urban areas and is in the process of producing microzonation seismic hazard maps for high seismic risk urban areas (Frankel and Safak, 1998). An example of such efforts is the earthquake scenario and probabilistic ground shaking maps produced for the Salt Lake Valley by Wong et al., (2002). Other planned improvements to the urban ground shaking maps include the addition of earthquake duration estimates and the incorporation of near source effects (Frankel and Safak, 1998).

Topographical Effects

Faccioli, et al. (2002) discuss evidence of complex site effects in 2D profiles and discuss the difficultly in interpreting recorded ground motion observed in three Alpine valleys in northern Italy, using weak motion data. Also, they investigate the amplification of strong motion by topography using historic earthquakes in mountainous regions. However, this study is not applicable to the relatively flat (i.e., ancestral lake bottom) geomorphology that predominates in areas where the soft Lake Bonneville sediments are found. Thus, we do not recommend that topographical effects be included in most site specific response analyses for UDOT bridges. However, for bridge crossings with large embankments (heights greater than 8 m), we recommend that the design consider the effects of the embankment response on the bridge foundation performance. Theses types of analyses can be done with 2D response analyses computer programs that are currently available.

Multi-Span Bridges

We have limited the scope of our guidance to developing rock outcrop motions that are compatible with a the target response spectrum for a candidate bridge location. These guidelines do not cover the generation of coherency-compatible multiple-support rock motion time histories and response spectra. Such considerations are important for multi-span structures and/or structures having multiple-supports. Design considerations regarding the potential for spatial and temporal variations in the input ground motions is required for multi-span bridges. This variation is caused by wave scattering and wave passage effects and these should be incorporated in the design ground motions (Abrahamson, Schneider, and Stepp, 1991; CALTRANS 1996a).

References

AASHTO, 1996. "Standard Specifications for Highway Bridges, 16th Edition.

Abrahamson, N. A., Schneider, J. F., and Stepp, J. C. 1991. "Empirical Spatial Coherency Functions for Applications to Soil-Structure Interaction Analyses," Earthquake Spectra, Vol. 7, No. 1, 1991.

Abrahamson, N. A., 1992. "Non-Stationary Spectral Matching," Presented in 87th Annual Meeting of Seismological Society of America, also in Seismological Research Letter, Vol. 63, No. 1.

Abrahamson, N. A., and Silva, W. J., 1996. "Empirical Response Spectral Attenuation Relations for Shallow Crustal Earthquakes," Seismological Research Letters, 68, 94-109.

Adan, S. M. and Rollins, K. M., 1993. "Damage Potential Index Mapping for Salt Lake Valley, Utah," Utah Geological Survey Miscellaneous Paper 93-4.

Arnow, T., Van Horn, R., and LaPray, R., 1970. "The pre-Quaternary Surface in the Jordan Valley, Utah; U.S. Geological Survey Professional Paper 700, p. D257-D261.

Baseline User's Manual, unpublished.

BAP (1992). "Basic Strong-Motion Accelerogram Processing Software; Version 1.0," U.S.G.S. Open-File Report 92-296A by April M. Converse and A. Gerald Brady.

Boore, D. M., Joyner W. B., and Fumal T. E., 1997. "Equations for Estimating Horizontal Reponse Spectra and Peak Acceleration from Western North American Earthquakes: A Summary of Recent Work," Seismological Research Letters, Vol. 68, No. 1, January/February 1997.

Boore, D. M. and Joyner, W. B., 1997. "Site Amplification for Generic Rock Sites," Bulletin of the Seismological Society of America, Vol. 87, No. 2, pp. 327-341, April 2997.

Boore, D. M., 1986, "Short period P- and S-wave radiation from large earthquakes: Implications for spectral scaling relations:" Bulletin of the Seismological Society of America, v. 76, p. 43-46.

Boore, D. M., 1983, "Stochastic simulation of high frequency-ground motions based on seismological modes of the radiated spectra:" Bulletin of the Seismological Society of America, v. 73, p. 1865-1894.

Borcherdt, R. D., 1997. "Estimates of Site-Dependent Response Spectra for New and Existing Highway Facilities (Methodology and Justification), Proceedings of the FHWA/NCEER Workshop on the National Representation of Seismic Ground Motion for New and Existing Highway Facilities, National Center for Earthquake Engineering Research Report No. NCEER-97-0010, pp. 171-201.

Borcherdt, R. D. 1994. "Simplified Site Classes and Empirical Amplification Factors for Site-Dependent Code Provisions." In *Proceedings of the NCEER/SEAOC/BSSC Workshop on Site Response During Earthquakes and Seismic Code Provision*s, University of Southern California, Los Angeles, November 18-20, edited by G. M. Martin.

Borcherdt, R. D., and G. Glassmoyer. 1993. "Influence of Local Geology and Weak Ground Motions in the San Francisco Bay Region, California, and Their Implications for Site-Specific Code Provisions." In *The Loma Prieta Earthquake of October 17, 1989 - Strong Ground Motio*n, USGS Professional Paper 1551-A, edited by R. D. Borcherdt.

CALTRANS, 1996a. "Guidelines for Generation of Response-Spectrum-Compatible Rock Motion Time Histories for Application to CALTRANS Toll Bridge Seismic Retrofit Projects," Caltrans Seismic Advisory Board, Ad Hoc Committee on Soil-Foundation-Structure Interaction, November, 25, 1996.

CALTRANS, 1996b. "Guidelines for Performing Site Response Analysis to Develop Seismic Ground Motions for Application to Caltrans Toll Bridge Seismic Retrofit Projects," Caltrans Seismic Advisory Board, Ad Hoc Committee on Soil-Foundation-Structure Interaction, Revised November, 25, 1996.

CALTRANS, 1996c. "Caltrans Procedures for Development of Site-Specific Acceleration Response Spectra," Caltrans, DNTMR, Office of Geotechnical Engineering.

Campbell, K. W. 1997. "Empirical Near Source Attenuation Relationships for Horizontal and Vertical Components of Peak Ground Acceleration, Peak Ground Velocity, and Pseudo-Absolute Acceleration Response Spectra," Seismological Research Letters, Vol. 68, No. 1, January/February 1997.

Chang, W. S., Bray, J. D., Gookin, W. B., and Riemer, M. F. 1997. "Seismic Response of Deep Stiff Soil Deposits in the Los Angeles, California Area During the 1994 Northridge Earthquake," Geotechnical Research Report No. UCB/GT/97-01, University of California, Berkeley.

Dames and Moore, 1996. "Seismic Hazard Analysis for the I-15 Corridor," Final Report submitted to the Utah Department of Transportation for the I-15 Reconstruction Project, Salt Lake City, Utah.

Dikmen, S. U. and Ghaboussi, J., 1984. "Effective stress analysis of seismic response and liquefaction theory," Journal of Geotechnical Engineering, ASCE, Vol. 110, No. 5, pp. 628-644.

Dobry, R., Ramos, R., Power, M. S., 1997. "Site Factors and Site Categories in Seismic Codes: A Perspective," Proceedings of the FHWA/NCEER Workshop on the National Representation of Seismic Ground Motion for New and Existing Highway Facilities, National Center for Earthquake Engineering Research Report No. NCEER-97-0010, pp. 137-169.

Electric Power Research Institute., 1993. *Guidelines for Determining Design Basis Ground Motions*, Report EPRI TR-102293. Palo Alto, California.

Faccioli, E., Vanini M., Frassine, L., 2002. "Complex site effects in earthquake ground motion, including topography," 12 European Conference on Earthquake Engineering, September 9-13, 2002.

Frankel, A. and Safak, E., 1998. "Recent Trends and Future Prospects in Seismic Hazard Analysis," Geotechnical Earthquake Engineerng and Soil Dynamics III," American Society of Civil Engineers Geotechnical Special Publication No. 75, Vol. 1, pp. 91-115.

Frankel, A., Mueller, C., Barnhard, T., Perkins, D., Leyendecker, E. V., Dickman, N., Hanson, S., and Hopper M., 1996. "National Seismic-Hazard Maps: Documentation June 1996," U.S.G.S. Open File Report 96-532.

Geomatrix, 2001a. "Development of Design Ground Motions for the Private Fuel Storage Facility, Revision 1," Private Fuel Storage Facility, Skull Valley, Utah, prepared for Stone and Webster Engineering Corporation, P.O. Box 5406, Denver Colorado 90217-5406.

Geomatrix, 2001b. "Development of Time Histories for 2,000-Year Return Period Design Spectra," Revision 1, "Private Fuel Storage Facility, Skull Valley, Utah, Calculation Number G(PO18)-3.

Geomatrix, 1999, "Fault Evaluation Study and Seismic Hazard Assessment, Private Fuel Storage Facility, Skull Valley Utah" Volume III, Appendix F, Prepared by Geomatrix Consultants, Inc., February 1999.

Geomatrix, 1996. "Recommendations for Site-Response Analyses of Vertical Excitation, Richmond-San Rafael Bridge Seismic Retrofit Design."

Gerber, T. M., 1996. "Ground Response at I-15 Bridge Sites on Soft Ground in Salt Lake Valley, Utah," Master's Thesis, Department of Civil and Environmental Engineering, Brigham Young University, Provo, Utah.

Hill, J. A., 1988. "A finite difference simulation of seismic wave propagation and resonance in Salt Lake Valley, Utah," M.S. Thesis, Dept. Of Geology and Geophysics, University of Utah.

Idriss, I. M. and Sun, J. I., 1992. "User's Manual for SHAKE91," Center for Geotechnical Modeling, Department of Civil and Environmental Engineering, University of California, Davis, California.

Idriss, I. M., 1990. "Response of Soft Soil Sites During Earthquakes," A memorial Symposium to Honor Professor Harry Bolton Seed, Department of Civil Engineering, University of California, Davis, CA.

International Building Code, 2000. IBCO publisher, ISBN: 10052K, paperback.

Joyner, W. B., 2000. "Strong Motion from Surface Waves in Deep Sedimentary Basins," Bulletin of the Seismological Society of America, 90, 6B, pp. S95-S112, December, 2000.

Joyner, W. B. and Chen, A. T. F., 1975. "Calculation of nonlinear ground response in earthquakes," Bulletin of Seismological Society of America, Vol. 65, pp. 1315-1336.

Joyner W. B., and Boore, D. M., 1982. "Prediction of earthquake response spectra," U.S. Geological Survey Open File Report 92-977, 16 pp.

Kramer, S. L., 1996. Geotechnical Earthquake Engineering, Prentice-Hall Inc.

Martin, P. P. and Seed, H. B., 1978. "MASH - A computer program for the nonlinear analysis of vertically propagating shear waves in horizontally layered soil deposits," Report No. UCB/EERC-78/23, Earthquake Engineering Research Center, University of California at Berkeley.

MCEER, 2001a. "Recommended LRFD Guidelines for the Seismic Design of Highway Bridges, Part I: Specifications," based on NCHRP Project 12-49, FY'98, "Comprehensive Specification for the Seismic Design of Bridges," Prepared under MCEER Highway, Project 094, Task F3-1, Multidisciplinary Center for Earthquake Engineering Research, State University of New York at Buffalo, April 9, 2001.

MCEER, 2001b. "Recommended LRFD Guidelines for the Seismic Design of Highway Bridges, Part II: Commentary and Appendices," based on NCHRP Project 12-49, FY'98, "Comprehensive Specification for the Seismic Design of Bridges," Prepared under MCEER Highway, Project 094, Task F3-1, Multidisciplinary Center for Earthquake Engineering Research, State University of New York at Buffalo, April 9, 2001.

Murphy, M., 1989. "Finite difference simulation of seismic P- and SV-wave amplification in Salt Lake Valley, Utah," Master of Science Thesis, University of Utah, Salt Lake City, Utah.

NCEER, 1997. "Proceedings of the FHWA/NCEER Workshop on the National Representation of Seismic Ground Motion for New and Existing Highway Facilities," National Center for Earthquake Engineering Research Report No. NCEER-97-0010.

NEHRP, 2000a. "NEHRP Recommended Provisions for Seismic Regulations for New Buildings and Other Structures," Part 1: Provisions (FEMA 368), Building Seismic Safety Council.

NEHRP, 2000b. "NEHRP Recommended Provisions for Seismic Regulations for New Buildings and Other Structures," Part 2:Commentary (FEMA 369), Building Seismic Safety Council.

NEHRP, 1997a. "Recommended Provisions for Seismic Regulations for New Buildings and Other Structures," Part 1: Provisions (FEMA 302), Building Seismic Safety Council.

NEHRP, 1997b. “Recommended Provisions for Seismic Regulations for New Buildings and Other Structures,” Part 2: Commentary (FEMA 303), Building Seismic Safety Council.

NEHRP, 1994, “Recommended Provisions for Seismic Regulations for New Buildings,” FEMA 222A/223A, May, Vol. 1 (Provisions) and Vol. 2 (Commentary).

NUREG/CR-6728, “Technical Basis for Revision of Regulatory Guidance on Design Ground Motions: Hazard- and Risk-consistent Ground Motion Spectra Guidelines,” U.S. Nuclear Regulatory Commission, Office of Nuclear Regulatory Research, Washington D.C. 20555-0001.

Olsen, K., Pechmann, J. C., and Schuster, G. T. “Simulation of 3D Elastic Wave Propagation in the Salt Lake Basin,” Bulletin of Seismological Society of America, Vol. 85, No. 6, pp. 1688-1710, December 1995.

Oyo Corporation, 1992. “Operation Manual, Model-3331, Suspension PS Log 170,” June 1992.

ProShake, Version 1.1, User’s Manual, EduPro Civil Systems, Inc., Redmond Washington.

Rinne, E., and R. Dobry. 1992. Preliminary Site Recommendations, Memorandum to Roland Sharpe, Chairman TS 2, Building Seismic Safety Council, December 11.

Rollins, K. M., Evans, M. D., Diehl, N. B., Daily, W. D. III., 1998. “Shear Modulus and Damping Relationships for Gravels,” Journal of Geotechnical and Geoenvironmental Engineering, Vol. 124, No. 5, May, 1998, pp. 396-405.

RSPMATCH, “User Guide for Spectral Matching Program RSPMATCH (Version 2.2).

RSPMATCH, “Manual for Program: RSPM22B,” Version: 5/22/97.

Sadigh, K., Chang, C.-Y., Egan, J. A., Makdisi, F., and Youngs, R. R., 1997. “Attenuation Relations for Shallow Crustal Earthquakes Based on California Strong Motion Data,” Seismological Research Letters, Vol. 68, No. 1, January/February 1997.

Saye S. R., and Ladd, C. C., 2000. “Design and Performance of the Foundation Stabilization Treatments for the Reconstruction of Interstate 15 in Salt Lake City, Utah,” URS Corporation specialty conference, June 2000.

Schnabel, P. B., Lysmer, J. and Seed H. B., 1972. “SHAKE - A computer program for earthquake analysis of horizontally layered sites,” Earthquake Engineering Research Center, University of California, Berkeley, Report No. EERC 72-12.

Seed, R. B., Cetin, K. O., Moss, R. E. S., Kammerer, A. M., Wu, J., Petana, J. M., Riemer, M. F. (2001). “Recent Advances in Soil Liquefaction Engineering and Seismic Site Response Evaluation,”

Fourth International Conference on Recent Advances in Geotechnical Earthquake Engineering and Soil Dynamics, University of Missouri-Rolla, Rolla, Missouri, 2001, 45 pages, Paper No. SPL-2.

Seed, R. B., Chang, S. W., Dickenson, S. E., and Bray, J. D., 1997. "Site-Dependent Seismic Response Including Recent Strong Motion Data." Proceedings Special Session on Earthquake Geotechnical Engineering, XIV International Conference on Soil Mechanics and Foundation Engineering, Hamburg, Germany, A. A. Balkema Publication, September 6-12, pp. 125-134.

Seed, R. B., Dickenson, S.E., and Mok, C. M., 1992. "Recent Lessons Regarding Seismic Response Analyses of Soft and Deep Clay Sites," Seminar Proceedings - Seismic Design and Retrofit of Bridges, University of California at Berkeley, Department of Civil Engineering and California Department of Transportation, Berkeley, California, June 8 and 9, 1996.

Seed, H. B., and Sun, J. I., 1989. "Implications of Site Effects in the Mexico City Earthquake of Sept. 19, 1985 for Earthquake-Resistant Design Criteria in the San Francisco Bay Area of California," Earthquake Engineering Research Center, College of Engineering, University of California at Berkeley, Report No. UCB/EERC-89/03, March 1989, 124 p.

Seed, H. B., Romo, M. P., Sun, J., Jaime, A., and Lysmer, J., 1987. "Relationships between Soil Conditions and Earthquake Ground Motions in Mexico City in the Earthquake of Sept. 19, 1985," Earthquake Engineering Research Center, College of Engineering, University of California at Berkeley, Report No. UCB/EERC-87/15, October 1987, 112 p.

Seed, H.B., R. T. Wong, I. M. Idriss, and K. Tokimatsu, 1986. "*Moduli and Damping Factors for Dynamic Analyses of Cohesionless Soil*s", Journal of Geotechnical Engineering, ASCE, Vol. 112, No. 11: 1016-1032.

Seed, H. B. and I. M. Idriss, 1982. "Ground motions and soil liquefaction during earthquakes," Earthquake Engineering Research Institute Monograph Series, v. 4, 134 p.

Seed, H. B., R. Murarka, J. Lysmer, and I. M. Idriss. 1976a. "Relationships Between Maximum Acceleration, Maximum Velocity, Distance from Source and Local Site Conditions for Moderately Strong Earthquakes." *Bulletin of the Seismological Society of America* 66 (4):1323--1342.

Seed, H. B., C. Ugas, and J. Lysmer, 1976b. "Site Dependent Spectra for Earthquake-Resistant Design." *Bulletin of the Seismological Society of America* 66 (1):221-244.

Seed, H.B., and I. M. Idriss, 1970. *Soil Moduli and Damping Factors for Dynamic Response Analyse*s, Report EERC 70-10. Berkeley: University of California, Earthquake Engineering Research Center.

Silva, W. J., Wong, I. G., and Darragh, R. B., 1999. "Surface Geology Based Strong Motion Amplification Factors for the San Francisco Bay and Los Angeles Areas," Final Report prepared for Pacific Gas and Electric Task 5.B, September 27, 1999.

Silva, W. J., and R. B. Darragh, 1995. "Engineering Characterization of Strong Ground Motion Recorded at Rock sites, Electric Power Research Institute, Palo Alto, California, Report No. TR-102262.

Silva, W. J., and Lee, K. 1987. "WES RASCAL code for synthesizing earthquake ground motions: State-of-the-art for assessing earthquake hazards in the United States: U.S. Army Waterways Experiment Station, Report 24, Miscellaneous Paper S-73-1, 120 p.

Silva, W. J., 1997. "Characteristics of Vertical Strong Ground Motions for Applications to Engineering Design," Proceedings of the FHWA/NCEER Workshop on the National Representation of Seismic Ground Motion for New and Existing Highway Facilities," Technical Report NCEER 97-0010, September 22, 1997, pp. 205 - 252.

Silva, W. J., 1988. "Soil response to earthquake ground motion," EPRI Report NP-5747, Electric Power Research Institute, Palo Alto, California.

Somerville, P. G., 2002. "Characterizing Near Fault Ground Motion for the Design and Evaluation of Bridges," Third National Seismic Conference and Workshop on Bridges and Highways, Portland, Oregon, April 29 - May 1, 2002.

Somerville, P. G., 1998a. "Emerging Art: Earthquake Ground Motion," Geotechnical Earthquake Engineerng and Soil Dynamics III," American Society of Civil Engineers Geotechnical Special Publication No. 75, Vol. 1, pp 1-38.

Somerville, P. G., 1998b. "The Characterization and Quantification of Near-Fault Ground Motion, with Implications for the Basin and Range Province," Proceedings Volume Basin and Range Province Seismic-Hazards Summit," Western States Seismic Policy Council, Utah Geological Survey Publication 98-2, pp. 96-109.

Somerville, P. G., Smith, N. F., Graves, R. W., and Abrahamson, N. A., 1997, "Modification of Empirical Strong Ground Motion Attenuations Relations to Include the Amplitude and Duration Effects of Rupture Directivity," Seismological Research Letters, v. 68, p. 199-222.

Somerville, P. G., 1997. "The Characteristics and Quantification of Near Fault Ground Motion," Proceedings of the FHWA/NCEER Workshop on the National Representation of Seismic Ground Motion for New and Existing Highway Facilities, National Center for Earthquake Engineering Research Report No. NCEER-97-0010, pp. 293-318.

Sun, J. I., R. Golesorkhi, and H. B. Seed. 1988. *Dynamic Moduli and Damping Ratios for*

*Cohesive Soil*s, Report UBC/EERC-88/15. Berkeley: University of California, Earthquake Engineering Research Center.

Toro, G. R., McGuire, R. K., and Silva, W. J., 1988. "Engineering model of earthquake ground motion for eastern North America," prepared by Risk Engineering, Inc., EPRI Final Report NP-6074.

UBC, 1997. "Uniform Building Code."

Vucetic, M., and R. Dobry. 1991. "*Effect of Soil Plasticity on Cyclic Response*", Journal of Geotechnical Engineering, ASCE, Vol. 117, No. 1: 89-107.

Wong, I. G., Silva, W., Olig, S., Thomas, P., Wright, D., Ashland, F., Gregor, N., Pechmann, J., Dober, M., Christenson, G., and Gerth, R., 2002. "Earthquake Scenario and Probabilistic Ground Shaking Maps for the Salt Lake City, Utah, Metropolitan Area," Utah Geological Survey Miscellaneous Publication 02-5.

Wong I. G. and Silva, W. J., 1993. "Site-Specific Strong Ground Motion Estimates for the Salt Lake Valley, Utah," Utah Geological Survey Miscellaneous Publication 93-9.

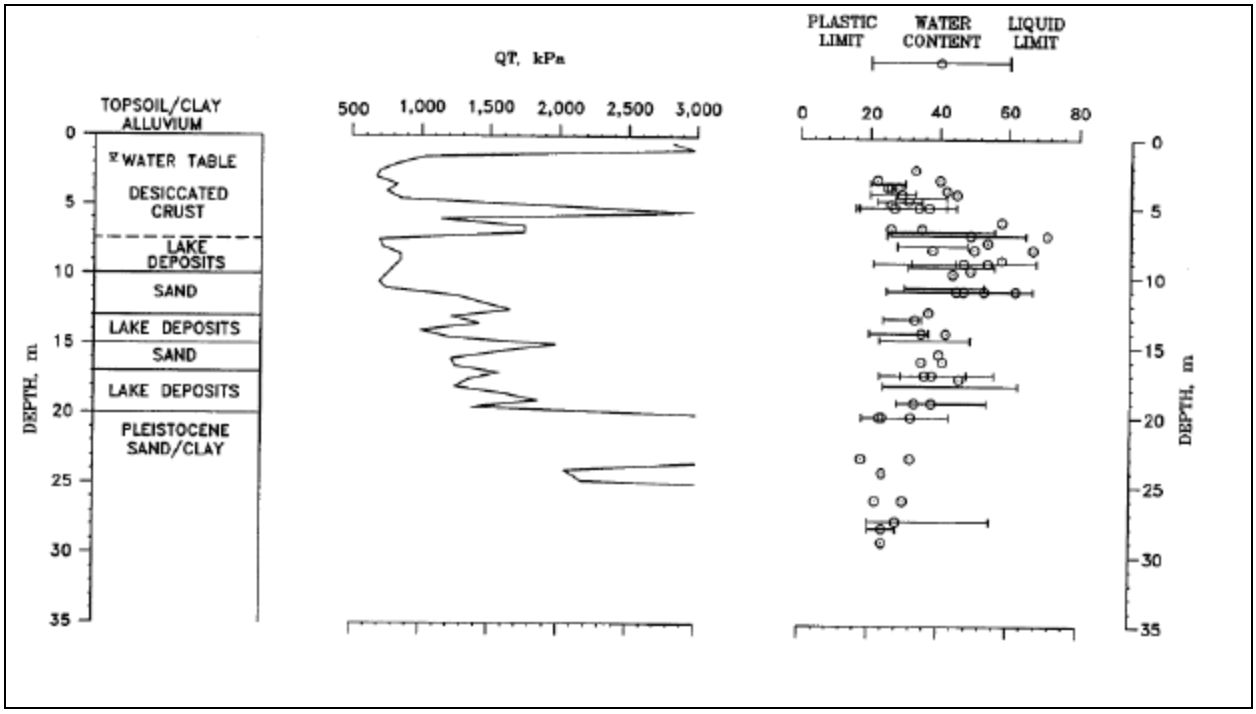

Figure 1. Generalized geotechnical and cone penetrometer profile for the 600 South interchange area, Salt Lake City, Utah.

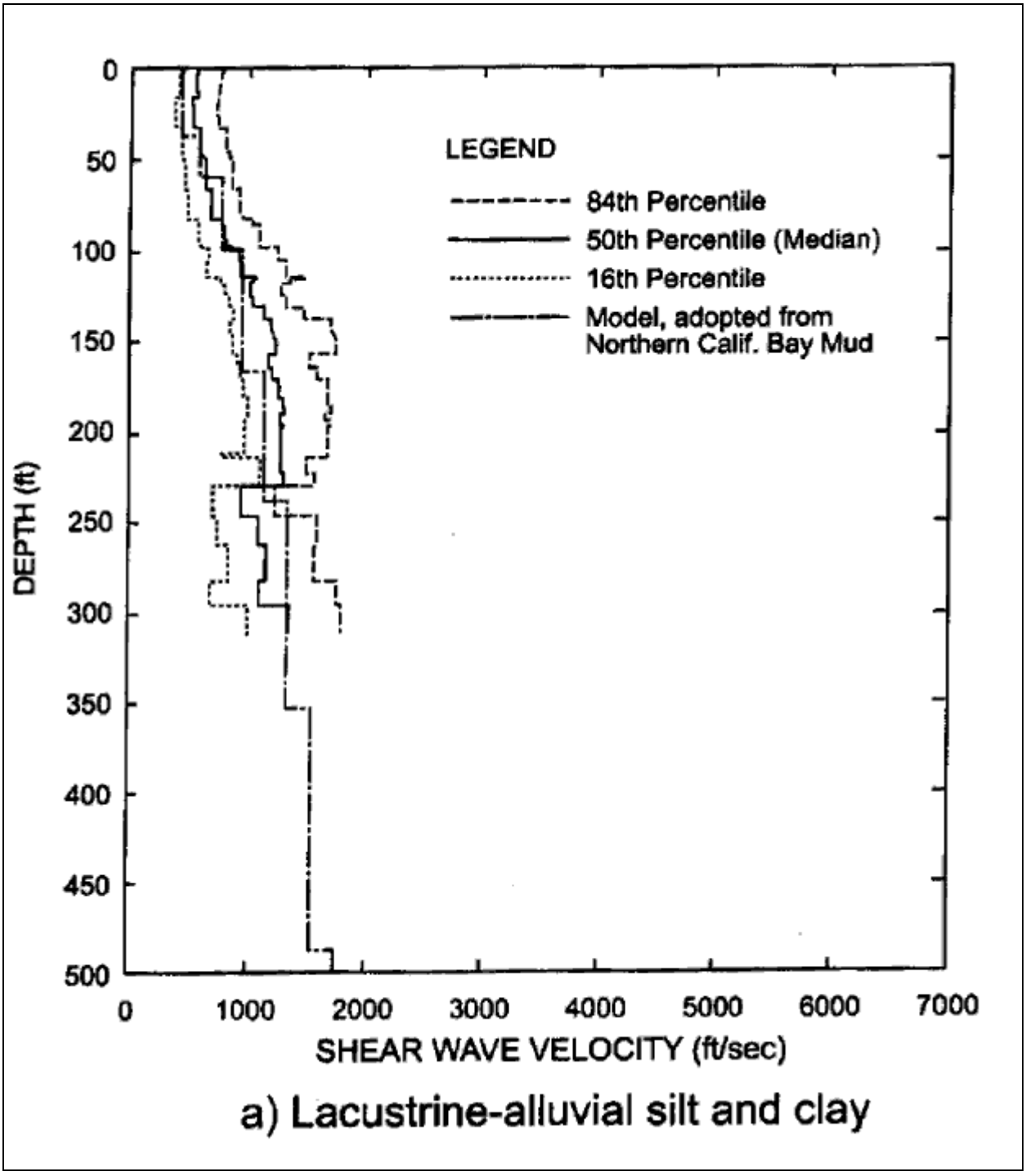

Figure 2. Lacustrine-alluvial silt and clay unit for the Salt Lake Valley (after Wong et al., 2002.)

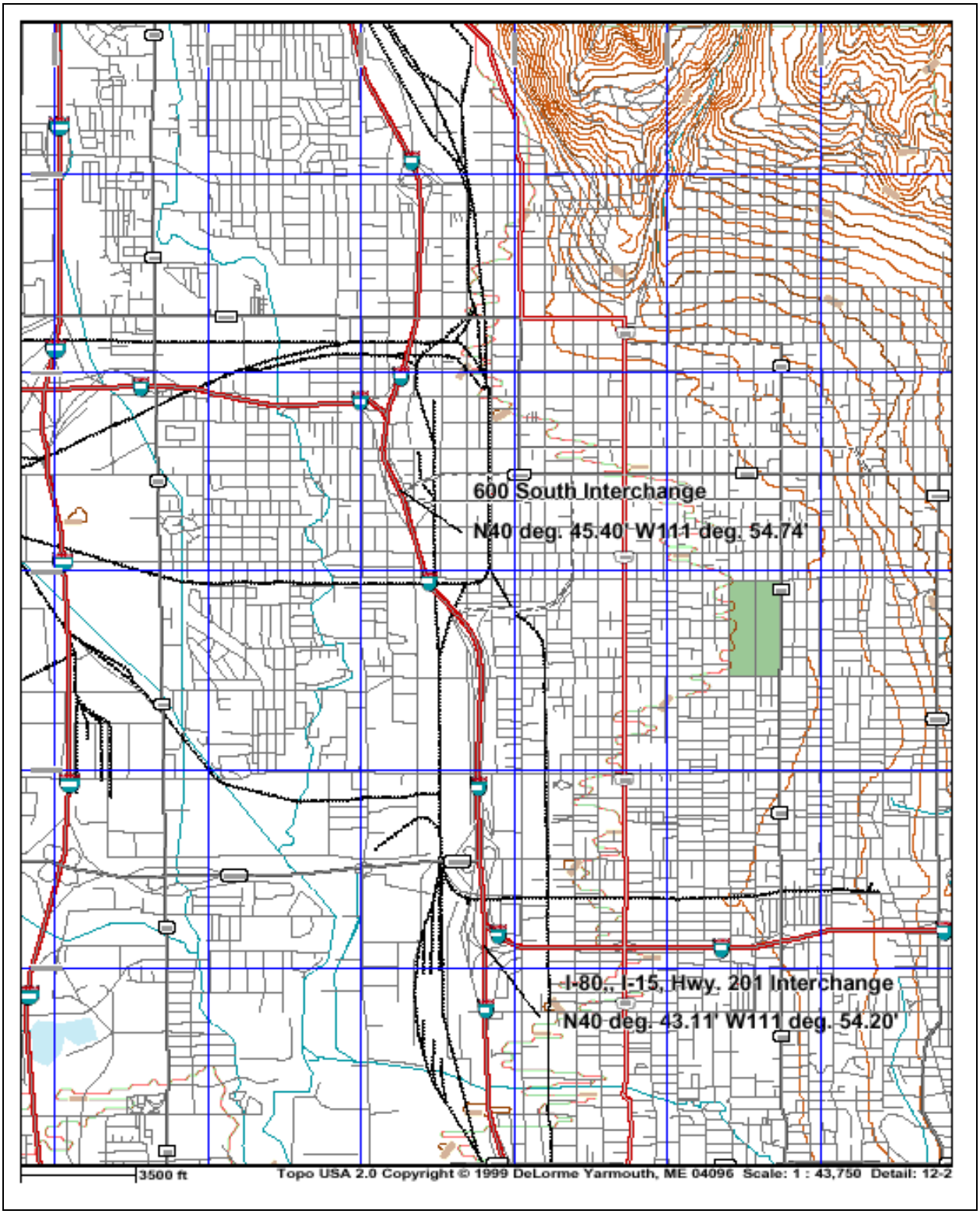

Figure 3. Index Map for 600 South Interchange and I-80, I-15, Highway 201 Interchange.

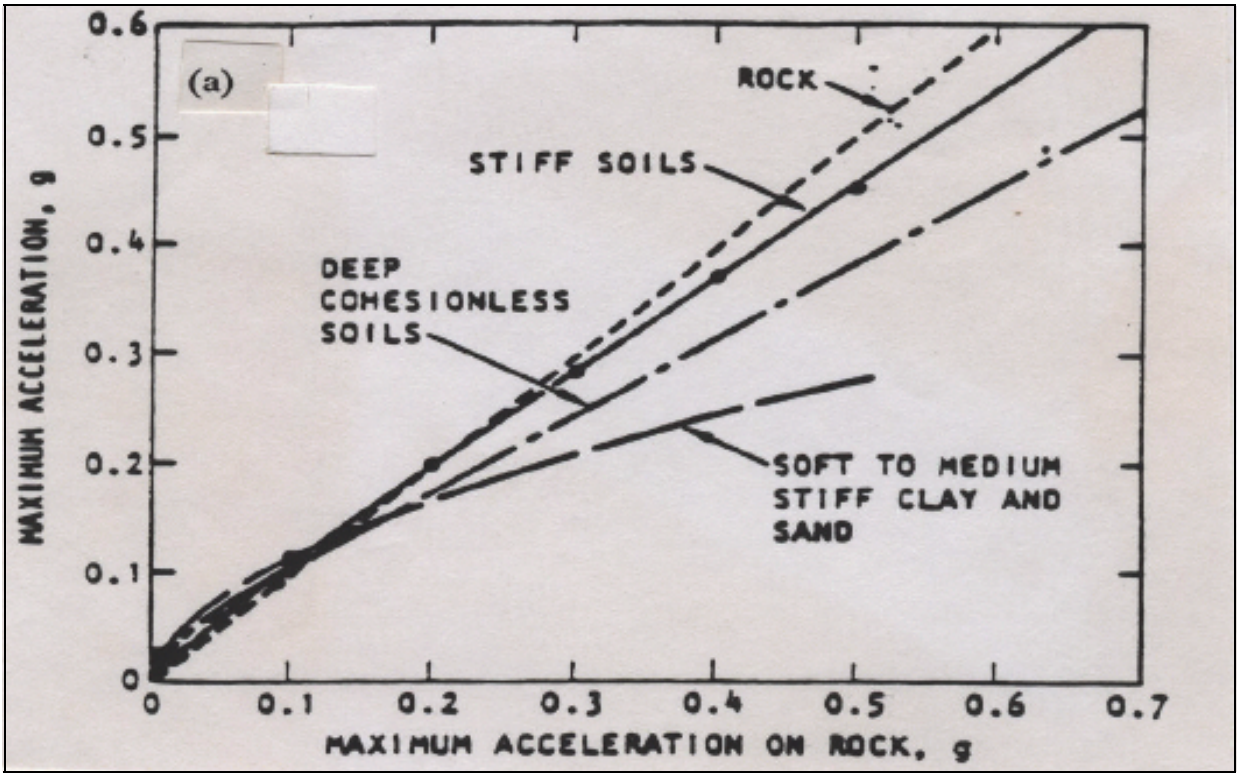

Figure 4. Comparison of maximum acceleration for soil sites with maximum acceleration on rock (Seed et al., 1976a).

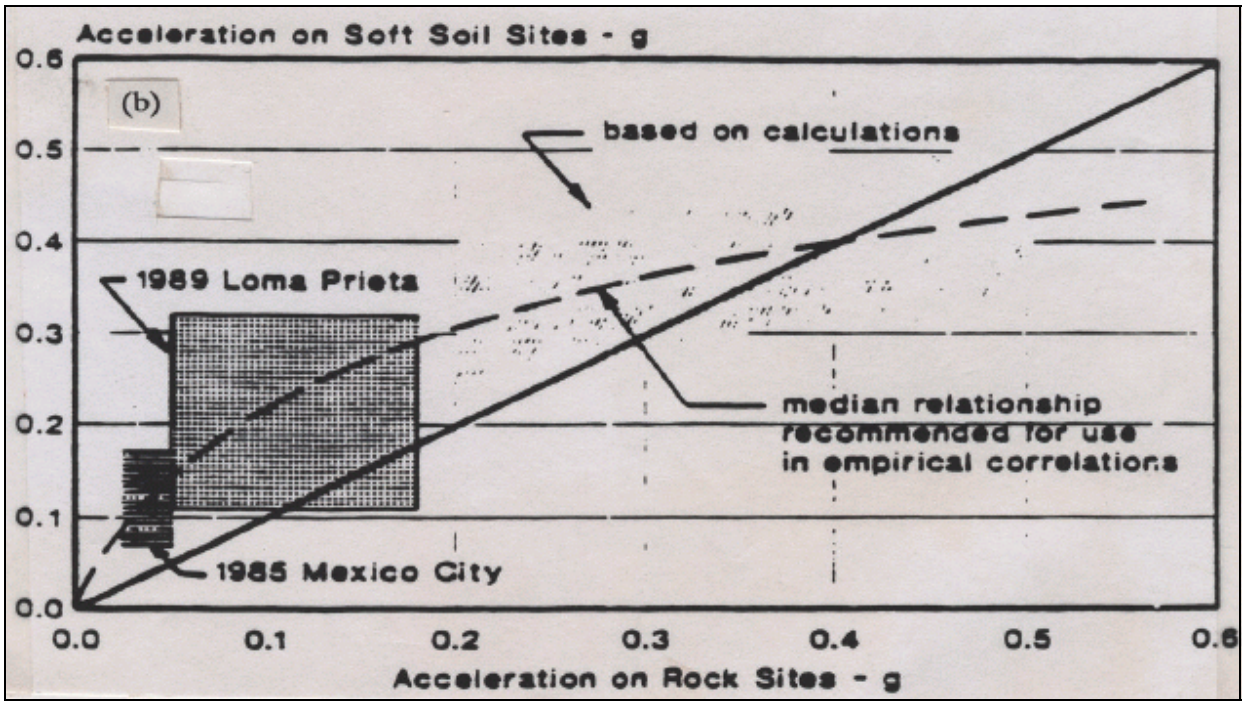

Figure 5. Relationship between maximum acceleration on rock and soft soil sites (Idriss, 1990).

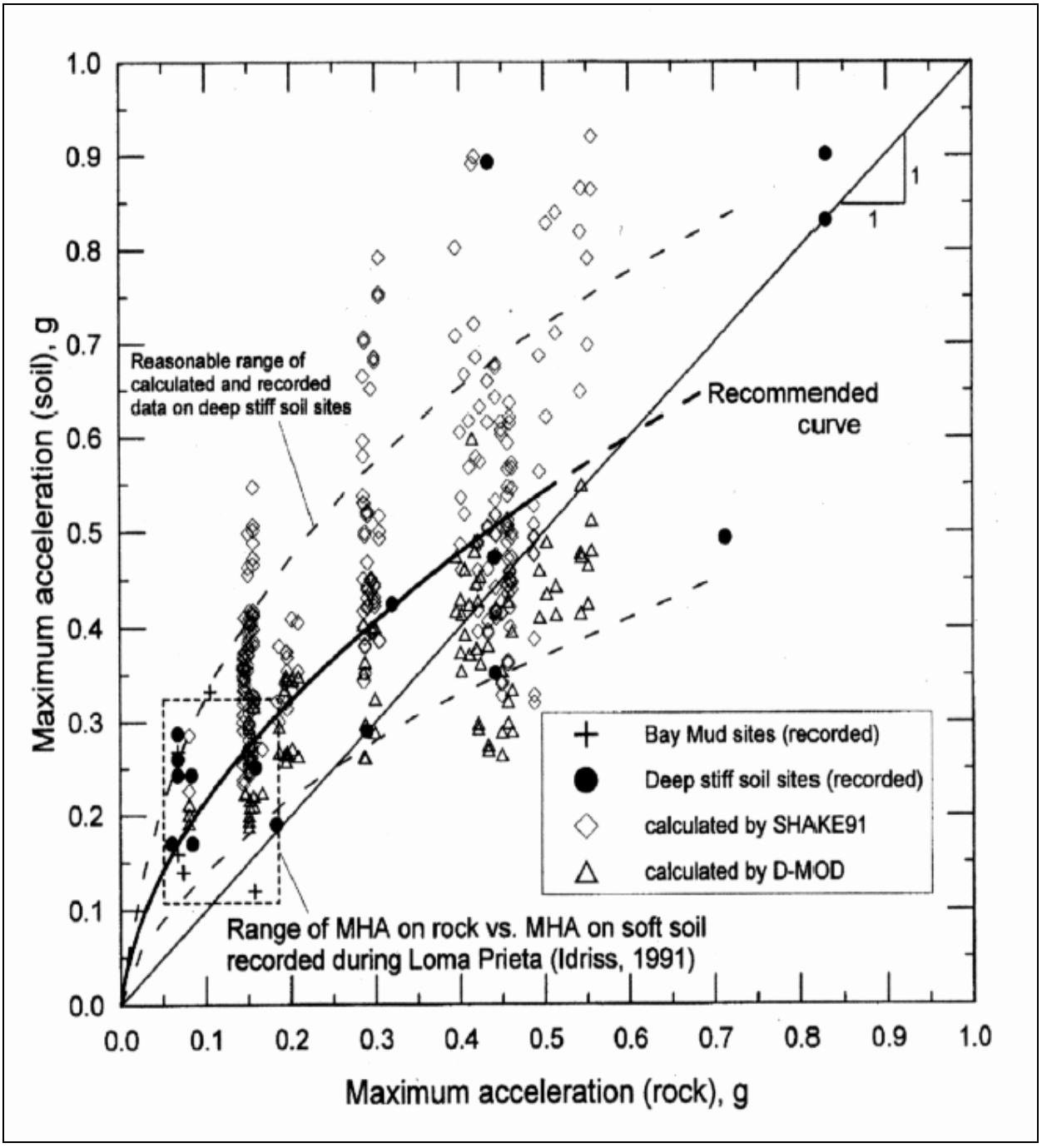

Figure 6. Relationship for a_{max} and $a_{max\ rock}$ for deep stiff soil sites using data from Loma Prieta and Northridge earthquakes and calculations from ground response methods (after Chang et al., 1997).

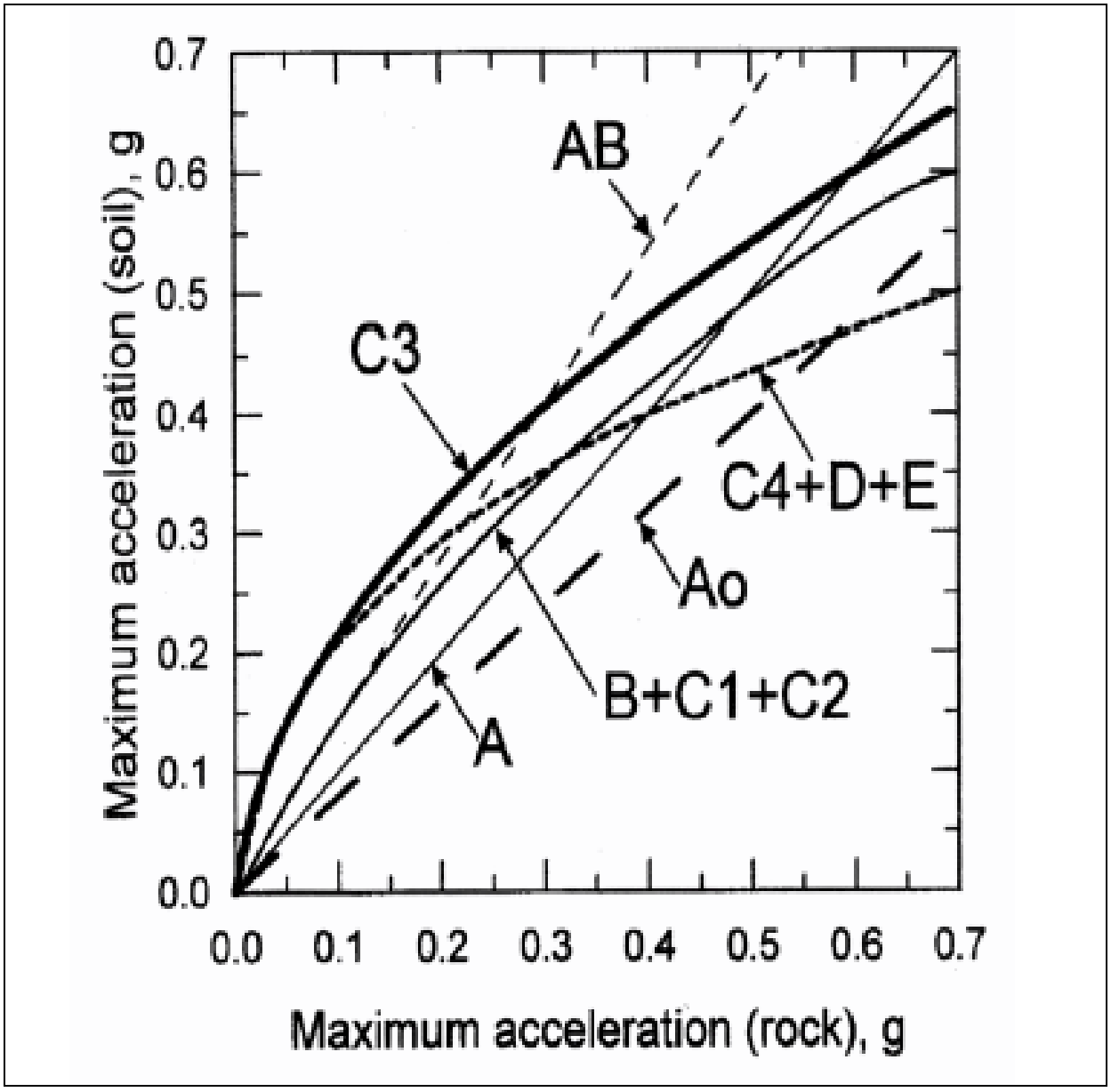

Figure 7. Proposed site-dependent relation between a_{max} and a_{max} for competent rock sites (after Seed et al., 1997).

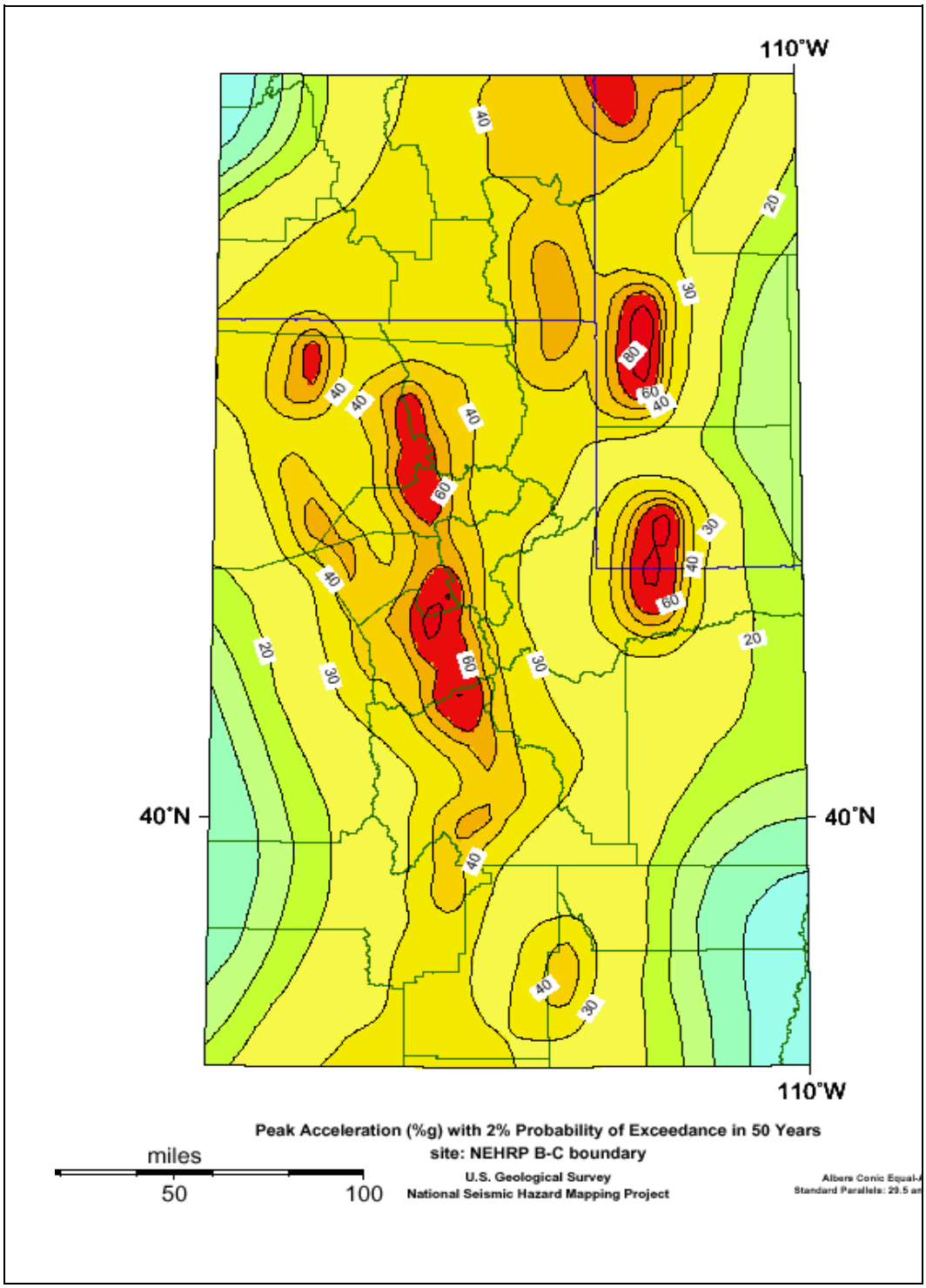

Figure 8. Pga values with 2 percent probability of exceedance in 50 years for Salt Lake and surrounding counties (U.S.G.S. National Seismic Hazard Mapping Project.

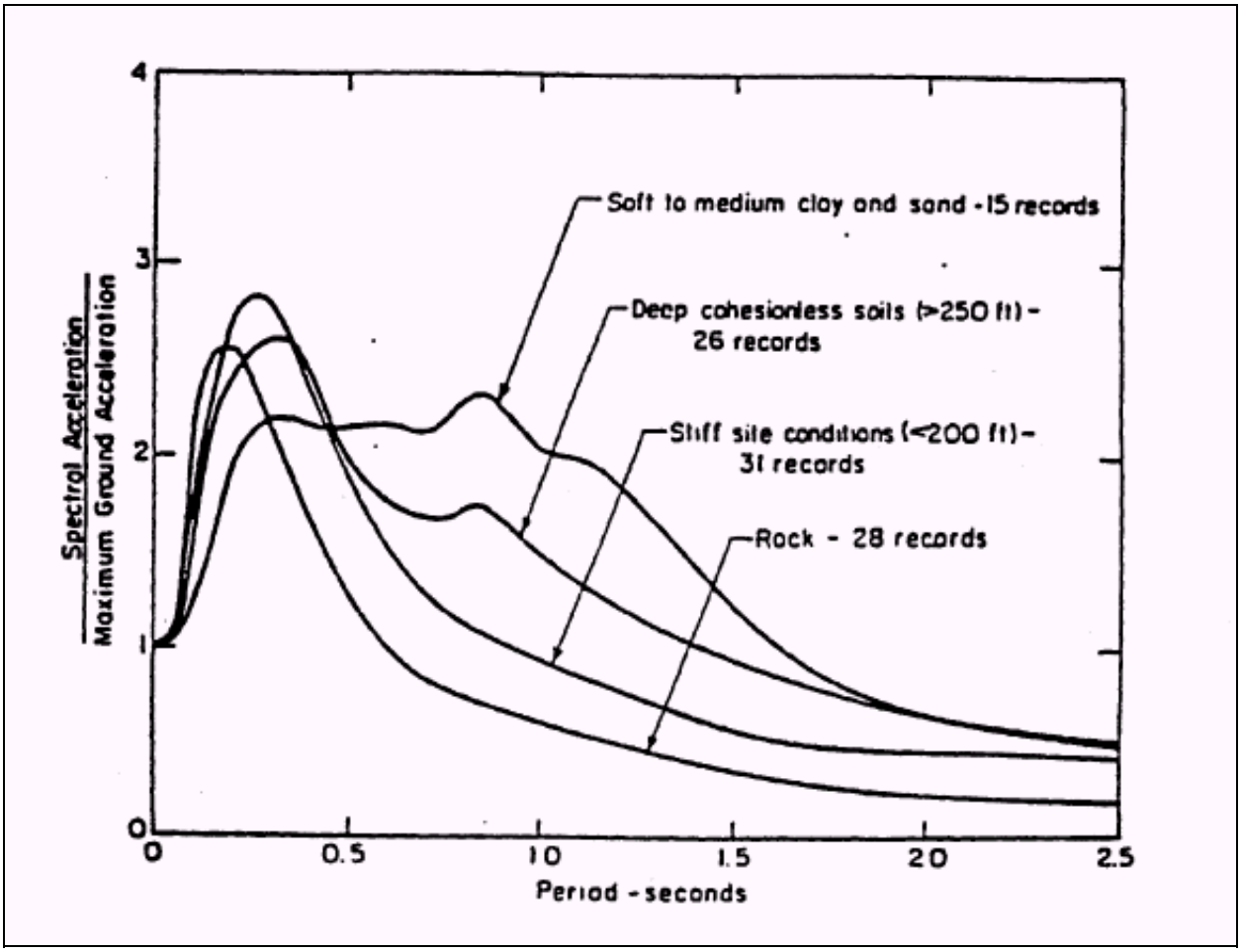

Figure 9. Normalized acceleration response spectra for different soil types (Seed et al., 1976a, 1976 b).

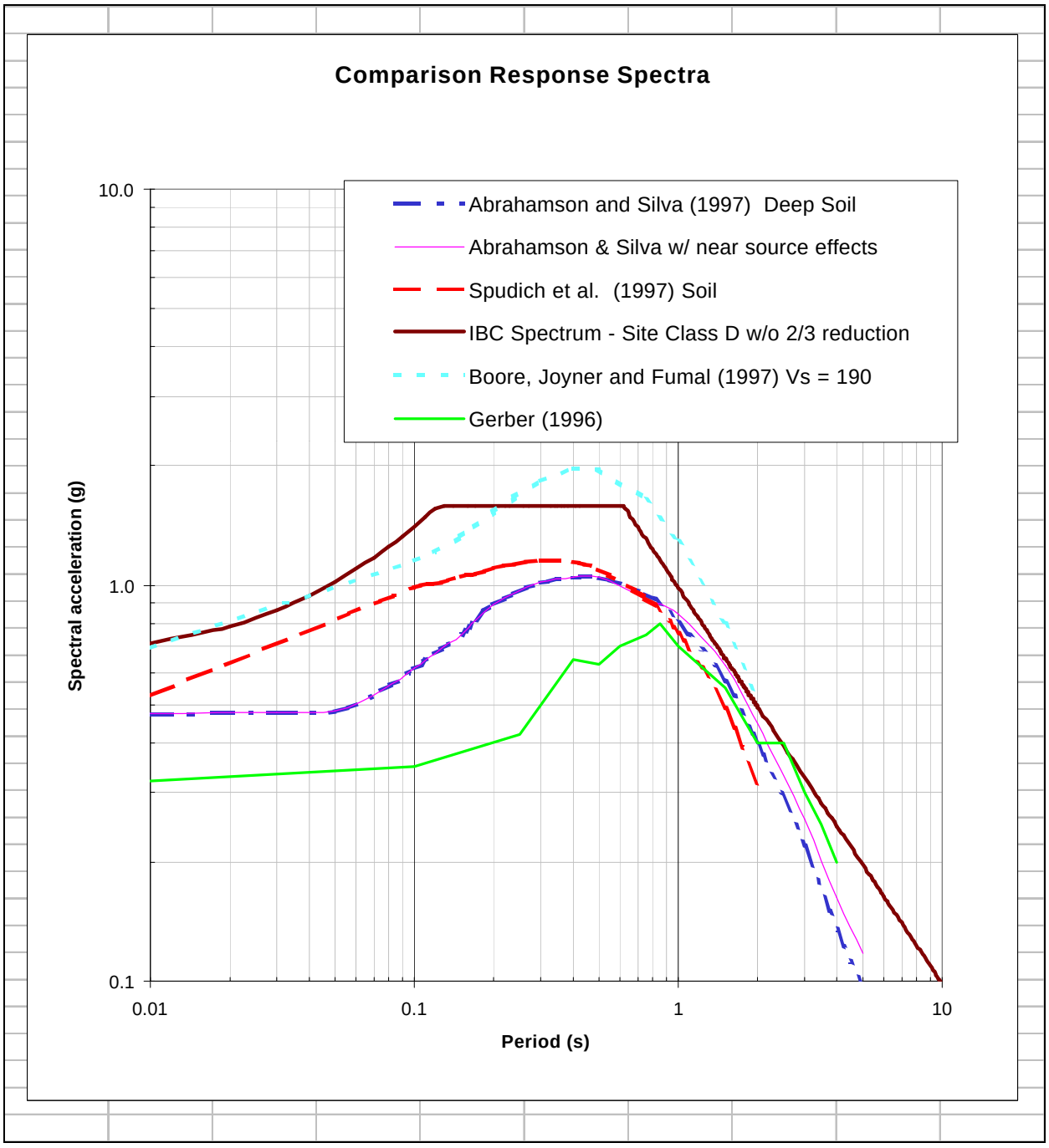

Figure 10. Comparison of IBC site class E soil spectrum with deterministic spectra and ground response modeling for 600 South interchange by Gerber (1996). Deterministic spectra are for soil sites with M = 6.78 and R = 2.9 km.

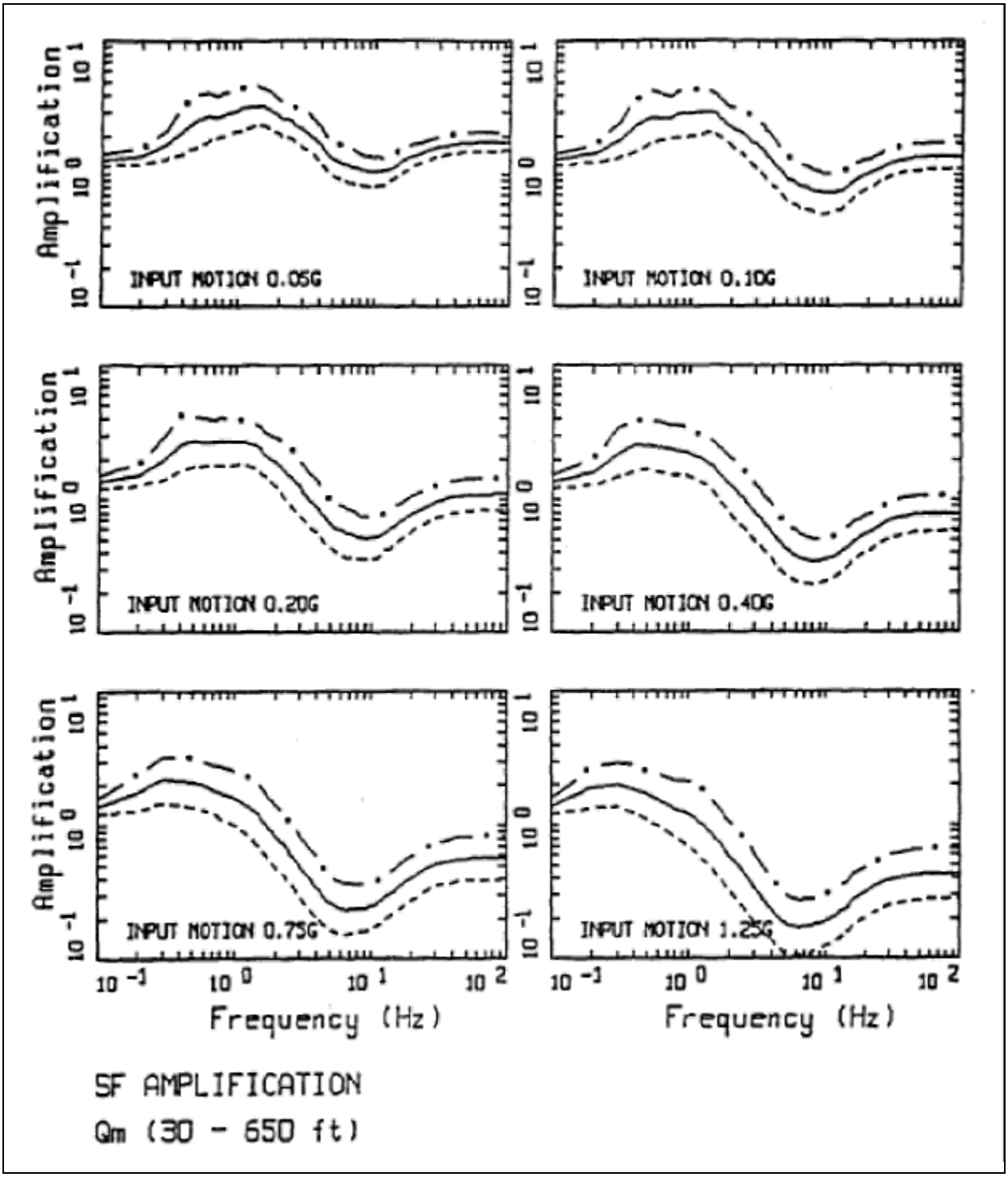

Figure 11. Median and ± 1 sigma amplification factors for the San Francisco Area surficial unit Qm (Bay Mud), Silva et al. 1990.

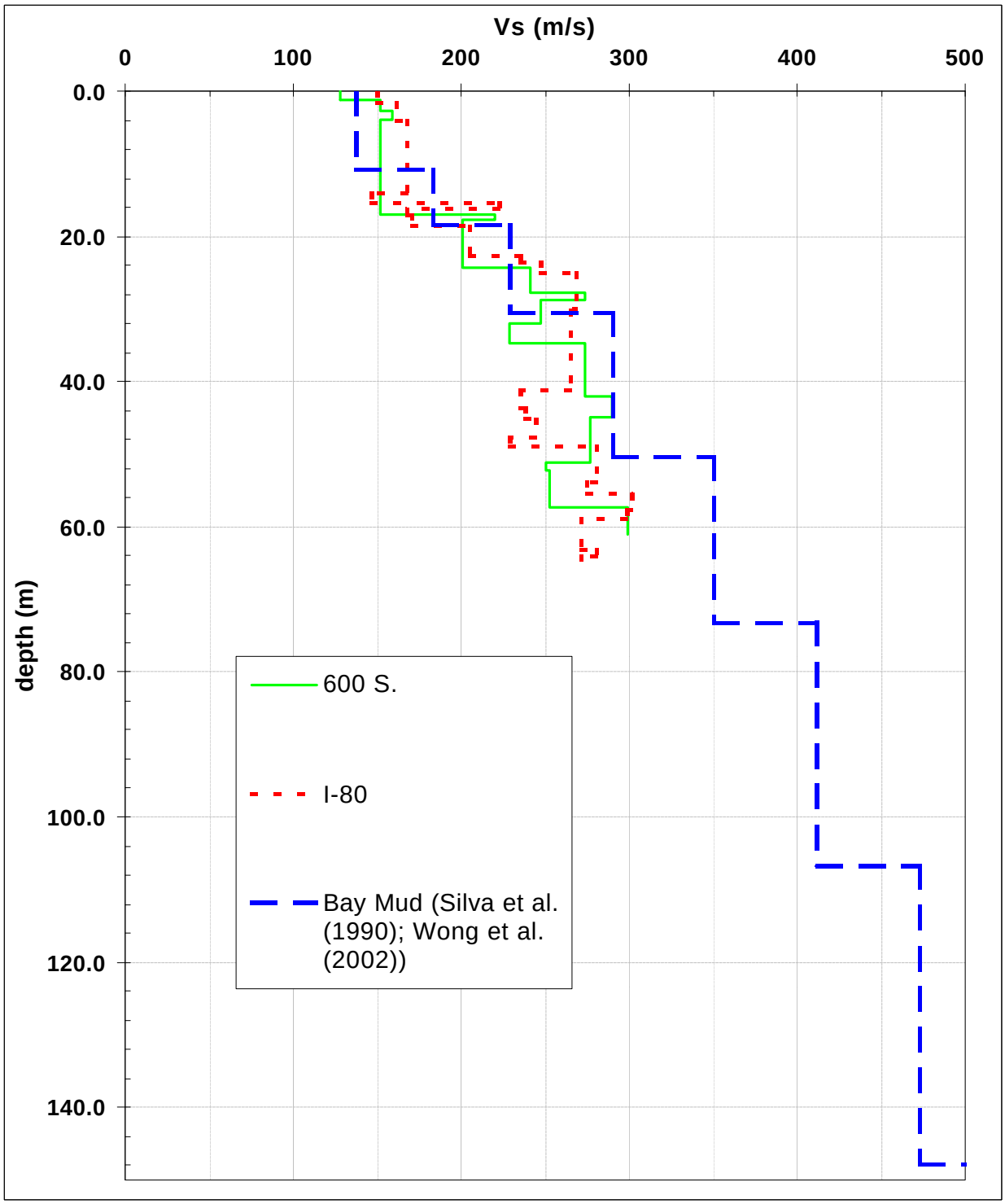

Figure 12. Comparison of the 600 South and I-80 Interchange shear wave velocity profiles from Salt Lake City, Utah with San Francisco Bay mud profile from Silva et al., 1990.

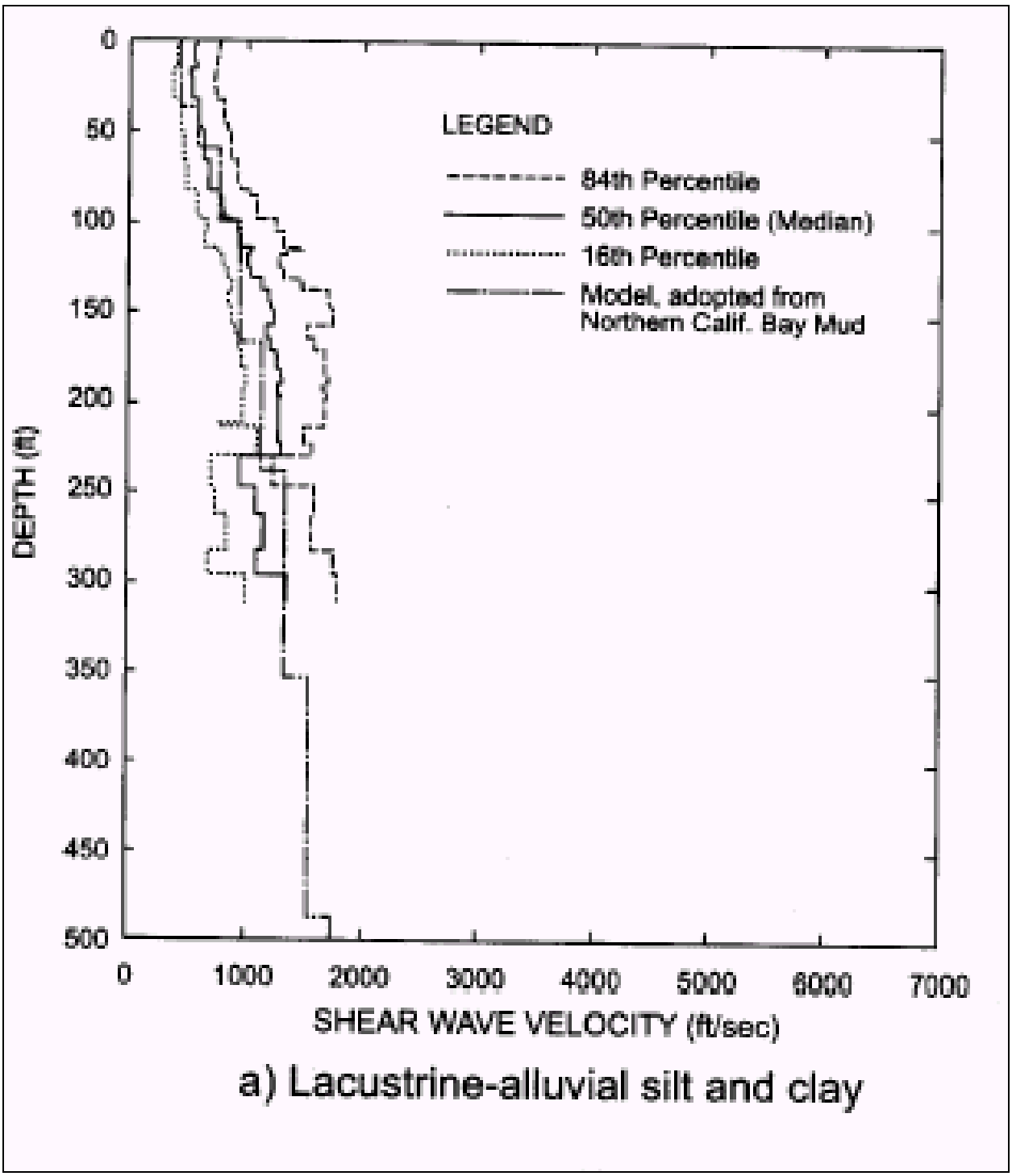

Figure 13. Median, 84th percentile and 16 percentile Vs profiles for the Salt Lake Valley (Wong et al., 2002).

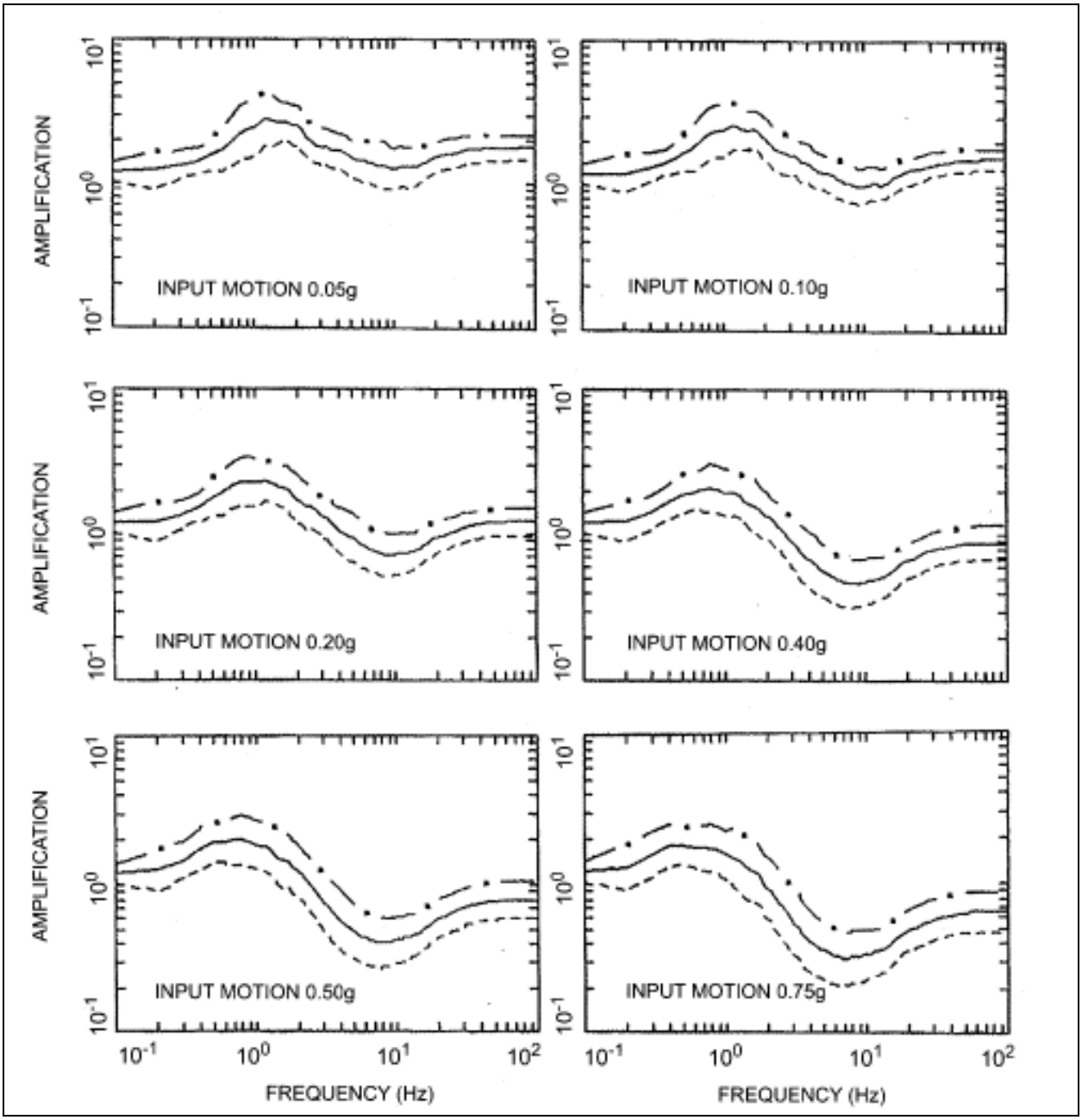

Figure 14. Amplification factors for the lacustrine-alluvial silts and clays (15.2 to 61.0 m thick) as a function of input peak acceleration. The three curves (bottom to top) represent the 16th, median and 84th percentile values (Wong et al., 2002).

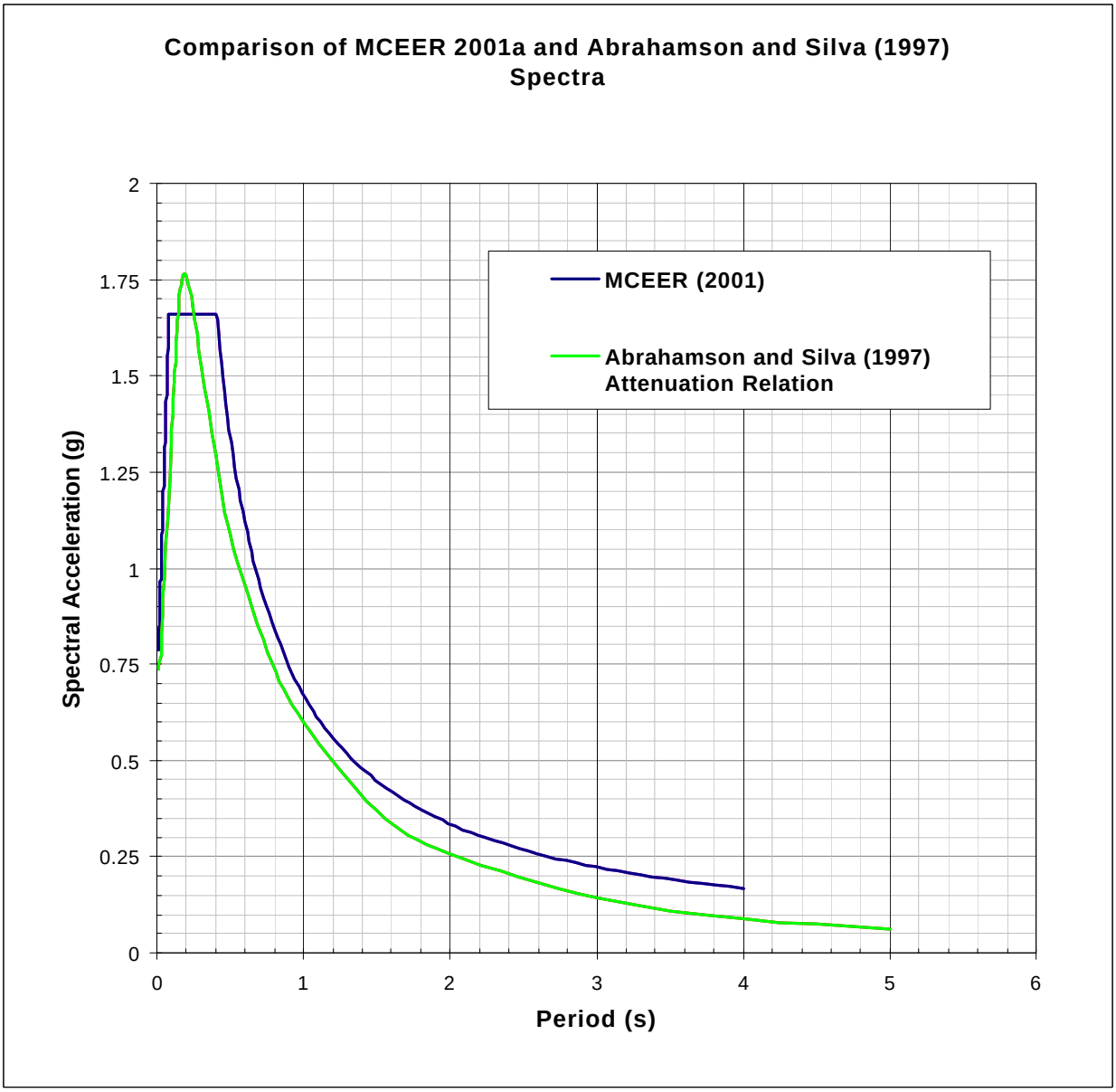

Figure 15. Comparison of response spectra for the I-80 interchange. The MCEER (2001) response spectrum is equivalent to an IBC (2000) spectrum for the MCE. The Abrahamson and Silva (1997) rock spectrum is for M = 7.2, R = 2.5 km.

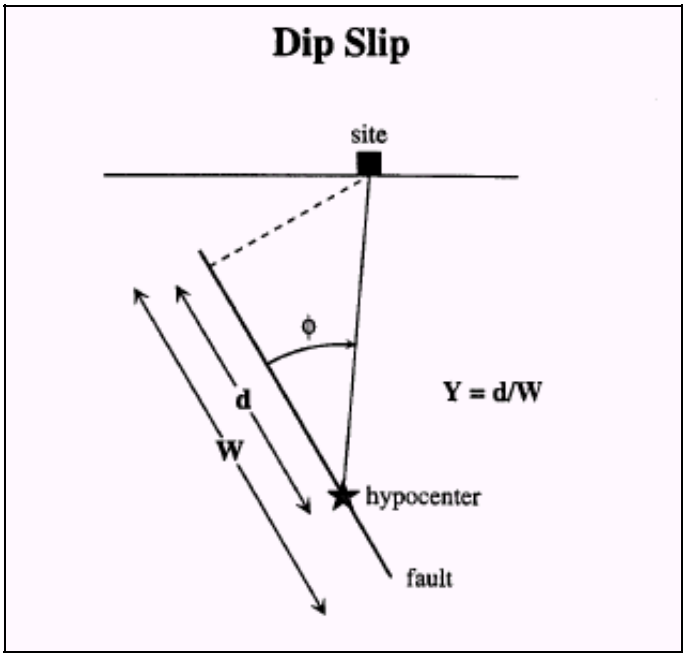

Figure 16a. Definition of rupture directivity parameters for dip slip faults (Sommerville et al., 1997).

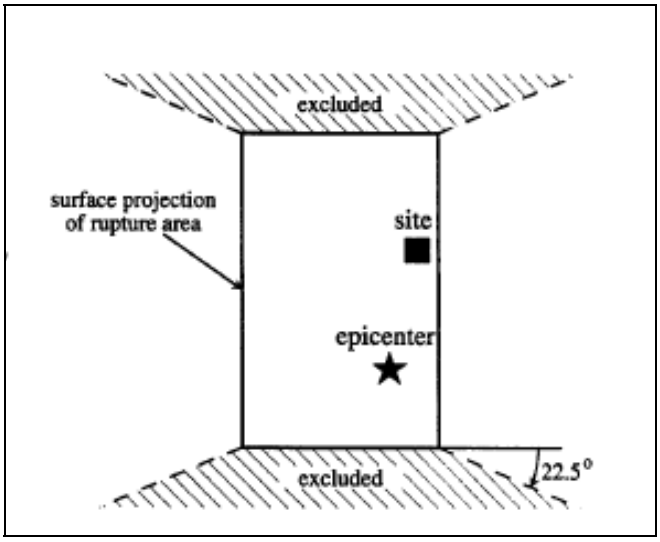

Figure 16b. Region off the end of dip-slip faults is excluded from the model (Sommerville et al., 1997).

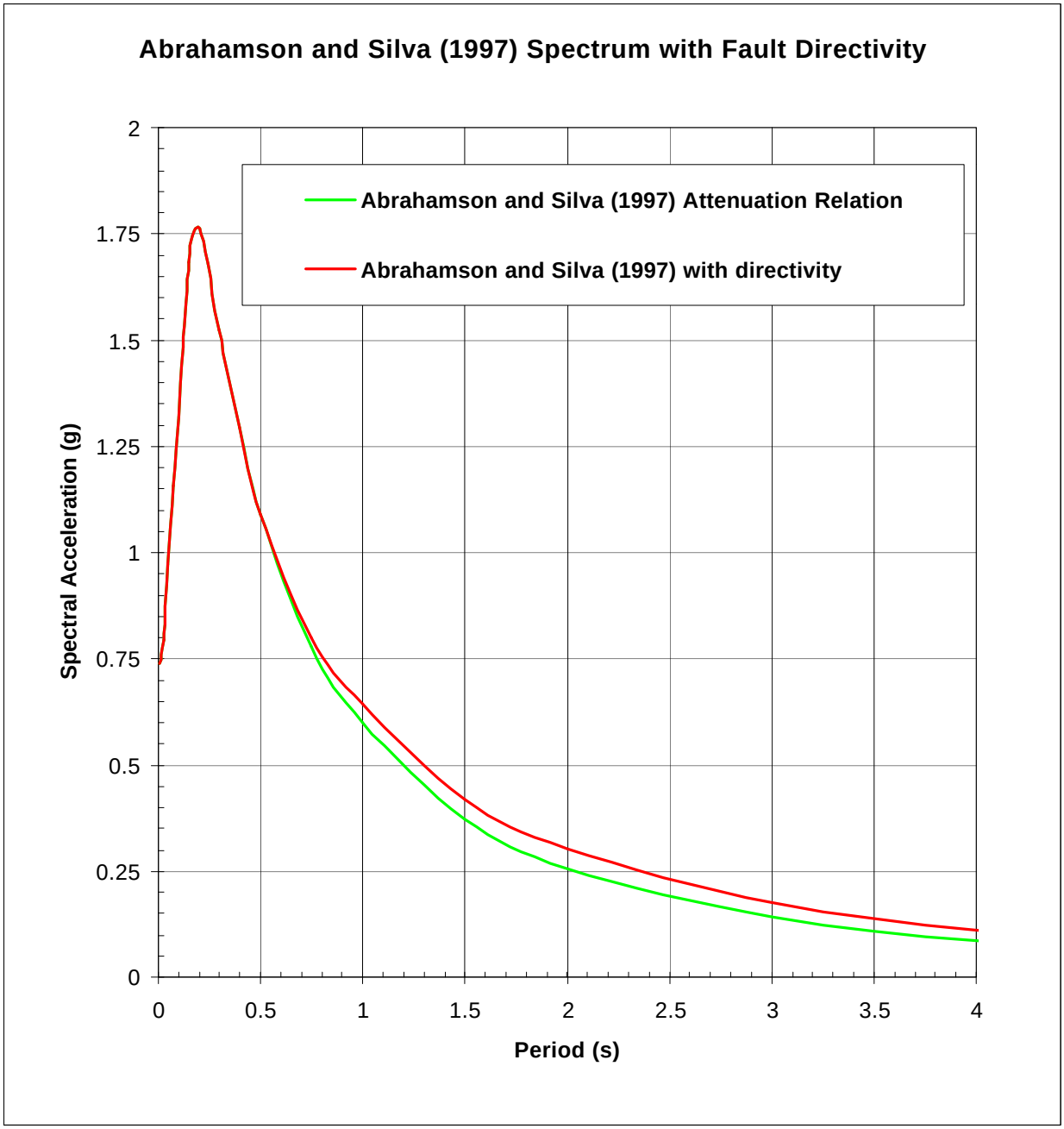

Figure 17. Adjustment of the Abrahamson and Silva (1997) spectrum for fault directivity for the I-80 interchange.

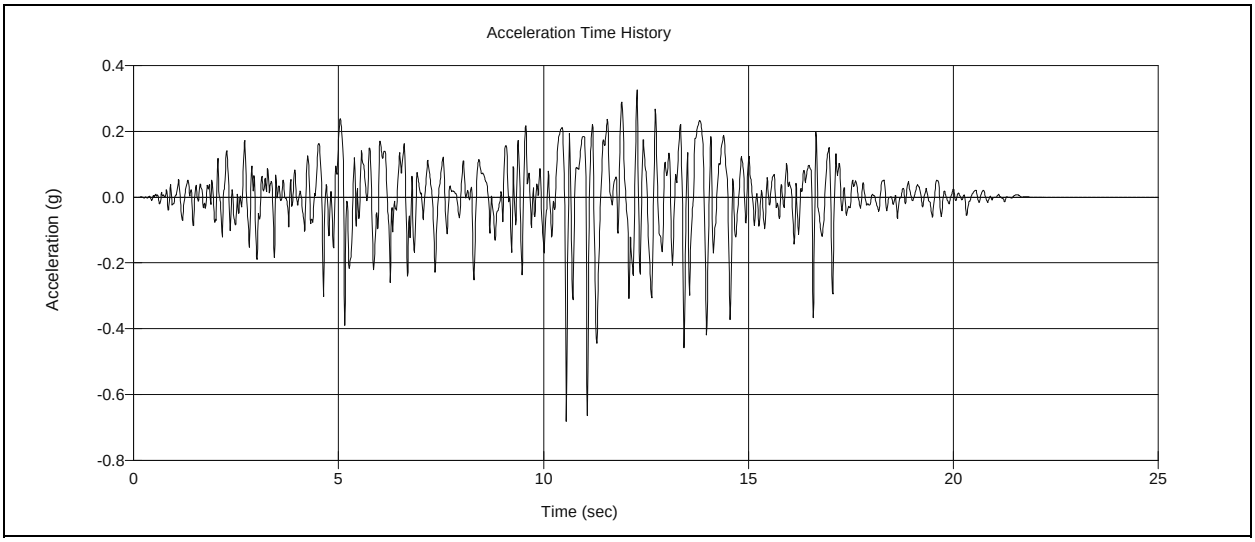

Figure 18a. Unrotated 1987 Superstition Hills Earthquake acceleration time history (45 deg. component).

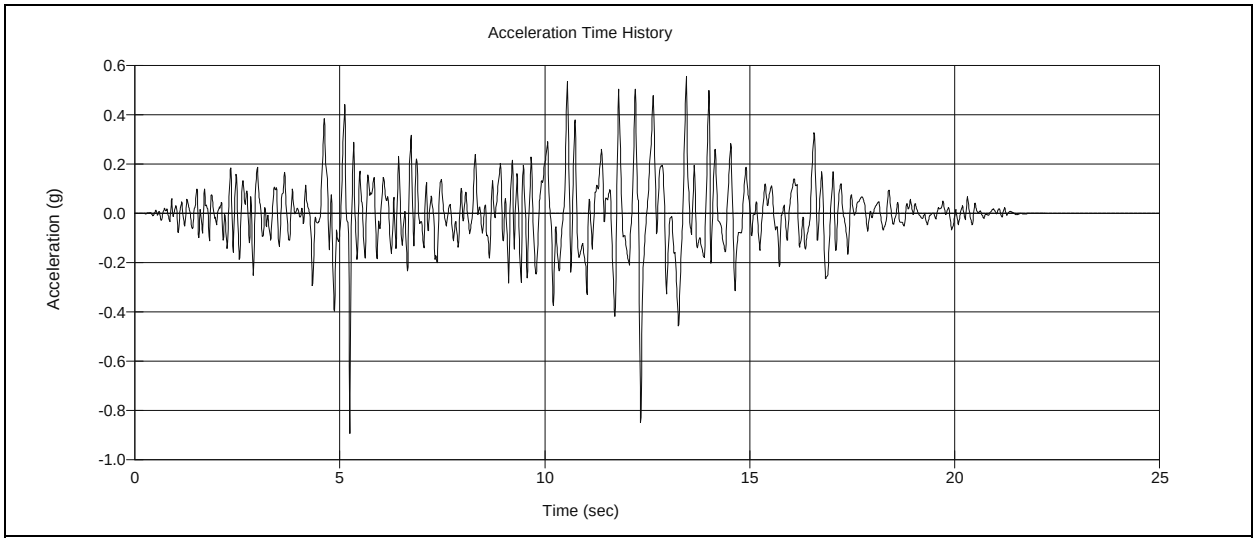

Figure 18b. Unrotated 1987 Superstition Hills Earthquake acceleration time history (135 deg. component).

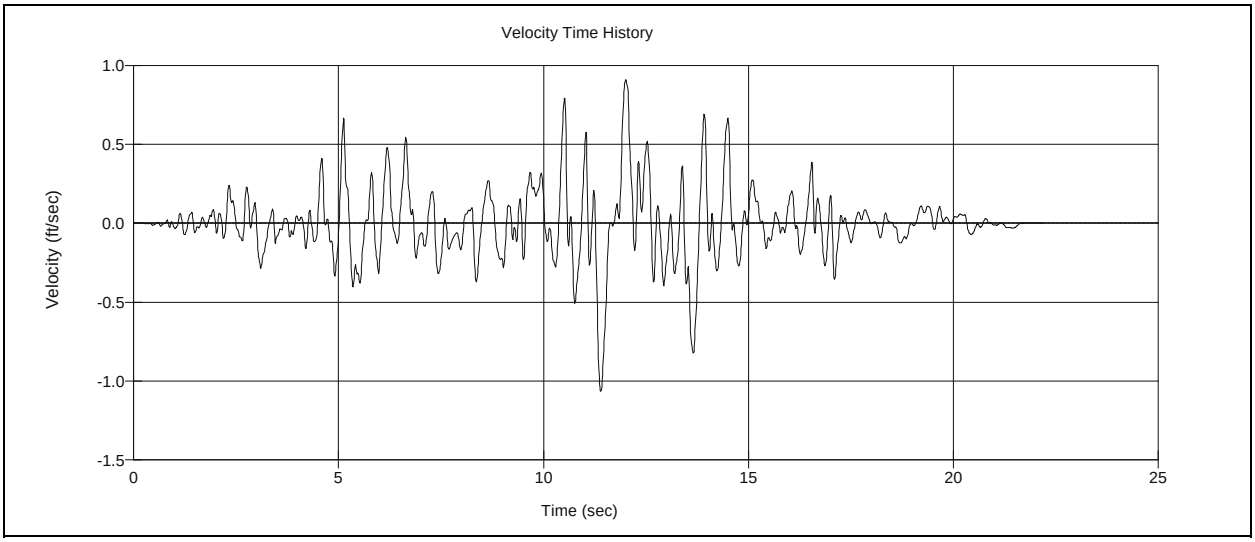

Figure 18c. Unrotated 1987 Superstition Hills Earthquake velocity time history (45 deg. component).

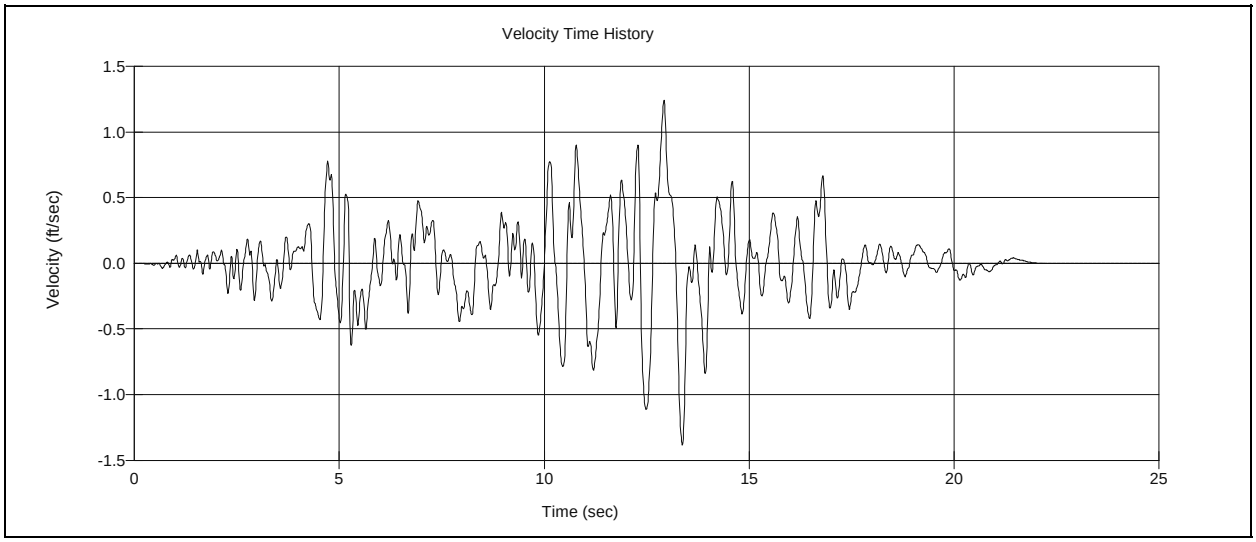

Figure 18d. Unrotated 1987 Superstition Hills Earthquake velocity time history (135 deg. component).

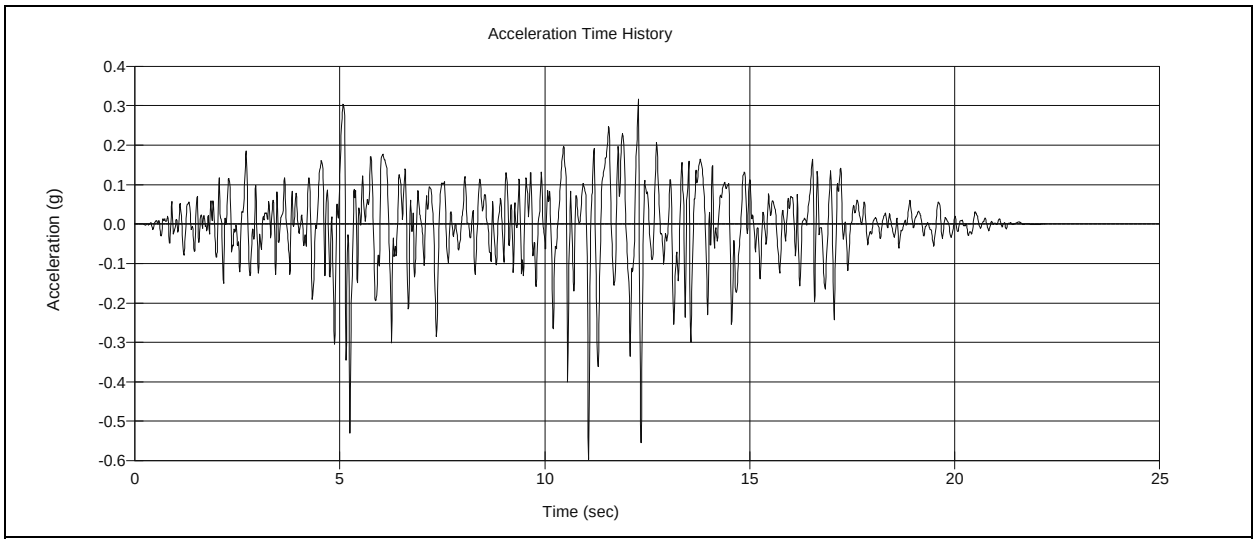

Figure 19a. Rotated 1987 Superstition Hills Earthquake acceleration time history. The time history has been rotated 25 degrees counter-clockwise from the 45 degree direction and is the minor principal component.

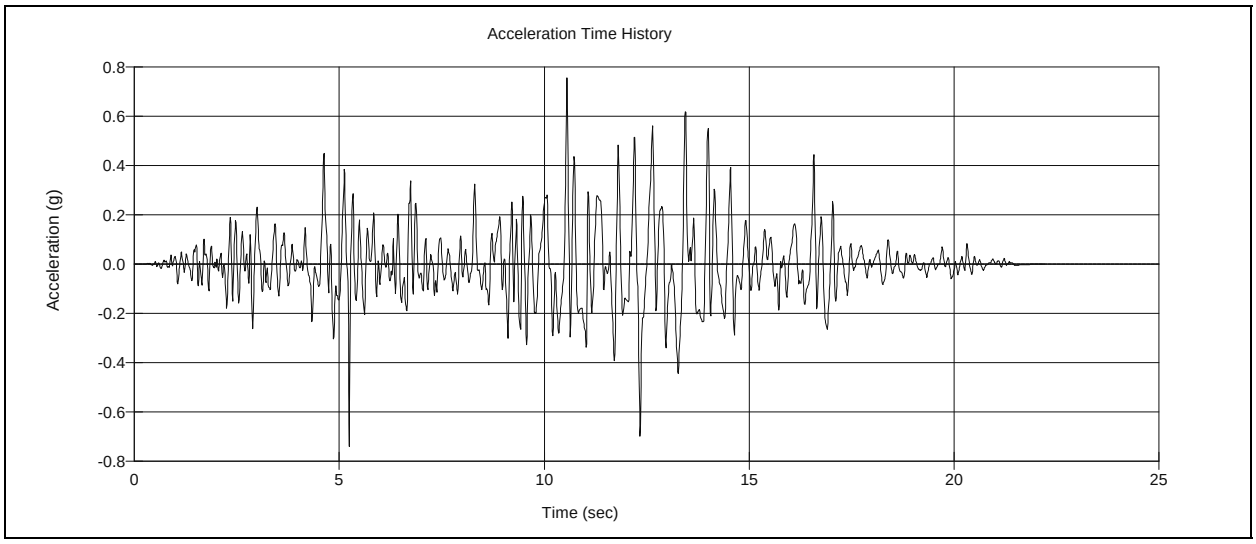

Figure 19b. Rotated 1987 Superstition Hills Earthquake acceleration time history. The time history has been rotated 25 degrees counter-clockwise from the 135 degree direction and is the major principal component.

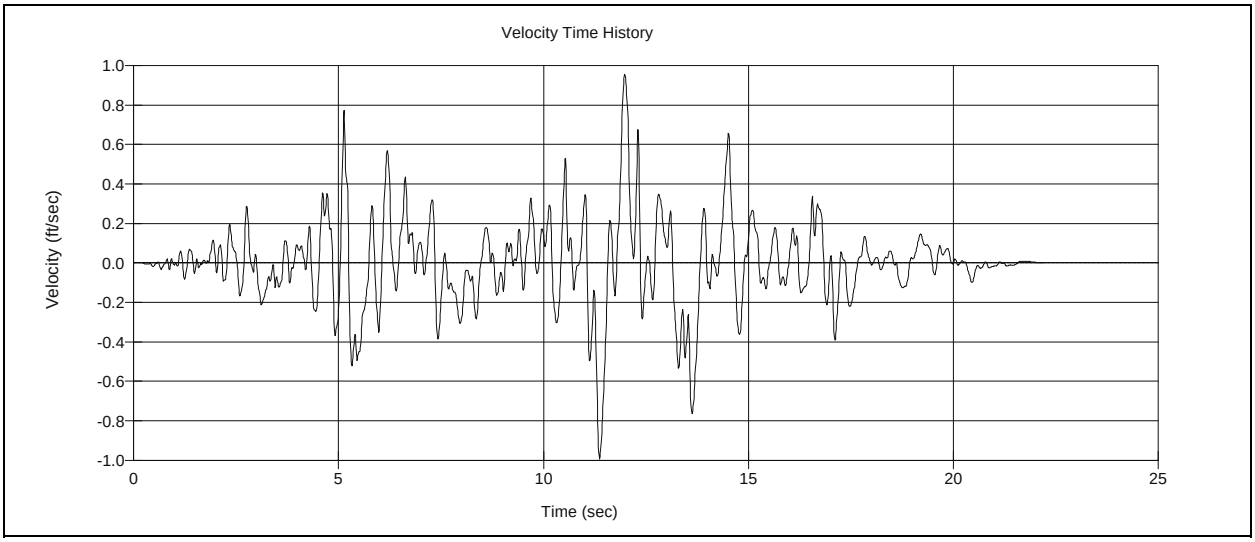

Figure 19c. Rotated 1987 Superstition Hills Earthquake velocity time history. The time history has been rotated 25 degrees in counter-clockwise from the 45 degree direction and is the minor principal component.

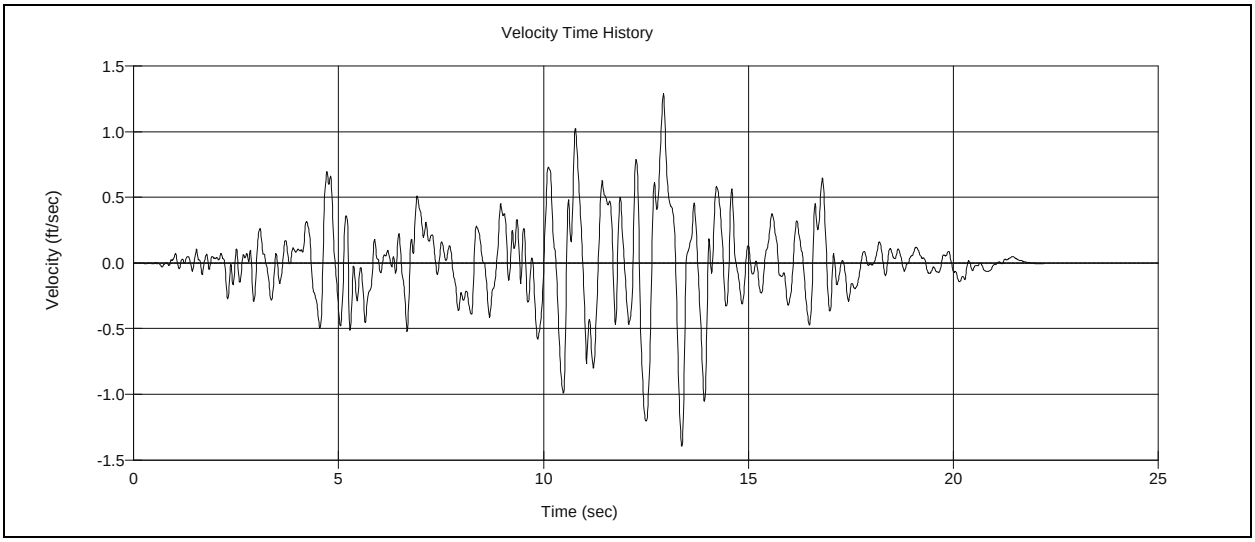

Figure 19d. Rotated 1987 Superstition Hills Earthquake velocity time history. The time history has been rotated 25 degrees in counter-clockwise from the 135 degree direction and is the major principal component.

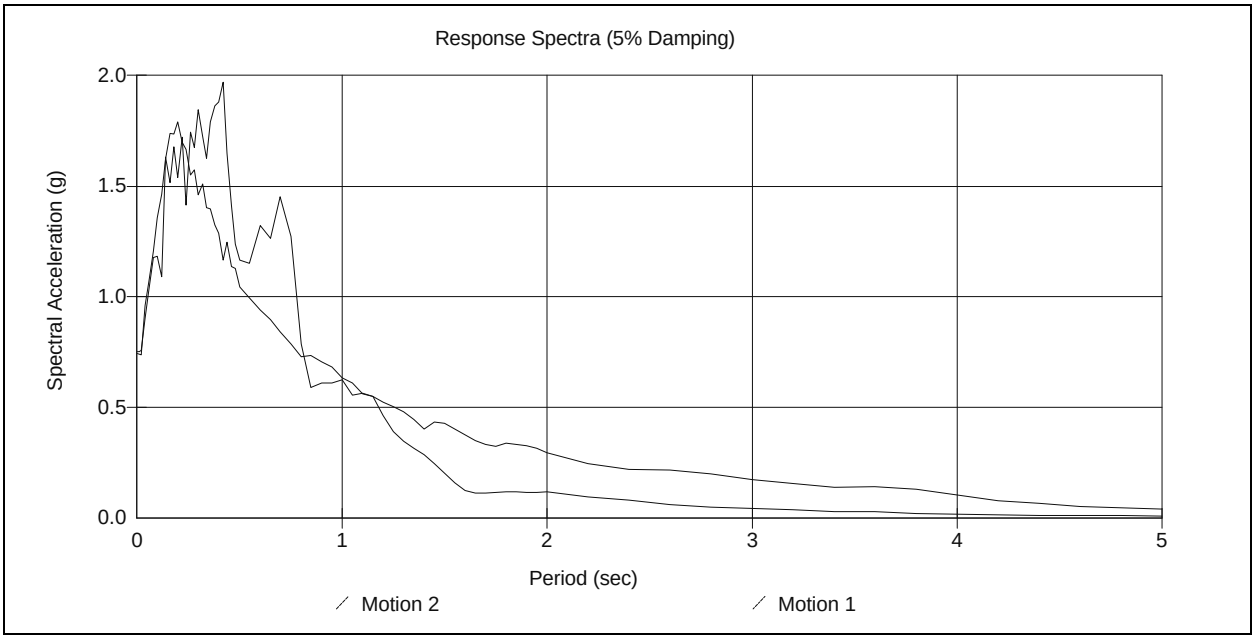

Figure 20a. Comparison of response spectra. Motion 1 is the unmatched major principal component of the 1987 Superstition Hills record and Motion 2 is the spectrally matched major principal component.

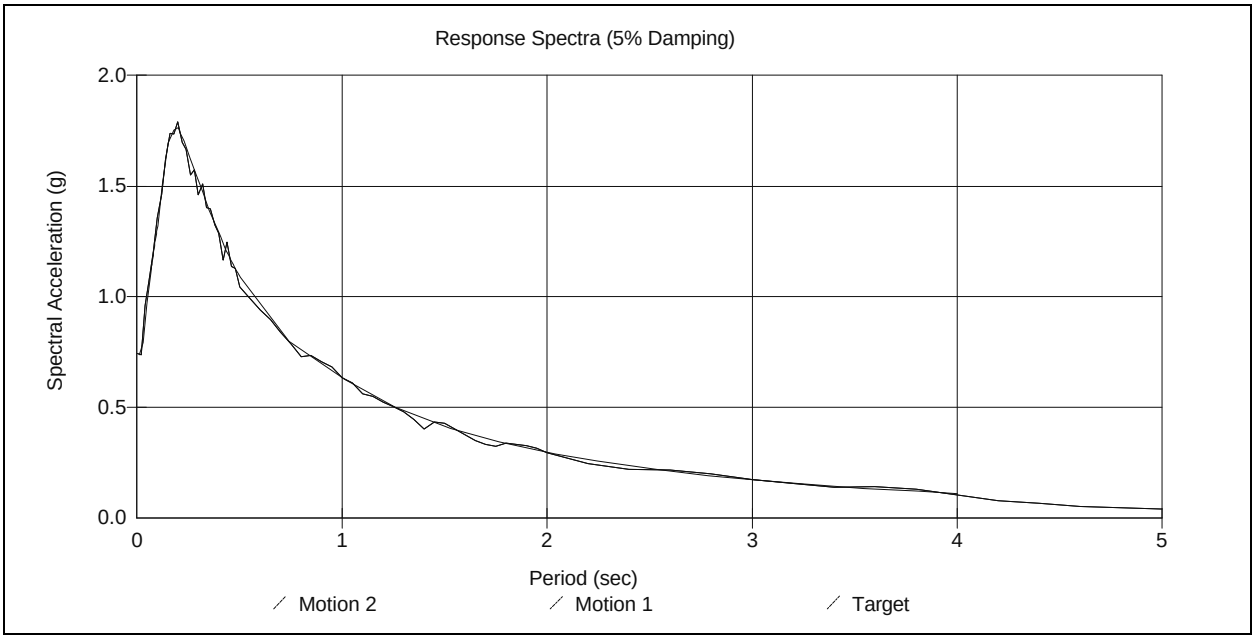

Figure 20b. Comparison of spectrally matched major principal component of 1987 Superstition Hills record with the Abrahamson and Silva I-80 interchange target spectrum with directivity effects.

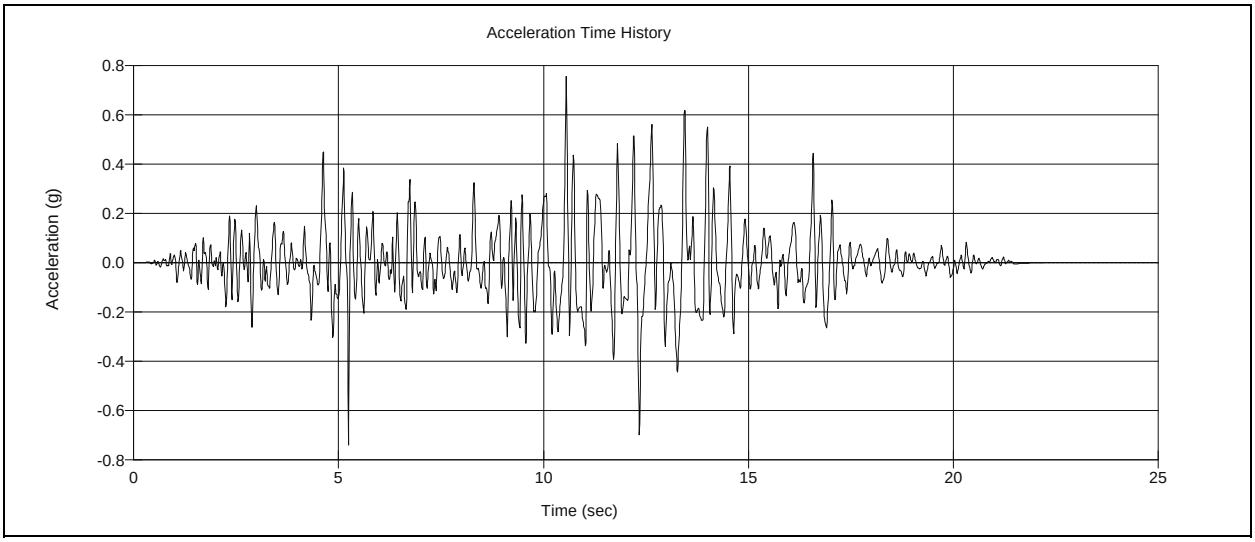

Figure 21a. Acceleration time history for rotated major principal component of the 1987 Superstition Hills acceleration time history.

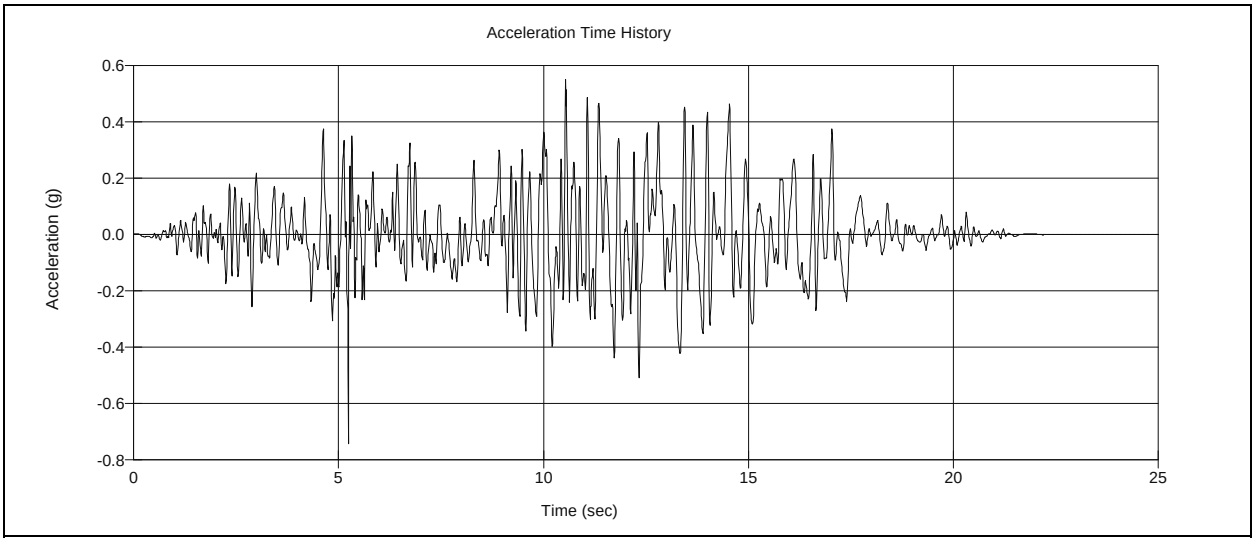

Figure 21b. Acceleration time history for rotated, spectrally matched and baseline corrected major principal component of the 1987 Superstition Hills acceleration time history. Target spectrum is rock Abrahamson and Silva spectrum for the I-80 interchangewith directivity effects.

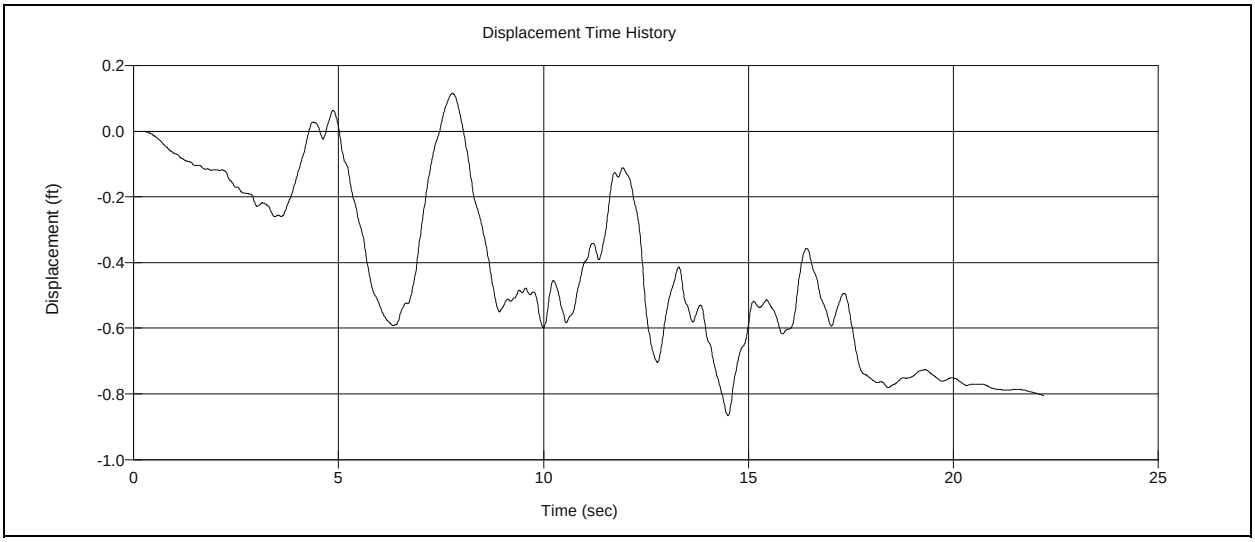

Figure 22a. Spectrally matched and rotated major principal component of 1987 Superstition Hills Earthquake displacement record showing drift in the displacement time history.

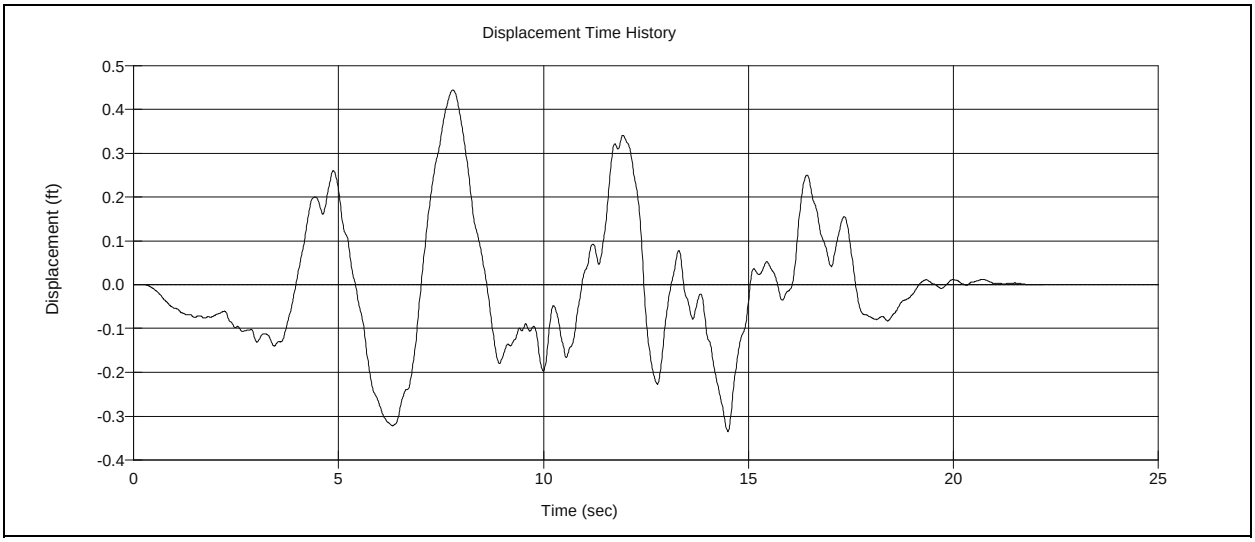

Figure 22b. Spectrally matched and rotated major principal component of 1987 Superstition Hills Earthquake displacement record that has been corrected for baseline drift using computer program BASELINE.

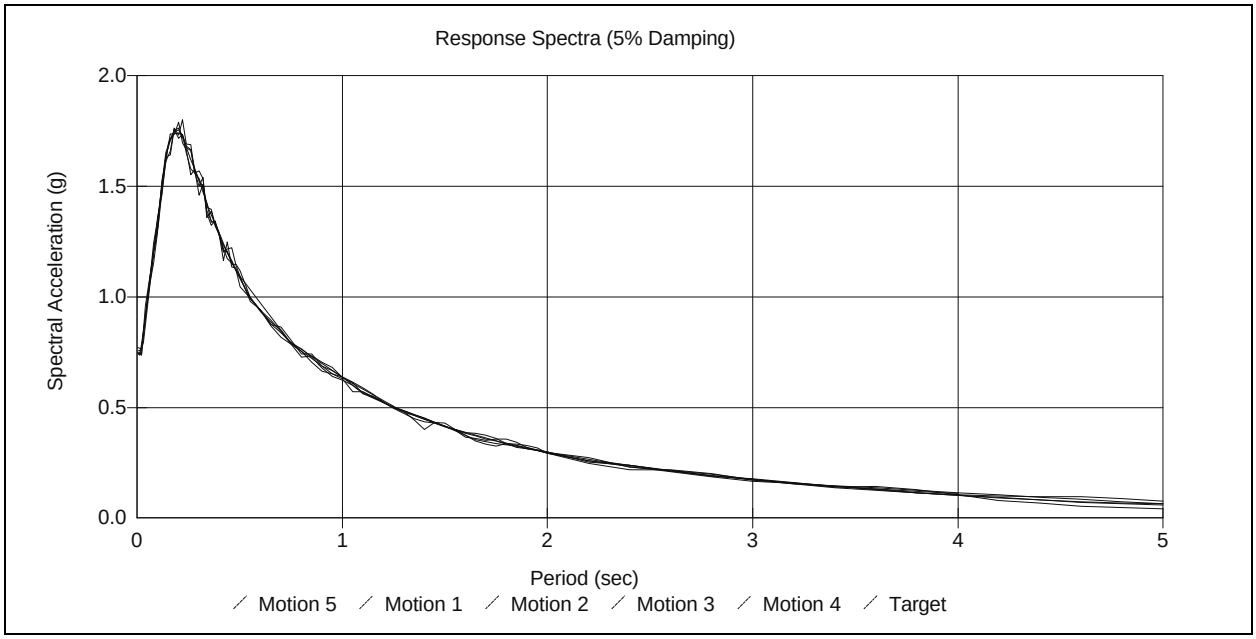

Figure 23a. Comparison of spectrally matched time histories with the target spectrum for the I-80 interchange design spectrum with fault directivity.

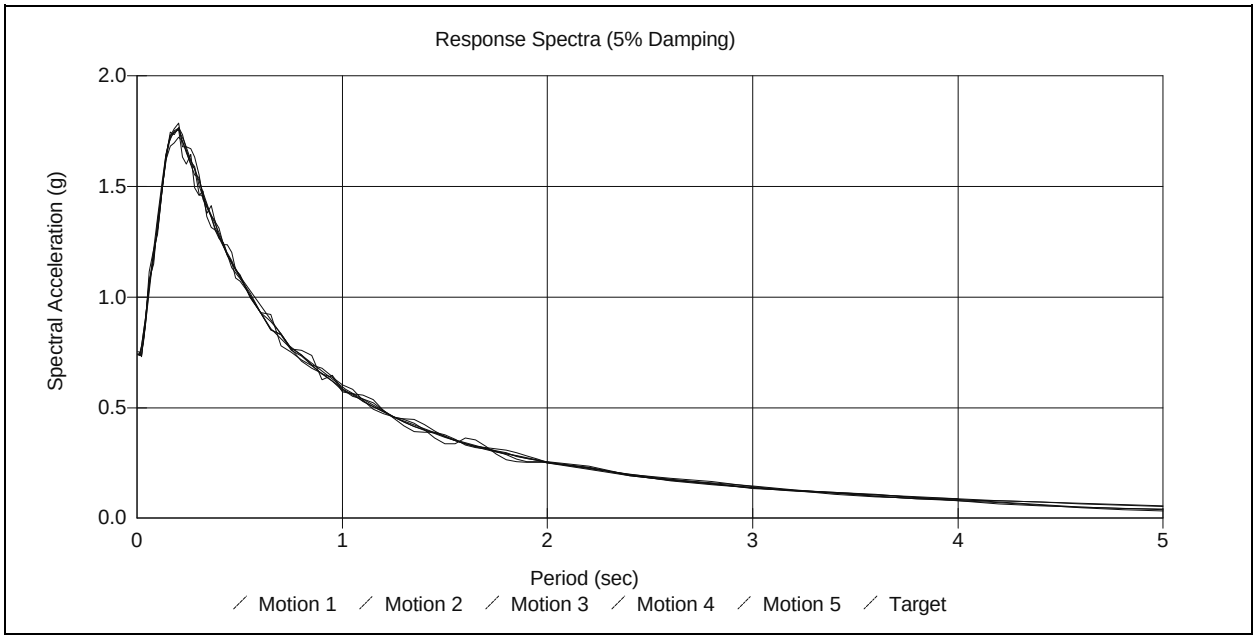

Figure 23b. Comparison of spectrally matched time histories with the target spectrum for the I-80 interchange design spectrum without fault directivity.

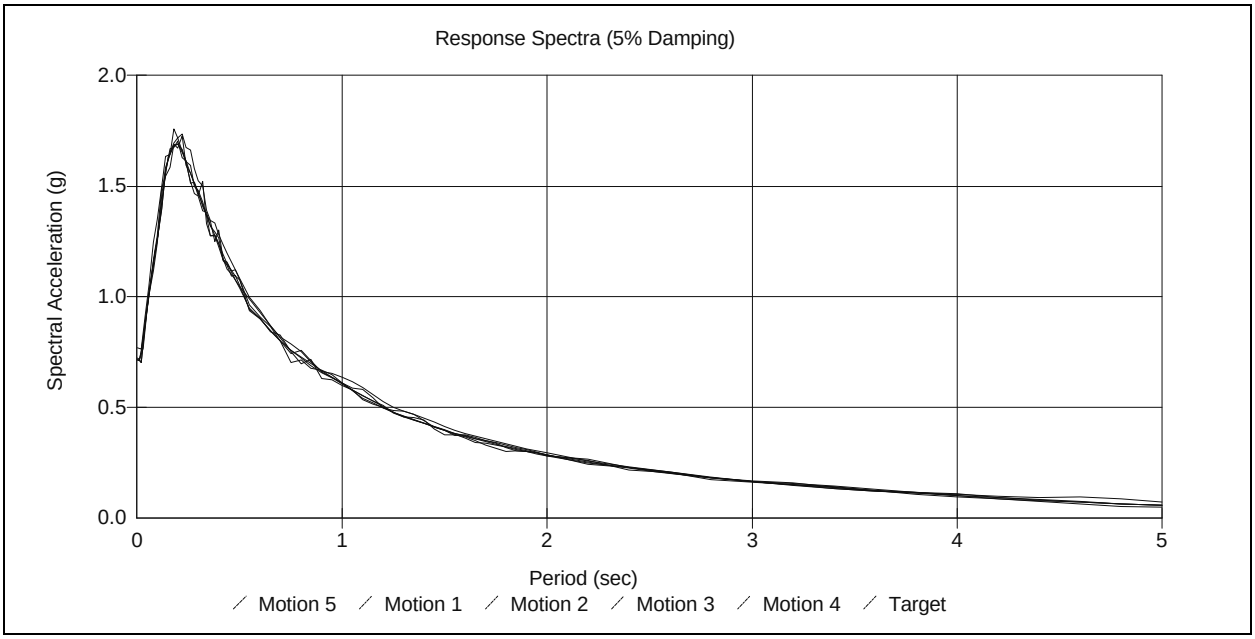

Figure 24a. Comparison of spectrally matched time histories with the target spectrum for the 600 South interchange design spectrum with fault directivity.

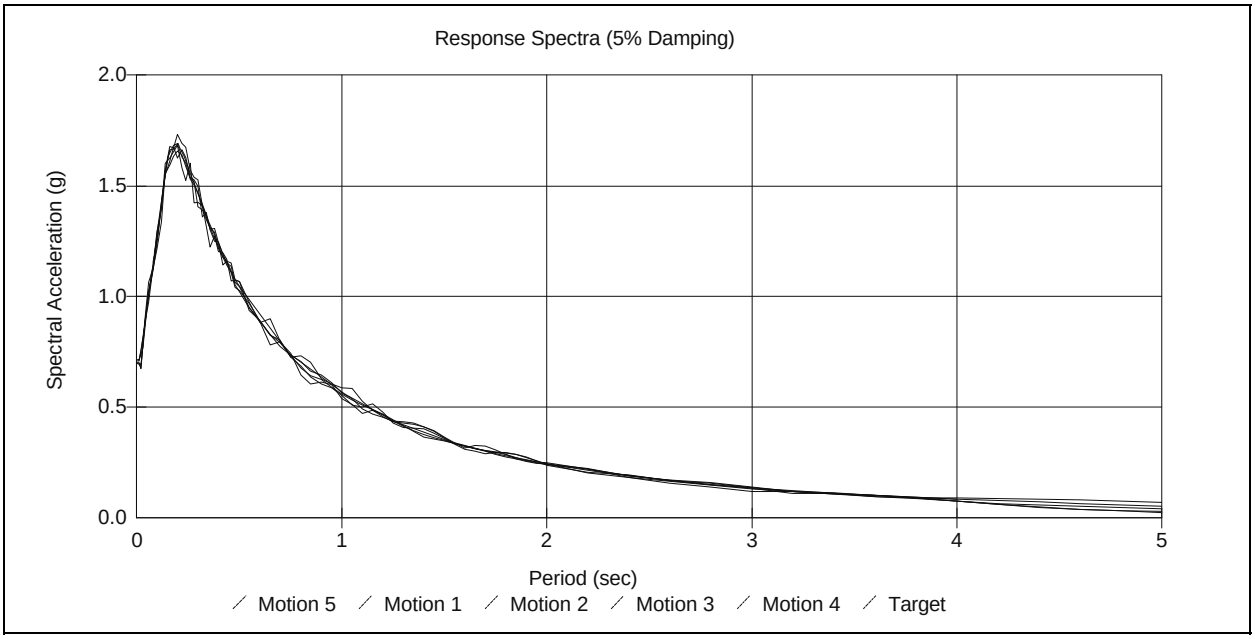

Figure 24b. Comparison of spectrally matched time histories with the target spectrum for the 600 South interchange design spectrum without fault directivity.

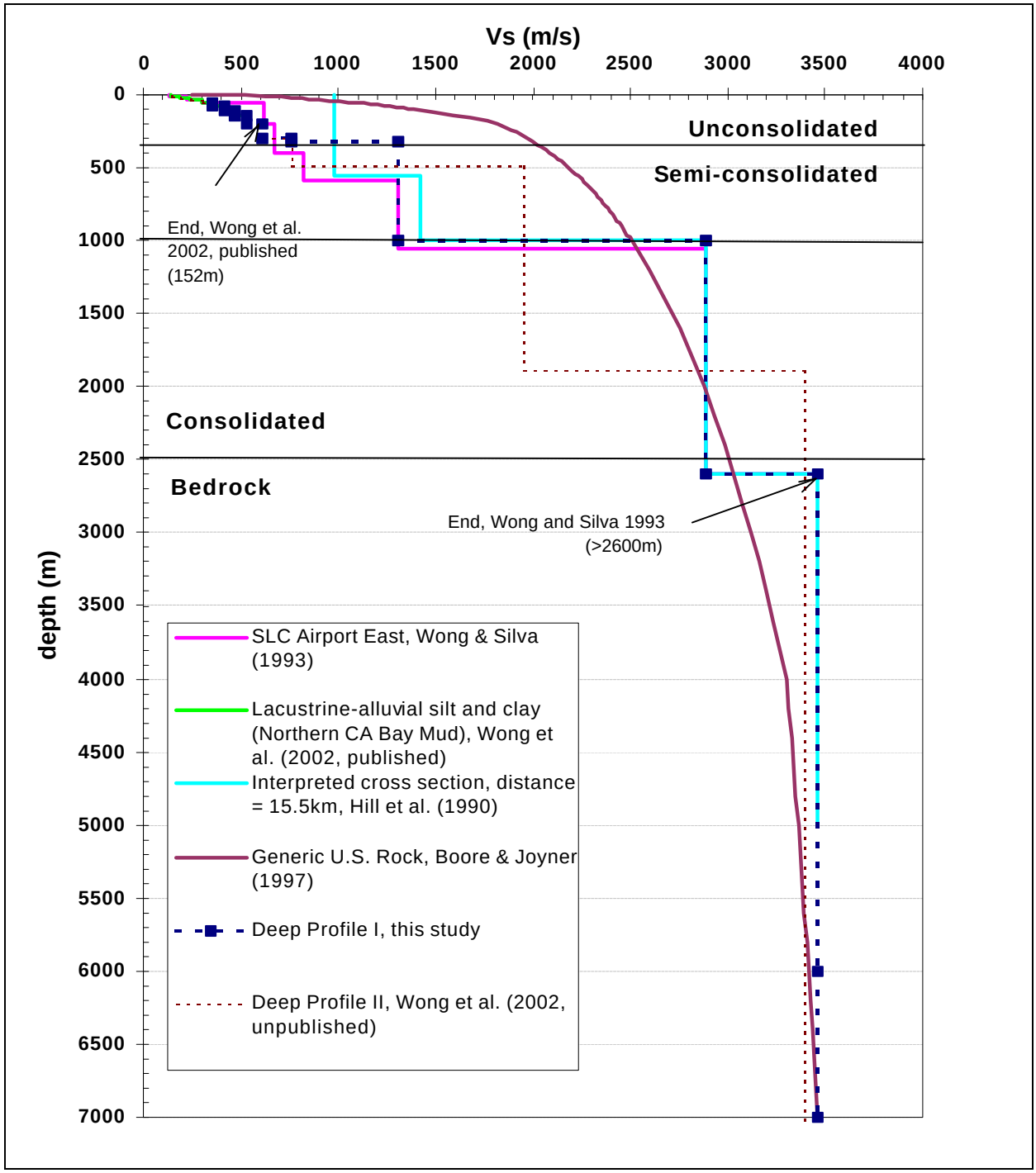

Figure 25. Comparison of the generic western U.S. rock Vs profile (Boore and Joyner, 1997) with Vs profiles for the Salt Lake Valley.

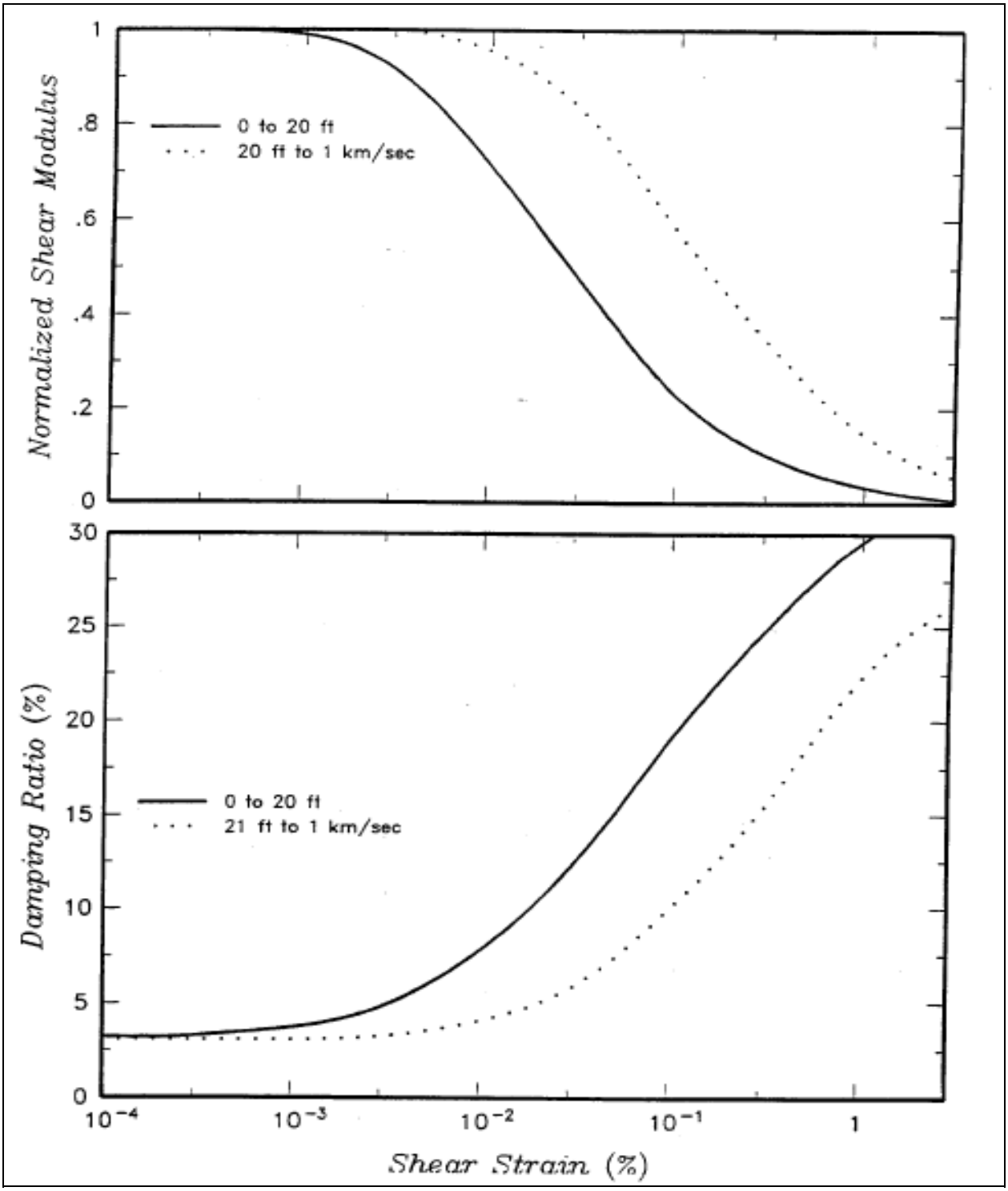

Figure 26. Shear modulus reduction and damping curves for weathered rock (Geomatrix, 1999).

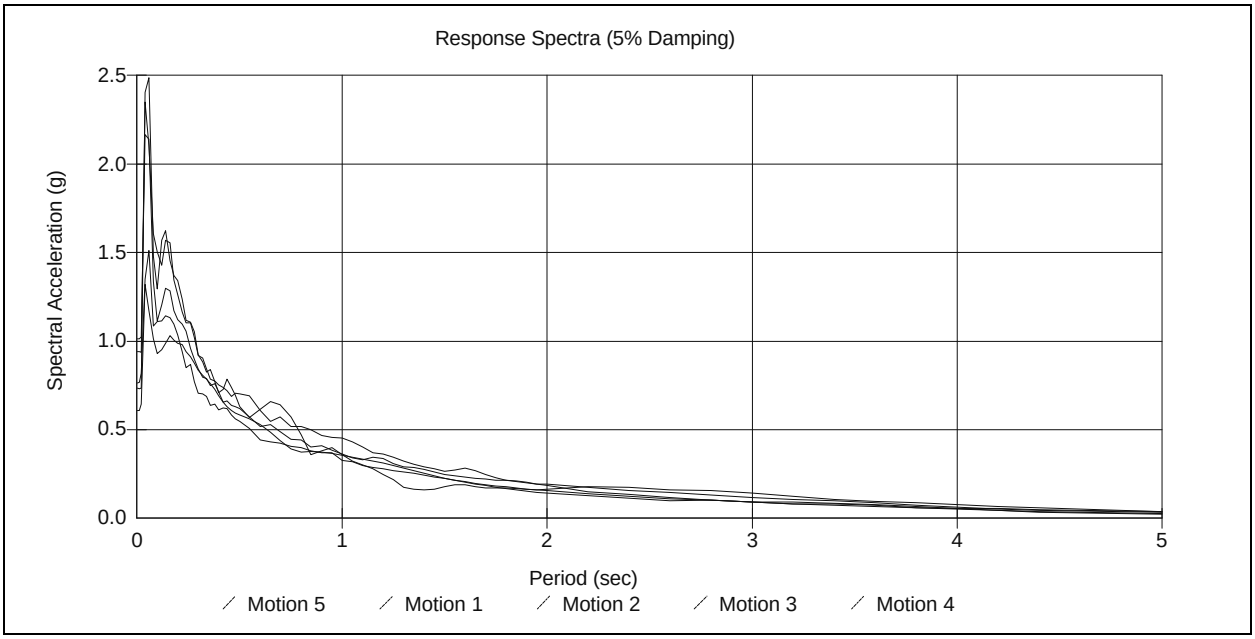

Figure 27. Results of 5 km deconvolution analysis using I-80 target spectrum for case without fault directivity and using 25 Hz cutoff frequency in ProShake.

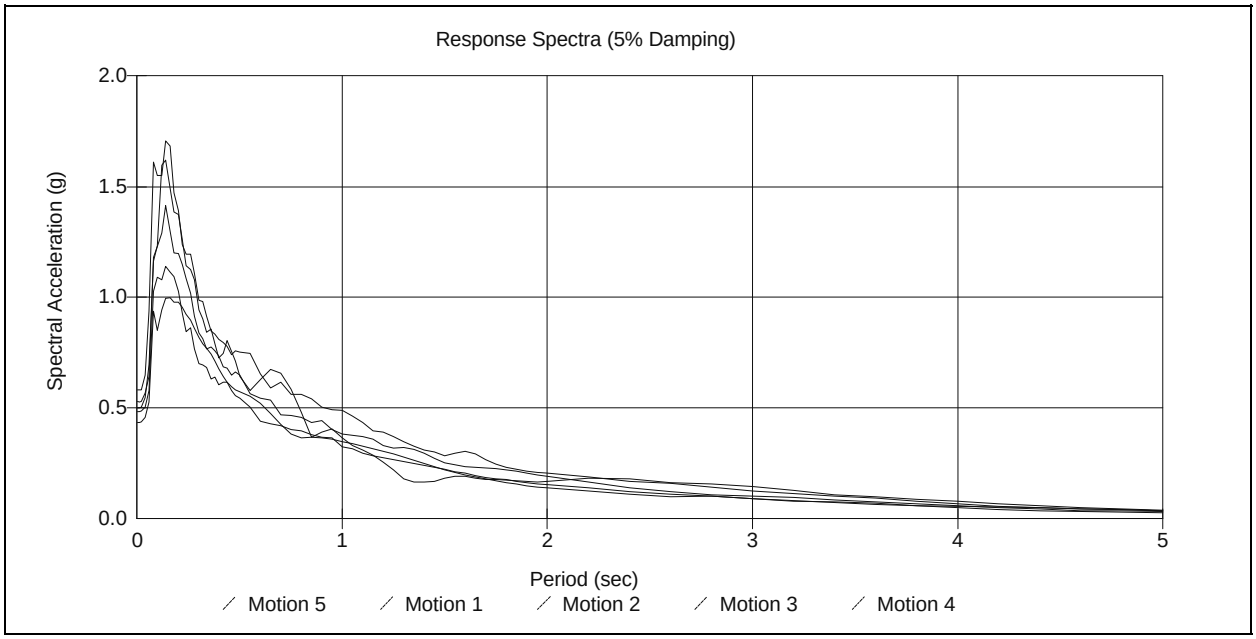

Figure 28. Results of 5 km deconvolution analysis using I-80 target spectrum for case without fault directivity and using 15 Hz cutoff frequency in ProShake.

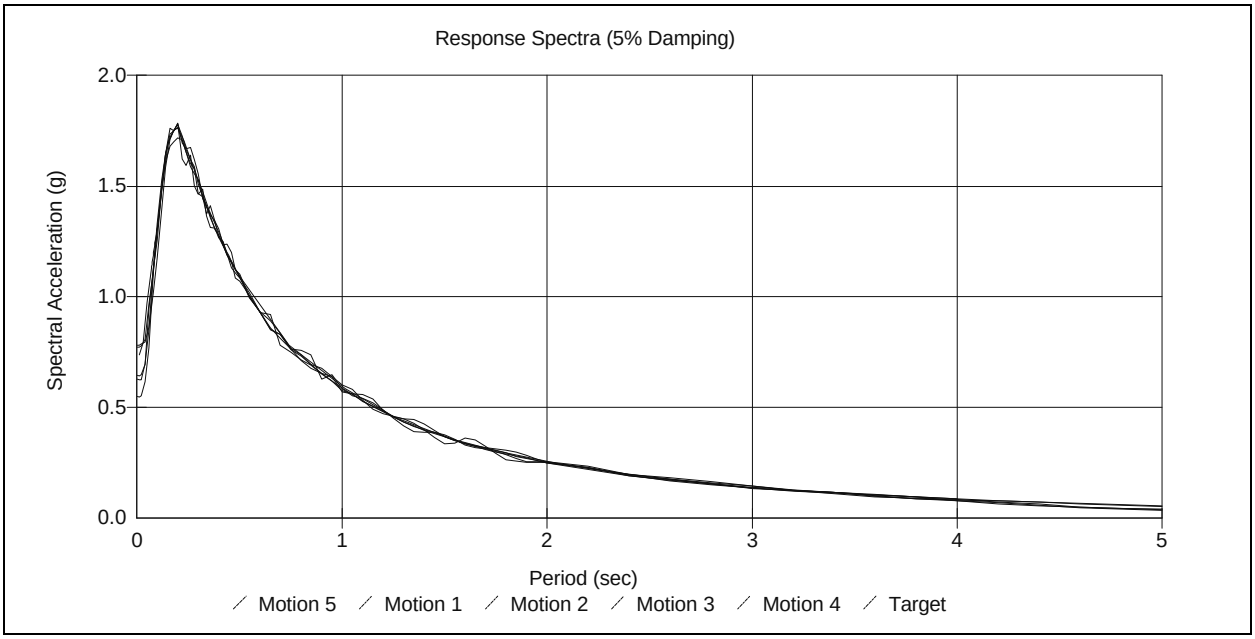

Figure 29a. Input rock spectra for the deconvolution analysis for the I-80 site for case without fault directivity. These input time histories have been filtered at 15 Hz using a low pass 4th order Butterworth filter.

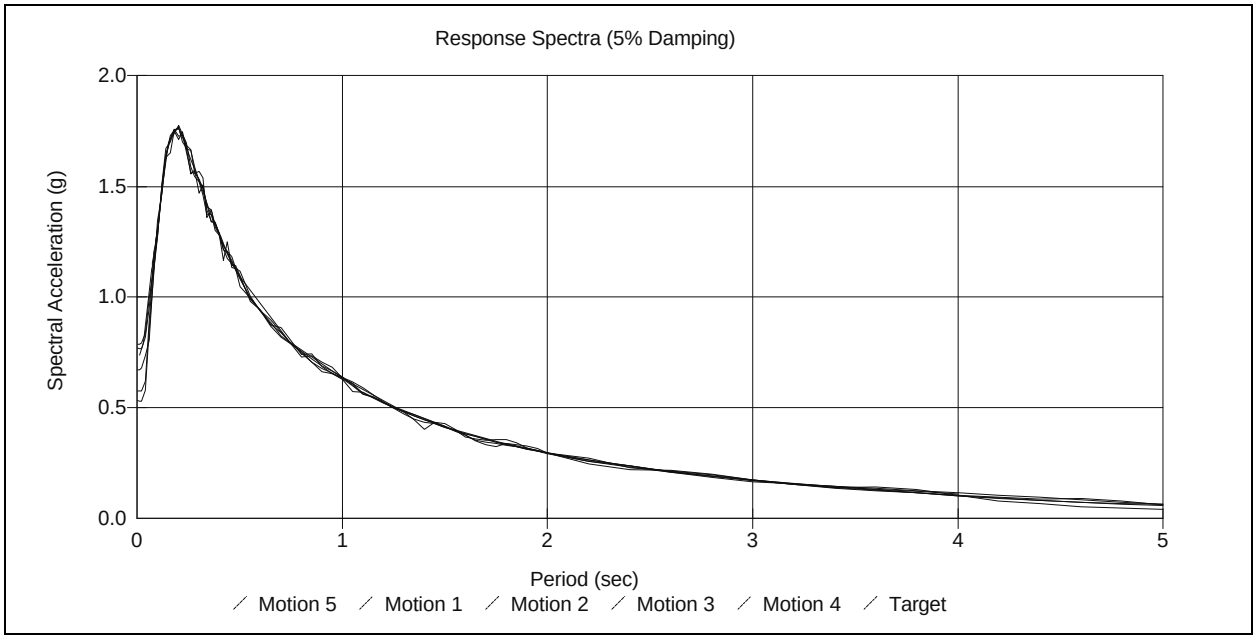

Figure 29b. Input rock spectra for the deconvolution analysis for the I-80 site for case with fault directivity. These input time histories have been filtered at 15 Hz using a low pass 4th order Butterworth filter.

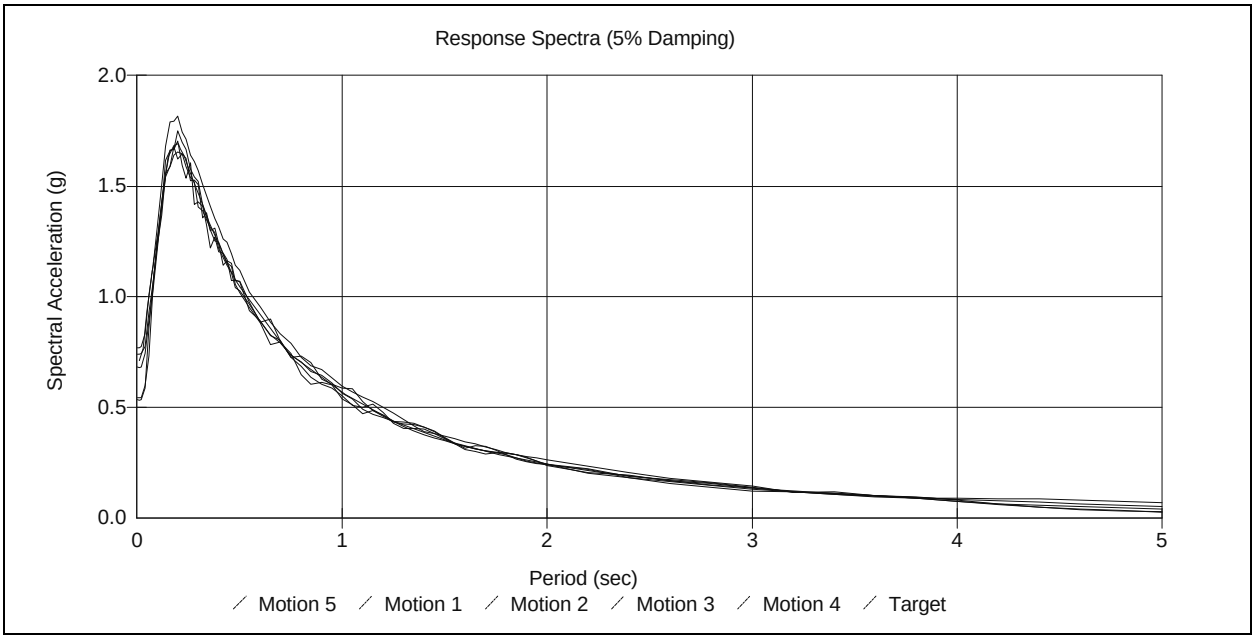

Figure 30a. Input rock spectra for the deconvolution analysis for the 600 S. site for case without fault directivity. These input time histories have been filtered at 15 Hz using a low pass 4th order Butterworth filter.

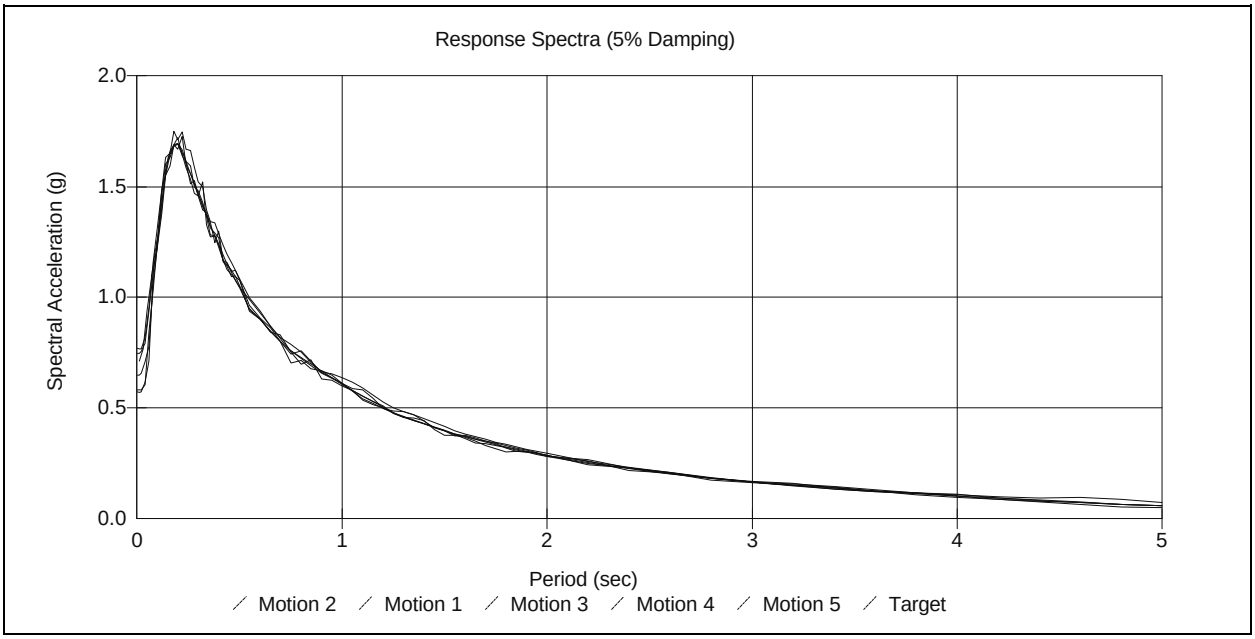

Figure 30b. Input rock spectra for the deconvolution analysis for the 600 S. site for case with fault directivity. These input time histories have been filtered at 15 Hz using a low pass 4th order Butterworth filter

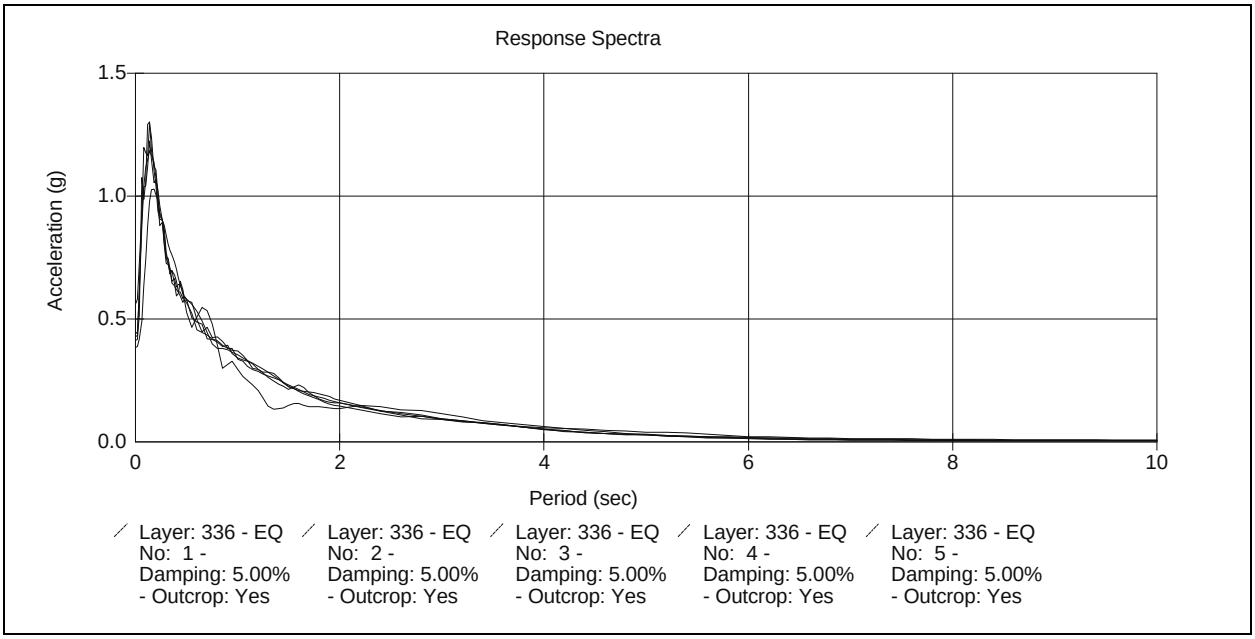

Figure 31a. Results of 5 km deconvolution analysis using I-80 target spectrum for case without fault directivity and preprocessing time histories with a 15 Hz Butterworth filter.

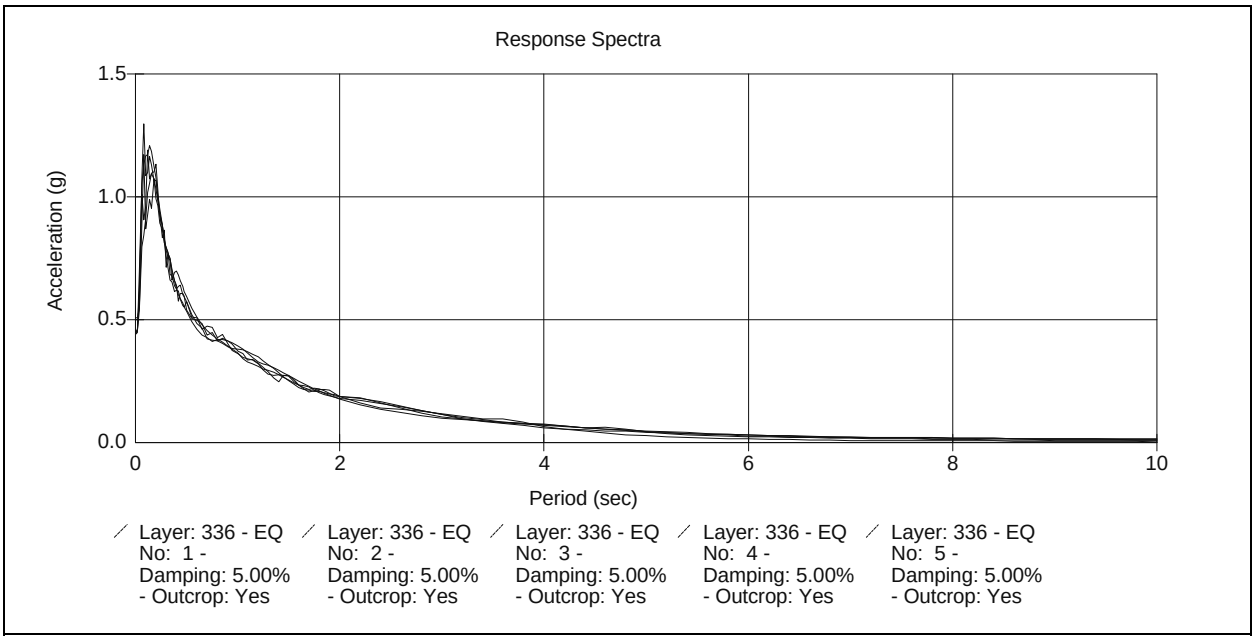

Figure 31b. Results of 5 km deconvolution analysis using I-80 target spectrum for case with fault directivity and preprocessing time histories with a 15 Hz Butterworth filter.

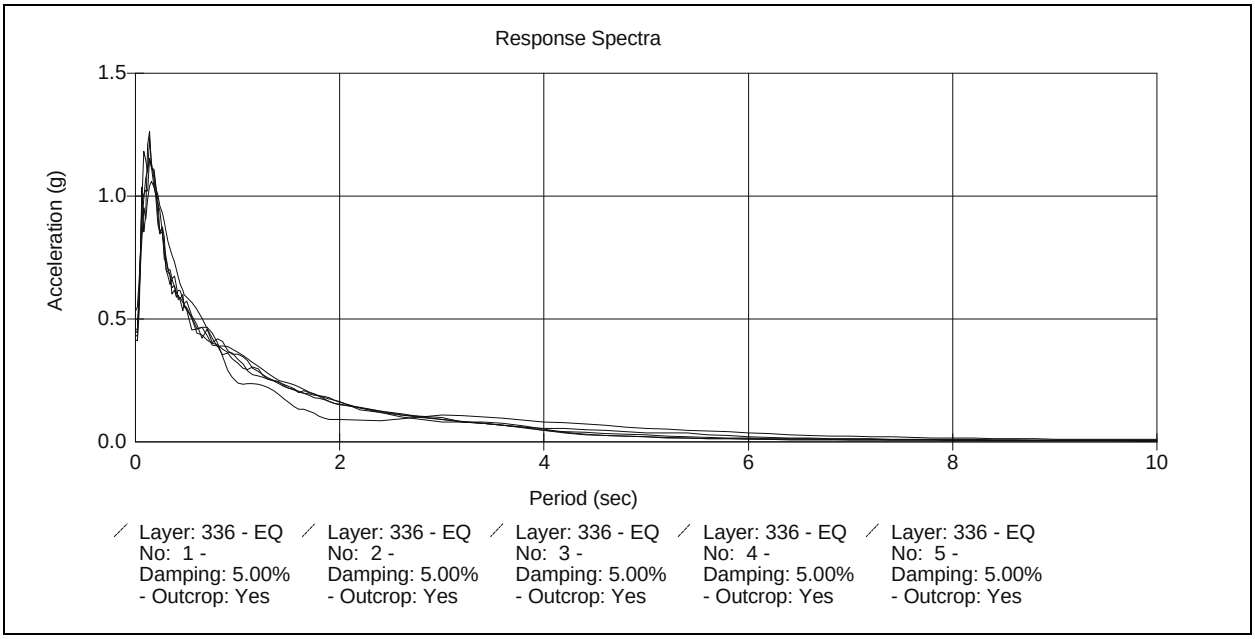

Figure 32a. Results of 5 km deconvolution analysis using 600 South target spectrum for case without fault directivity and preprocessing time histories with a 15 Hz Butterworth filter.

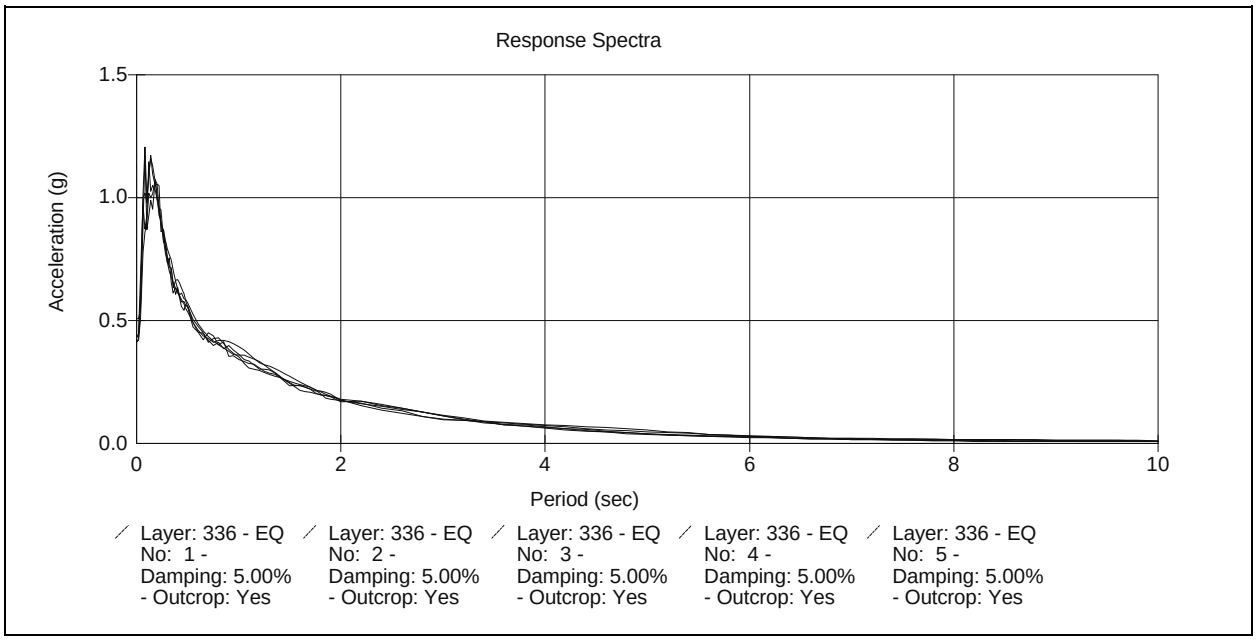

Figure 32b. Results of 5 km deconvolution analysis using 600 South target spectrum for case with fault directivity and preprocessing time histories with a 15 Hz Butterworth filter.

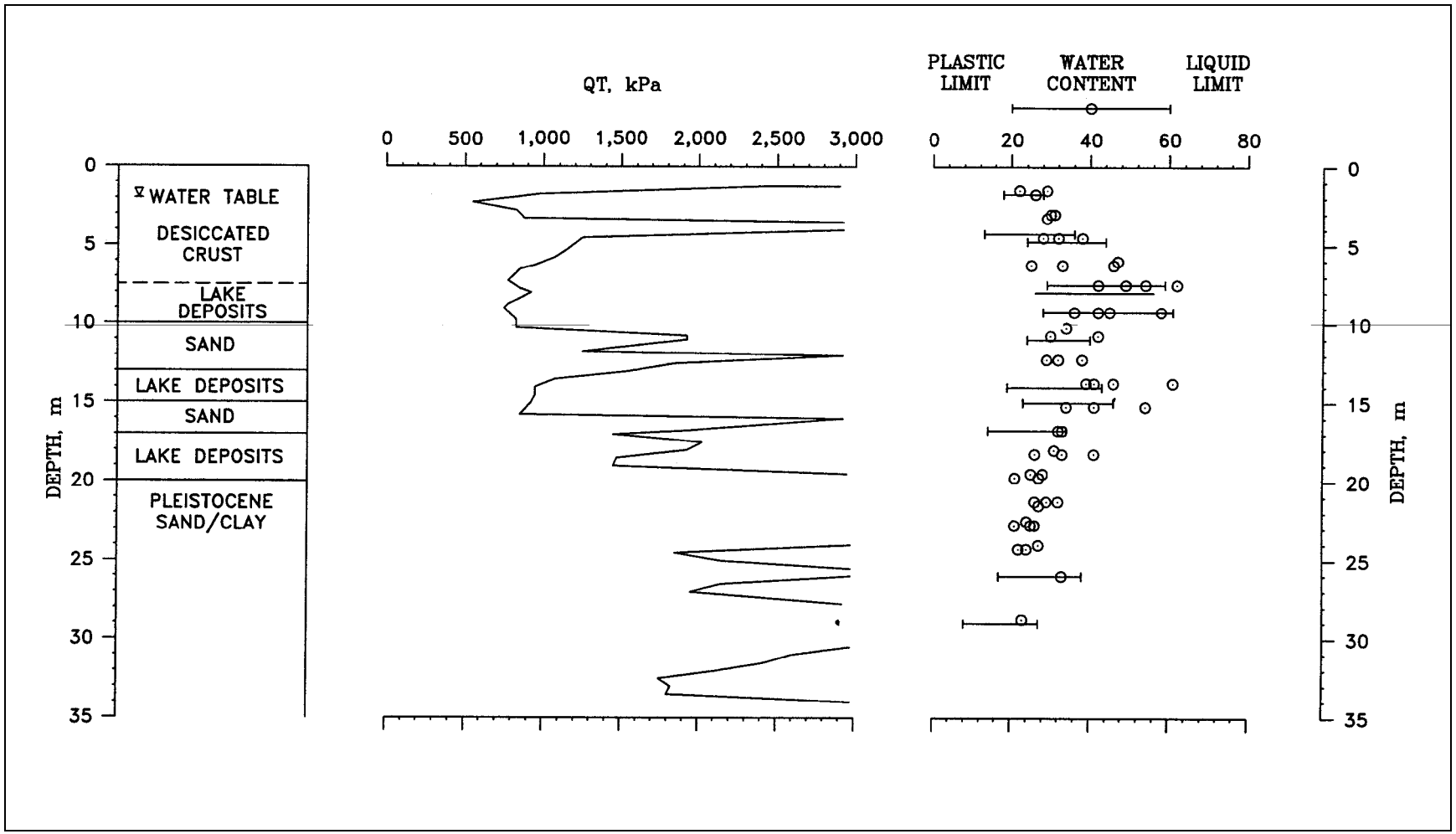

Figure 33. Generalized geotechnical profile for the I-80 interchange (Woodward-Clyde, unpublished).

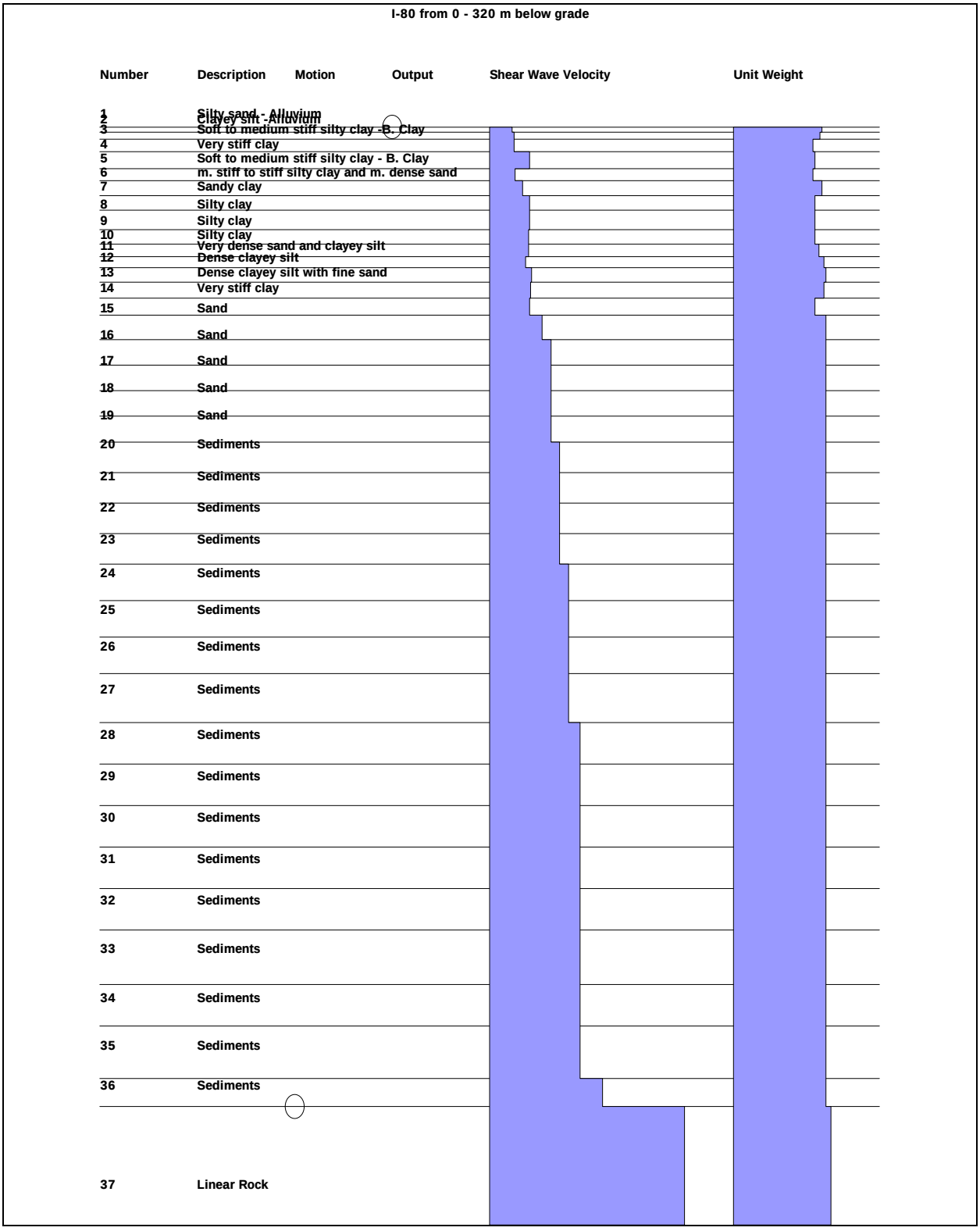

Figure 34. Best Estimate V_s profile for the upper 320 m for the I-80 interchange.

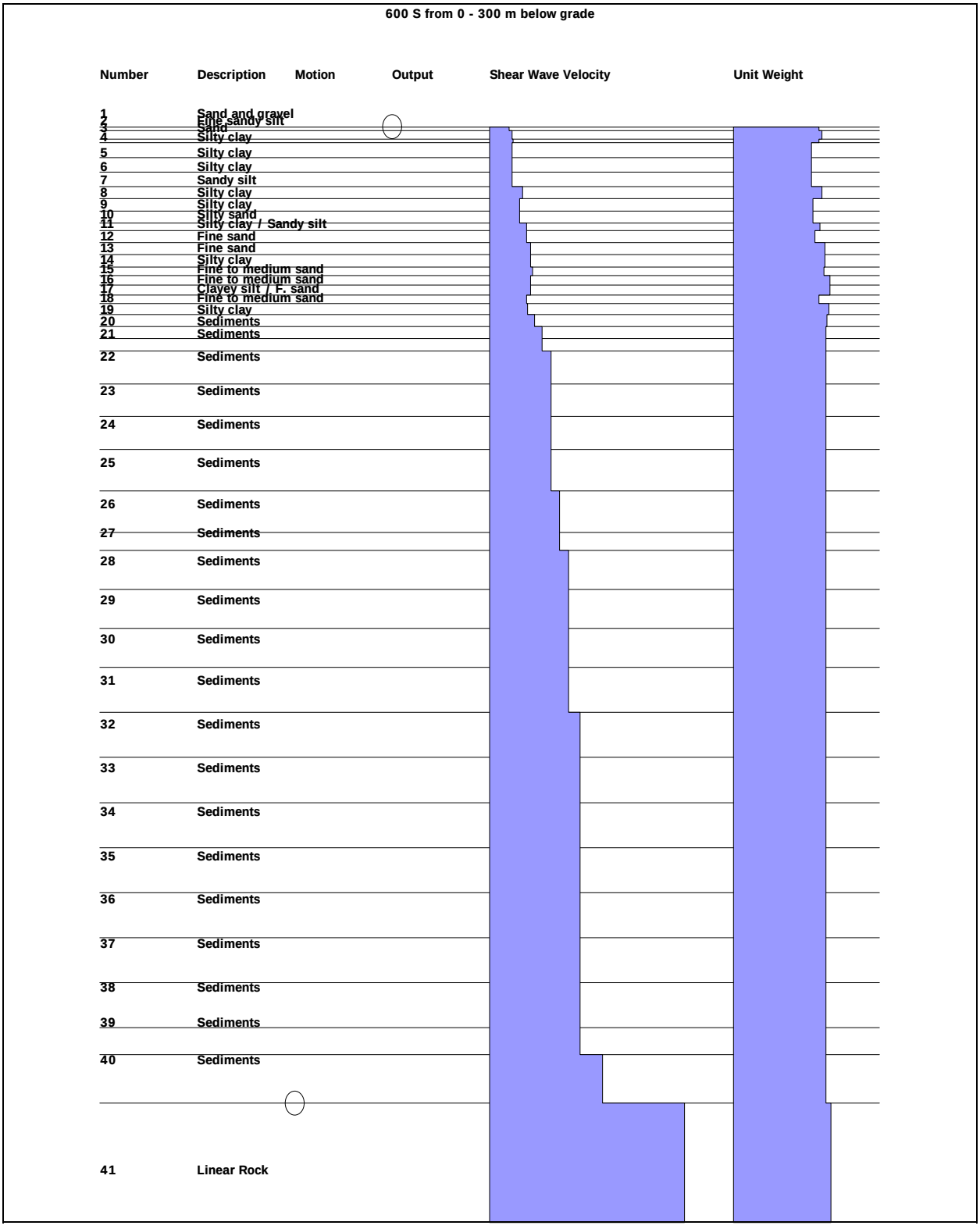

Figure 35. Best Estimate V_s profile for the upper 300 m for the 600 South interchange.

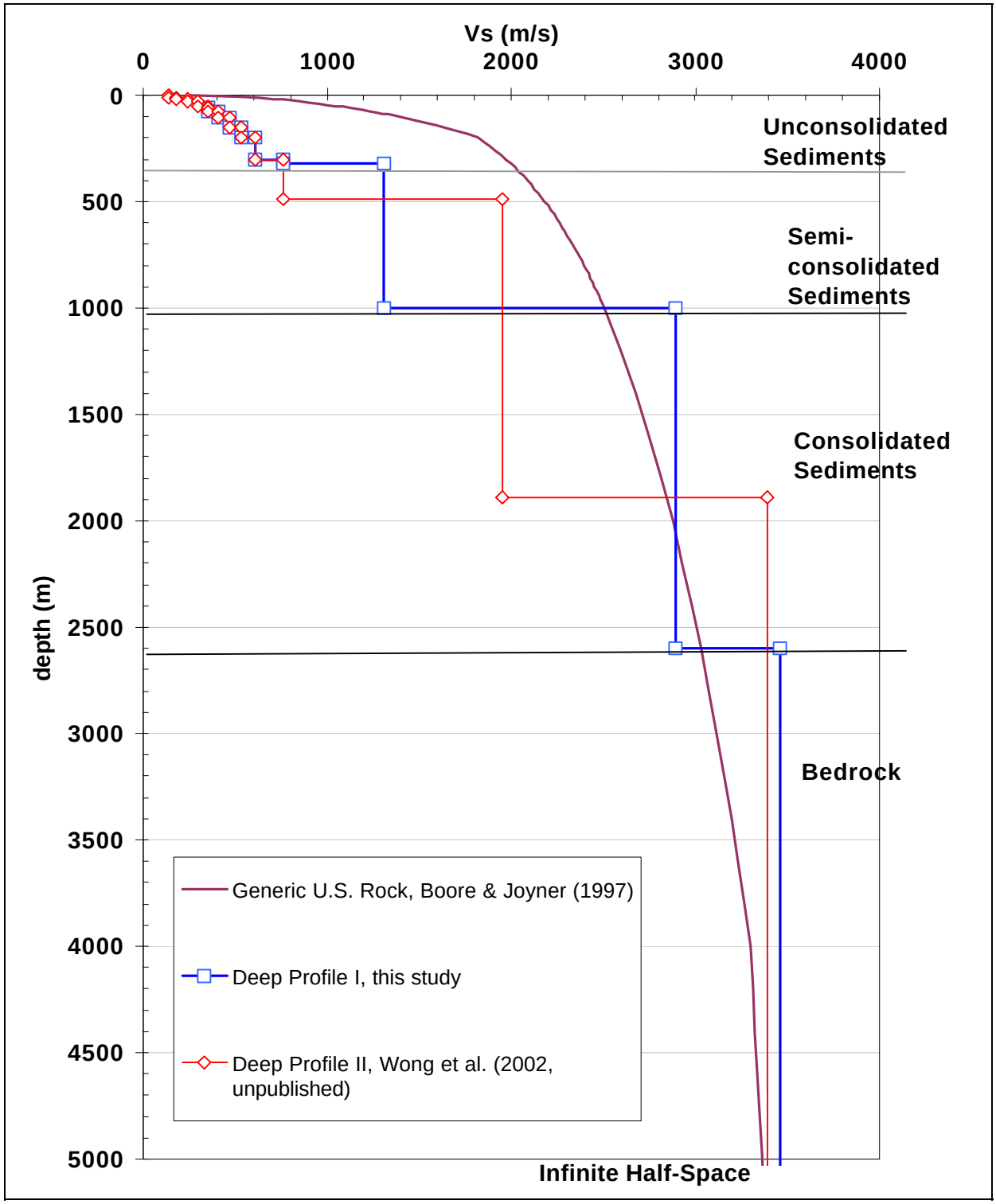

Figure 36. Deep Vs Profile for ProShake Modeling.

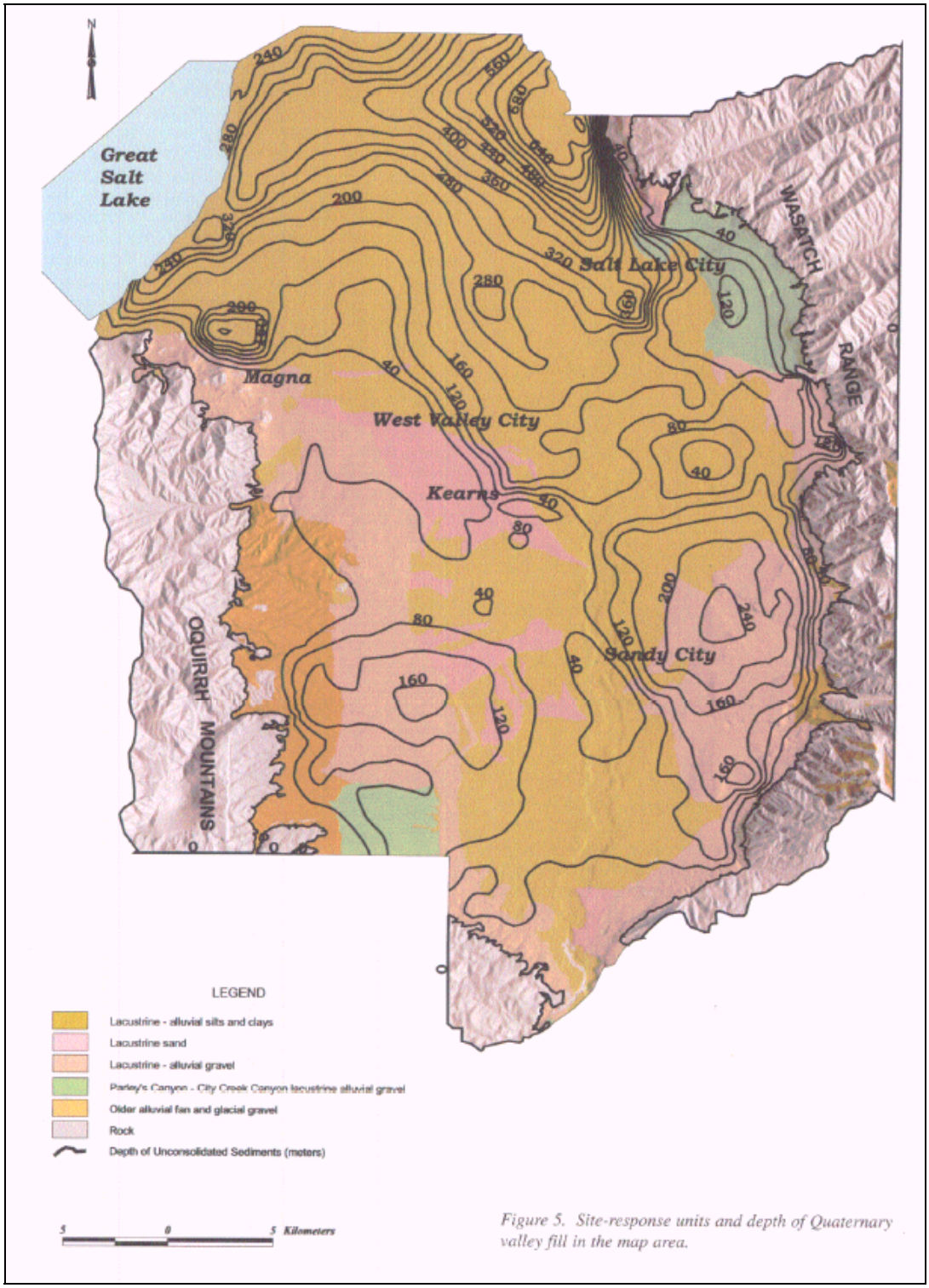

Figure 37. Depth to base of unconsolidated sediments in Salt Lake Valley (from Wong et al., 2002.)

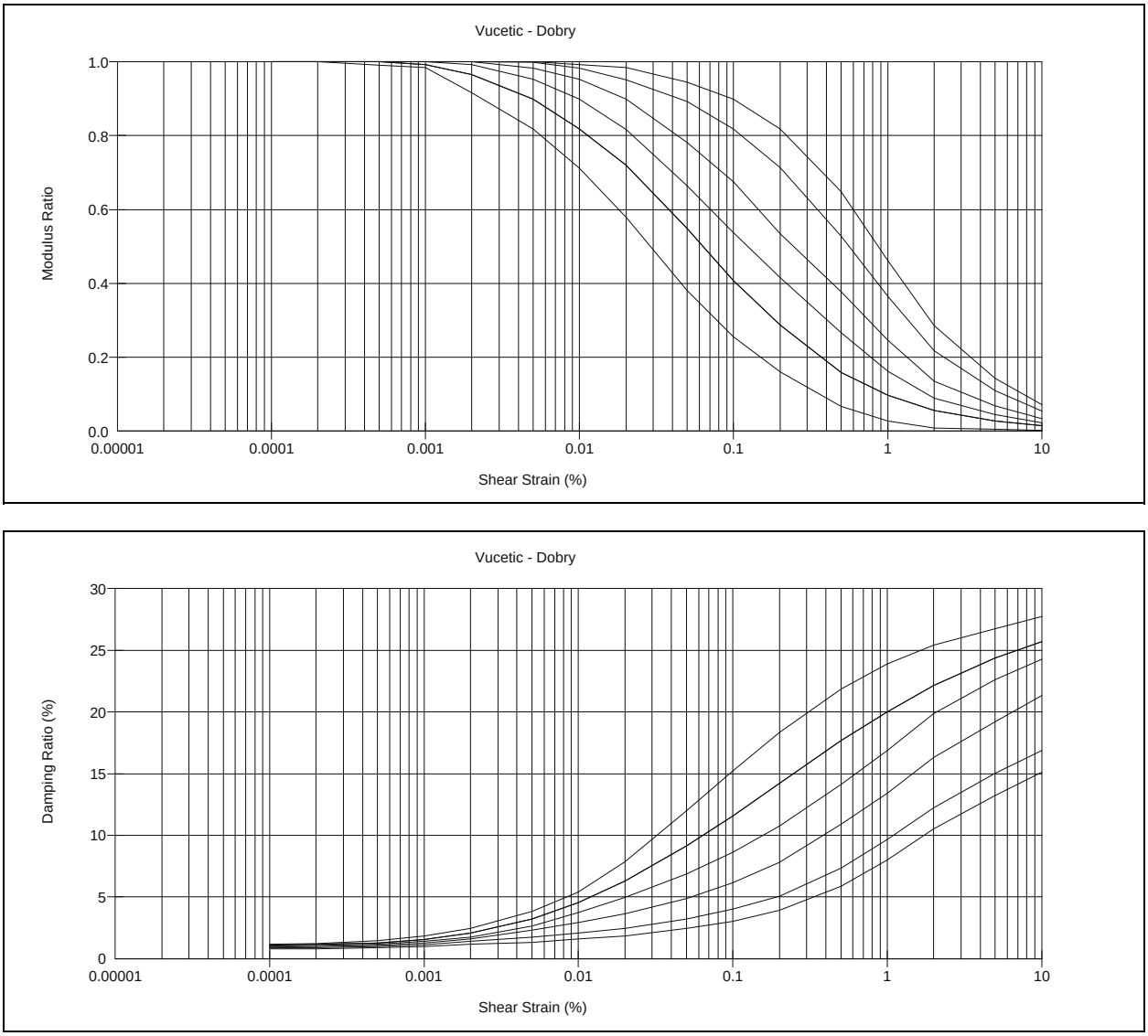

Figure 38. Vucetic and Dobry (1991) shear modulus reduction and damping curves for clayey soils.

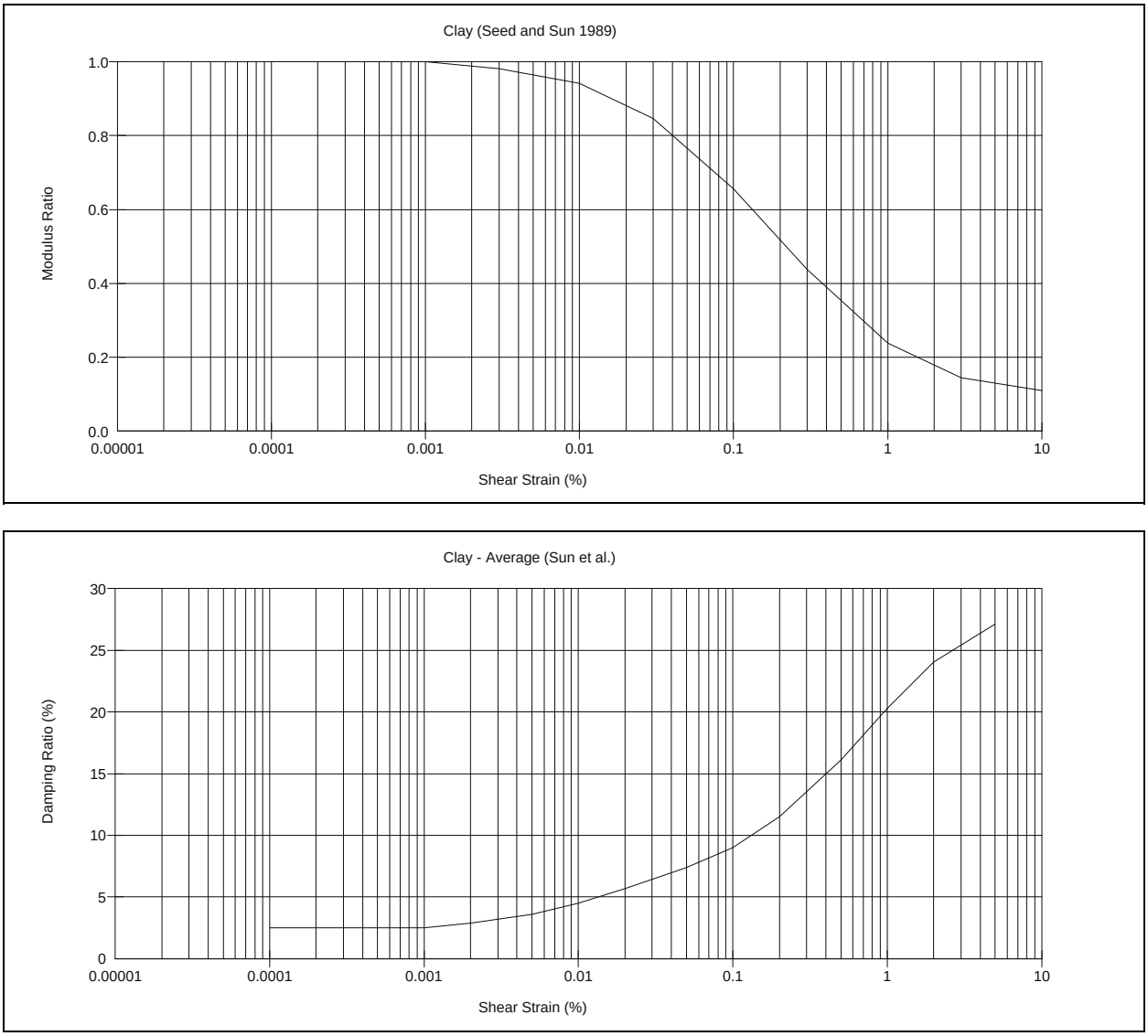

Figure 39. Seed and Sun (1989) shear modulus and damping curves for clay.

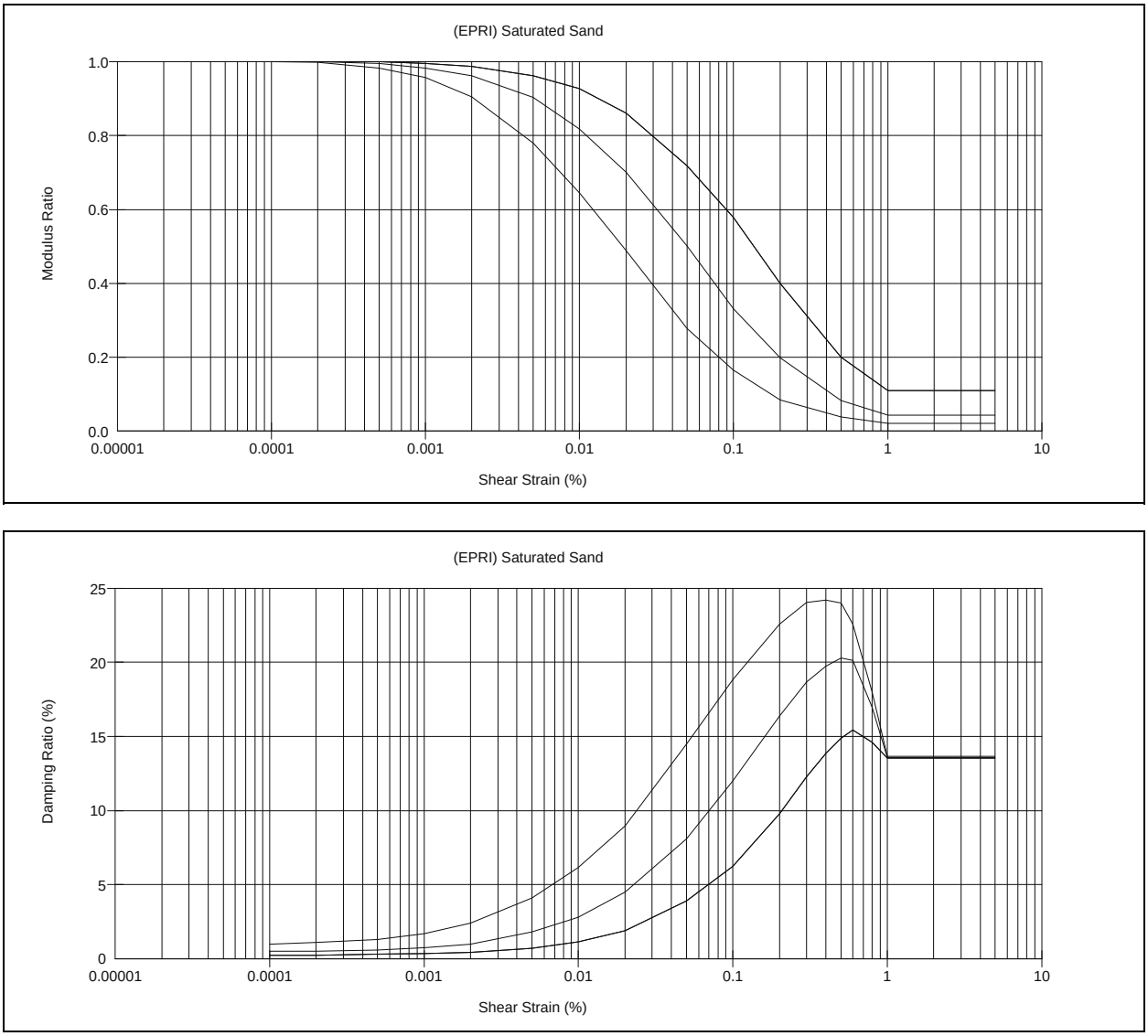

Figure 40. EPRI (1993) shear modulus and damping curves for saturated sands.

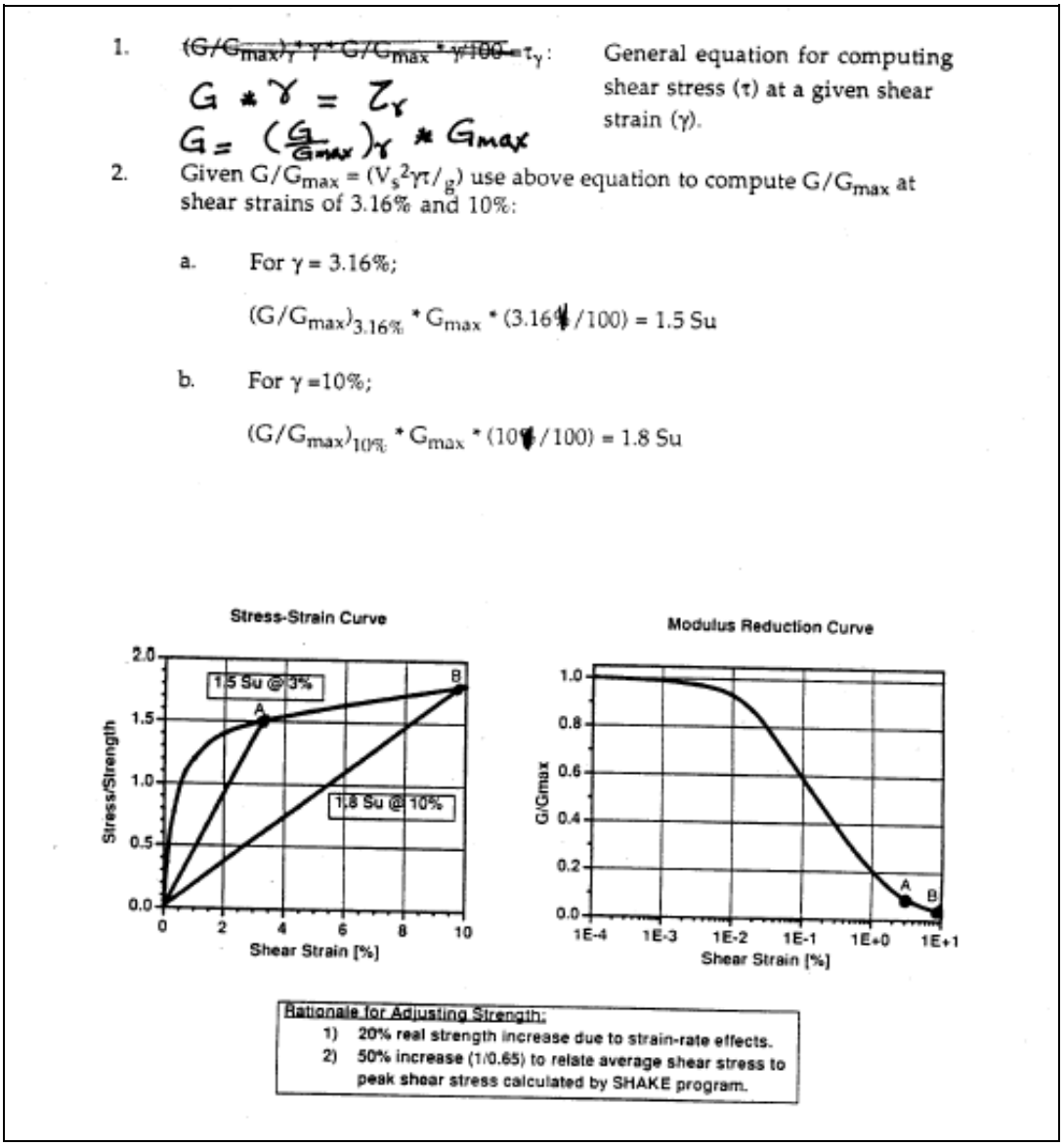

Figure 41. Procedure for extending G/G_{max} curves for higher levels of shear strain (CALTRANS, 1996c).

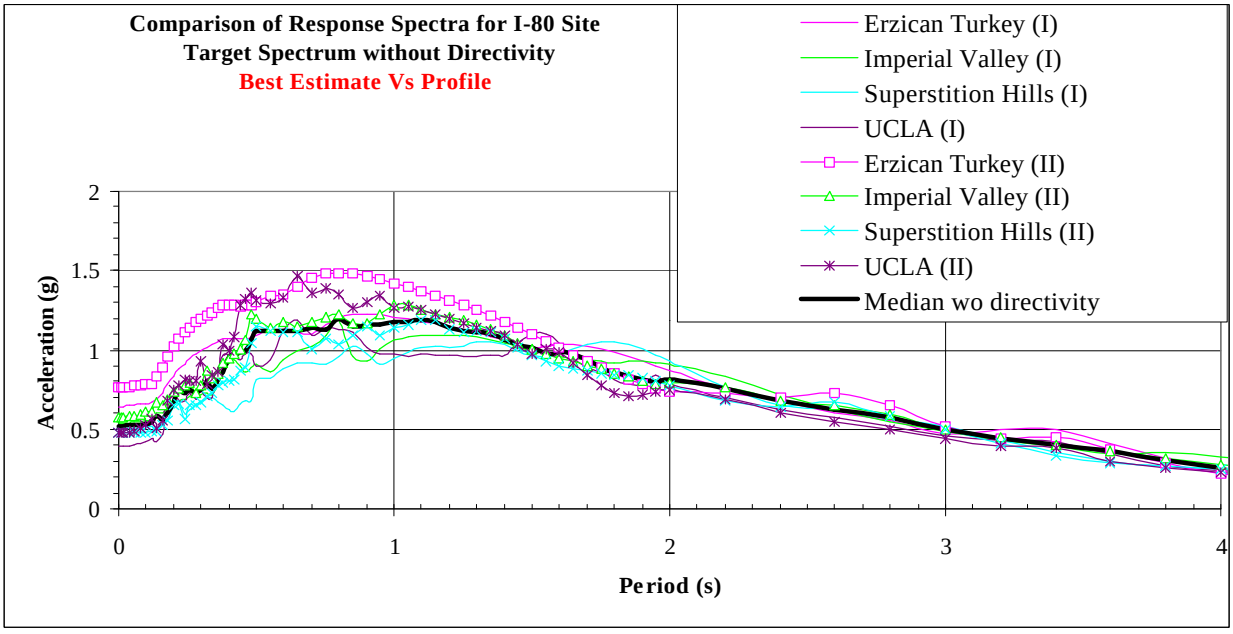

Figure 42a. SHAKE response spectra from convolution analysis of the I-80 best-estimate profile for case of input rock spectrum without fault directivity. Median response spectrum is heavy black line

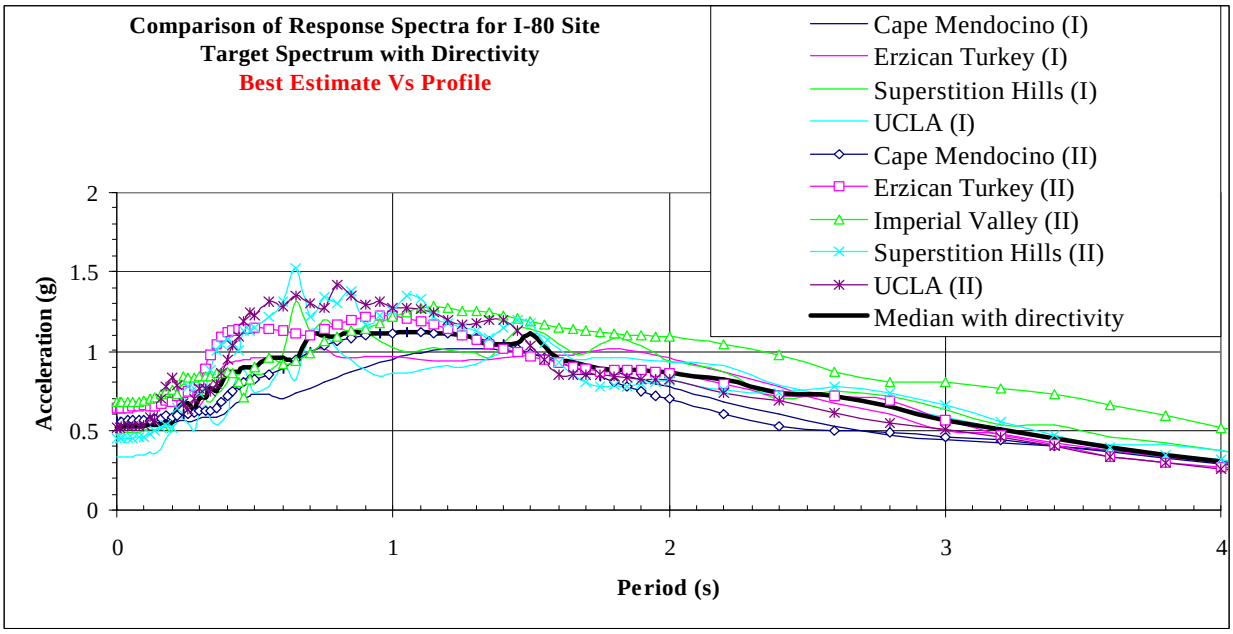

Figure 42b. SHAKE response spectra from convolution analysis of the I-80 best-estimate profile for case of input rock spectrum with fault directivity. Median response spectrum is heavy black line.

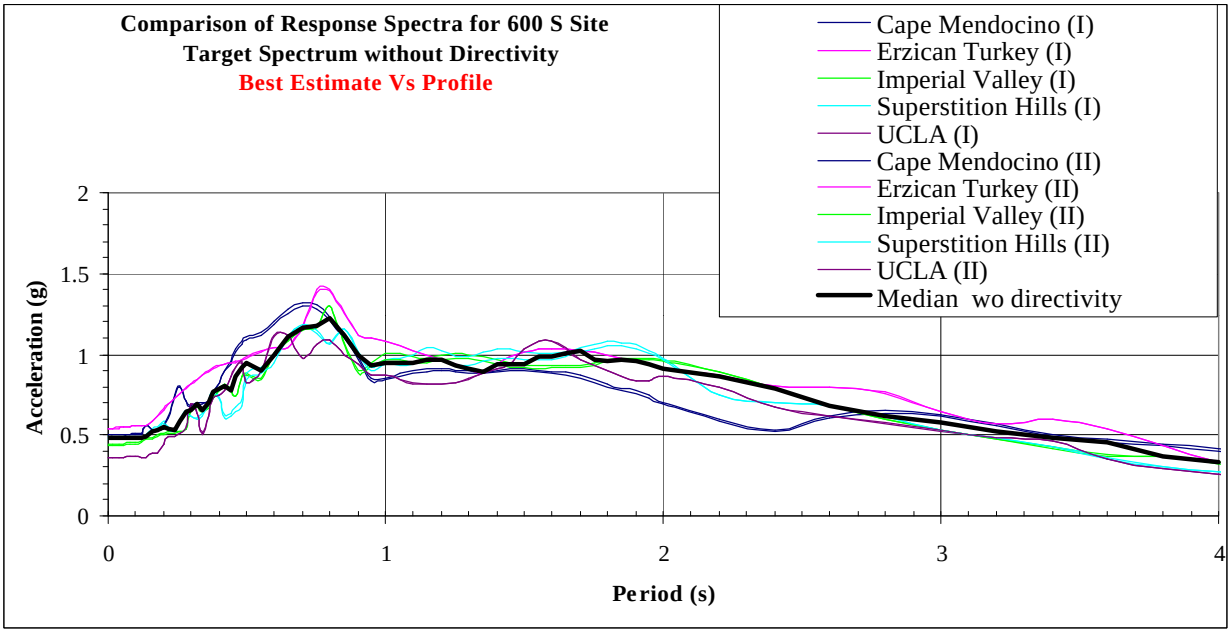

Figure 43a. SHAKE response spectra from convolution analysis of the 600 S. best-estimate profile for case of input rock spectrum without fault directivity. Median response spectrum is heavy black line.

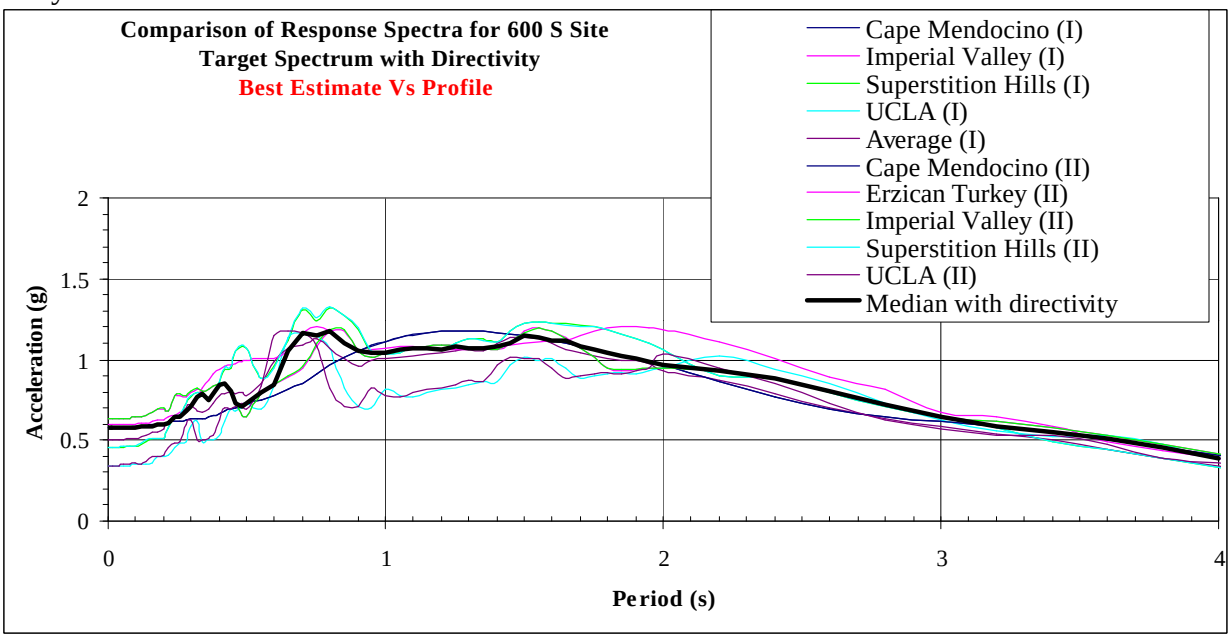

Figure 43b. SHAKE response spectra from convolution analysis of 600 S. best-estimate profile for case of input rock spectrum with fault directivity. Median response spectrum is heavy black line.

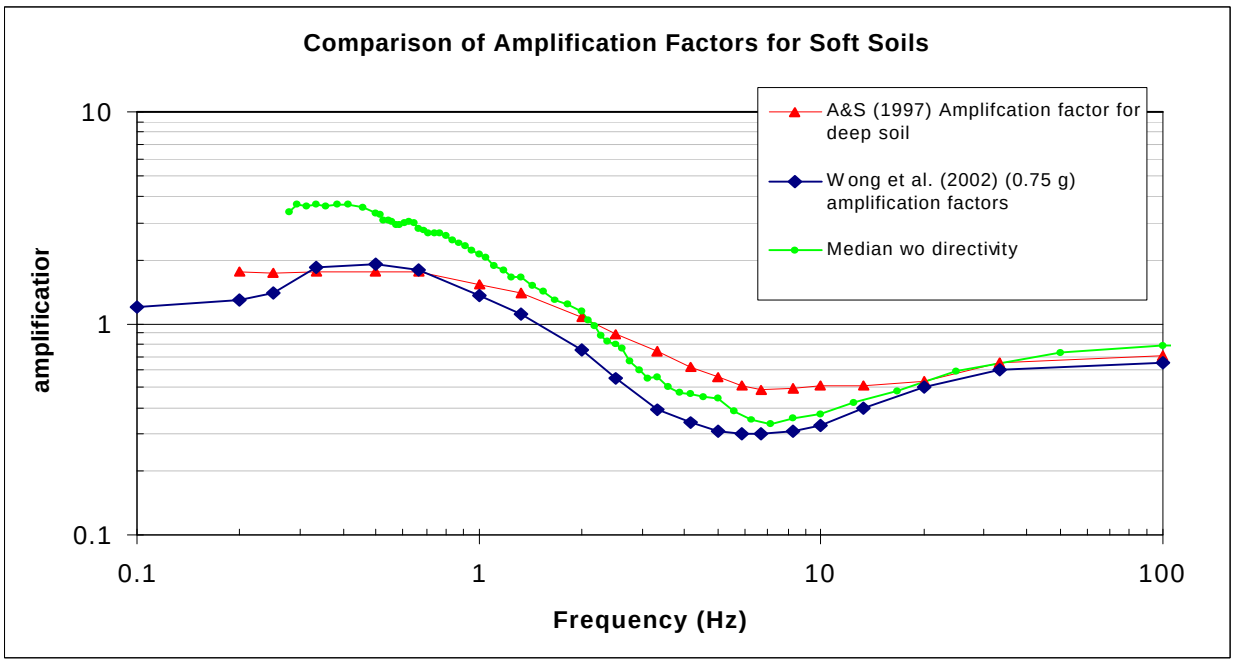

Figure 44a. Median amplification factors for the I-80 interchange for the best-estimate soil profile and for the case without fault directivity.

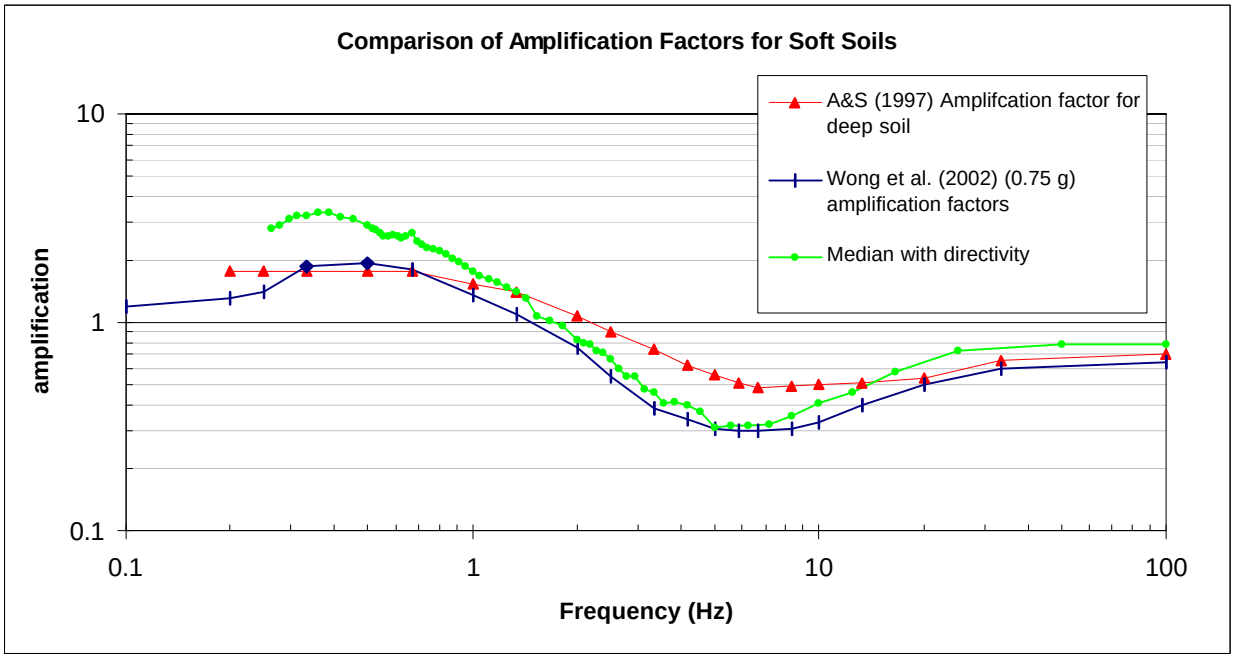

Figure 44b. Median amplification factors for the I-80 interchange for the best-estimate soil profile and for the case with fault directivity.

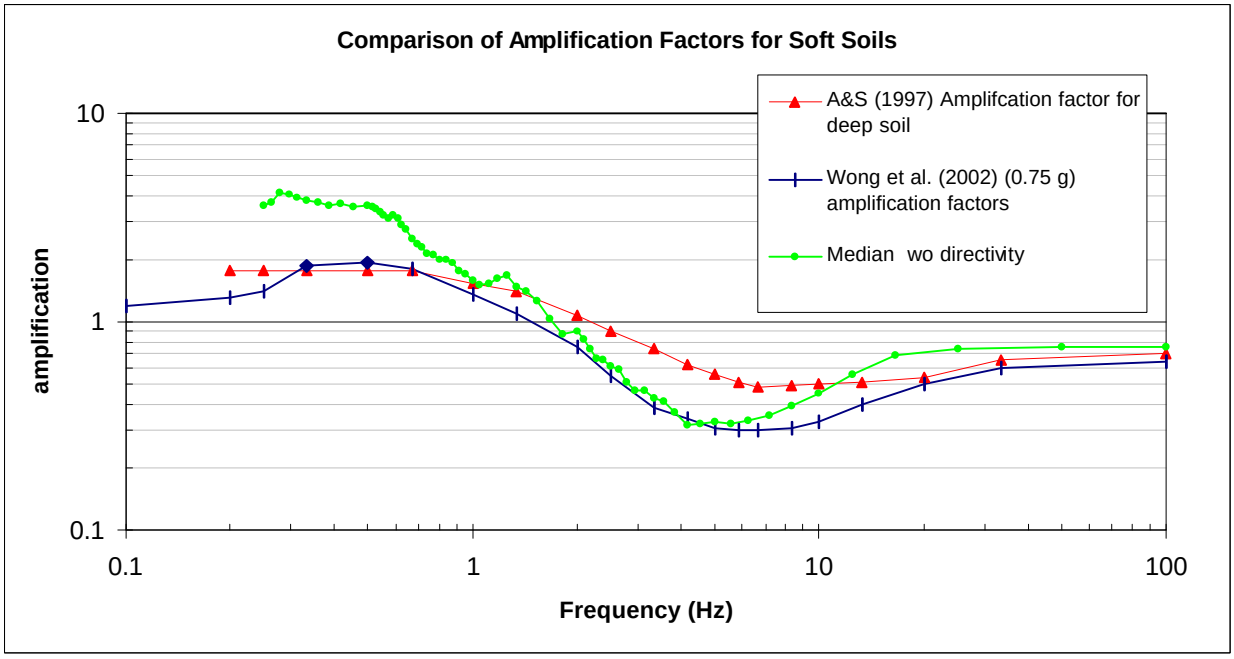

Figure 45a. Median amplification factors for the 600 S. interchange for the best-estimate soil profile and for the case without fault directivity.

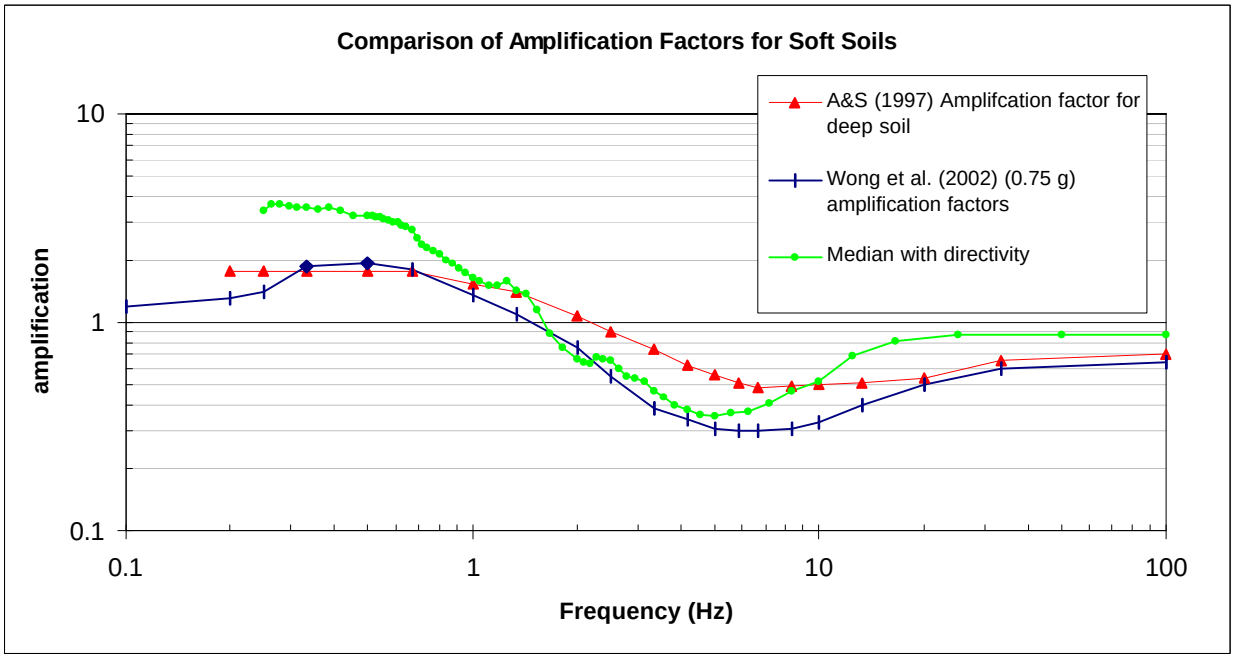

Figure 45b. Median amplification factors for the 600 S. interchange for the best-estimate soil profile and for the case with fault directivity.

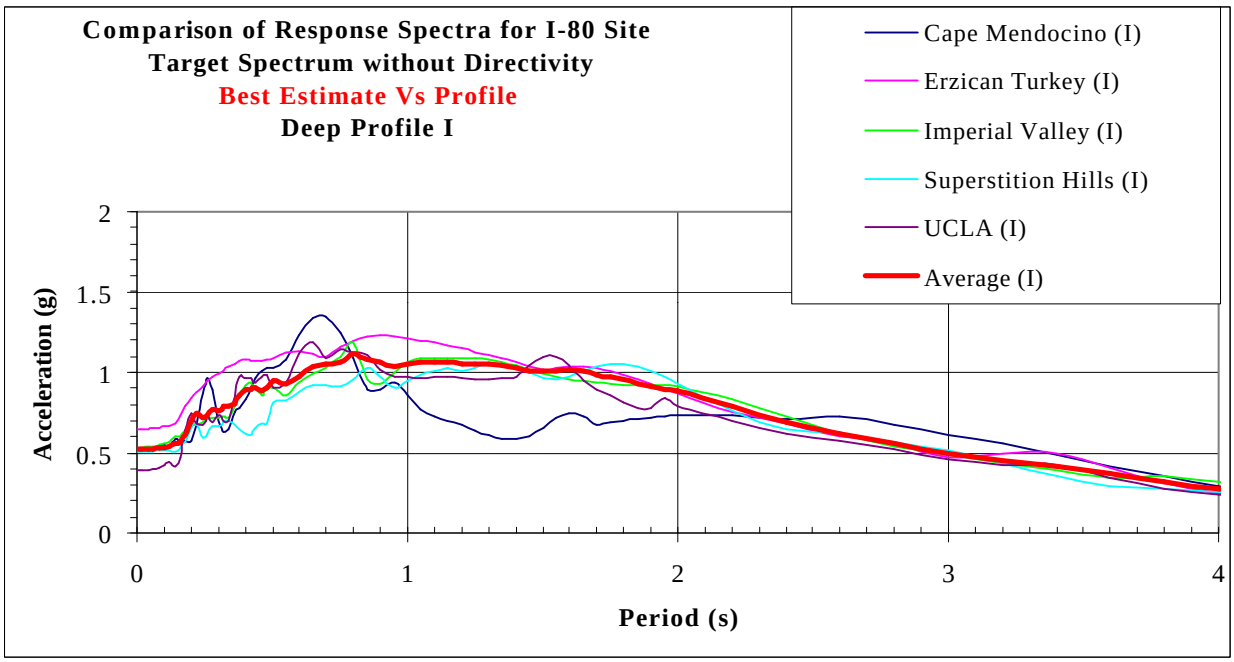

Figure 46a. Results of the SHAKE analyses for the best estimate I-80 interchange profile and deep profile I for the case of the input spectrum without fault directivity.

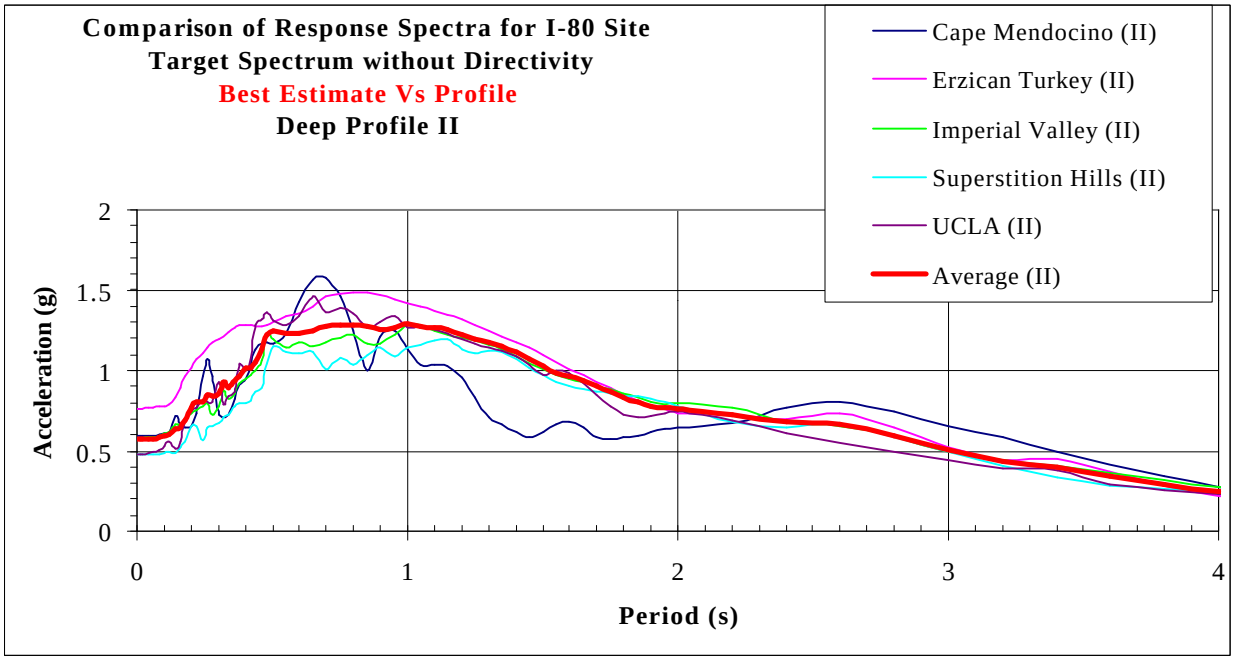

Figure 46b. Results of the SHAKE analyses for the best estimate I-80 interchange profile and deep profile II for the case of an input spectrum without fault directivity.

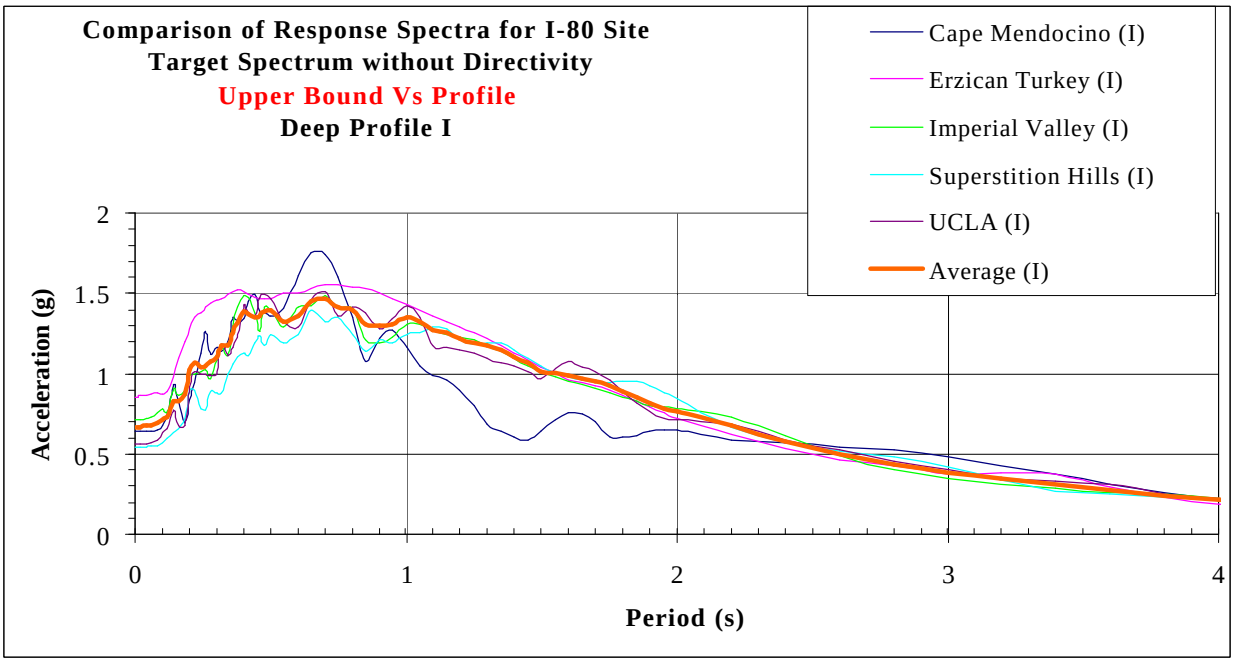

Figure 46c. Results of the SHAKE analyses for the upper bound I-80 interchange profile and deep profile I for the case of the input spectrum without fault directivity.

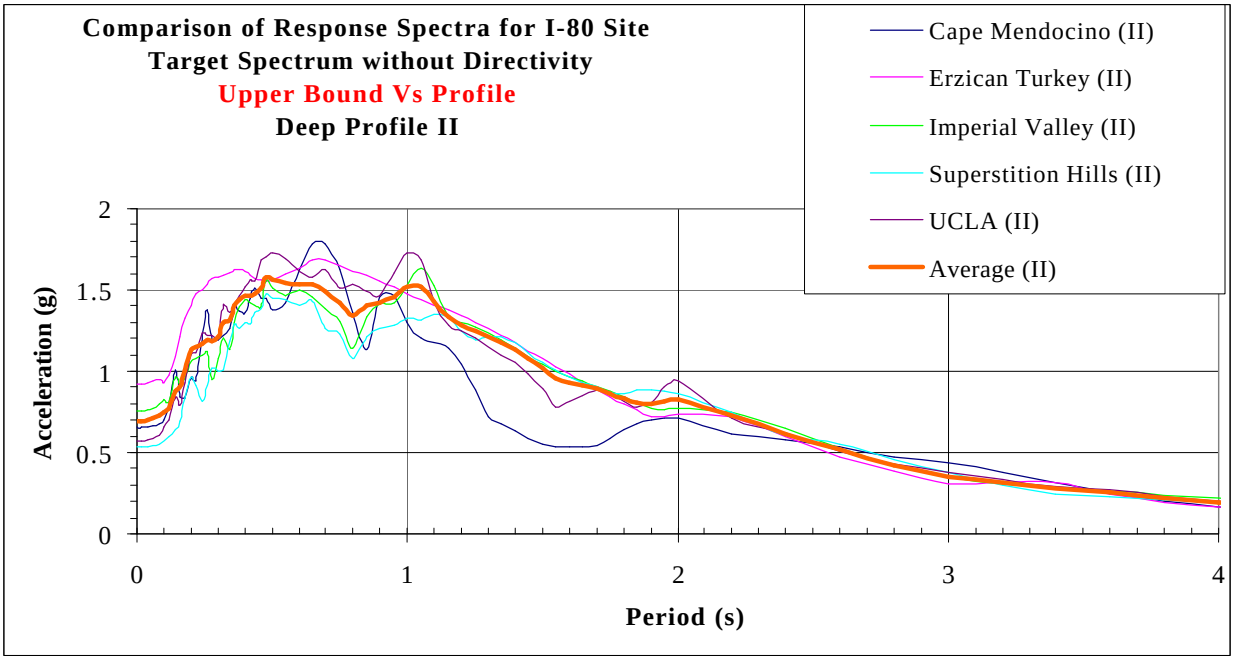

Figure 46d. Results of the SHAKE analyses for the upper bound I-80 interchange profile and deep profile II for the case of the input spectrum without fault directivity.

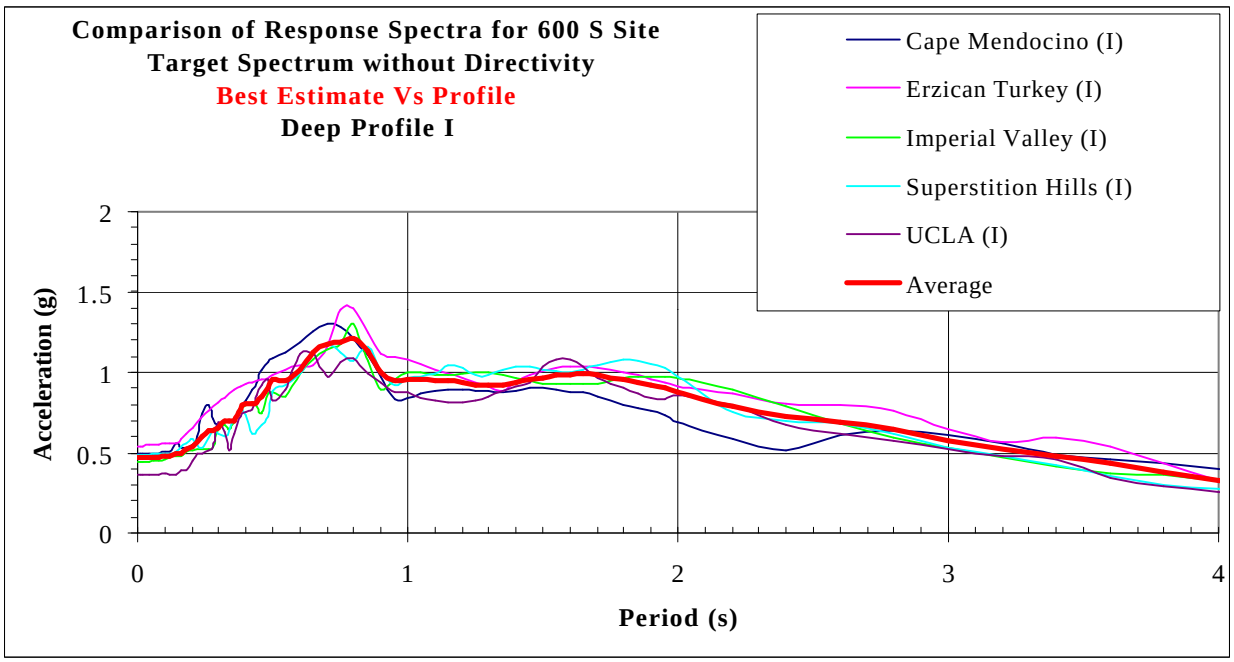

Figure 47a. Results of the SHAKE analyses for the best estimate 600 S. interchange profile and deep profile I for the case of the input spectrum without fault directivity.

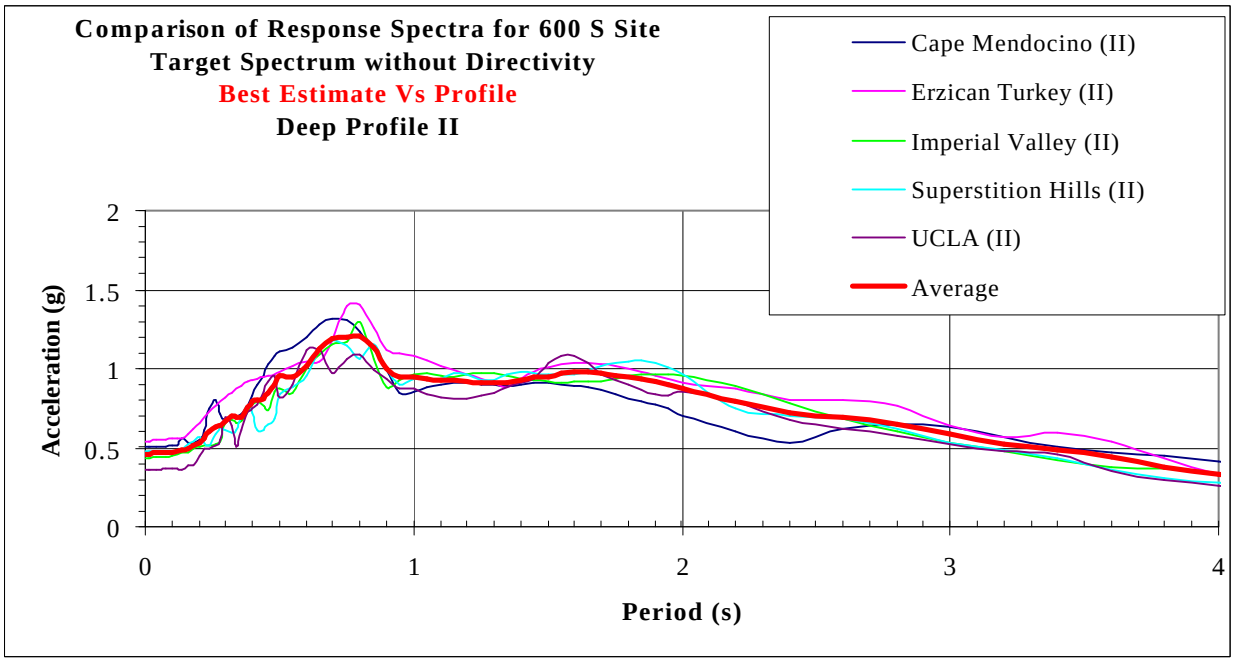

Figure 47b. Results of the SHAKE analyses for the best estimate 600 S. interchange profile and deep profile II for the case of the input spectrum without fault directivity.

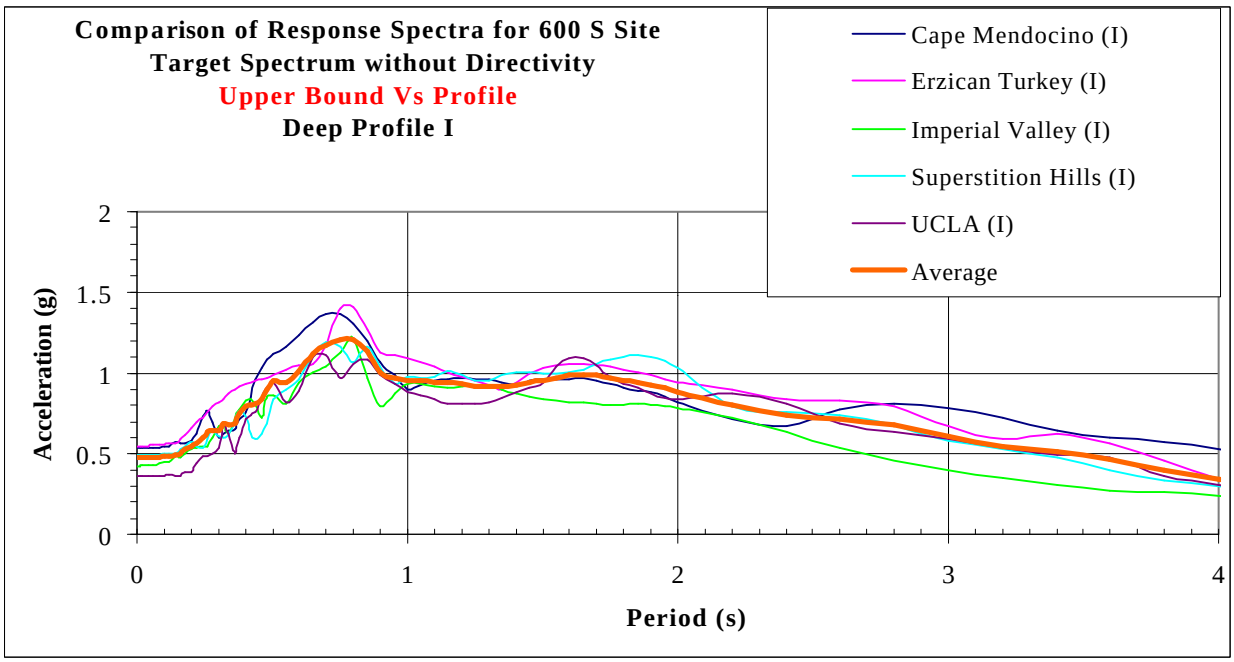

Figure 47c. Results of the SHAKE analyses for the upper bound 600 S. interchange profile and deep profile I for the case of the input spectrum without fault directivity.

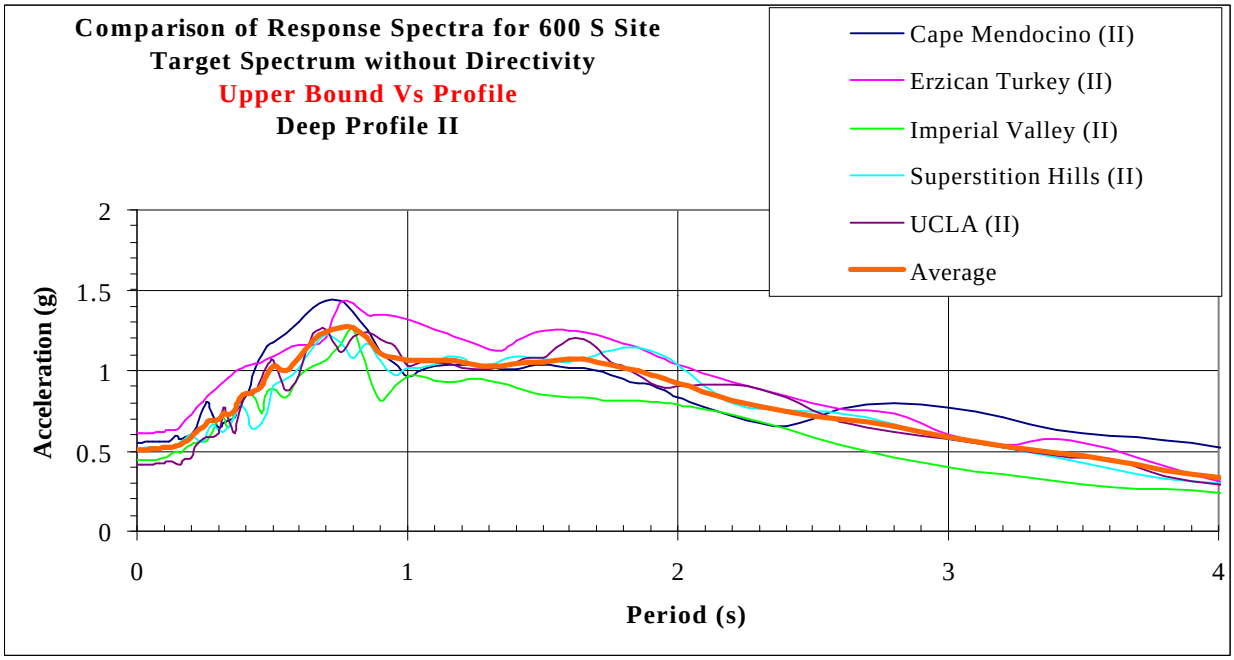

Figure 47d. Results of the SHAKE analyses for the upper bound 600 S. interchange profile and deep profile II for the case of the input spectrum without fault directivity.

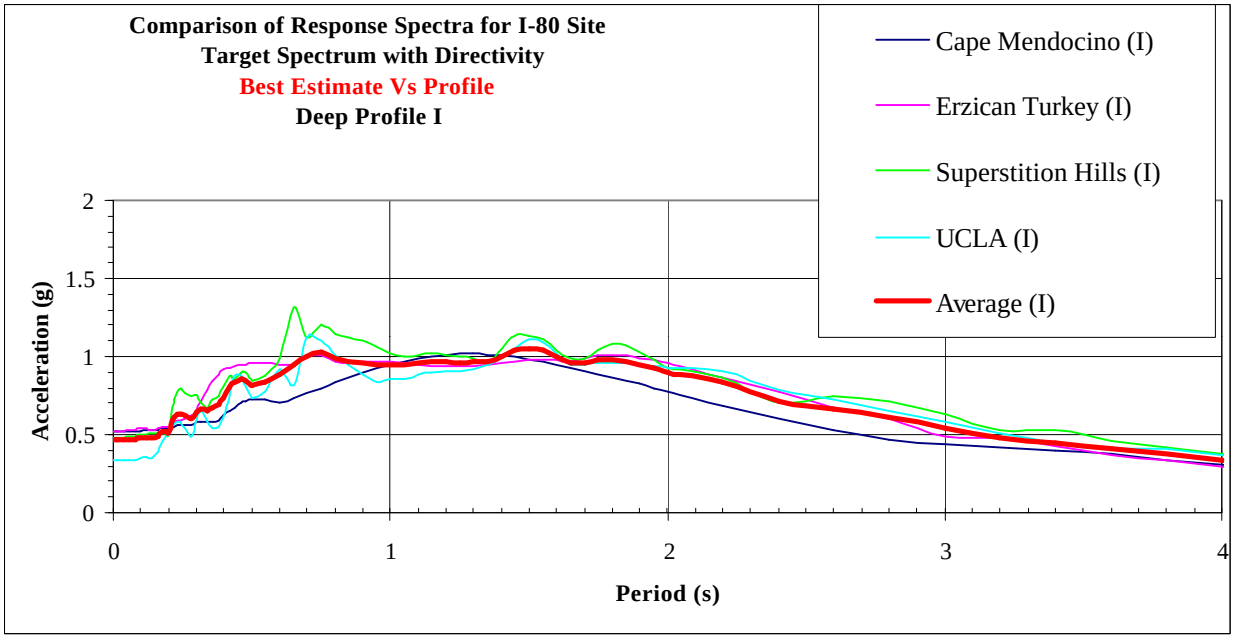

Figure 48a. Results of the SHAKE analyses for the best estimate I-80 interchange profile and deep profile I for the case of the input spectrum with fault directivity.

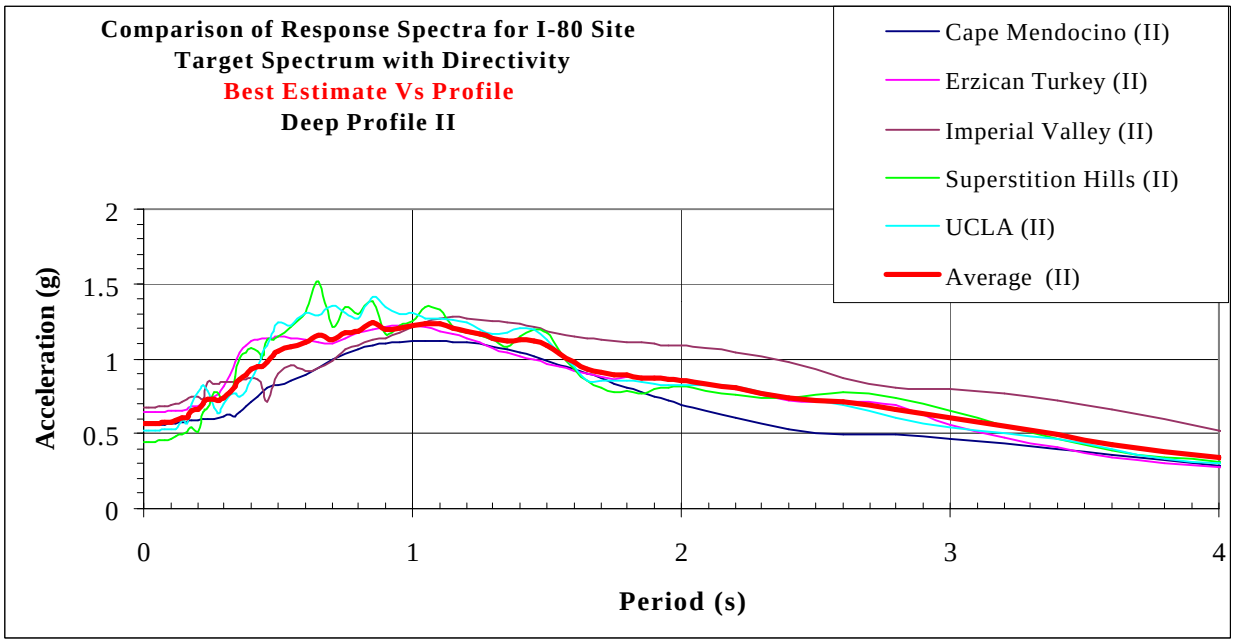

Figure 48b. Results of the SHAKE analyses for the best estimate I-80 interchange profile and deep profile II for the case of the input spectrum with fault directivity.

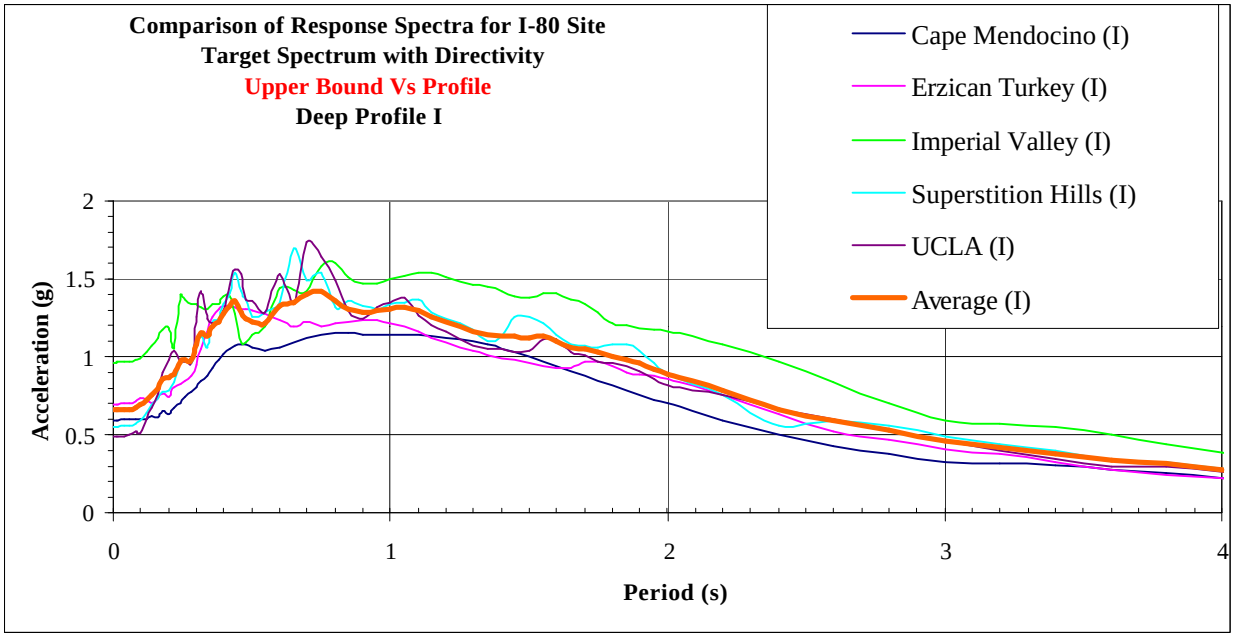

Figure 48c. Results of the SHAKE analyses for the upper bound I-80 interchange profile and deep profile I for the case of the input spectrum with fault directivity.

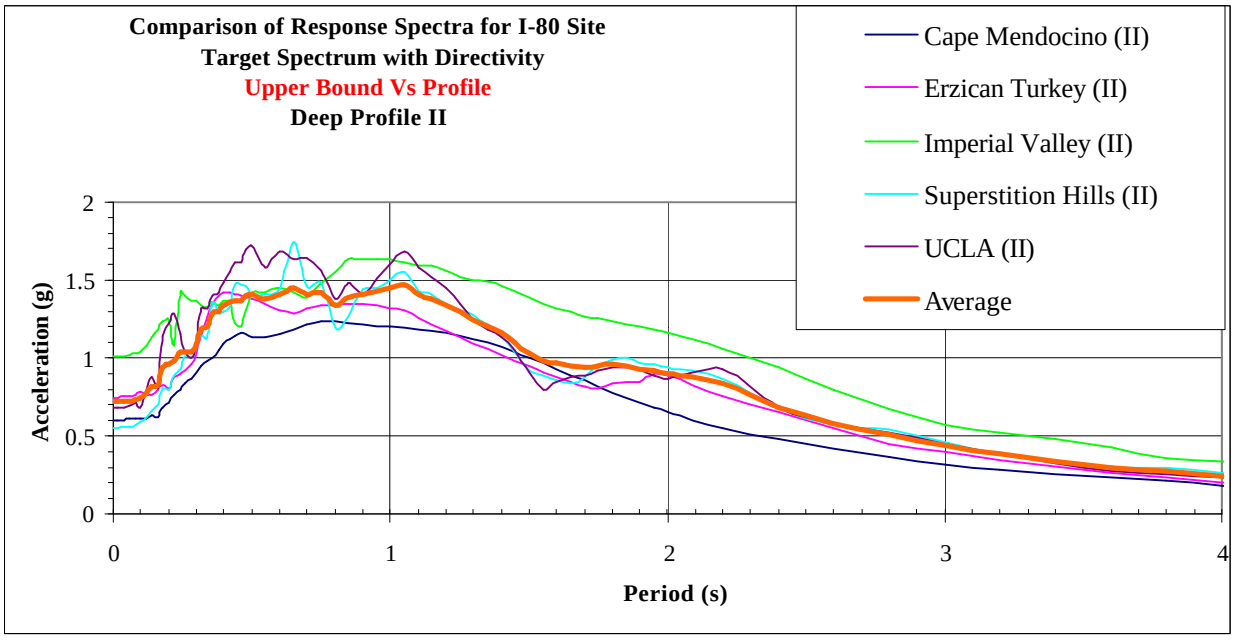

Figure 48d. Results of the SHAKE analyses for the upper bound I-80 interchange profile and deep profile II for the case of the input spectrum with fault directivity.

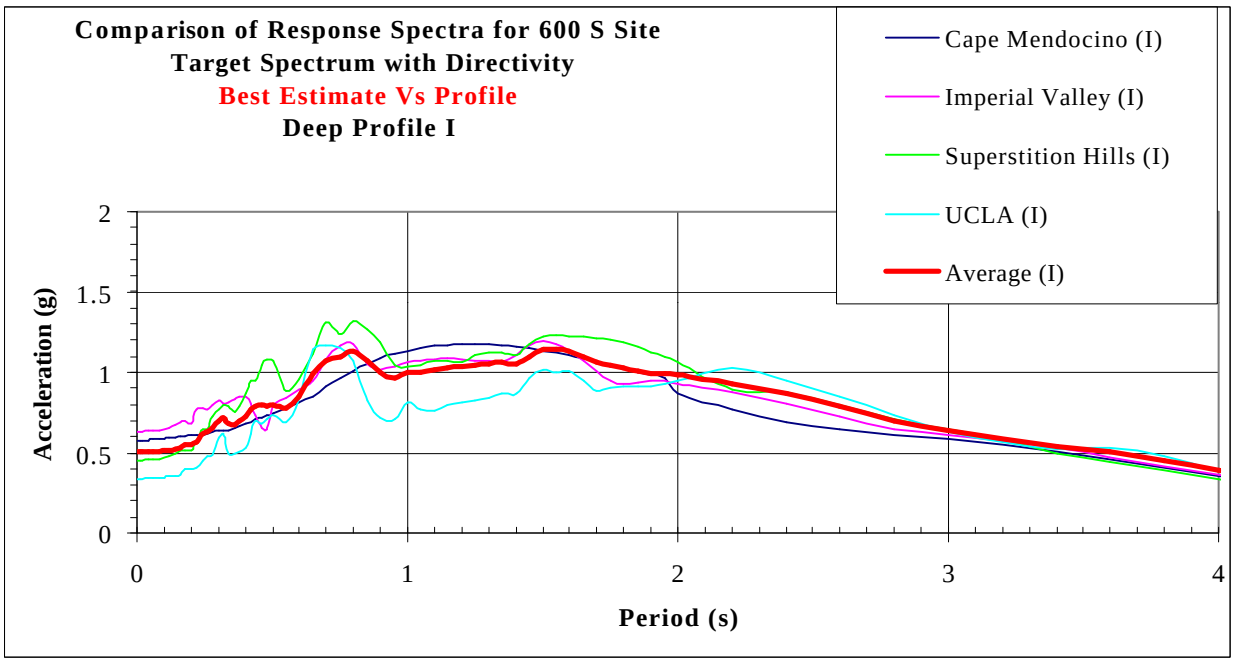

Figure 49a. Results of the SHAKE analyses for the best estimate 600 S. interchange profile and deep profile I for the case of the input spectrum with fault directivity.

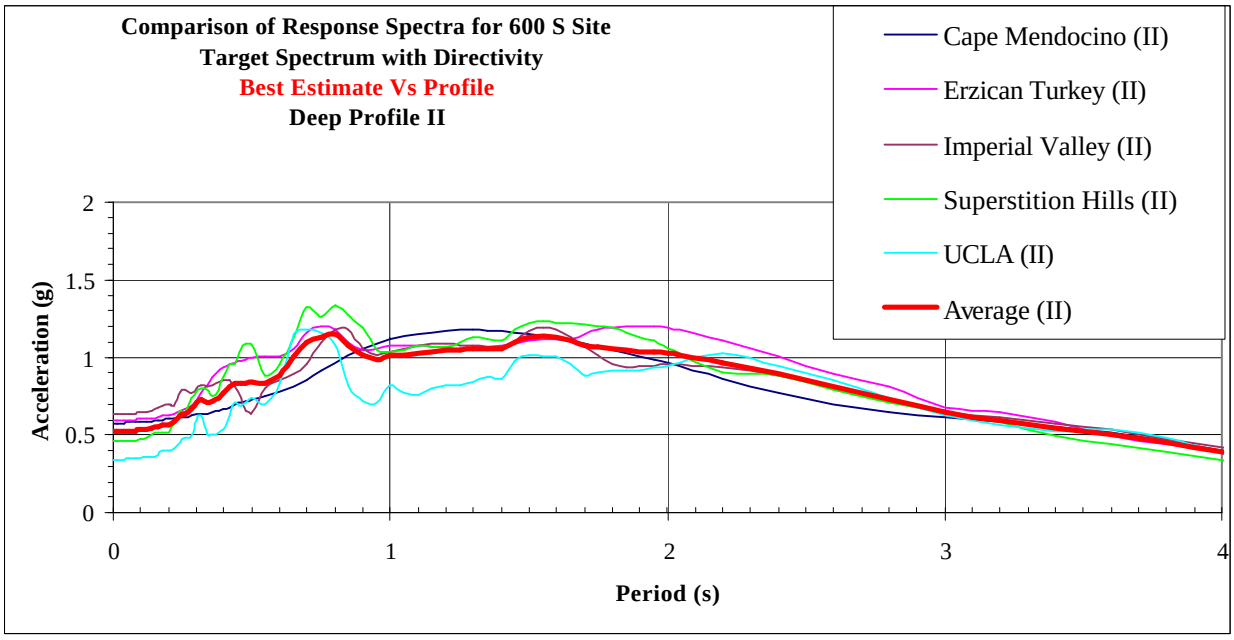

Figure 49b. Results of the SHAKE analyses for the best estimate 600 S. interchange profile and deep profile II for the case of the input spectrum with fault directivity.

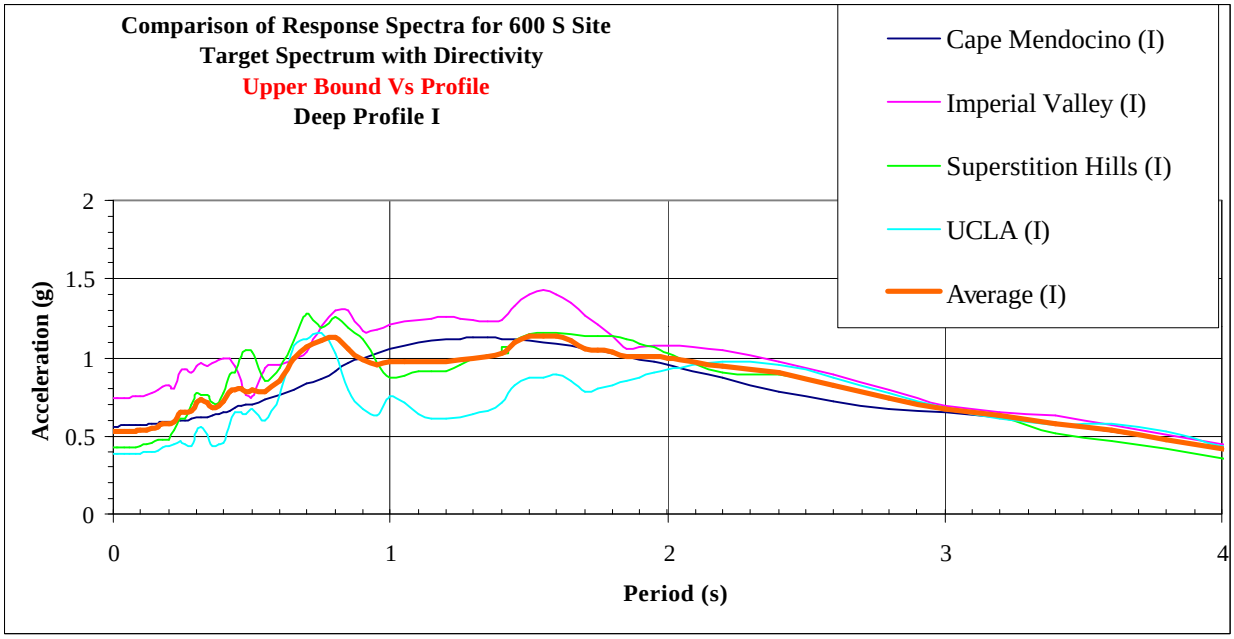

Figure 49c. Results of the SHAKE analyses for the upper bound 600 S. interchange profile and deep profile I for the case of the input spectrum with fault directivity.

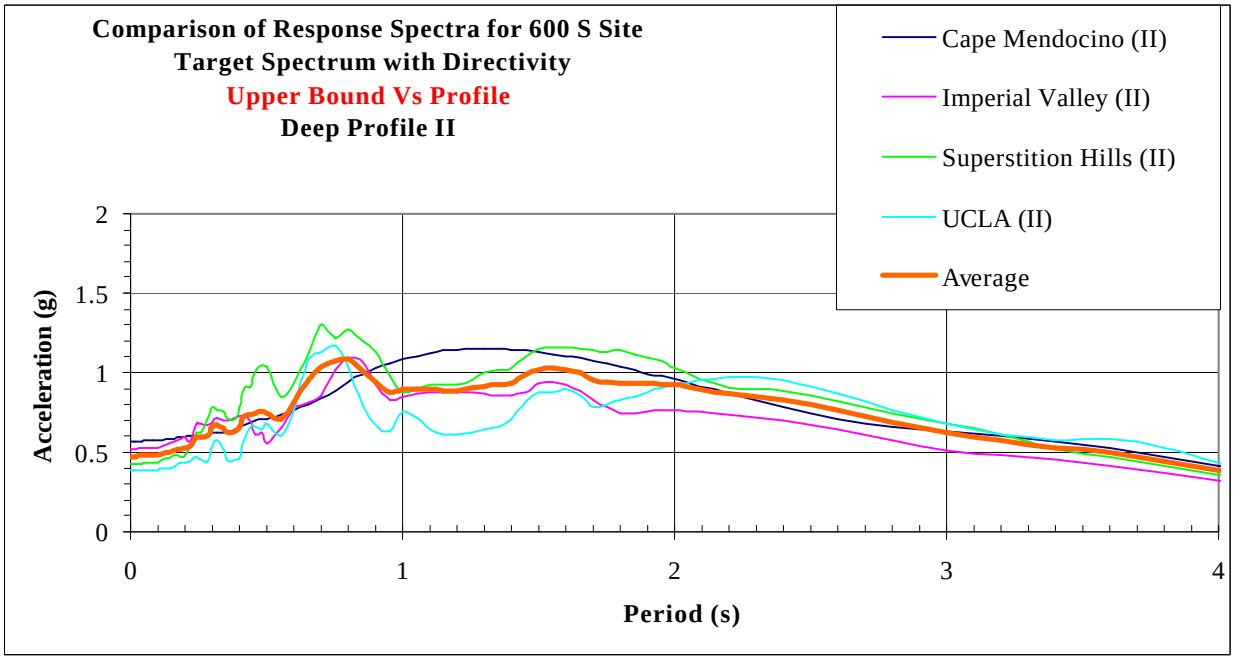

Figure 49d. Results of the SHAKE analyses for the upper bound 600 S. interchange profile and deep profile II for the case of the input spectrum with fault directivity.

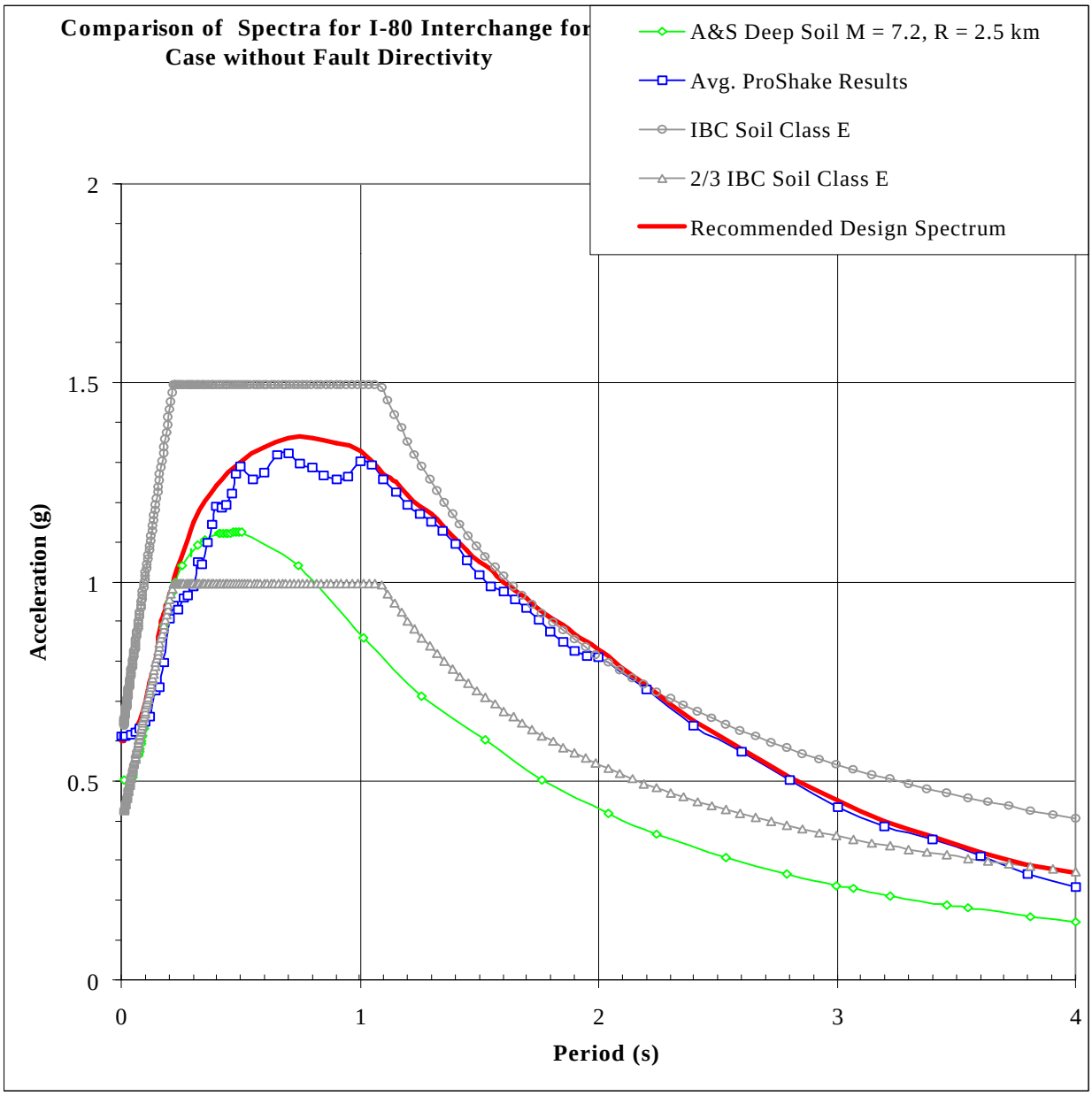

Figure 50. Recommended Design Surface Soil Spectrum for the I-80 Interchange for the case without fault directivity. Note that the recommended spectrum bounds the SHAKE, Abrahamson and Silva (1997) and two-thirds IBC spectra.

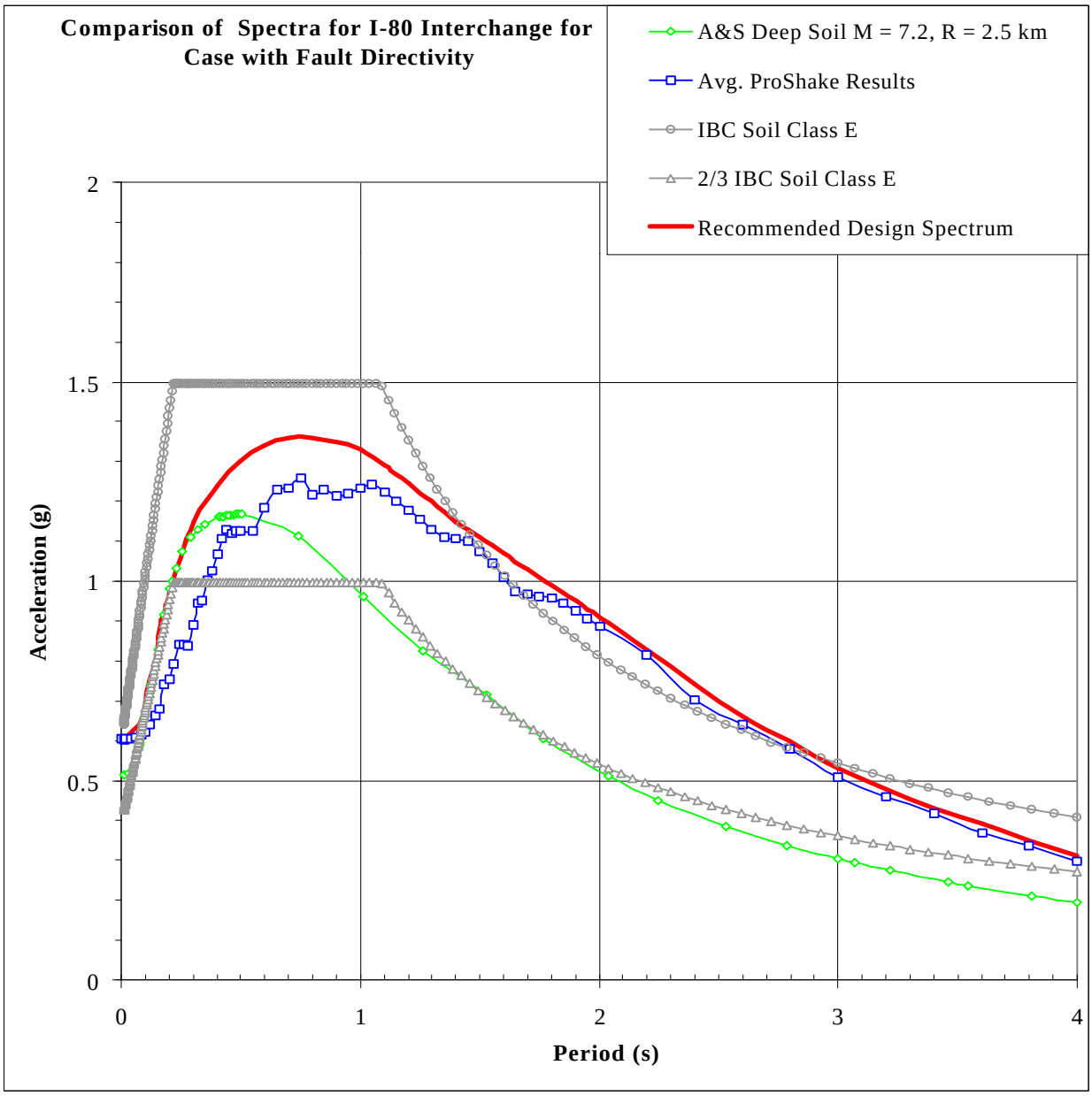

Figure 51. Recommended Design Surface Soil Spectrum for the I-80 Interchange for the case with fault directivity. Note that the recommended spectrum bounds the SHAKE, Abrahamson and Silva (1997) and two-thirds IBC spectra.

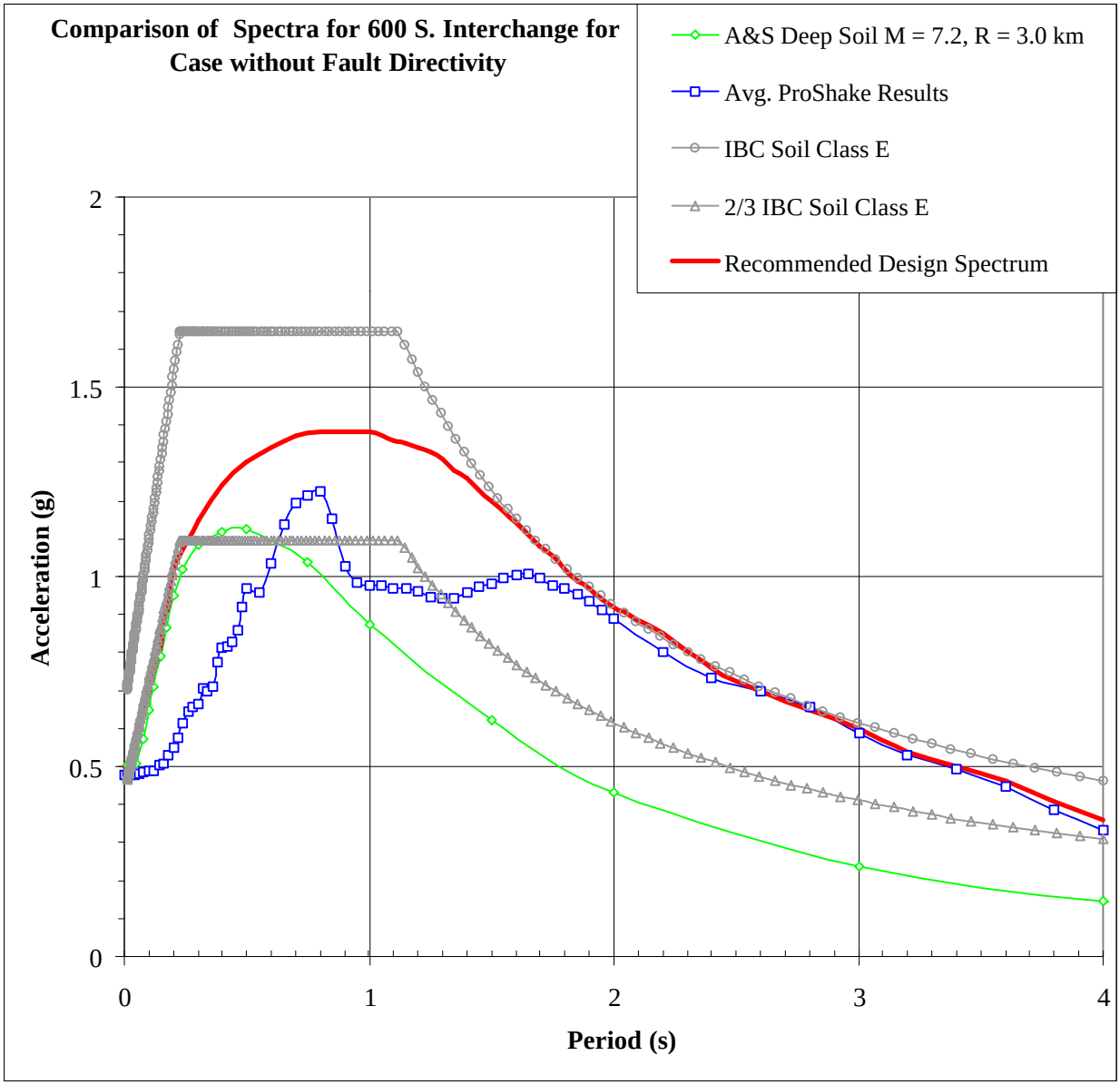

Figure 52. Recommended Design Surface Soil Spectrum for the 600 S. Interchange for the case without fault directivity. Note that the recommended spectrum bounds the SHAKE, Abrahamson and Silva (1997) and two-thirds IBC spectra.

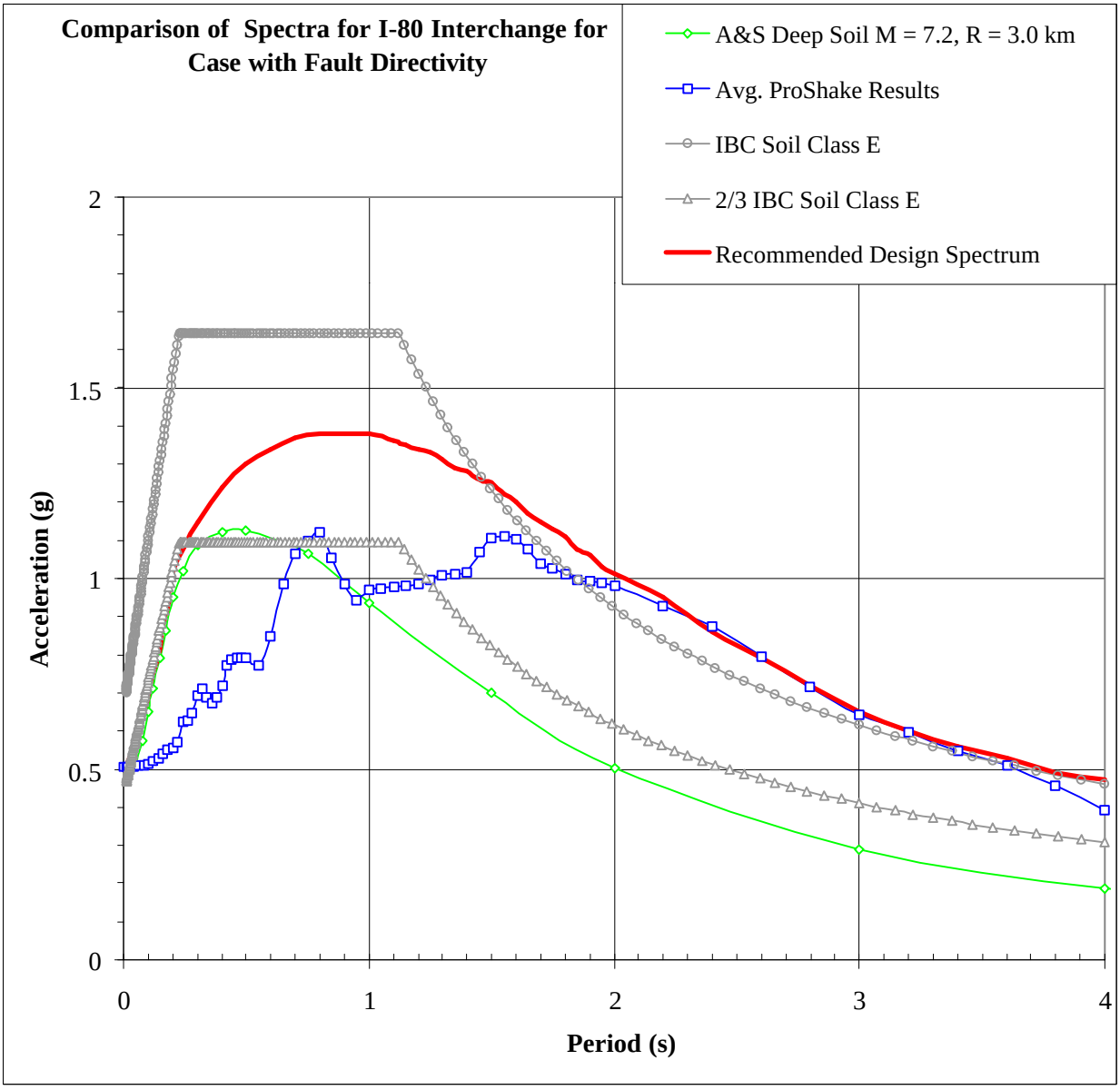

Figure 53. Recommended Design Surface Soil Spectrum for the 600 S. Interchange for the case with fault directivity. Note that the recommended spectrum bounds the SHAKE, Abrahamson and Silva (1997) and two-thirds IBC spectra.

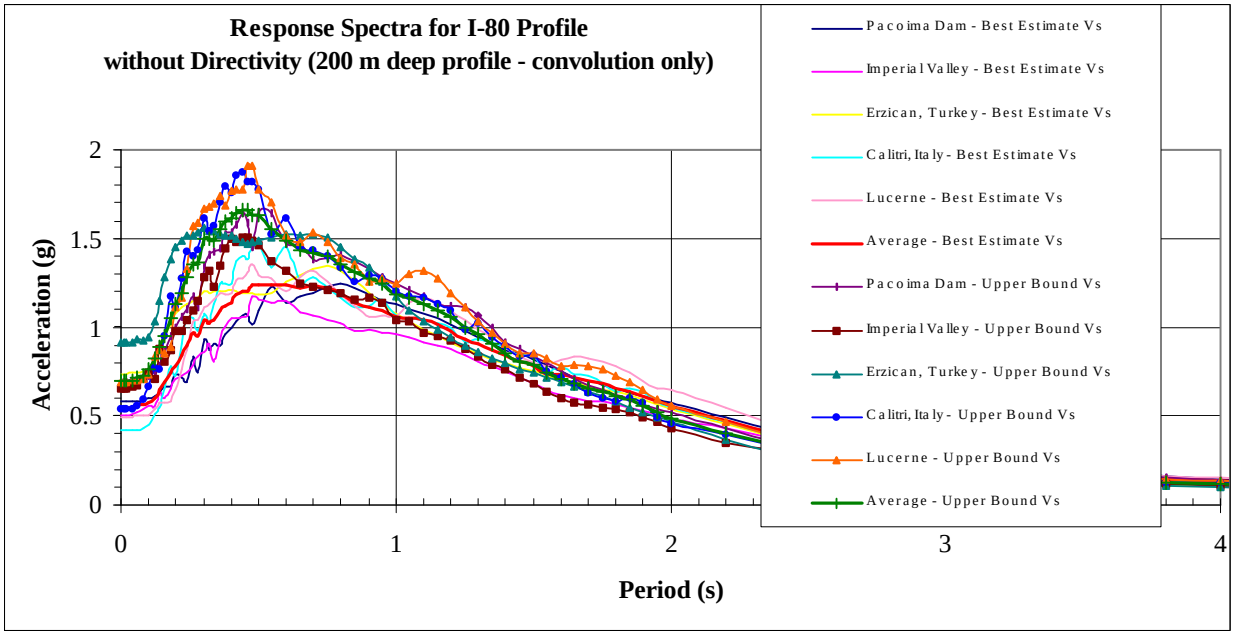

Figure 54a. Results of the 200 m convolution analysis for the I-80 interchange for the case of the input motion without fault directivity.

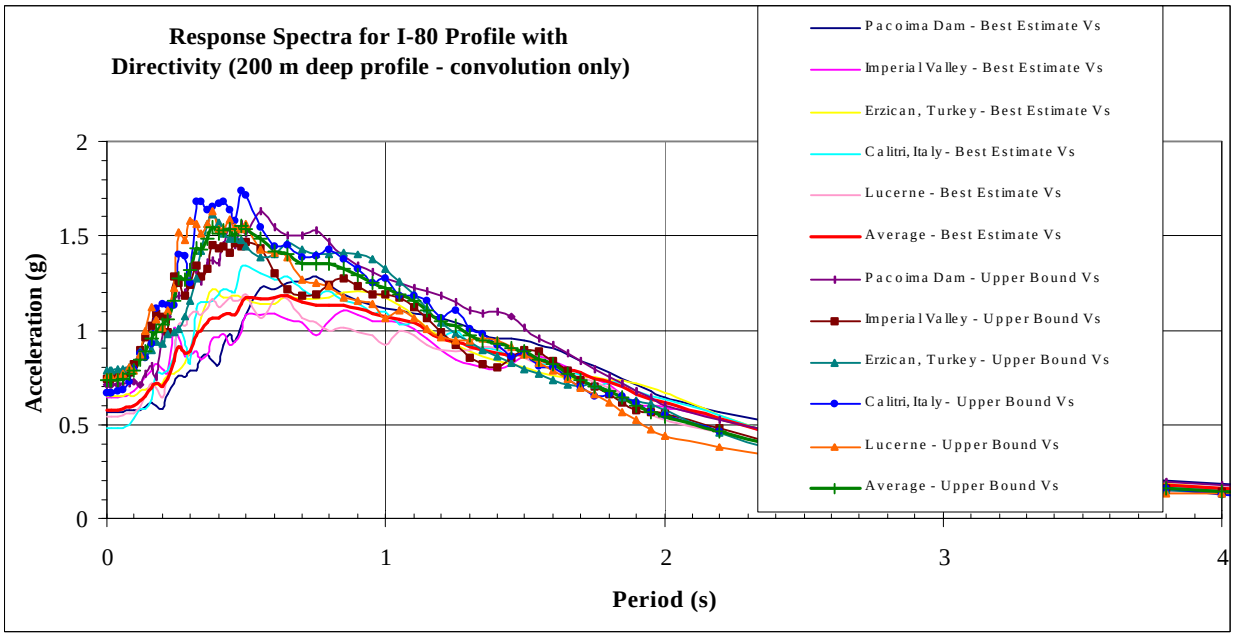

Figure 54b. Results of the 200 m convolution analysis for the I-80 interchange for the case of the input motion with fault directivity.

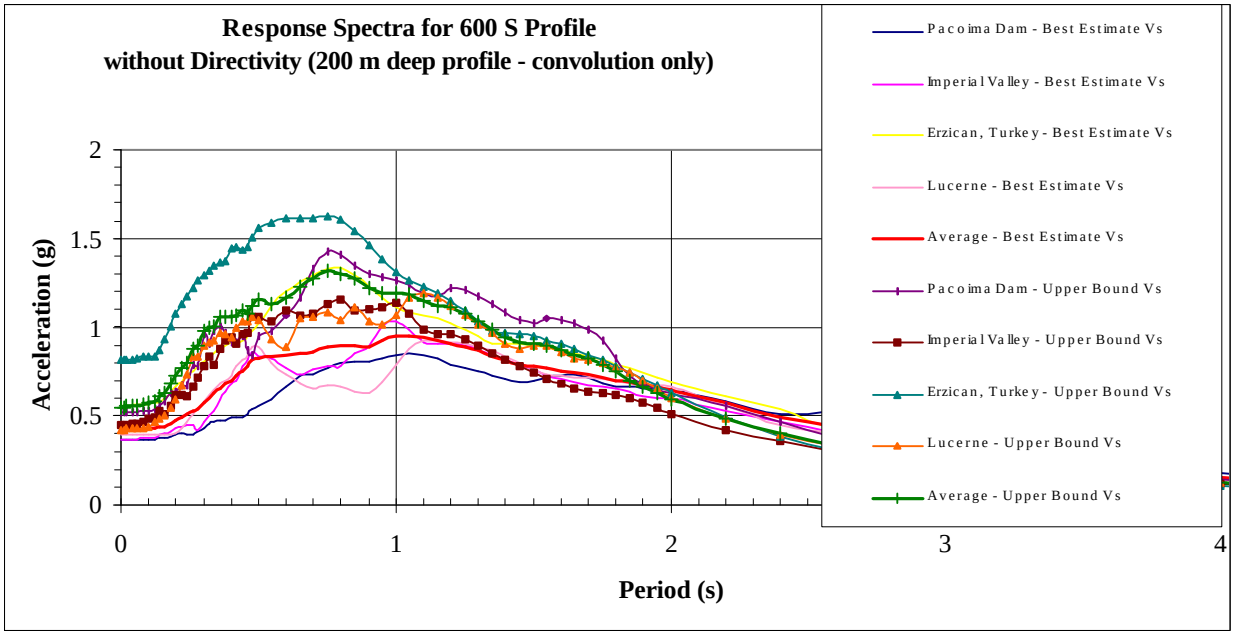

Figure 55a. Results of the 200 m convolution analysis for the 600 S. interchange for the case of the input motion without fault directivity.

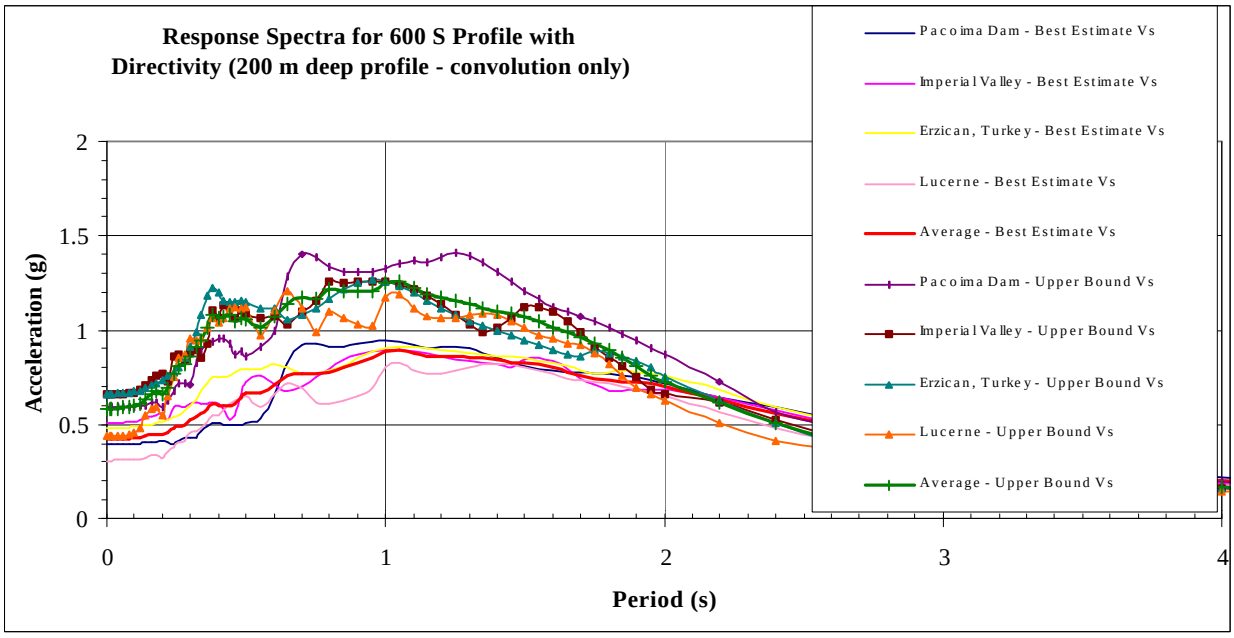

Figure 55b. Results of the 200 m convolution analysis for the 600 S. interchange for the case of the input motion without fault directivity.

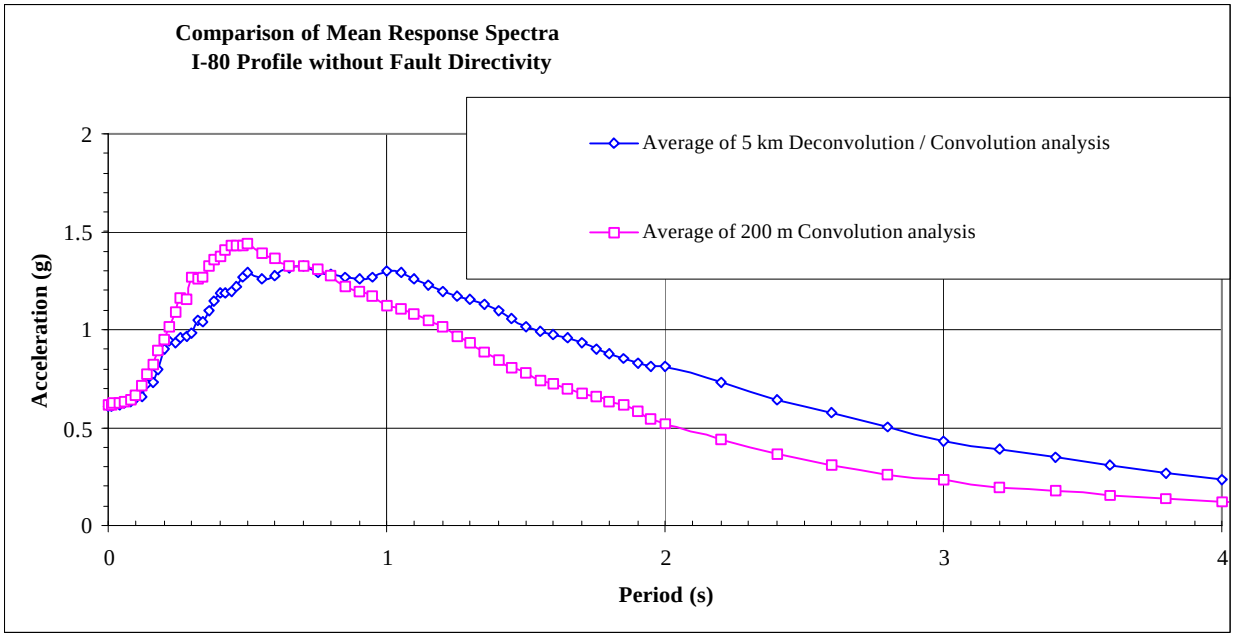

Figure 56a. Comparison of the 5 km Deconvolution / Convolution Analyses results with the 200 m Convolution Analyses results for the I-80 interchange for the case without fault directivity.

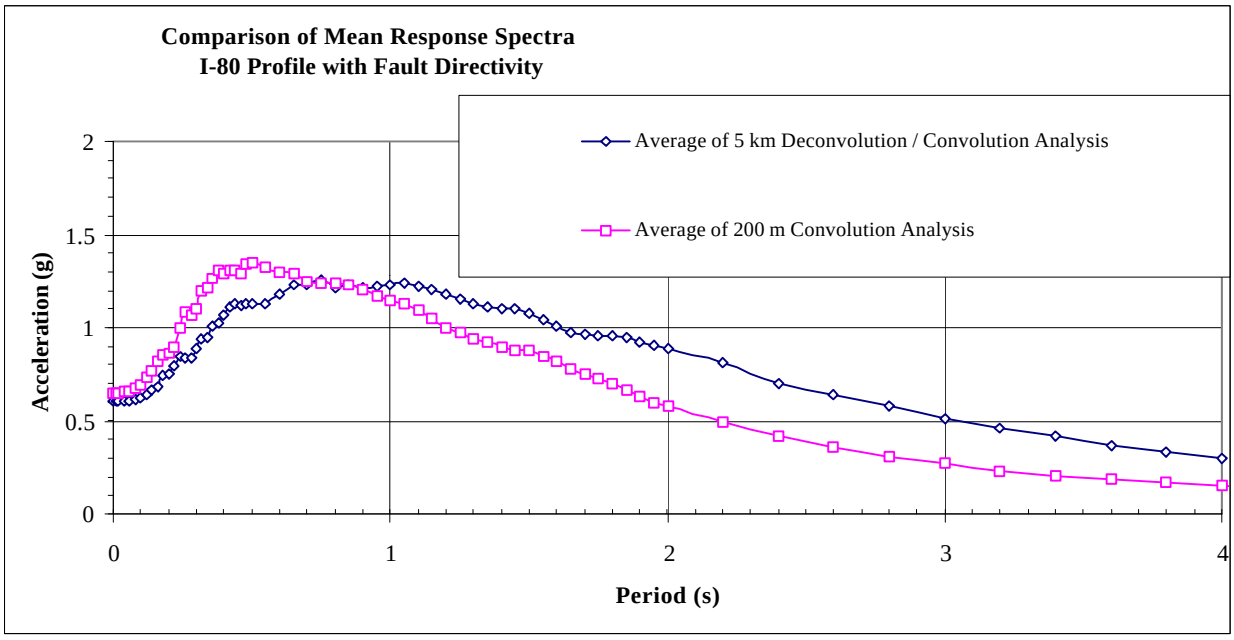

Figure 56b. Comparison of the 5 km Deconvolution / Convolution Analyses results with the 200 m Convolution Analyses results for the I-80 interchange for the case with fault directivity.

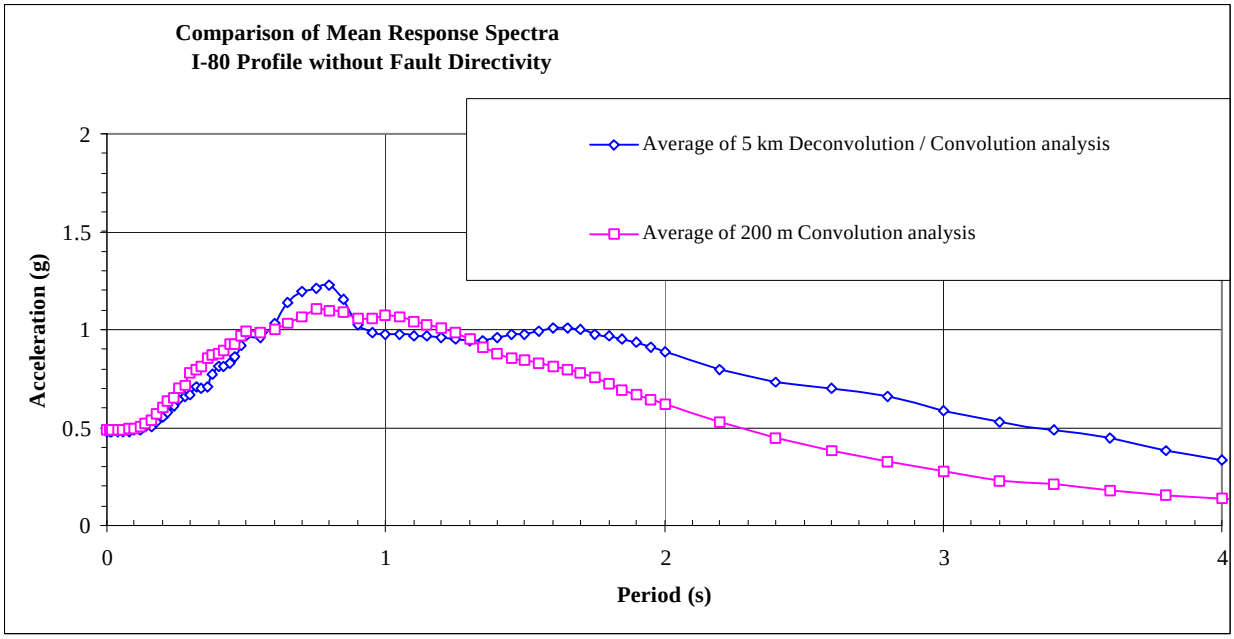

Figure 57a. Comparison of the 5 km Deconvolution / Convolution Analyses results with the 200 m Convolution Analyses results for the 600 S. interchange for the case without fault directivity.

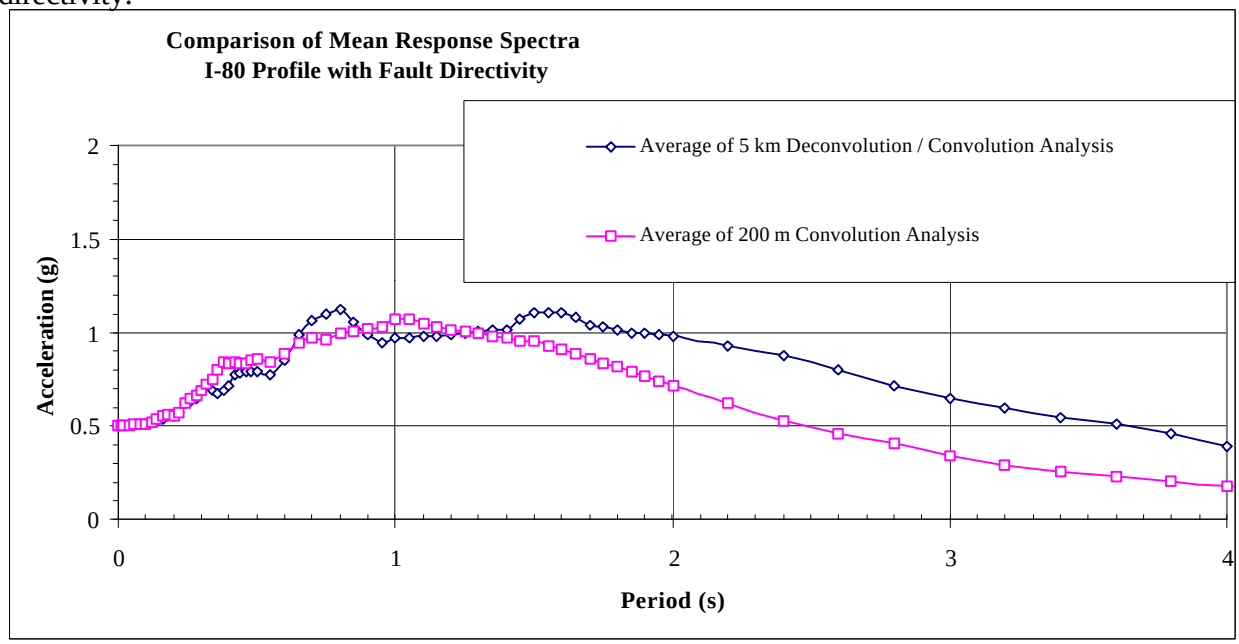

Figure 57b. Comparison of the 5 km Deconvolution / Convolution Analyses results with the 200 m Convolution Analyses results for the 600 S. interchange for the case with fault directivity.

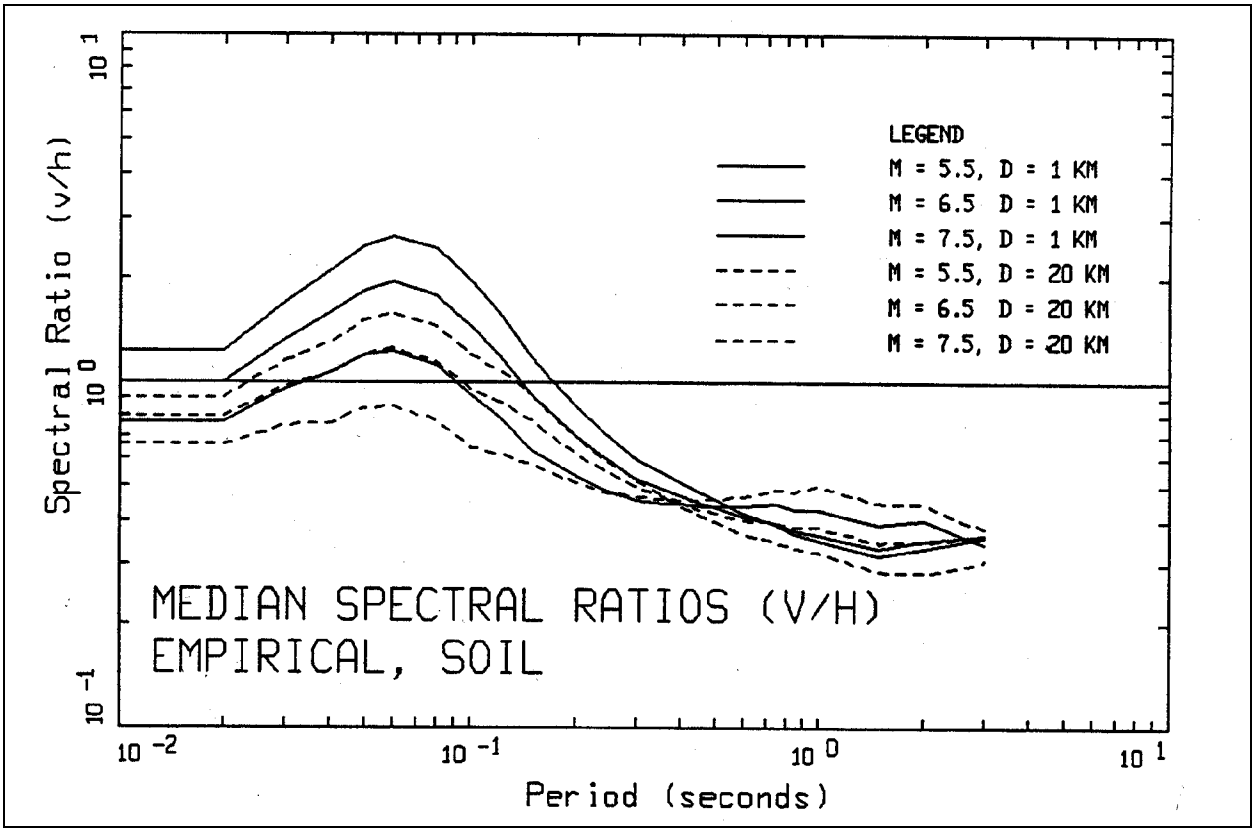

Figure 58. Vertical to horizontal spectral ratios for soil (Silva, 1997).

Table 1.
Proposed Site Classification System for Seismic Site Response (after Seed et al. 1997).

Site Class	Site Condition	General Description	Site Characteristics
(A_0)	A_0	Very hard rock	V_s(avg.)>5,000 ft/s in top 50 ft.
A	A_1	Competent rock with little or no soil and/or weathered rock veneer.	2,500 ft/s ≤ V_s(rock) ≤ 5,000 ft/s, and $H_{soil+weathered\ rock}$ ≤ 40 ft, with V_s > 800 ft/s (in all but the top few feet[3])
AB	AB_1	Soft, fractured and/or weathered rock.	For both AB_1 and AB_2: 40 ft ≤ $H_{soil+weathered\ rock}$ ≤ 150 ft, and V_s > 800 ft/s (in all but the top few feet[3])
	AB_2	Stiff, very shallow soil over rock and/or weathered rock.	
B	B_1	Deep, primarily cohesionless[4] soils. (H_{soil} ≤ 300 ft.)	No "soft clay" (see note 5), and $H_{cohesive\ soil}$ > 0.2 $H_{cohesionless\ soil}$
	B_2	Medium depth, stiff cohesive soils and/or mix of cohesionless with stiff cohesive soils; no "soft clay".	$H_{all\ soils}$ ≤ 200 ft, and V_s (cohesive soils) > 600 ft/s (see Note 5)
C	C_1	Medium depth, stiff cohesive soils and/or mix of cohesionless with stiff cohesive soils; thin layer(s) of soft clay.	Same as B_2 above, except 0 ft < $H_{soft\ clay}$ ≤ 10 ft. (see Note 5)
	C_2	Very deep, primarily cohesionless soils.	Same as B_1 above, except H_{soil} > 300 ft.
	C_3	Deep, stiff cohesive soils and/or mix of cohesionless with still cohesive soils; no "soft clay".	H_{soil} > 200 ft., and V_s (cohesive soils) > 600 ft/s
	C_4	Soft, cohesive soil at small to moderate levels of shaking.	10 ft < $H_{soft\ clay}$ ≤ 90 ft, and $A_{max,rock}$ ≤ 0.25 g
D	D_1	Soft, cohesive soil at medium to strong levels of shaking.	10 ft < $H_{soft\ clay}$ ≤ 90 ft, and 0.25 g < $A_{max,rock}$ ≤ 0.45 g, or (0.25 g < $A_{max,rock}$ ≤ 0.55 g and M ≤ 7-1/4)
(E)[6]	E_1	Very deep, soft cohesive soil.	$H_{soft\ clay}$ > 90 ft (see Note 5)
	E_2	Soft, cohesive soil and very strong shaking.	$H_{soft\ clay}$ > 10 ft and either: $A_{max,rock}$ > 0.55 g or $A_{max,rock}$ > 0.45 g and M > 7-1/4
	E_3	Very high plasticity clays.	H_{clay} > 30 ft with PI > 75% and V_s < 800 ft/s
(F)[7]	F_1	Highly organic and/or peaty soils.	H > 10 ft of peat and/or highly organic soils.
	F_2	Sites likely to suffer ground failure due either to significant soil liquefaction or other potential modes of ground instability.	Liquefaction and/or other types of ground failure analysis required.

Notes:
1. H = total (vertical) depth of soils of the type or types referred to.
2. V_s = seismic shear wave velocity (ft/s) at small shear strains (shear strain ~ 10^{-4}%).
3. If surface soils are cohesionless, V_s may be less than 800 ft/s in top 10 feet.
4. "Cohesionless soils" = soils with less than 30% "fines" by dry weight. "Cohesive soils" = soils with more than 30% "fines" by dry weight, and 15% ≤ PI (fines) ≤ 90%. Soils with more than 30% fines, and PI (fines) < 15% are considered "silty" soils herein, and these should be (conservatively) treated as "cohesive" soils for site classification purposes in this Table.
5. "Soft Clay" is defined as cohesive soil with: (a) Fines content ≥ 30%, (b) PI(fines) ≥ 20%, and (c) V_s ≤ 600 ft/s.
6. Site-specific geotechnical investigations and dynamic site response analyses are strongly recommended for these conditions. Response characteristics within this Class (E) of sites tends to be more highly variable than for Classes A_0 through D, and the response projections herein should be applied conservatively in the absence of (strongly recommended) site-specific studies.
7. Site-specific geotechnical investigations and dynamic site response analyses are *required* for these conditions. Potentially significant ground failure must be mitigated, and/or it must be demonstrated that the proposed structure/facility can be engineered to satisfactorily withstand such ground failure.

Table 2
Spectral Acceleration Values from National Hazard Maps
Source: http://eqint.cr.usgs.gov/eq/html/lookup.shtml)
2 Percent Probability of Exceedance in 50 years

600 S. Interchange

The ground motion values for the requested point:
LOCATION 40.7566 Lat. -111.9123 Long.
DISTANCE TO
NEAREST GRID POINT 4.93001371348276 kms
NEAREST GRID POINT 40.80000 Lat. -111.9000 Long.
Probabilistic ground motion values, in %g, at the Nearest Grid point are:

	10%PE in 50 yr	5%PE in 50 yr	**2%PE in 50 yr**
PGA	28.94103	52.59599	**87.49070**
0.2 sec SA	64.65861	117.7811	**182.5703**
0.3 sec SA	60.87698	113.4463	**177.7571**
1.0 sec SA	22.00630	43.82281	**76.85534**

I-80 / I-15 / Hwy 201 Interchange

The ground motion values for the requested point:
LOCATION 40.7185 Lat. -111.9033 Long.
DISTANCE TO
NEAREST GRID POINT 2.07318184354735 kms
NEAREST GRID POINT 40.70000 Lat.
-111.9000 Long.
Probabilistic ground motion values, in %g, at the Nearest Grid point are:

	10%PE in 50 yr	5%PE in 50 yr	**2%PE in 50 yr**
PGA	26.73019	45.23461	**75.53425**
0.2 sec SA	60.98087	108.3717	**166.0577**
0.3 sec SA	56.84623	103.2921	**160.1968**
1.0 sec SA	20.61572	38.61566	**67.68243**

Table 3a
Sample deaggregation for 600 S. Interchange
Source: (http://eqint1.cr.usgs.gov/eq/html/deaggint.shtml)
2 percent probability of exceedance in 50 years
0.2 Second Spectral Acceleration

****

PSHA Deaggregation. %contributions. site: 600_South long: 111.9120 W., lat: 40.7560 N.
Return period: 2475yrs. 0.20 s. PSA =1.5921819g. Computed annual rate=.40421E-03

DIST(KM)	MAG(MW)	ALL-EPS	EPSILON>2	1<EPS<2	0<EPS<1	-1<EPS<0	-2<EPS<-1	EPS<-2
8.3	5.20	0.751	0.735	0.015	0.000	0.000	0.000	0.000
14.3	5.21	0.180	0.177	0.003	0.000	0.000	0.000	0.000
8.3	5.60	0.723	0.617	0.098	0.008	0.000	0.000	0.000
14.5	5.62	0.194	0.176	0.018	0.000	0.000	0.000	0.000
7.1	6.24	3.228	1.271	1.928	0.028	0.001	0.000	0.000
14.4	6.27	0.557	0.505	0.044	0.008	0.000	0.000	0.000
24.0	6.28	0.053	0.044	0.009	0.000	0.000	0.000	0.000
0.9	6.51	49.931	3.760	20.145	26.023	0.003	0.000	0.000
14.2	6.79	0.397	0.323	0.061	0.012	0.000	0.000	0.000
23.3	6.80	0.068	0.057	0.008	0.002	0.000	0.000	0.000
3.9	7.20	42.826	3.928	24.948	13.948	0.001	0.000	0.000
18.1	7.10	0.846	0.840	0.002	0.004	0.001	0.000	0.000
21.6	7.09	0.086	0.082	0.002	0.002	0.000	0.000	0.000

Summary statistics for above 0.2s PSA deaggregation, R=distance, e=epsilon:
Mean src-site R= 2.9 km; M= 6.78; e0= 0.60; e= 1.23 for all sources.
Modal src-site R= 0.9 km; M= 6.51; e0= 0.30 from peak (R,M) bin
Primary distance metric: HYPOCENTRAL
MODE R*= 0.7 km; M*= 6.50; EPS.INTERVAL: 0 to 1 sigma % CONTRIB.= 26.023

Principal sources (faults, subduction, random seismicity having >10% contribution)

Source:	% contr.	R(km)	M	epsilon0 (mean values)
Wasatch Salt Lake City	**42.82**	3.9	7.20	0.72
West Valley	**47.89**	0.6	6.50	0.26

****

Table 3b
Sample deaggregation for I-80/I-15/Hwy. 201 Interchange
Source: (http://eqint1.cr.usgs.gov/eq/html/deaggint.shtml)
2 percent probability of exceedance in 50 years
0.2 Second Spectral Acceleration

****

PSHA Deaggregation. %contributions. site: I_80 long: 111.9030 W., lat: 40.7190 N.
Return period: 2475yrs. 0.20 s. PSA =1.5929723g. Computed annual rate=.40452E-03

DIST(KM)	MAG(MW)	ALL-EPS	EPSILON>2	1<EPS<2	0<EPS<1	-1<EPS<0	-2<EPS<-1	EPS<-2
7.5	5.20	0.869	0.761	0.108	0.001	0.000	0.000	0.000
15.0	5.21	0.150	0.147	0.003	0.000	0.000	0.000	0.000
7.4	5.60	0.826	0.568	0.248	0.010	0.000	0.000	0.000
15.1	5.62	0.163	0.147	0.015	0.000	0.000	0.000	0.000
6.9	6.25	2.805	1.077	1.664	0.063	0.001	0.000	0.000
14.3	6.24	0.596	0.566	0.023	0.007	0.000	0.000	0.000
24.1	6.23	0.058	0.045	0.013	0.000	0.000	0.000	0.000
0.7	6.51	56.599	3.719	20.251	27.301	5.328	0.000	0.000
14.2	6.79	0.472	0.386	0.076	0.010	0.000	0.000	0.000
23.9	6.80	0.055	0.040	0.011	0.003	0.000	0.000	0.000
3.8	7.20	37.037	3.925	24.341	8.769	0.001	0.000	0.000
22.2	7.10	0.180	0.175	0.003	0.003	0.000	0.000	0.000

Summary statistics for above 0.2s PSA deaggregation, R=distance, e=epsilon:
Mean src-site **R= 2.5 km; M= 6.74**; e0= 0.47; e= 1.15 for all sources.
Modal src-site **R= 0.7 km; M= 6.51**; e0= 0.10 from peak (R,M) bin
Primary distance metric: HYPOCENTRAL
MODE R*= 0.6km; M*= 6.50; EPS.INTERVAL: 0 to 1 sigma % CONTRIB.= 27.301

Principal sources (faults, subduction, random seismicity having >10% contribution)

Source:	% contr.	R(km)	M	epsilon0 (mean values)
Wasatch Salt Lake City	**37.03**	3.8	7.20	0.80
West Valley	**54.71**	0.5	6.50	0.07

****

Table 4
Recommended Time Histories for Response Analysis of I-80 and 600 South Interchanges

Earthquake, Magnitude	**Distance**	**Site**	**Channel**	**Direction**	**pga**	**v_{max}** (cm/s)	**Site Conditions**	**Tectonic Regime**	**Directivity ratio v_{max} / v**	**Source Files**
1987 Superstition Hills, CA., M = 6.7	4.3 km to fault rupture	286 Super-stition Mtn.	SUP045 SUP135	45 deg 135 deg	0.682 g 0.894 g	32.5 42.2	rock, U.S.G.S. site class B	strike slip	42.2/32.5 =1.298	PEER website, SUPERST/B-SUP045;SUPERST/B-SUP135
1994 Northridge, CA., M = 6.7	14.9 km to fault rupture	LA - UCLA Grounds	UCL090 UCL360	90 deg 360 deg.	0.278 g 0.474 g	20.0 22.2	rock, U.S.G.S. site class B	compressional	112.5 / 54.3 = 2.072	PEER website, PCD164.AT2 PCD254.AT2
1992 Cape Mendocino, CA, M = 7.1	13.7 km to fault rupture	Fortuna Blvd.	FOR 090 FOR 000	EW NS	0.114 0.116	21.7 30.0	rock, U.S.G.S. site class B	compressional	30.0 / 21.7 = 1.38	PEER website, NORTHR/UCL090;NORTHR/UCL090
1979 Imperial Valley, Ms = 6.9	14.2 km to fault rupture, 14.0 (r_{jb}),	Parachute Test site	H-PTS315 H-PTS225	315 deg 225 deg	0.204 g 0.111 g	16.1 17.8	rock, U.S.G.S site class B	extensional	16.1 / 17.8 = 0.904	PEER website, H-PTS315.AT2 H-PTS225.AT2
1992 Erzincan, Turkey, M = 6.7	2.0 km to fault rupture	Erzincan	ERZ-NS ERZ-EW	0 deg 90 deg.	0.515 g 0.496	83.9 64.3	stiff soil, U.S.G.S. site class C (V_s = 180 to 360 m/s)	extensional	83.9 / 64.3 = 1.305	PEER website, ERZ-NS.AT2 ERZ-EW.AT2

Table 5
Kappa Calculations for the Upper 70 m (246 ft)
Generic Western U.S. Rock Profile

upper profile (above 246 ft)

	thickness (ft)	Vs (ft/s)	H/V_{s2}	Qs	lamda	layer k
3.28	3.28	803.81	5.08E-06	12.5	**0.0400**	0.0003265
9.84	6.56	1031.06	6.17E-06	12.5	**0.0400**	0.0005091
16.40	6.56	1485.56	2.97E-06	12.50	**0.0400**	0.0003534
24.61	8.20	1801.66	2.53E-06	15.15	**0.0330**	0.0003005
32.81	8.20	1979.35	2.09E-06	15.15	**0.0330**	0.0002735
49.21	16.40	2188.76	3.42E-06	15.15	**0.0330**	0.0004947
65.62	16.40	2403.32	2.84E-06	15.15	**0.0330**	0.0004505
82.02	16.40	2575.43	2.47E-06	15.15	**0.0330**	0.0004204
98.43	16.40	2721.02	2.22E-06	15.15	**0.0330**	0.0003979
114.83	16.40	2878.94	1.98E-06	15.15	**0.0330**	0.0003761
131.23	16.40	3052.33	1.76E-06	15.15	**0.0330**	0.0003547
147.64	16.40	3212.23	1.59E-06	15.15	**0.0330**	0.0003370
164.04	16.40	3361.26	1.45E-06	15.15	**0.0330**	0.0003221
180.45	16.40	3501.22	1.34E-06	15.15	**0.0330**	0.0003092
196.85	16.40	3633.45	1.24E-06	15.15	**0.0330**	0.0002980
213.25	16.40	3759.00	1.16E-06	15.15	**0.0330**	0.0002880
229.66	16.40	3878.72	1.09E-06	15.15	**0.0330**	0.0002791
246.06	16.40	3993.27	1.03E-06	15.15	**0.0330**	0.0002711
					k upper	**0.0063618**
					k remaining	**0.0336382**

Table 6
Kappa Calculations for Depth between 70 m and 1.5 km
Generic Western U.S. Rock Profile

lower profile to a depth of 1.5 km

depth (bottom) (ft)	thickness (ft)	Vs (ft/s)	H/V_s^2	Qs	lamda	layer k
262.47	16.40	4103.22	9.74E-07	10.8037789	0.0463	0.0003700
278.87	16.40	4209.03	9.26E-07	11.0823808	0.0451	0.0003517
295.28	16.40	4311.10	8.83E-07	11.3511257	0.0440	0.0003352
311.68	16.40	4409.76	8.44E-07	11.6108989	0.0431	0.0003204
328.08	16.40	4505.30	8.08E-07	11.8624629	0.0421	0.0003069
360.89	32.81	4639.99	1.52E-06	12.2170991	0.0409	0.0005788
393.70	32.81	4815.32	1.41E-06	12.6787353	0.0394	0.0005374
426.51	32.81	4982.35	1.32E-06	13.1185244	0.0381	0.0005020
459.32	32.81	5141.08	1.24E-06	13.5364664	0.0369	0.0004714
492.13	32.81	5293.34	1.17E-06	13.9373622	0.0359	0.0004447
524.93	32.81	5439.12	1.11E-06	14.3212119	0.0349	0.0004212
557.74	32.81	5579.68	1.05E-06	14.6913047	0.0340	0.0004002
590.55	32.81	5715.02	1.00E-06	15.0476405	0.0332	0.0003815
623.36	32.81	5828.56	9.66E-07	15.3466069	0.0326	0.0003668
656.17	32.81	5920.32	9.36E-07	15.5882036	0.0321	0.0003555
688.98	32.81	5994.76	9.13E-07	15.7842	0.0317	0.0003467
721.78	32.81	6051.88	8.96E-07	15.9345959	0.0314	0.0003402
754.59	32.81	6106.99	8.80E-07	16.0797008	0.0311	0.0003341
787.40	32.81	6160.09	8.65E-07	16.2195147	0.0308	0.0003284
820.21	32.81	6211.47	8.50E-07	16.3548075	0.0306	0.0003230
853.02	32.81	6261.14	8.37E-07	16.4855792	0.0303	0.0003179
885.83	32.81	6309.32	8.24E-07	16.6124386	0.0301	0.0003130
918.64	32.81	6356.01	8.12E-07	16.7353855	0.0299	0.0003084
951.44	32.81	6401.41	8.01E-07	16.85491	0.0297	0.0003041
984.25	32.81	6445.50	7.90E-07	16.9710121	0.0295	0.0002999
1017.06	32.81	6488.45	7.79E-07	17.0840926	0.0293	0.0002960
1049.87	32.81	6530.25	7.69E-07	17.1941513	0.0291	0.0002922
1082.68	32.81	6571.03	7.60E-07	17.3015206	0.0289	0.0002886
1115.49	32.81	6610.79	7.51E-07	17.4062004	0.0287	0.0002851
1148.29	32.81	6649.63	7.42E-07	17.5084694	0.0286	0.0002818
1181.10	32.81	6687.55	7.34E-07	17.6083276	0.0284	0.0002786
1213.91	32.81	6724.65	7.26E-07	17.706011	0.0282	0.0002755
1246.72	32.81	6760.93	7.18E-07	17.8015198	0.0281	0.0002726
1279.53	32.81	6796.45	7.10E-07	17.895056	0.0279	0.0002698

1312.34	32.81	6831.23	7.03E-07	17.9866196	0.0278	0.0002670
1345.14	32.81	6865.32	6.96E-07	18.0763848	0.0277	0.0002644
1377.95	32.81	6898.73	6.89E-07	18.1643516	0.0275	0.0002618
1410.76	32.81	6931.51	6.83E-07	18.2506715	0.0274	0.0002593
1443.57	32.81	6963.67	6.77E-07	18.3353445	0.0273	0.0002570
1476.38	32.81	6995.25	6.70E-07	18.4185031	0.0271	0.0002546
1509.19	32.81	7026.26	6.65E-07	18.5001472	0.0270	0.0002524
1541.99	32.81	7056.74	6.59E-07	18.5803936	0.0269	0.0002502
1574.80	32.81	7086.69	6.53E-07	18.6592421	0.0268	0.0002481
1607.61	32.81	7116.14	6.48E-07	18.7367961	0.0267	0.0002461
1640.42	32.81	7145.10	6.43E-07	18.8130554	0.0266	0.0002441
1673.23	32.81	7173.61	6.38E-07	18.888112	0.0265	0.0002421
1706.04	32.81	7201.66	6.33E-07	18.9619659	0.0264	0.0002403
1738.85	32.81	7229.28	6.28E-07	19.034699	0.0263	0.0002384
1771.65	32.81	7256.48	6.23E-07	19.1063116	0.0262	0.0002366
1804.46	32.81	7283.28	6.18E-07	19.1768771	0.0261	0.0002349
1837.27	32.81	7309.68	6.14E-07	19.2463956	0.0260	0.0002332
1870.08	32.81	7335.71	6.10E-07	19.3149336	0.0259	0.0002316
1902.89	32.81	7361.37	6.05E-07	19.3824911	0.0258	0.0002299
1935.70	32.81	7386.68	6.01E-07	19.449128	0.0257	0.0002284
1968.50	32.81	7411.64	5.97E-07	19.5148445	0.0256	0.0002268
2001.31	32.81	7436.27	5.93E-07	19.579695	0.0255	0.0002253
2034.12	32.81	7460.57	5.89E-07	19.6436796	0.0255	0.0002239
2066.93	32.81	7484.56	5.86E-07	19.706848	0.0254	0.0002224
2099.74	32.81	7508.24	5.82E-07	19.7692001	0.0253	0.0002210
2132.55	32.81	7531.63	5.78E-07	19.8307814	0.0252	0.0002197
2165.35	32.81	7554.73	5.75E-07	19.8915918	0.0251	0.0002183
2198.16	32.81	7577.54	5.71E-07	19.9516729	0.0251	0.0002170
2230.97	32.81	7600.09	5.68E-07	20.0110247	0.0250	0.0002157
2263.78	32.81	7622.36	5.65E-07	20.0696854	0.0249	0.0002145
2296.59	32.81	7644.38	5.61E-07	20.1276551	0.0248	0.0002132
2329.40	32.81	7666.15	5.58E-07	20.1849688	0.0248	0.0002120
2362.20	32.81	7687.67	5.55E-07	20.2416265	0.0247	0.0002108
2395.01	32.81	7708.95	5.52E-07	20.2976608	0.0246	0.0002097
2427.82	32.81	7729.99	5.49E-07	20.3530717	0.0246	0.0002085
2460.63	32.81	7750.81	5.46E-07	20.4078891	0.0245	0.0002074
2493.44	32.81	7771.41	5.43E-07	20.462113	0.0244	0.0002063
2526.25	32.81	7791.79	5.40E-07	20.5157714	0.0244	0.0002052
2559.06	32.81	7811.95	5.38E-07	20.5688641	0.0243	0.0002042
2591.86	32.81	7831.91	5.35E-07	20.6214171	0.0242	0.0002031
2624.67	32.81	7851.66	5.32E-07	20.6734304	0.0242	0.0002021
2657.48	32.81	7871.22	5.30E-07	20.724928	0.0241	0.0002011
2690.29	32.81	7890.58	5.27E-07	20.7759099	0.0241	0.0002001

2723.10	32.81	7909.76	5.24E-07	20.8263986	0.0240	0.0001992
2755.91	32.81	7928.75	5.22E-07	20.876394	0.0240	0.0001982
2788.71	32.81	7947.56	5.19E-07	20.9259171	0.0239	0.0001973
2821.52	32.81	7966.19	5.17E-07	20.974968	0.0238	0.0001964
2854.33	32.81	7984.64	5.15E-07	21.0235662	0.0238	0.0001954
2887.14	32.81	8002.93	5.12E-07	21.0717117	0.0237	0.0001946
2919.95	32.81	8021.05	5.10E-07	21.1194228	0.0237	0.0001937
2952.76	32.81	8039.00	5.08E-07	21.1666997	0.0236	0.0001928
2985.56	32.81	8056.80	5.05E-07	21.2135594	0.0236	0.0001920
3018.37	32.81	8074.44	5.03E-07	21.2600021	0.0235	0.0001911
3051.18	32.81	8091.93	5.01E-07	21.3060439	0.0235	0.0001903
3083.99	32.81	8109.26	4.99E-07	21.3516847	0.0234	0.0001895
3116.80	32.81	8126.45	4.97E-07	21.3969399	0.0234	0.0001887
3149.61	32.81	8143.49	4.95E-07	21.4418095	0.0233	0.0001879
3182.41	32.81	8160.39	4.93E-07	21.4863077	0.0233	0.0001871
3215.22	32.81	8177.15	4.91E-07	21.5304346	0.0232	0.0001864
3248.03	32.81	8193.77	4.89E-07	21.5742038	0.0232	0.0001856
3280.84	32.81	8210.26	4.87E-07	21.6176152	0.0231	0.0001849
3313.65	32.81	8226.10	4.85E-07	21.6593092	0.0231	0.0001841
3346.46	32.81	8241.28	4.83E-07	21.6992859	0.0230	0.0001835
3379.27	32.81	8256.46	4.81E-07	21.7392626	0.0230	0.0001828
3412.07	32.81	8271.64	4.80E-07	21.7792394	0.0230	0.0001821
3444.88	32.81	8286.83	4.78E-07	21.8192161	0.0229	0.0001815
3477.69	32.81	8302.01	4.76E-07	21.8591928	0.0229	0.0001808
3510.50	32.81	8317.19	4.74E-07	21.8991695	0.0228	0.0001801
3543.31	32.81	8332.38	4.73E-07	21.9391462	0.0228	0.0001795
3576.12	32.81	8347.56	4.71E-07	21.9791229	0.0227	0.0001788
3608.92	32.81	8362.74	4.69E-07	22.0190996	0.0227	0.0001782
3641.73	32.81	8377.92	4.67E-07	22.0590764	0.0227	0.0001775
3674.54	32.81	8393.11	4.66E-07	22.0990531	0.0226	0.0001769
3707.35	32.81	8408.29	4.64E-07	22.1390298	0.0226	0.0001762
3740.16	32.81	8423.47	4.62E-07	22.1790065	0.0225	0.0001756
3772.97	32.81	8438.66	4.61E-07	22.2189832	0.0225	0.0001750
3805.77	32.81	8453.84	4.59E-07	22.2589599	0.0225	0.0001744
3838.58	32.81	8469.02	4.57E-07	22.2989366	0.0224	0.0001737
3871.39	32.81	8484.21	4.56E-07	22.3389133	0.0224	0.0001731
3904.20	32.81	8499.39	4.54E-07	22.3788901	0.0223	0.0001725
3937.01	32.81	8514.57	4.53E-07	22.4188668	0.0223	0.0001719
3969.82	32.81	8528.80	4.51E-07	22.4563301	0.0223	0.0001713
4002.62	32.81	8542.07	4.50E-07	22.4912802	0.0222	0.0001708
4035.43	32.81	8555.35	4.48E-07	22.5262302	0.0222	0.0001702
4068.24	32.81	8568.62	4.47E-07	22.5611802	0.0222	0.0001697
4101.05	32.81	8581.90	4.45E-07	22.5961302	0.0221	0.0001692

4133.86	32.81	8595.17	4.44E-07	22.6310802	0.0221	0.0001687
4166.67	32.81	8608.44	4.43E-07	22.6660303	0.0221	0.0001681
4199.48	32.81	8621.72	4.41E-07	22.7009803	0.0220	0.0001676
4232.28	32.81	8634.99	4.40E-07	22.7359303	0.0220	0.0001671
4265.09	32.81	8648.26	4.39E-07	22.7708803	0.0220	0.0001666
4297.90	32.81	8661.54	4.37E-07	22.8058304	0.0219	0.0001661
4330.71	32.81	8674.81	4.36E-07	22.8407804	0.0219	0.0001656
4363.52	32.81	8688.09	4.35E-07	22.8757304	0.0219	0.0001651
4396.33	32.81	8701.36	4.33E-07	22.9106804	0.0218	0.0001646
4429.13	32.81	8714.63	4.32E-07	22.9456304	0.0218	0.0001641
4461.94	32.81	8727.91	4.31E-07	22.9805805	0.0218	0.0001636
4494.75	32.81	8741.18	4.29E-07	23.0155305	0.0217	0.0001631
4527.56	32.81	8754.46	4.28E-07	23.0504805	0.0217	0.0001626
4560.37	32.81	8767.73	4.27E-07	23.0854305	0.0217	0.0001621
4593.18	32.81	8781.00	4.25E-07	23.1203806	0.0216	0.0001616
4658.79	65.62	8799.47	8.47E-07	23.1690095	0.0216	0.0003218
4724.41	65.62	8823.14	8.43E-07	23.2313173	0.0215	0.0003201
4790.03	65.62	8846.80	8.38E-07	23.2936251	0.0215	0.0003184
4855.64	65.62	8870.46	8.34E-07	23.3559329	0.0214	0.0003167
4921.26	65.62	8894.13	8.29E-07	23.4182407	0.0214	0.0003150
						3.36E-02

Table 7
Soil Properties and V_s Profile
Generic Western U.S. Profile
(Upper 75 m only)

Layer Number	Material Name	Thickness (m)	Unit Weight (kN/m^3)	Gmax (MPa)	Vs (m/sec)	Modulus Curve	Damping Curve	Mod. Parameter	Damp. Parameter
1	Weathered Rock	1.00	18.60	113.85	245.00	Weathered Rock above 20ft (Silva et al.)	Weathered Rock above 20ft (Silva et al.)		
2	Weathered Rock	2.00	18.60	188.19	315.00	Weathered Rock above 20ft (Silva et al.)	Weathered Rock above 20ft (Silva et al.)		
3	Weathered Rock	2.00	18.60	389.21	453.00	Weathered Rock above 20ft (Silva et al.)	Weathered Rock above 20ft (Silva et al.)		
4	Weathered Rock	2.50	18.60	571.65	549.00	Weathered Rock below 20ft (Silva et al.)	Weathered Rock below 20ft (Silva et al.)		
5	Weathered Rock	2.50	18.60	691.93	604.00	Weathered Rock below 20ft (Silva et al.)	Weathered Rock below 20ft (Silva et al.)		
6	Weathered Rock	5.00	18.60	846.33	668.00	Weathered Rock below 20ft (Silva et al.)	Weathered Rock below 20ft (Silva et al.)		
7	Weathered Rock	5.00	18.60	1,019.05	733.00	Weathered Rock below 20ft (Silva et al.)	Weathered Rock below 20ft (Silva et al.)		
8	Weathered Rock	5.00	18.60	1,168.76	785.00	Weathered Rock below 20ft (Silva et al.)	Weathered Rock below 20ft (Silva et al.)		
9	Weathered Rock	5.00	18.60	1,306.60	830.00	Weathered Rock below 20ft (Silva et al.)	Weathered Rock below 20ft (Silva et al.)		
10	Weathered Rock	5.00	18.60	1,462.09	878.00	Weathered Rock below 20ft (Silva et al.)	Weathered Rock below 20ft (Silva et al.)		
11	Weathered Rock	5.00	18.60	1,643.94	931.00	Weathered Rock below 20ft (Silva et al.)	Weathered Rock below 20ft (Silva et al.)		
12	Weathered Rock	5.00	18.60	1,821.54	980.00	Weathered Rock below 20ft (Silva et al.)	Weathered Rock below 20ft (Silva et al.)		
13	Weathered Rock	5.00	18.60	1,992.66	1,025.00	Weathered Rock below 20ft (Silva et al.)	Weathered Rock below 20ft (Silva et al.)		
14	Weathered Rock	5.00	18.60	2,163.36	1,068.00	Weathered Rock below 20ft (Silva et al.)	Weathered Rock below 20ft (Silva et al.)		
15	Weathered Rock	5.00	18.60	2,328.44	1,108.00	Weathered Rock below 20ft (Silva et al.)	Weathered Rock below 20ft (Silva et al.)		
16	Weathered Rock	5.00	20.40	2,731.95	1,146.00	Weathered Rock below 20ft (Silva et al.)	Weathered Rock below 20ft (Silva et al.)		
17	Weathered Rock	5.00	20.40	2,911.20	1,183.00	Weathered Rock below 20ft (Silva et al.)	Weathered Rock below 20ft (Silva et al.)		
18	Weathered Rock	5.00	20.40	3,086.01	1,218.00	Weathered Rock below 20ft (Silva et al.)	Weathered Rock below 20ft (Silva et al.)		

Table 8
ProShake Profile for I-80 Interchange
Best-Estimate (mean) Vs values
(0 to 320 m)

Layer Number	Material Name	Thickness (m)	Unit Weight (kN/m^3)	Gmax (MPa)	Vs (m/sec)	Modulus Curve	Damping Curve	Mod. Parameter	Damp. Parameter
1	Silty sand - Alluvium	1.52	19.64	44.63	149.35	(EPRI) Saturated Sand	(EPRI) Saturated Sand	7.50	7.50
2	Clayey silt - Alluvium	2.44	19.16	50.96	161.54	Vucetic - Dobry	Vucetic - Dobry	15.00	15.00
3	Soft to medium stiff silty clay - B. Clay	4.11	17.75	47.20	161.54	Vucetic - Dobry	Vucetic - Dobry	25.00	25.00
4	Very stiff clay	5.79	18.07	135.45	271.27	Clay (Seed and Sun 1989)	Clay - Average (Sun et al.)		
5	Soft to medium stiff silty clay - B. Clay	4.11	17.75	52.69	170.69	Vucetic - Dobry	Vucetic - Dobry	30.00	30.00
6	m. stiff to stiff silty clay and m. dense sand	4.85	19.64	96.35	219.46	Vucetic - Dobry	Vucetic - Dobry	20.00	20.00
7	Sandy clay	4.88	18.07	132.42	268.22	Vucetic - Dobry	Vucetic - Dobry	20.00	20.00
8	Silty clay	6.40	18.07	130.92	266.70	Vucetic - Dobry	Vucetic - Dobry	20.00	22.00
9	Silty clay	4.88	18.07	129.43	265.18	Vucetic - Dobry	Vucetic - Dobry	20.00	22.00
10	Silty clay	3.96	18.85	135.06	265.18	Vucetic - Dobry	Vucetic - Dobry	20.00	22.00
11	Very dense sand and clayey silt	3.66	20.11	121.81	243.84	Clay (Seed and Sun 1989)	Clay - Average (Sun et al.)		
12	Dense clayey silt	4.88	20.42	163.61	280.42	Clay (Seed and Sun 1989)	Clay - Average (Sun et al.)		
13	Dense clayey silt with fine sand	5.18	20.11	154.17	274.32	Clay (Seed and Sun 1989)	Clay - Average (Sun et al.)		
14	Very stiff clay	5.79	18.07	135.45	271.27	Clay (Seed and Sun 1989)	Clay - Average (Sun et al.)		
15	Sand	8.17	20.42	255.65	350.52	(EPRI) Saturated Sand	(EPRI) Saturated Sand	587.00	587.00
16	Sand	8.69	20.42	352.30	411.48	(EPRI) Saturated Sand	(EPRI) Saturated Sand	676.50	676.50
17	Sand	8.69	20.42	352.30	411.48	(EPRI) Saturated Sand	(EPRI) Saturated Sand	768.80	768.80
18	Sand	8.69	20.42	352.30	411.48	(EPRI) Saturated Sand	(EPRI) Saturated Sand	861.00	861.00
19	Sand	8.69	20.42	352.30	411.48	(EPRI) Saturated Sand	(EPRI) Saturated Sand	953.30	953.30
20	Sediments	10.36	20.42	464.41	472.44	(EPRI) Saturated Sand	(EPRI) Saturated Sand	957.60	957.60
21	Sediments	10.36	20.42	464.41	472.44	(EPRI) Saturated Sand	(EPRI) Saturated Sand	957.60	957.60
22	Sediments	10.36	20.42	464.41	472.44	(EPRI) Saturated Sand	(EPRI) Saturated Sand	957.60	957.60
23	Sediments	10.36	20.42	464.41	472.44	(EPRI) Saturated Sand	(EPRI) Saturated Sand	957.60	957.60
24	Sediments	12.19	20.42	592.00	533.40	(EPRI) Saturated Sand	(EPRI) Saturated Sand	957.60	957.60
25	Sediments	12.19	20.42	592.00	533.40	(EPRI) Saturated Sand	(EPRI) Saturated Sand	957.60	957.60
26	Sediments	12.19	20.42	592.00	533.40	(EPRI) Saturated Sand	(EPRI) Saturated Sand	957.60	957.60
27	Sediments	16.25	20.42	592.00	533.40	(EPRI) Saturated Sand	(EPRI) Saturated Sand	957.60	957.60
28	Sediments	13.90	20.42	773.22	609.60	(EPRI) Saturated Sand	(EPRI) Saturated Sand	957.60	957.60

29	Sediments	13.90	20.42	773.22	609.60	(E P R I) Saturated Sand	(EPRI) Saturated Sand	957.60	957.60
30	Sediments	13.90	20.42	773.22	609.60	(E P R I) Saturated Sand	(EPRI) Saturated Sand	957.60	957.60
31	Sediments	13.90	20.42	773.22	609.60	(E P R I) Saturated Sand	(EPRI) Saturated Sand	957.60	957.60
32	Sediments	13.90	20.42	773.22	609.60	(E P R I) Saturated Sand	(EPRI) Saturated Sand	957.60	957.60
33	Sediments	18.53	20.42	773.22	609.60	(E P R I) Saturated Sand	(EPRI) Saturated Sand	957.60	957.60
34	Sediments	13.90	20.42	773.22	609.60	(E P R I) Saturated Sand	(EPRI) Saturated Sand	957.60	957.60
35	Sediments	17.68	20.42	773.22	609.60	(E P R I) Saturated Sand	(EPRI) Saturated Sand	957.60	957.60
36	Sediments	9.45	20.42	1,208.16	762.00	(E P R I) Saturated Sand	(EPRI) Saturated Sand	957.60	957.60
37	Linear Rock	0.00	21.52	3,763.17	1,310.03	Linear	Linear		0.71

Table 9
ProShake Profile for 600 S. Interchange
Best-Estimate (mean) Vs values
(0 to 300 m)

Layer Number	Material Name	Thickness (m)	Unit Weight (kN/m^3)	Gmax (MPa)	Vs (m/sec)	Modulus Curve	Damping Curve	Mod. Parameter	Damp. Parameter
1	Sand and gravel	1.22	18.85	31.50	128.02	(EPRI) Saturated Sand	(EPRI) Saturated Sand	5.50	5.50
2	Fine sandy silt	2.74	19.64	46.51	152.40	(EPRI) Saturated Sand	(EPRI) Saturated Sand	25.00	25.00
3	Sand	1.22	18.85	48.29	158.50	(EPRI) Saturated Sand	(EPRI) Saturated Sand	31.53	31.50
4	Silty clay	4.37	17.28	40.92	152.40	Vucetic - Dobry	Vucetic - Dobry	30.00	30.00
5	Silty clay	4.37	17.28	40.92	152.40	Vucetic - Dobry	Vucetic - Dobry	30.00	30.00
6	Silty clay	4.37	17.28	40.92	152.40	Vucetic - Dobry	Vucetic - Dobry	30.00	30.00
7	Sandy silt	3.66	19.64	96.43	219.46	(EPRI) Saturated Sand	(EPRI) Saturated Sand	153.00	153.00
8	Silty clay	3.66	17.59	72.61	201.17	Clay (Seed and Sun 1989)	Clay - Average (Sun et al.)		
9	Silty clay	3.66	17.59	72.61	201.17	Clay (Seed and Sun 1989)	Clay - Average (Sun et al.)		
10	Silty sand	2.44	19.16	119.12	246.89	(EPRI) Saturated Sand	(EPRI) Saturated Sand	239.41	239.40
11	Silty clay / Sandy silt	3.66	18.07	112.28	246.89	(EPRI) Saturated Sand	(EPRI) Saturated Sand	265.90	265.90
12	Fine sand	3.66	20.26	155.50	274.32	(EPRI) Saturated Sand	(EPRI) Saturated Sand	300.20	300.20
13	Fine sand	3.66	20.26	155.50	274.32	(EPRI) Saturated Sand	(EPRI) Saturated Sand	338.40	338.40
14	Silty clay	2.74	20.11	171.91	289.56	Clay (Seed and Sun 1989)	Clay - Average (Sun et al.)		
15	Fine to medium sand	3.20	21.36	167.60	277.37	(EPRI) Saturated Sand	(EPRI) Saturated Sand	404.30	404.30
16	Fine to medium sand	3.20	21.36	167.60	277.37	(EPRI) Saturated Sand	(EPRI) Saturated Sand	441.30	441.30
17	Clayey silt / F. sand	2.83	18.85	120.08	249.94	(EPRI) Saturated Sand	(EPRI) Saturated Sand	472.70	472.70
18	Fine to medium sand	3.26	21.05	137.38	252.98	(EPRI) Saturated Sand	(EPRI) Saturated Sand	503.80	503.80
19	Silty clay	3.92	20.58	187.23	298.70	Clay (Seed and Sun 1989)	Clay - Average (Sun et al.)		
20	Sediments	3.92	20.42	255.85	350.52	(EPRI) Saturated Sand	(EPRI) Saturated Sand	585.20	585.20
21	Sediments	3.92	20.42	255.85	350.52	(EPRI) Saturated Sand	(EPRI) Saturated Sand	626.90	626.90
22	Sediments	10.33	20.42	352.59	411.48	(EPRI) Saturated Sand	(EPRI) Saturated Sand	702.50	702.50
23	Sediments	10.33	20.42	352.59	411.48	(EPRI) Saturated Sand	(EPRI) Saturated Sand	812.20	812.20
24	Sediments	10.33	20.42	352.59	411.48	(EPRI) Saturated Sand	(EPRI) Saturated Sand	922.00	922.00
25	Sediments	13.08	20.42	352.59	411.48	(EPRI) Saturated Sand	(EPRI) Saturated Sand	957.60	957.60
26	Sediments	13.08	20.42	464.79	472.44	(EPRI) Saturated Sand	(EPRI) Saturated Sand	957.60	957.60
27	Sediments	5.55	20.42	464.79	472.44	(EPRI) Saturated Sand	(EPRI) Saturated Sand	957.60	957.60
28	Sediments	12.16	20.42	592.48	533.40	(EPRI) Saturated Sand	(EPRI) Saturated Sand	957.60	957.60
29	Sediments	12.16	20.42	592.48	533.40	(EPRI) Saturated Sand	(EPRI) Saturated Sand	957.60	957.60
30	Sediments	12.16	20.42	592.48	533.40	(EPRI) Saturated Sand	(EPRI) Saturated Sand	957.60	957.60

31	Sediments	13.99	20.42	592.48	533.40	(EPRI) Saturated Sand	(EPRI) Saturated Sand	957.60	957.60
32	Sediments	13.90	20.42	773.85	609.60	(EPRI) Saturated Sand	(EPRI) Saturated Sand	957.60	957.60
33	Sediments	13.90	20.42	773.85	609.60	(EPRI) Saturated Sand	(EPRI) Saturated Sand	957.60	957.60
34	Sediments	13.90	20.42	773.85	609.60	(EPRI) Saturated Sand	(EPRI) Saturated Sand	957.60	957.60
35	Sediments	13.90	20.42	773.85	609.60	(EPRI) Saturated Sand	(EPRI) Saturated Sand	957.60	957.60
36	Sediments	13.90	20.42	773.85	609.60	(EPRI) Saturated Sand	(EPRI) Saturated Sand	957.60	957.60
37	Sediments	13.90	20.42	773.85	609.60	(EPRI) Saturated Sand	(EPRI) Saturated Sand	957.60	957.60
38	Sediments	13.90	20.42	773.85	609.60	(EPRI) Saturated Sand	(EPRI) Saturated Sand	957.60	957.60
39	Sediments	8.41	20.42	773.85	609.60	(EPRI) Saturated Sand	(EPRI) Saturated Sand	957.60	957.60
40	Sediments	15.21	20.42	1,209.13	762.00	(EPRI) Saturated Sand	(EPRI) Saturated Sand	957.60	957.60
41	Linear Rock	0.00	21.52	3,766.21	1,310.03	Linear	Linear		0.68

ATTACHMENT A
RSPMATCH MANUAL

ATTACHMENT B
FAULT DIRECTIVITY CALCULATION

ATTACHMENT C
RSPMATCH INPUT FILES

ATTACHMENT D
BASELINE USER'S MANUAL

ATTACHMENT E
PROSHAKE INPUT FILE
GENERIC WESTERN U.S. ROCK PROFILE

ATTACHMENT F
BEST ESTIMATE SOIL PROFILE
I-80 INTERCHANGE

ATTACHMENT G
BEST ESTIMATE SOIL PROFILE
600 S. INTERCHANGE

ATTACHMENT H
UPPER BOUND SOIL PROFILE
I-80 INTERCHANGE

ATTACHMENT I
UPPER BOUND SOIL PROFILE
600 S. INTERCHANGE

ATTACHMENT J
DAMPING CALCULATIONS
I-80 PROFILES

ATTACHMENT K
DAMPING CALCULATIONS
600 SOUTH PROFILES